The Design and Synthesis of Novel AOX and cytochrome bc_1 complex inhibitors which act as Phytopathogenic Fungicides

James Misselbrook

Submitted in partial fulfilment towards the requirements for the degree of Doctor of Philosophy (DPhil)

University of Sussex

February 2019

I hereby declare that this thesis has not been and will not be, submitted in whole or in part to another University for the award of any other degree.

University of Sussex

Doctor of Philosophy

The Design and Synthesis of Novel AOX and cytochrome *bc$_1$* complex inhibitors which act as Phytopathogenic Fungicides

Summary

The metabolic pathway for oxidative phosphorylation has remained a reliable target for the development of novel fungicides. The reliance on single target site fungicides within this pathway has increased the selection pressure for point mutations within a number of key complexes, including the cytochrome *bc$_1$* complex. The alternative oxidase (AOX) provides an alternative route for respiration, introducing a mechanism by which selection pressure and pathogenicity can be increased. In particular, the fungal pathogen *Septoria tritici* has developed a highly fungicide resistant strain. The design and synthesis of inhibitors targeting the fungal AOX, or the AOX and the cytochrome *bc$_1$* complex, represents a new class of fungicides improving crop yield outcomes.

Investigation into the AOX found in *S. tritici* (StAOX), led to new techniques to fully characterise and overexpress the protein in a haem deficient *Escherichia coli* strain, which has then been compared to that of the well-studied protozoan AOX, *Trypanosoma brucei brucei* (TAO). The enzymatic activity of StAOX was found to be significantly lower in comparison to AOXs from other species, but responded dramatically to the nucleotide regulators, GMP and IMP. The purified protein has also been shown to be sensitive to its lipid environment with full enzymatic recovery following re-introduction into a lipid membrane.

The natural quinol analogue, ascofuranone, displays selectivity towards the AOX and was selected for further design and lead modification. Several ascofuranone derivatives were synthesised according to a new synthetic route. A variety of new methods were utilised to analyse the inhibitors providing IC_{50}, K_D, thermodynamic and cytotoxicity data. Two of the newly synthesised compounds provided selectivity for TAO over the cytochrome *bc$_1$* complex, but failed to show selectivity to the StAOX. *In vitro* data suggests a single phenylalanine residue restricts inhibitor's tail length to within an 8-carbon chain length, supported by an *in-silico* docking screen.

Table of Contents

Abbreviations Used

Abbreviation	Full Name
5'-NT	'5-Nucleotidase
ABC transporter	ATP-binding cassette transporter
Acetyl-CoA	Acetyl Coenzyme A
ADP	Adenosine diphosphate
ADSL	Adenylsuccinate lyase
AdSS	Adenylosuccinate synthase
ALA	α-Linolenic acid
AMP	Adenosine monophosphate
AMPD	Adenosine monophosphate deaminase
AOX	Alternative oxidase
AP	All purpose
APS	Ammonium persulfate
ATP	Adenosine triphosphate
BSA	Bovine serum albumin
CYP51	Lanosterol 14α-demethylase
DBU	1,8-Diazabicyclo[5.4.0]undec-7-ene
DCE	Dichloroethane
DCM	Dichloromethane
DCPIP	Dichlorophenolindophenol
DDM	*n*-Dodecyl β-D-maltoside
DMF	Dimethylformamide
DMI	Demethylation inhibitor
DMSO	Dimethyl sulfoxide
EFSA	European Food Safety Authority
EGTA	Ethylene glycol-bis (β-aminoethyl ether)-*N*,*N*,*N*′,*N*′-tetraacetic acid
EPR	Electron paramagnetic resonance
ETC	Electron transport chain
EtOAc	Ethyl acetate
FAD	Flavin adenine dinucleotide
$FADH_2$	Flavin adenine dinucleotide hydroquinone
FAO	Food and Agriculture Organisation

Abbreviations Cont'd

FC-12	Fos-choline 12
FMN	Flavin mononucleotide
FPLC	Fast protein liquid chromatography
FRAC	Fungicide Resistance Action Committee
GAPDH	Glyceraldehyde 3-phosphate dehydrogenase
GMP	Guanosine monophosphate
GS	Glutamine synthetase
GST	Glutathione S-transferase
GTP	Guanosine triphosphate
HABA	4'-Hydroxyazobenzene-2-carboxylic acid
HBD	Hydrogen bond donors
HMPA	Hexamethylphosphoramide
IDH	Isocitrate dehydrogenase
IMP	Inosine monophosphate
IMS	Intermembrane space
IPTG	Isopropyl β-D-1-thiogalactopyranoside
ITC	Isothermal titration calorimetry
MMO	Methane monooxygenase
MOPS	3-(*N*-Morpholino)propanesulfonic acid
MPO	Multi parameter optimisation
MS	Mass spectrometry
MW	Molecular weight
NAD^+	Nicotinamide adenine dinucleotide oxidised
NADH	Nicotinamide adenine dinucleotide reduced
NBD-Cl	4-Chloro-7-nitrobenzofurazan
NCS	*N*-Chlorosuccinamide
NDI	Internal NADH Dehydrogenase
NDK	Nucleoside-diphosphate kinase
NMK	Nucleoside-phosphate kinase
NMR	Nuclear magnetic resonance
PCET	Proton coupled electron transfer
PDB	Protein database
pTLC	Preparative thin layer chromatography

Abbreviations Cont'd

Q	Quinone
Q_{10}	Quinone with 10 repeated isoprene units
Q_2	Quinone with 2 repeated isoprene units
Q_2H_2	Quinol with 2 repeated isoprene units
QH_2	Quinol with 1 isoprene unit
Q_iI	Quinone inside inihibtor
Q_oI	Quinone outside inhibitor
Q_oSI	Quinone stigmatellin binding
QSAR	Quantitative structure-activity relationship
RNR	Ribonucleotide reductase
ROS	Reactive oxygen species
R_f	Retention Factor
SDHI	Succinate dehydrogenase inhibitor
SDS-Page	Sodium dodecyl sulfate polyacrylamide gel electrophoresis
SgAOX	*Sauromattum guttatum* alternative oxidase
SHAM	Salicylhydroxamic acid
S_NAr	Nucleophilic aromatic substitution
StAOX	*Septoria tritici* alternative oxidase
STB	*Septoria tritci* blotch
TAO	*Trypanosoma brucei brucei* alternative oxidase
TBDMS-Cl	*tert*-Butyldimethylsilyl chloride
TBST	Tris buffered saline with Tween 20
t-BuLi	*tert*-Butyllithium
t-BuOOH	*tert*-Butyl hydroperoxide
TCA	Tricarboxylic acid cycle
TEA	Triethylamine
TEMED	Tetramethylethylenediamine
THF	Tetrahydrofuran
TLC	Thin layer chromatography
tPSA	Total polar surface area
UDAO	n-Undecyl-*N*,*N*-Dimethylamine-Oxide

Acknowledgments

I would like to thank my supervisor, Professor Anthony Moore, for giving me the opportunity to undertake a PhD research project. His continued guidance and support throughout my time as a doctoral researcher has been invaluable and greatly appreciated.

I would also like to thank my industrial sponsor, Agform Ltd., for funding the project and supporting a considerable research effort at their facilities. In particular my thanks are given to my industrial supervisor, Dr. Jonathan Sharp, who helped increase my knowledge in organic chemistry and taught me a large variety of lab techniques to complete this thesis.

Many thanks are extended to Mary Albury, Benjamin May, Alicia Rosell-Hidalgo and Alice Copsey for helping me in the lab and introducing me to new biochemical lab techniques. Thank you to Andrew McGown for allowing me to use his lab space and equipment for compound characterisation. A special thanks is extended to Luke Young, for both his contribution towards the fungicide research project and his support and patience when bombarding him with questions at 9am on a Monday morning!

Last but not least, I would like to thank my family and friends for their continued support throughout my research project and for believing in my abilities when pursuing a PhD. Without their support, the past 4 years would have been a lot harder.

Chapter 1: Introduction

1.1 Phytopathogenic Fungicides

The use of fungicides to control foliar crop disease, can be dated back to the nineteenth century, following the widespread infection of *Phytophthora infestans* (Potato Blight). Potato blight caused widespread famine and fatalities across the majority of Western Europe. Subsequently, the first fungicide, known as the Bordeaux mixture, was discovered by Millardet. It had been used for a number of years to treat powdery mildew (*Plasmopara viticola*) on grapevines; and after Millardet noticed the similarities between the two fungi, it was found it could be used against potato blight. This discovery[1], albeit too late, coincided with the creation of plant pathology and stressed the importance of understanding the target of fungicides.

Today, the Bordeaux mixture is still used as a fungicide treatment[2]; consisting of a 1% solution of copper sulfate ($CuSO_4$) and slaked lime ($Ca(OH)_2$), with a 1:1 ratio for both of these inorganic salts. The effective concentration of Cu^{2+} ions produces its fungistatic activity by inhibiting a broad spectrum of molecular targets including transport carriers and biologically important enzymes. The multi-site activity and lack of specificity for copper fungicides presents a number of toxic effects for the environment[3,4], aquatic life[5], plants[6], animals[7] and humans[8]. The accumulation of elemental copper residues following a fungicide treatment also poses concern for the long-term use of inorganic fungicides[3,9]. The European Union has therefore regulated[10] its use to reduce environmental damage and the probable health implications.

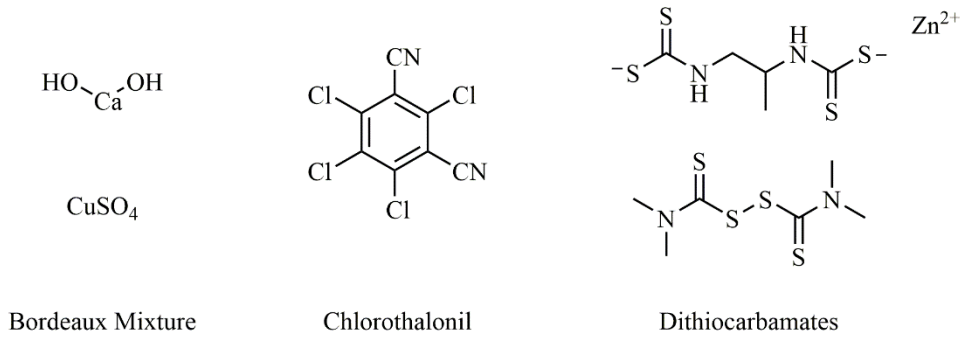

Bordeaux Mixture Chlorothalonil Dithiocarbamates

Figure 1 – Classical Multi Target Site Fungicides

Since the original discovery of the Bordeaux mixture, a number of multi target site fungicides (**Figure 1**) have been used to treat phytopathogenic fungal diseases. Chlorothalonil is one such fungicide with a broad spectrum of activity against both resistant (Q_oI and DMI) and non-resistant fungal species. The mode of action of chlorothalonil occurs through its reaction with thiol rich enzymes such as glutathione-S-transferase (GST) and glyceraldehyde-3-phosphate dehydrogenase (GAPDH)[11]. Chlorothalonil acts as an alkylating agent, reacting with thiol groups through a nucleophilic aromatic substitution (S_NAr) reaction, forming conjugated chlorothalonil-thiol derivatives[12]. This action depletes the cellular reserves of GST and GAPDH limiting the fungal cells ability to detoxify xenobiotic species and generate ATP through glycolysis, respectively.

The use of chlorothalonil has raised concerns following the discovery of non-target toxic effects on environmental organisms; including, aquatic life[13–15] and soil bacteria[16,17]. However, the risks posed by chlorothalonil on both of these organisms is diminished, due to its inherent physicochemical properties. The low water solubility (0.81 g/kg[18]) and high adherence to soil[19] prevents any considerable accumulation in water systems, and therefore within aquatic species. Recent discoveries of chlorothalonil degrading bacteria[20–23] show a breakdown of the compound once adsorbed to the soil surface reducing leftover treatment residues. Furthermore, soil samples containing chlorothalonil demonstrate a half-life of <9 days[24] following spraying under laboratory conditions. Human toxicity reports suggest genotoxic and carcinogenic properties when assessed against *in vitro* human lymphoma cells[25] and animal studies[26] but the EFSA peer reviewed study[27] highlights inadequacies with the data obtained for these studies including the use of 2-60 times the residue concentrations found in the field[28]. Nevertheless; the EU commission has decided not to renew the approval for chlorothalonil as a phytopathogenic fungicide, eliminating a powerful tool for the treatment of resistant and non-resistant fungal species.

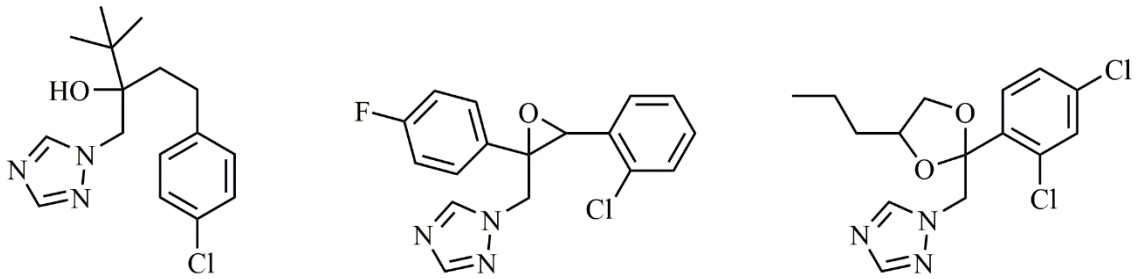

Tebuconazole Epoxiconazole Propiconazole

Figure 2 - Most Commonly used Demethylation Inhibitors (DMIs) Fungicides

To overcome possible ecological and non-target toxicity, modern fungicides exhibit single-site inhibition. The demethylation inhibitors (DMIs) are a class of fungicides that disrupt the biosynthesis of ergosterol an essential component of the fungal cell membrane[11]. More specifically; the inhibition of lanosterol 14α-demethylase, a protein from the cytochrome P450 family, is responsible for an essential step in the biosynthetic ergosterol pathway. The triazole family of compounds display high selectivity to this enzyme and represent the most commonly used fungicides in the UK and globally[29]. Tebuconazole, Epoxiconazole and Propiconazole[29] (**Figure 2**) represent the majority of the market share within the triazole class, helping to control fungal pathogens affecting cereals[30], rice[31], vegetable and fruits[32]. The relatively low cost and effectiveness against a broad spectrum of fungal species has led to extensive use of this fungicide class. Unfortunately, this extensive use has led to an increase of triazole resistant fungal strains[33], limiting their ability to solely control plant diseases.

In recent years, the most significant discoveries for the treatment of phytopathogenic fungicides has arisen from the inhibition of fungal respiration[34,35]. The inhibition of energy production and oxidative phosphorylation remains a key target for current and future fungicide design, due to the high energy demands required for successful spore germination and host penetration for phytopathogenic fungi[32]. The strobilurins represent the largest and most commonly used fungicides within this group (**Figure 6**). Much like the triazoles, the strobilurins offer broad spectrum control against fungal pathogens but provide a much higher efficacy[36]. The lower use rates, yield and grain quality improvements offer a number of advantages over the older triazole fungicides but their specificity to single target site has resulted in the establishment of highly resistant fungal strains[37–39].

The succinate dehydrogenase inhibitors, SDHIs, are another class of fungicides that inhibit the respiration of phytopathogenic fungi (**Figure 5**). The use of the SDHI inhibitors has grown in recent years following the emergence of resistant fungal strains to both triazole and strobilurin fungicides[37–40]. In a similar manner to the strobilurins, the SDHI inhibitors offer a single site of action posing a potential opportunity for the selection pressure for resistant fungal species. The eradication of fungal pathogens with multiple respiratory inhibitors introduces a novel treatment for economically important crops, increasing the efficacy of fungicide treatments and manages the threat of emerging resistance[41]. Scientists are therefore focussing efforts towards understanding the fungal respiratory chain and the mechanism by which both of these groups of respiratory fungicides exhibit their mode of action.

1.2 Fungal Respiration

The metabolism and respiration of phytopathogenic fungi is well adapted to the survival within host systems, utilising abundant (*in planta*) or sometimes limiting nutrient resources (prior to host invasion)[42]. The use of a carbon source is vital to a fungal species survival within a host to initiate respiration and generate ATP for the cell[42]. Preferentially glucose is used as a carbon source which is converted into two pyruvate, two NADH and two ATP molecules *via* the metabolic process known as glycolysis[43]. Under aerobic conditions pyruvate enters the mitochondrial matrix where it is decarboxylated into acetyl coenzyme A (acetyl-coA) by pyruvate dehydrogenase; linking the glycolytic pathway with the cyclical metabolic pathway of the Citric acid cycle (TCA).

The citric acid cycle is a key metabolic pathway responsible for the generation of important precursors for amino acid synthesis, as well as NADH and succinate that feed into the electron transport chain. The full cycle consumes one molecule of acetyl-CoA generating three NADH, one $FADH_2$, two CO_2 and one GTP molecule, through a series of enzymatic reactions. The regulation of the citric acid cycle occurs through feedback inhibition[37–40] through a build-up of intermediates such as NADH, inhibiting crucial enzymes for TCA turnover.

The availability of glucose within the plant host and through fungal reserves, plays a significant role in the turnover of the TCA cycle for fungi[44], resulting in less productive mycelium growth. In fact, the combination of all three elements of fungal metabolism are required for ATP demanding processes such as host penetration and spore germination[42]. One glucose molecule provides a theoretical maximum yield of 38 equivalents of ATP which involves glycolysis, TCA cycle and oxidative phosphorylation. However, observed yields are closer to 30 ATP equivalents due to inefficiencies with oxidative phosphorylation[37–40]. The significance of the electron transport within the yield of ATP is that without oxidative phosphorylation, glycolysis only provides 2 molecules of ATP per glucose molecule. The inhibition of the electron transport chain, through the design of fungicides targeted to the respiratory chain, could therefore be detrimental to fungal respiration.

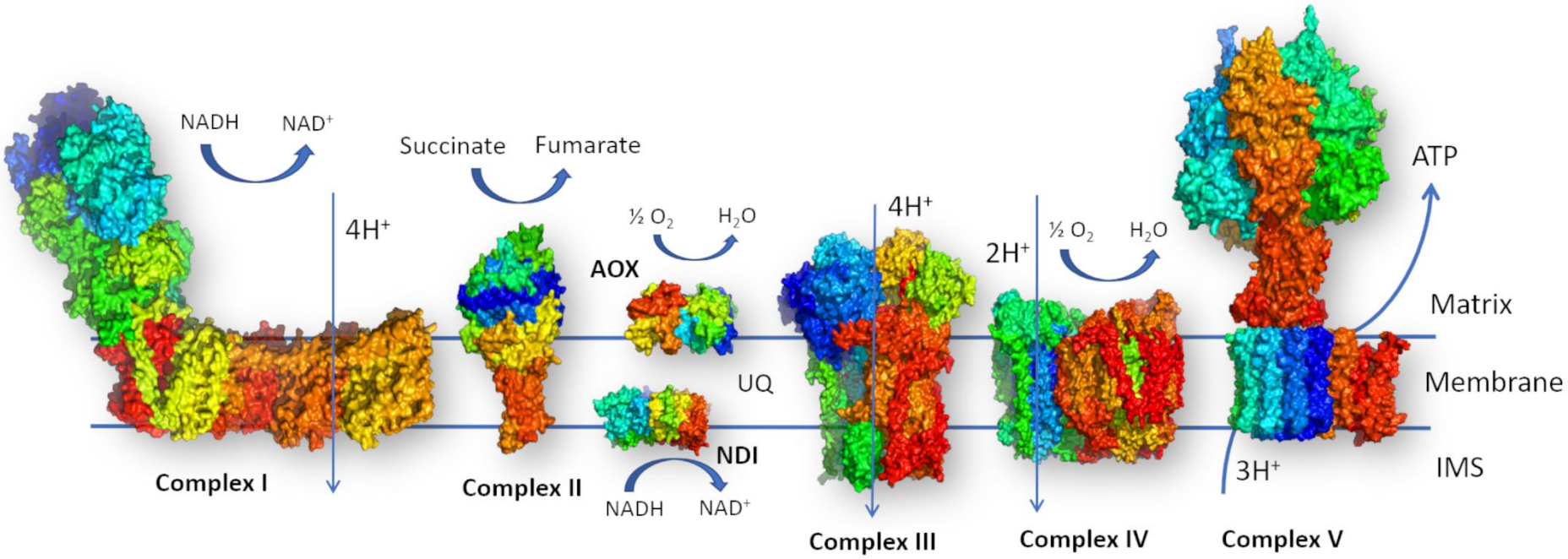

Figure 3 - A Fungal-like Electron Transport Chain (ETC) with all its components. Crystal Structures of Complex I from Yarrowia lipolytica (PDB ID: 6GCS), Complex II from porcine heart (PDB ID: 1ZOY), Complex III from chicken (PDB ID: 3H1L), Complex IV from yeast (PDB ID: 6GIQ), ATP synthase from yeast (PDB ID: 2WPD), AOX from Trypanosoma brucei brucei (PDB ID: 3W54) and NDI from yeast (PDB code: 4G9K). AOX refers to the alternative oxidase, NDI refers to the external NADH dehydrogenase. UQ refers to the ubiquinone pool. Each complex and enzymatic function is described in Section 1.3.

1.3 Oxidative Phosphorylation *via* the Electron Transport Chain

The mitochondria are the main site for oxidative phosphorylation for fungi and most eukaryotic life forms and contains the electron transport chain (ETC). The majority of ATP production within the fungal cell occurs through the ETC. The classical ETC consists of 5 multi-enzyme complexes, isoprenoid charge carriers (Ubiquinone and Ubiquinol) (**Figure 4**) and cytochrome c. Electrons enter the ETC *via* NADH from glycolysis and the TCA cycle, passing through Complex 1 whereby its transferred to quinone. Quinone is also reduced by Complex II, passing the electrons to Complex III which transfers its electrons to cytochrome *c*. Cytochrome *c* passes electrons to Complex IV which catalyses the reduction of O_2 to H_2O. This process effectively shuttles protons across the inner mitochondrial membrane from the matrix into the intermembrane space (IMS), thus creating a proton electrochemical potential gradient. This potential is used to drive the ATP synthase in the forward direction phosphorylating ADP to ATP, generating energy for the fungal cell. An overview of this process is summarised in **Figure 3**.

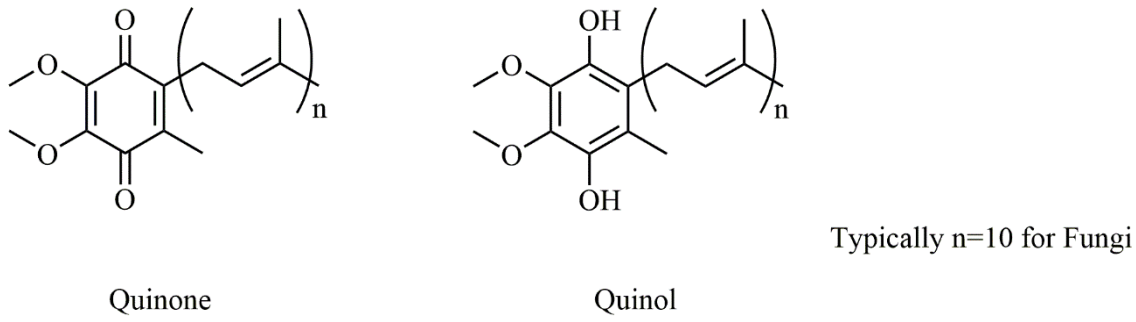

Figure 4 - Structure of the Isoprenoid charge carriers, Quinone and Quinol, which are concentrated within the inner mitochondrial membrane.

1.3.1 Complex I

NADH dehydrogenase or Complex I is the first respiratory complex in the ETC, catalysing the oxidation of NADH produced by the TCA cycle and sparingly from β-oxidation of fatty acids. The redox reaction proceeds following the binding of NADH to the matrix side of the protein, at which point it is oxidised by the flavin mononucleotide (FMN) to NAD^+. A series of FeS clusters transfer electrons from NADH to reduce a bound ubiquinone to ubiquinol. The electron transfer reaction is coupled with the translocation of four protons[45–47] across the inner mitochondrial membrane and contributing to the chemiosmotic potential.

$$NADH + 4H^{+}_{Matrix} + Q \rightarrow NAD^{+} + QH_2 + 4H^{+}_{IMS}$$

Complex I is the largest of the mitochondrial membrane proteins at around 1MDa with an L-shaped structure, consisting of membrane bound domain and a mitochondrial matrix dendritic hydrophilic arm[48]. The total number of subunits for the protein complex is species dependent but all share a core of 14 central subunits. Assessment of the Complex I found in fungi[48–50] have shown a total number of subunits between 35 and 37. High resolution X-Ray crystal structures[51,52] of Complex I have also revealed previously debated positions of the quinone reduction site which may allow for the design of novel inhibitors.

There are very few reported inhibitors of Complex I for the control of phytopathogenic fungi mostly due to the poorly understood mechanism of inhibition. Pyrimidine fungicides have recently[53] been designated by the fungicide resistance action committee (FRAC) to inhibit complex I, with pyrazole-MET1 like tolfenpyrad[54] remaining the only commercialised fungicide with this mode of action. Ongoing research[55–57] is focussed on adaptation of diflumetorim derivatives to treat a wider range of fungal rusts diseases. Since there are very few research groups investigating Complex I inhibitors for their potential as fungicides, the protein complex offers a unique mode of action to introduce a new class of fungicides.

1.3.2 Succinate dehydrogenase (Complex II)

Succinate dehydrogenase or Complex II is unique, in that it is both present in the citric acid cycle and the ETC, catalysing the oxidation of succinate to fumarate. After oxidation, a transfer of electrons to bound ubiquinone occurs and in contrast to other respiratory complexes does not translocate protons across the membrane. X ray crystallographic examination[58,59] along with EPR studies[60,61] demonstrate the stepwise removal of protons and electrons from the quinone molecule and successfully identify the precise quinone binding sites. A detailed mechanism for the mechanism of catalysis has been reviewed by Iverson *et al*[62] but can be summarised as follows:

$$Succinate + Q \rightarrow Fumarate + QH_2$$

The structure of succinate dehydrogenases display high conservation across all species for two of the four subunits which are encoded by nuclear DNA[63,64]. Two of the complex II subunits extend into the matrix side of the mitochondrial membrane (SdhA and SdhB) and contain the main catalytic groups of the flavin (FAD) and three FeS clusters (2Fe-2S, 3Fe-4S and 4Fe4S). The two other subunits (SdhC and SdhD) span the membrane and contain the sites for quinone binding and b-type haem. Succinate binds to the SdhA subunit and transfers protons and electrons to reduce FAD to $FADH_2$. The electrons transfer between the FeS centres in subunit SdhB and onto the b-type haem, reducing a bound ubiquinone molecule.

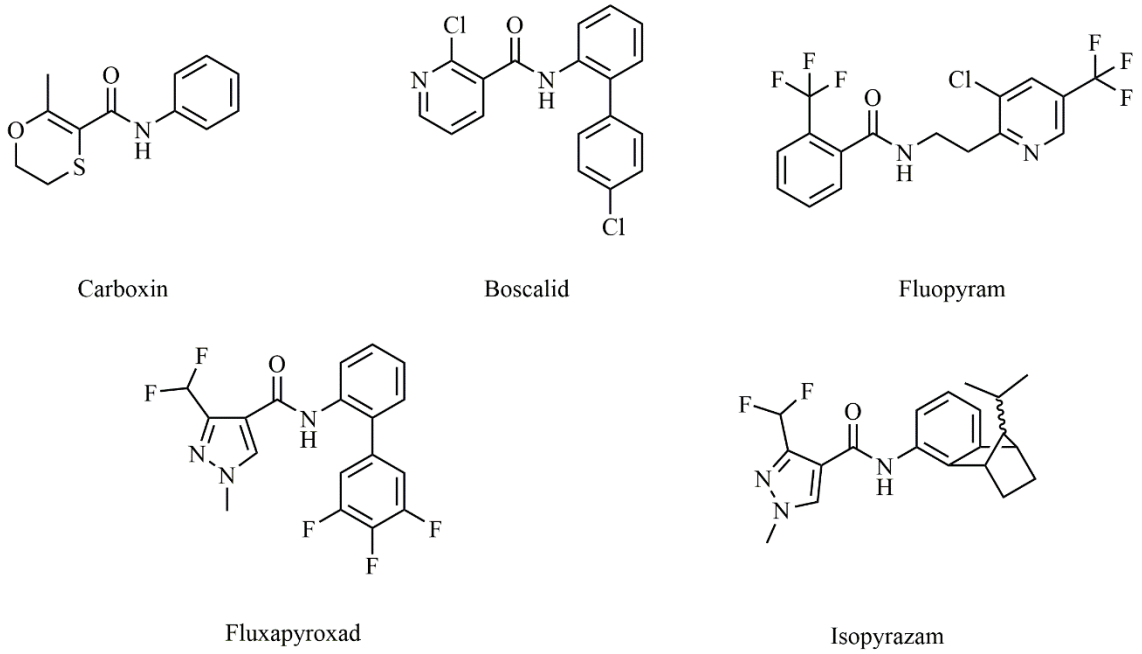

Figure 5 - SDHI Fungicides used to Treat a Spectrum of Fungal Species

The SDHI family of fungicides target Complex II by binding to the ubiquinone site within the trans membranous domain of the complex, confirmed by X-ray crystallographic studies[65–67]. The majority of SDHI inhibitors share common chemical structures that allow for a high affinity to the ubiquinone binding site. The central amide moiety within the chemical structures shown in **Figure 5**, is essential for hydrogen bonding to Y130, W224 and indirectly S83 (*S. tritici* numbering) within the quinone binding site of Complex II. These residues are highly conserved across species since they are directly involved in the binding of ubiquinone[61,68,69]. The head group (attached to the carbonyl of the amide bond), by which the compounds family classification is derived, binds deeper into the polar cleft of the binding site than the substrate ubiquinone. The rest of the compound lies within the hydrophobic region of the cavity representing a large diversity in chemical structures.

1.3.3 Cytochrome bc_1 complex (Complex III)

The cytochrome bc_1 complex catalyses the oxidation of quinol transferring electrons onto cytochrome *c* concomitantly translocating four protons across the mitochondrial membrane. Its structural similarity across all species including prokaryotic systems allow for direct comparisons between structures. The cytochrome bc_1 complex contains a catalytic core consisting of three transmembrane subunits, the central unit of these is the membrane spanning cytochrome *b* homodimer subunit. The cytochrome *b* subunit contains two *b*-type hemes (b_L and b_H) adjacent to the two quinol binding sites, one site being responsible for the oxidation of quinol (Q_o) and the other for the reduction of quinone or semiquinone to quinol, known as the Q_i site. Each cytochrome *b* subunit is attached to a subunit either containing the cofactor cytochrome c or the Rieske-type iron sulfur cluster (2Fe-2S). These two subunits extend into the intermembrane space (IMS) which is the location under normal physiological conditions of the water-soluble cytochrome *c*.

$$QH_2 + 2\ cytochrome\ c\left(Fe^{3+}\right) + 2H^+_{Matrix} \rightarrow Q + 2\ cytochrome\ c\left(Fe^{2+}\right) + 4H^+_{IMS}$$

The above equation summarises the reaction catalysed by Complex III but a detailed mechanism, known as the protonmotive Q cycle, for the oxidation of quinol was established by Mitchell[70,71] and later updated by others[72–74]. The updated Q cycle determines the oxidation of quinol at the Q_o site followed by the transfer of two electrons along two separate pathways within the protein complex. The first route follows along through the subunit containing the Rieske-type iron sulfur cluster (2Fe-2S) and through the subunit containing the c-type heme towards the soluble cytochrome c molecule. The second route sees the electron pass through the cytochrome b subunit and hemes at b_L and b_H and through to a semiquinone at the Q_i binding site. The interaction of common inhibitors associated with the Q_i site have provided confirmation[75,76] of the Q cycle model along with EPR studies[77,78] and oxidant induced reduction[79] of the b-cytochromes.

Fungicides that target respiration *via* the cytochrome bc_1 complex can be categorised into two groups as classified by FRAC[53]: the quinone outside inhibitors (Q_oIs) and quinone inside inhibitors (Q_iIs). The Q_oI fungicide class is well established and represents the strobilurin compounds along with more recent discoveries that share the same Q_o ubiquinol binding site[80,81]. The newly discovered fungicides which inhibit the Q_i site offer an alternative binding site within Complex III and therefore treat Q_oI resistant fungal species. A selection of fungicides from each group are shown in **Figure 6**.

Strobilurins (Q_o site)
Fungicides:

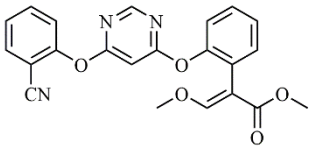

Azoxystrobin

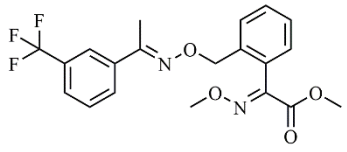

Trifloxystrobin

New Q_o Fungicides:

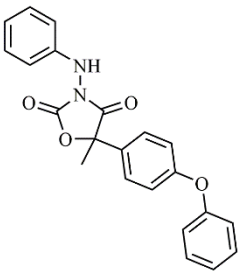

Famoxadone

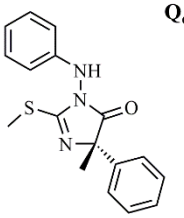

Fenamidone

Q_oSI Fungicide:

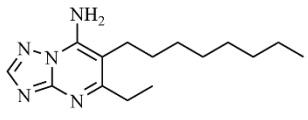

Amectotradin

Q_o site Inhibitors:

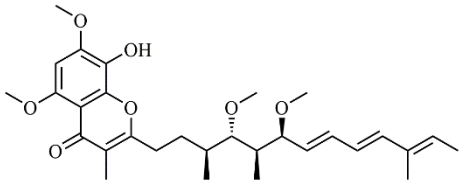

Stigmatellin

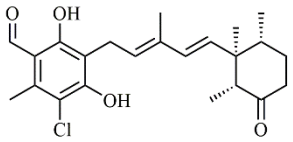

Ascochlorin

Q_i site Fungicides:

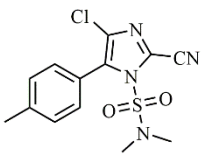

Cyazofamid

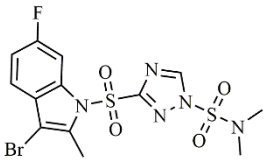

Amisulbrom

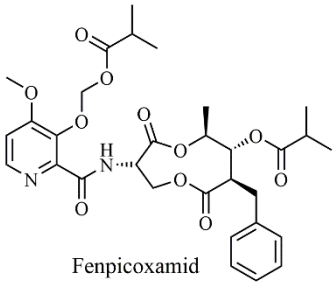

Fenpicoxamid

Q_i site Inhibitors:

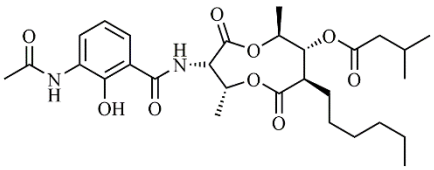

Antimycin A

Figure 6 - A selection of Fungicides and Inhibitors of the fungal cytochrome bc_1 complex (Complex III). Strobilurins Azoxystrobin and Trifloxystrobin represent the Q_o fungicides with a common methoxy acrylate like binding motif. Famoxadone and Fenamidone provide a representation of recent Q_o Fungicide discoveries. Amectotradin is the sole commercial fungicide contributing to the Q_oSI class. Stigmatellin and Ascochlorin provide examples of inhibitors with a 'distal' binding mode. Q_i Fungicides include Cyazofamid, Amisulbrom and Fenpicoxamid. Antimycin A is a well-established Q_i site inhibitor.

Binding of the Q_oI inhibitors to the Q_o site within the cytochrome b subunit occurs in a unique position in the bifurcated binding cavity. Strobilurins bind in what is known as the 'proximal' domain which does not affect the redox properties or mobility of Rieske iron sulfur cluster[82,83]. Alternatively, benzoquinone-like inhibitors such as Ascochlorin[84], Stigmatellin[37–40] and the fungicide Amectotradin[82] bind at the 'distal' position, directly interacting with the Rieske iron and stabilise this subunit to the protein.

The toxophore for the strobilurins is the methoxy acrylate group or chemically related derivatives. Binding of the methoxy acrylate group occurs adjacent to the fully conserved PEWY sequence (P270, E271, W272 and Y273) loop in the cytochrome b subunit (**Figure 7**). The carbonyl group on the toxophore is essential for inhibitor binding with hydrogen bonding to the amide bond of E271 as shown in solved bovine crystal structures. Within the adjacent pocket formed in between the rings of F128 and Y132 sits the ether group of the methoxy acrylate group. Whilst π-stacking interactions stabilise the intermediate ring which is present in the Azoxystrobin structure. The binding of azoxystrobin within this position allows for continued motility of the Rieske-iron containing subunit.

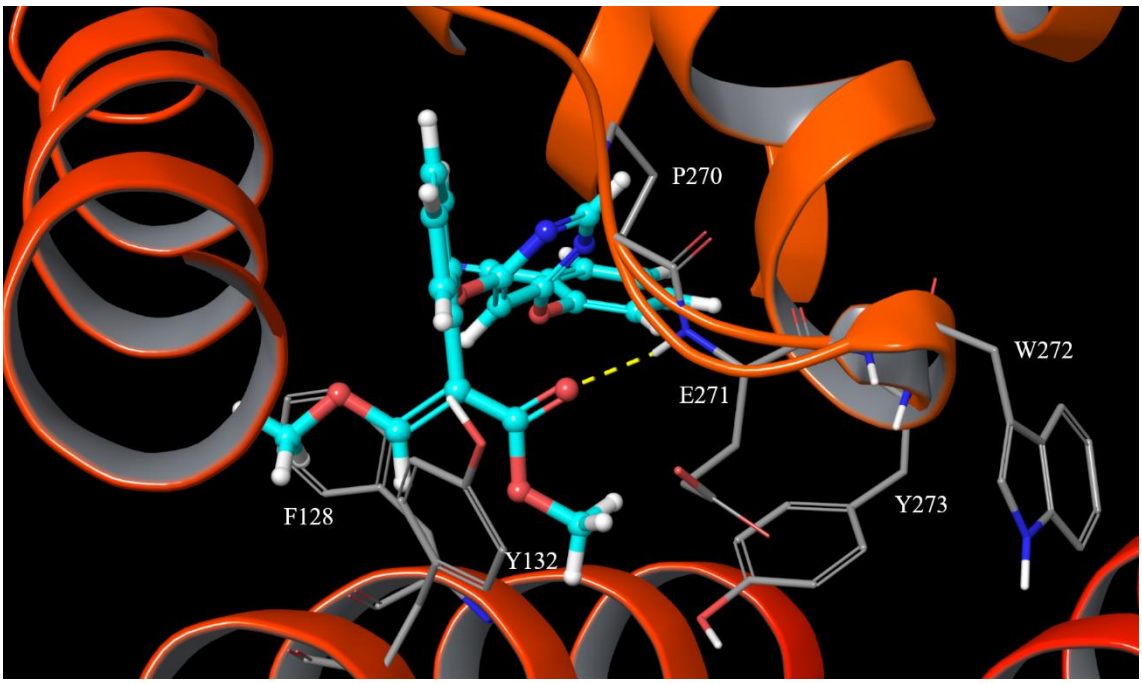

Figure 7 – Azoxystrobin binding position within the Q_o binding site of the cytochrome bc_1 complex (PDB code: 3L71), highlighting its proximity to the conserved PEWY amino acid sequence. The pocket formed by residues F128 and Y132 houses the methoxy acrylate toxophore common to Q_oIs.

The development of three resistant strains of fungal species considerably hampers the binding of the Q_oIs to the cytochrome *b* subunit and quinol binding site. Field isolates containing the amino

acid substitutions G143A[39,85,86], F129L[87,88] and G173R[89,90] confer complete or partial resistance, respectively. As shown in **Figure 8**, the most prevalent G143A mutation sterically hinders the binding of the methoxy acrylate toxophore within the Q_o binding site. Fungal species that contain any combination of these amino acid mutations is broad, with wide spread field identifications of the G143A mutation in *S. tritici*[91,92], *Venturia inaequalis*[86], *Magnaporthe oryzae*[93] and *Botrytis cinerea*[39]. The fitness cost of the G143A mutation is minor with only 87% remaining of the original activity of cytochrome bc_1 complex allowing for adoption to a wide range of fungal pathogens[94].

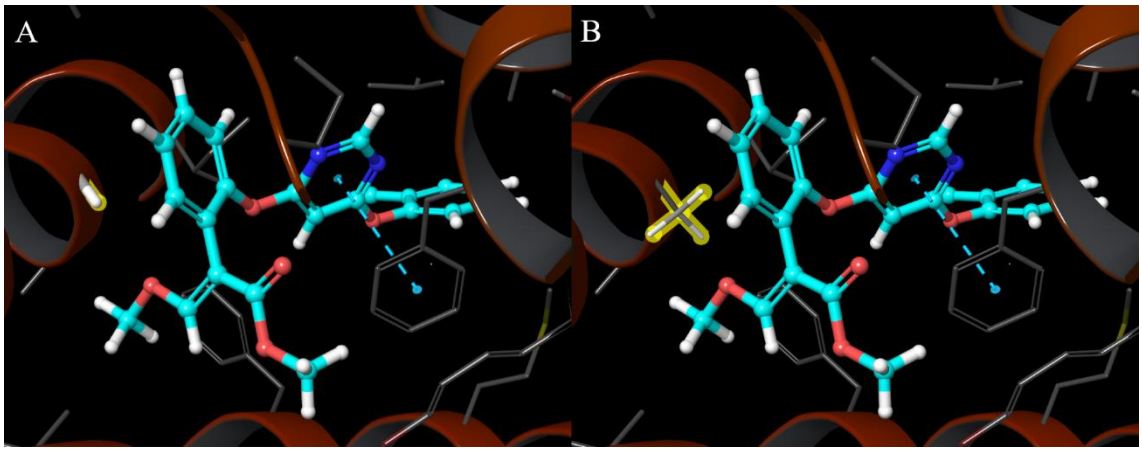

Figure 8 - Azoxystrobin bound within the Q_o binding site of the cytochrome bc_1 complex (PDB code 3L71) with the wildtype complex and G143 residue highlighted (A) and the Q_o resistant G143A strain with the alanine mutation highlighted (B).

The reduced sensitivity of fungicides binding to the 'proximal' position within the Q_o binding site severely limits fungal pathogen treatment. Fungicides binding in the 'distal' position of the Q_o binding site such as the natural fungicides stigmatellin, ascochlorin and amectotradin are unaffected by the G143A mutation[82,95–97]. Stigmatellin and amectotradin are therefore sometimes referred to as Q_oSI inhibitors due to their differential binding at the Q_o site of the cytochrome bc_1 complex. Famoxadone and Fenamidone fall somewhere in between the 'distal' and 'proximal' position with their point of contact within the fully conserved PEWY sequence of residues between the Y132 and P270 amino acid residue (**Figure 9**). These two relatively new Q_oIs display reduced sensitivity to the G143A resistant fungal species[98] and therefore offer little in the way of treating resistant fungal diseases.

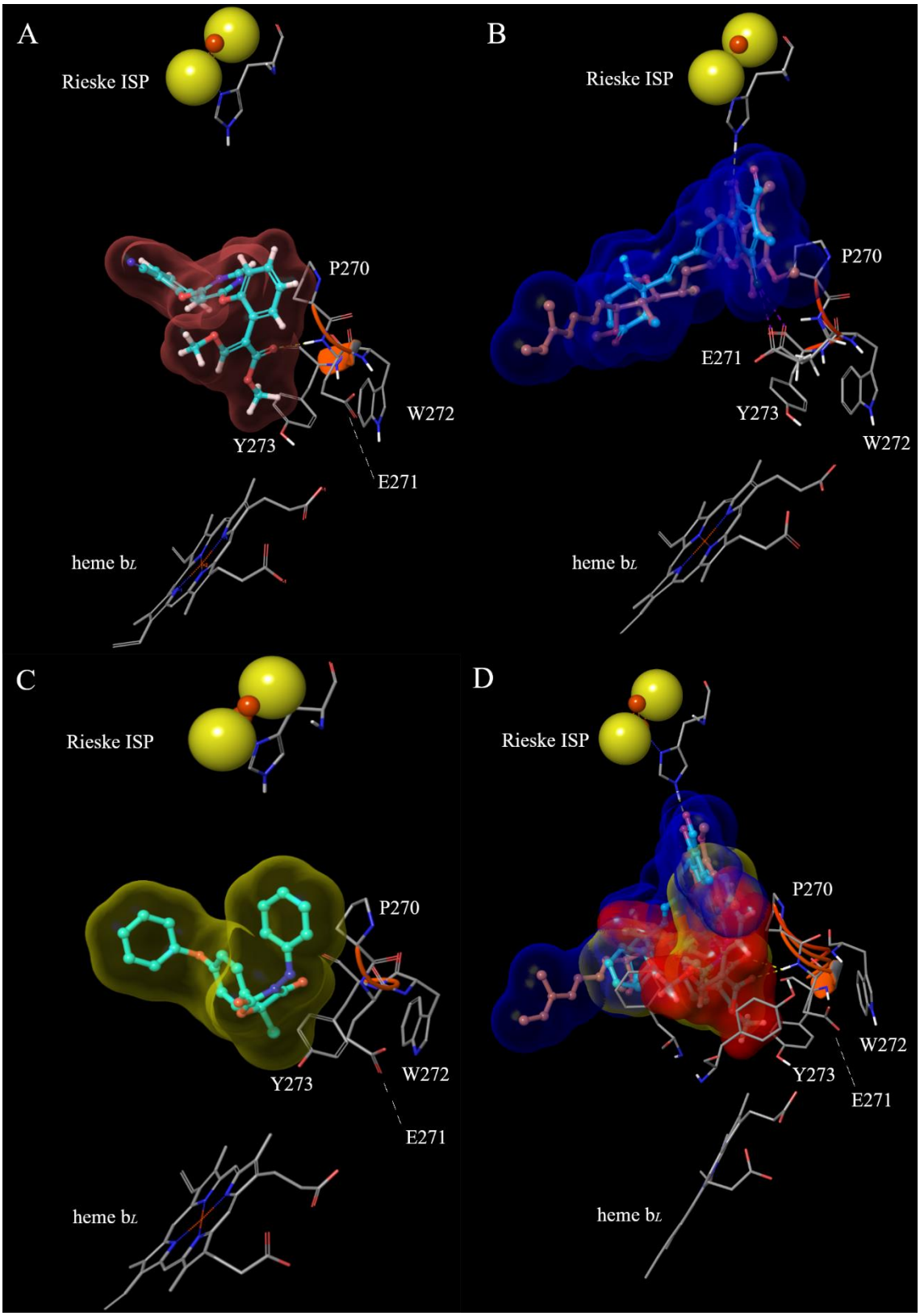

Figure 9 – The different binding modes of fungicide classes that inhibit the Q_o site of the cytochrome bc_1 complex (PDB IDs:3H1L,3L71, 1PPJ and 3L74). The position of each fungicide within the Q_o site is displayed in relation to the Rieske Iron Sulfur Protein (ISP) and heme b_L. The binding of Azoxystrobin is described to be within a 'distal' position (A), stigmatellin and ascochlorin bind in a 'proximal' position (B) and famoxadone binds between these two positions (C). The combination of the binding modes (D) shows overlap for each fungicide binding mode. The residues that make up the fully conserved PEWY sequence are displayed.

Binding of the QiIs occurs at the Qi site in close proximity to the b_H heme and preventing the reduction of quinone or semiquinone at this binding site. Only three commercial fungicides make up this new group of Complex III inhibitors, namely cyazofamid, amisulbrom and the recently registered, fenpicoxamid. Since a common toxophore between these fungicides does not exist, all of the QiIs bind with unique binding positions within the Q_i bind site. Cyazofamid and amisulbrom have very little information regarding exact binding positions within the Q_i site. Nevertheless; conclusions have been made by Li *et al*[99], with only two hydrogen binding possibilities possible between D229 and the nitrile or imidazole ring (sulfoxide in amisulbrom). Fenpicoxamid, in a similar manner to that of cyazofamid and amisulbrom has only had its binding mode elucidated by docking studies. Young *et al*[35] propose a model by which UK-2A (the major metabolite of fenpicoxamid) binds to D229 *via* pyridyl atom adjacent to the dilactone ring *via* a salt bridge. The binding mode of Antimycin A (Classical Q_i Inhibitor) shows a similarity with that of UK-2A with a deeper binding position that that of cyazofamid or amisulbrom (**Figure 10**).

Since the introduction of the QiIs there only remains one amino acid substitution that may pose a threat to inhibitor binding, the G37V mutation. This mutation has been shown to impart resistance to Antimycin A but to date has only been isolated under laboratory conditions for *Saccharomyces cerevisae*[100,101]. It therefore remains that QiI or QoSI fungicide classes show no resistance in field but since they offer specific mechanisms of action, resistance may follow with overuse.

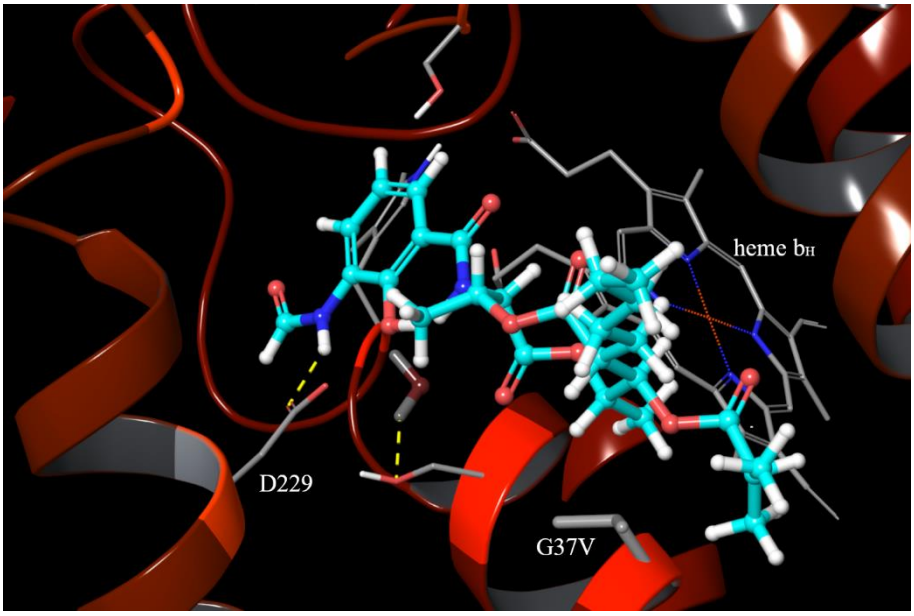

Figure 10 – The binding mode of Antimycin A within the Q_i active site for the cytochrome bc1 complex (PDB ID: 1PPJ) with the H-bonding interaction between D229 and the amide of Antimycin A highlighted. The G37V mutation conferring resistance to Q_i fungicides is also displayed and the proximity of Antimycin A to the catalytically essential heme b_L.

1.3.4 Complex IV

Complex IV or cytochrome *c* oxidase represents the terminal oxidase in the ETC, catalysing the oxidation of cytochrome *c* whilst translocating four protons across the membrane. This process is coupled with the reduction of O_2 to H_2O, completing the cellular respiration process. The enzyme contains eleven subunits in *S. cerevisiae*[102] with four catalytic subunits containing two copper redox active centres, Cu_A and Cu_B, and two hemes, heme *a* and heme a_3.

$$4\ cytochrome\ c\ (Fe^{2+}) + 8\ H^+_{Matrix} + O_2 \rightarrow 4\ cytochrome\ c\ (Fe^{3+}) + 2H_2O + 4\ H^+_{IMS}$$

The solution of the high-resolution X-ray structure of Complex IV has allowed for the elucidation of the detailed mechanism[103] by which the above reaction is catalysed. The initiation of the reaction mechanism occurs through the binding of the cytochrome *c* near to the Cu_A redox active site and transfers electrons to the Cu_A and on to heme *a*. The electrons are then transferred along to the O_2 reduction site formed between heme a_3 and Cu_B at which point O_2 is rapidly reduced with homolytic cleavage. The heme a_3 is oxidised to a Fe^{4+}=O complex with one oxygen atom receiving one electron from Cu_B and a second oxygen atom receiving an electron and proton from an adjacent tyrosyl radical resulting in the generation of hydroxide ion. A further electron received from another cytochrome c molecule is passed through to the Cu_B – heme a_3 centre converting the hydroxide ion into a water molecule. Another electron is passed down through from one more cytochrome c molecule reducing the aforementioned Fe^{4+}=O complex into a hydroxide and thus completing the cycle. Currently there are no reported fungicides that inhibit *via* Complex IV; but typical inhibitors include cyanide and nitric oxide, with a general mode of action by binding to the site of cytochrome *c* oxidation or to the copper active sites, respectively.

1.3.5 ATP Synthase

The ATP Synthase is an integral mitochondrial enzyme complex responsible for utilising the chemiosmotic electrochemical potential, generated by complex I, III and IV, and producing energy for the cell in the form of ATP. The overall reaction can be summarised as below:

$$ADP + P_i + H^+_{IMS} \rightarrow ATP + H^+_{Matrix} + H_2O$$

The structure of the ATP synthase is consistent between all species consisting of two main functional domains: the membrane integrated hydrophobic subunit, F_o, and the hydrophilic region located within the IMS, F_1. The F_1 domain is responsible for the catalytic function of the enzyme where ADP and P_i form ATP and consists of five separate subunits, α, β, γ, δ, ε in a 3:3:1:1:1 ratio, respectively. The three α subunits and three β subunits form a spherical structure with the γ subunit acting as central stalk. The central stalk formed by the γ subunit link the F_1 domain with the membrane spanning F_o domain with the help of the ε subunit. These subunits make up the rotation rotor mechanism for the utilisation of the chemiosmotic potential. The F_o domain is formed from three separate subunits, a, b, c, d and F6, with a cylinder consisting of ten c subunits connected to one a and two b subunits.

The detailed mechanism by which the chemiosmotic potential is used to create ATP has been extensively studied in a number of reviews[104–106]. Briefly, the high concentration of protons formed within the IMS flow across the membrane *via* F_o domain allowing the cylinder of alternating c subunits to rotate. The tight attachment of the cylinder with the γ- stalk of the F_1 domain, facilitates its rotation, altering the conformational structure of the nucleotide binding sites on the β subunits, leading to the release of tightly bound ATP.

There remains very little information on fungicides that target the ATP synthase since its inhibition poses considerable toxicity to non-target organisms. Nevertheless; the mode of action of previously unknown organotin complexes (fentin acetate, hydroxide and chloride) has been reclassified by FRAC[53]. The binding mechanism of the organotin fungicides has yet to be identified and therefore remains enigmatic. Ultimately, the banning of fentin derivatives for agricultural use by the European Union due to their toxicity to mammals[107], precludes them from future fungicide design and treatments.

1.4 Alternative Oxidase (AOX) and its Function between Species

The alternative oxidase (AOX) offers an alternative route to the classical ETC for respiration. The AOX is located on the matrix side of the inner mitochondrial membrane and catalyses the oxidation of quinol to quinone whilst reducing O_2 to H_2O[108]. The bypassing of electron transfer by AOX occurs before the cytochrome bc_1 complex and Complex IV; but importantly, the AOX's activity does not involve the translocation of protons across the gradient. Respiration *via* the AOX is therefore less energy efficient since its does not contribute to the chemiosmotic electrochemical potential[109].

The AOX is found ubiquitously in the plant kingdom[110] and also in a variety of fungi[111–114], protists[115–117] and some animals[118]. Its absence from humans offers a unique fungicide target reducing potential non-target toxic side effects. The physiological role of the AOX differs depending on the species but in general its role as oxygen scavenger and reducing reactive oxygen species can be attributed to all AOXs[109].

The role of the AOX in both thermogenic and non-thermogenic plants is well described, where it responds to a range of stress responses and environmental conditions. Within certain thermogenic plant species such as *Sauromatum guttatum*[119] and *Arum maculatum*[120], a high concentration and activity of AOX was found within the spadices or flowering organs during periods of raised temperature. The rise of temperature is utilised by the plant to volatise primary amines for the attraction of insects or other pollinators[120,121]. The rise in temperature occurs following the switch from the traditional cytochrome pathway towards the AOX. Since the AOX is non-protonmotive and is therefore not coupled to the generation of ATP, the excess energy is released as heat within the thermogenic tissue[121]. In non-thermogenic plants the role of the AOX can be diverse mediating changes in temperature and light intensity[122–124], drought[125–127], oxidative stress[128–131] and to plant hormones[132–134]. Ultimately, the AOX serves a role to regulate energy metabolism following times of biotic and abiotic stress conditions[135]. The turnover of the AOX allows the generation of Krebs cycle intermediates during times of limiting nutrient availability but at the sacrifice of reduced ATP generation. Studies carried out on *Arabidopsis thaliana* also suggest AOX knockout mutants hinder growth and exhibit an increase in reactive oxygen species (ROS) [136,137]. It's clear in thermogenic plants the AOX serves a role in both protection against ROS and optimising respiratory metabolism under stress conditions.

More recently the AOX has been shown to be present in the animal kingdom; with the mollusc *Artica islandica*, lugworm *Arenicola marina*, arthropod millipede *Euryurus leachii* and the chordate sea squirt *Ciona intestinalis* expressing the AOX[118]. The role of the AOX within these animal species is thought to allow the species to survive conditions in which the normal cytochrome pathway is inhibited. For example, in the lugworm *A. marina* the AOX may act as alternative route for respiration when oxygen is limiting and the species utilises hydrogen sulfide as respiratory substrate[138]. The mollusc *Arctica islandica* often lives at the bottom of the sea floor with a mixture of high and low oxygen concentrations. The AOX within this system acts to regulate the generation of high amounts of ROS when excess levels of oxygen are present, yielding an oxyregulating species[139]. In a similar manner to that of the lugworm *A. marina*, the role of the AOX in *C. intestinalis* provides an opportunity to continue respiration following the presence of high concentrations of sulfide. In fact, *C. intestinalis* contains an enzyme required to derive energy from sulfide by oxidising it to thiosulfate *via* the respiratory chain[140]. This route is

unavailable at high sulfide concentrations and therefore the AOX provides the route for electrons to be passed onto O_2 and hence continue respiration[141,142].

In some parasites (*T. brucei*[117], *Cryptosporidium parvum*[143] and *Acanthamoeba castelanii*[116,144]) AOX performs an integral role in respiration as it acts as the terminal oxidase and therefore offering a potential drug target[145,146]. The bloodstream form of TAO utilises the AOX as its only terminal oxidase within the mitochondrial electron transport chain. Bloodstream forms of *T. brucei* rely on the blood glucose as their sole source of energy and therefore cannot utilise the majority of their mitochondrial activity. The glucose is metabolised to pyruvate *via* glycolysis allowing for the generation of some ATP and the operation of the Krebs cycle. The $NADH/NAD^+$ ratio is also mediated through the reoxidation of glycolysis through reducing equivalents by glycerol kinase. Research by the Clayton lab[115] has shown that the AOX is vital in these circumstances and offers double the ATP generation in comparison to a AOX inhibited energy metabolism.

The physiological role of the AOX within fungi follows that of plants with an emphasis on the AOX as a rescue system under stress conditions, but dispensable for normal energy metabolism[114,147,148]. AOX is often induced following the use of typical fungicides which inhibit the cytochrome dependent respiratory complexes[110,115,149,150]. The induction of the AOX may play role in pathogenesis for phytopathogenic fungi whilst nutrients are limiting. For example, the fungus responsible for witches' broom disease in cacao, *Moniliophthora perniciosa*, offers a role for the AOX in the switch between the biotrophic and necrotrophic growth stages within the plant[151]. It also doubles up as a protective mechanism to the negate the plant's host defence systems following the release of high concentrations of nitric oxide[151]. Further *in vitro* studies on *Ustilago maydis*[114], *Fusarium graminearum*[152], *Sclerotinia sclerotiorum*[153] and *V. Inaequalis*[154] showed an increased upregulation of the fungal AOX following the use of the common cytochrome bc_1 complex inhibitor, azoxystrobin. The first *in planta* study for the role of the fungal AOX by Köller *et al*[111] provides evidence for the upregulation of the AOX following treatment with azoxystrobin. The role for the fungal AOX still requires research but existing studies have demonstrated similarities to AOXs found in other species.

1.5 AOX Regulation

The regulation of the AOX through allosteric ligands has long been accounted for within plant species[108,155] and more recently through fungi and amoeba[156,157]. A post-translational mechanism[108] by which the AOX is regulated supports its role as a rescue mechanism and provides a biological switch by which its activity can be regulated.

Regulation of the plant AOX occurs through the α-keto acid, pyruvate, which binds to a terminal cysteine residue to form a thiohemiacetal functional group[155]. The site of the cysteine-pyruvate interaction is known as the Cys_1 and is present on the N-terminus of the plant AOX. Furthermore, the presence of another cysteine, Cys_2, was thought to confirm sensitivity to pyruvate due to its high conservation throughout the plant kingdom. Plant AOXs with and without these cysteine residues in their structure demonstrated differential sensitivity to pyruvate[158], disproving the original hypothesis. Indeed, a further motif confirming the activation of plants by pyruvate required the presence of an ENV/QDC amino acid motif. Plant species containing the ENV motif are said to be sensitive to pyruvate whereas species with the QDC motif are insensitive[159].

Stimulation by allosteric compounds occurs through a different mechanism in fungi[160,161] and the protist *A. castelanii*[157,162]. Since fungi contain neither of the regulatory cysteines, stimulation by pyruvate does not occur[163]. The fungal AOXs, *Pichia stipitis* and *Neurospora crassa*[164] instead show a regulation through the addition of ADP, AMP and GMP nucleotides with GMP being essential for AOX activity. The binding site for nucleotide stimulation is suggested to be approximately 40 amino acids long creating a loop for activation[161]. This activation by GMP is also found in *A. castelanii* the addition of which resulting in over 2.5 times the baseline activity when stimulated with GMP (1.5 mM). The exact binding site for purine nucleotides is yet to be determined as by which the activity is increased within fungal or amoeba species.

1.6 AOX Structure and its Catalytic Mechanism

The recent elucidation of the AOX crystal structure from *T. brucei* (TAO) with a resolution of 2.3 Å,[165] confirms previous models[130,166] suggesting the AOX is a monotopic diiron carboxylate protein. The TAO crystal structure indicates that a dimeric structure is found with each monomer consisting of six long and four short α helices. The diiron active site is contained within a four-helix bundle comprising of helices α2, α3, α5 and α6. On one side of the protein at the membrane binding interface, a high conservation of hydrophobic residues extends from α1 and α4 helices allowing for monotopic interaction with the phospholipid membrane. The crystal structure[165] displays a bound inhibitor, colletochlorin B, within the quinol binding site between α1 and α4 helices (**Figure 11**).

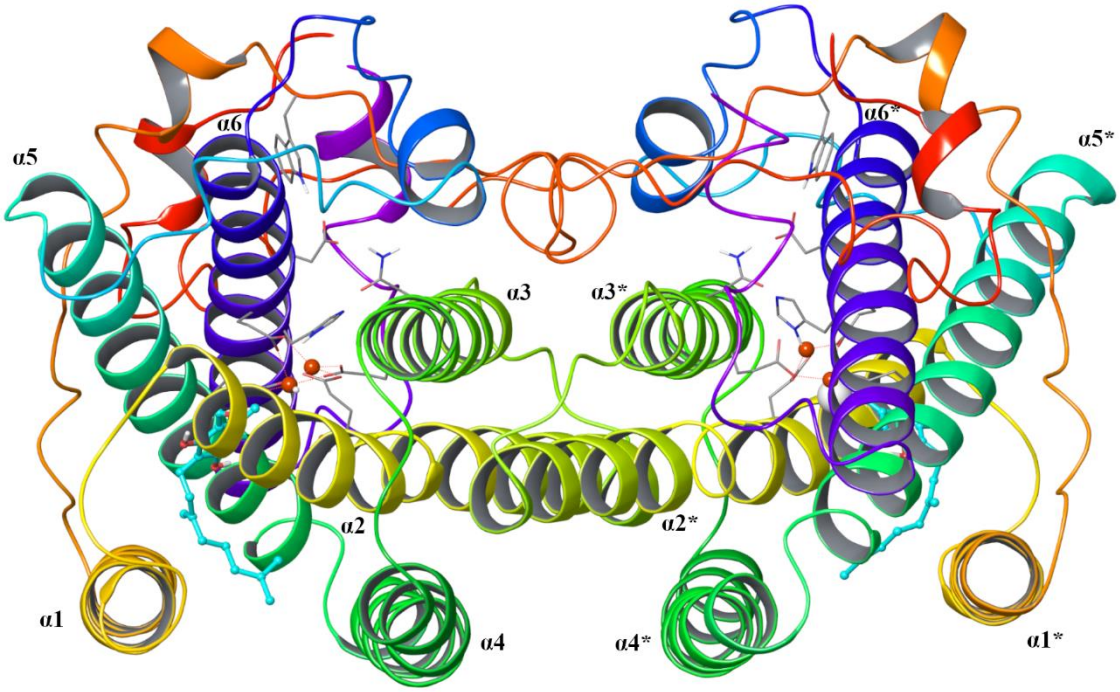

Figure 11 - Crystal Structure for TAO (PDB code: 3W54) with colletochlorin B bound within the hydrophobic cavity. Helices labelled (α1-6) with the corresponding monomer labelled (α1*-6*).

The diiron core active site is ligated by four glutamate residues (E123, E162, E213 and E266) and in close proximity to two histidine residues (H165 and H269), all fully conserved throughout all AOX species. A single hydroxo bridge between the two iron atoms completes the structure of the active site and the residues that make up the primary ligation sphere (**Figure 12**). Unusually the AOX displays histidine residues in a position too far away to coordinate with the diiron centre in contrast to other diiron proteins such as MMO[167], RNR[168] and rubrerythrin[169]. The presence of an amino acid chain (W65, N161, D265 and W247) similar to the proton coupled electron transport network (PCET) found in RNR[170] is proposed to fulfil the same role in the AOX. The amino acid chain runs from the diiron core towards the matrix side of the protein providing a route for proton and electron transfer from molecular O_2.

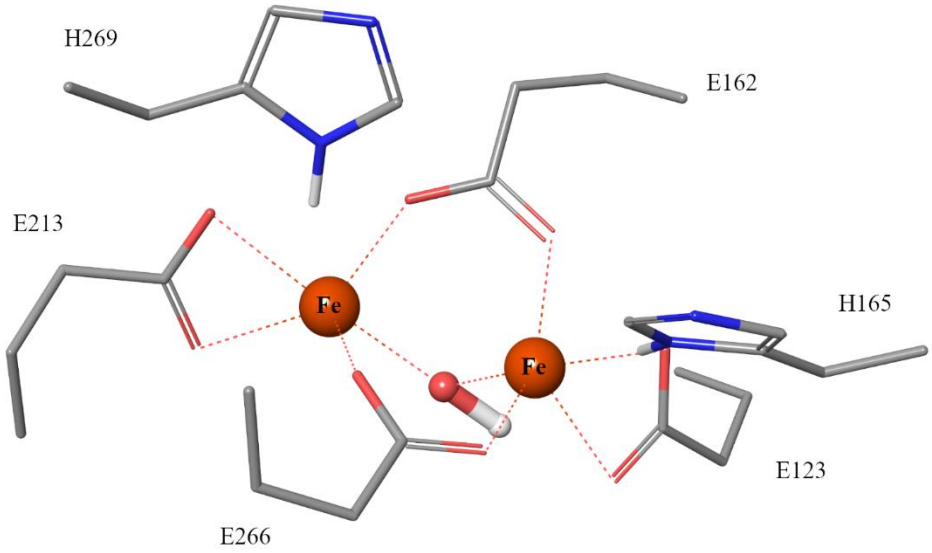

Figure 12 - Primary ligation sphere displaying the fully conserved residues bridged by a hydroxo group from the crystal structure of TAO (3W54)

Along with the crystal structure determined with colletochlorin B (PDB code:3W54) two more crystal structures with an ascofuranone derivative (PDB code: 3VVA) and no inhibitor (PDB code: 3VV9) were crystallised at 2.59 Å and 2.85 Å, respectively[165]. The generation of a range of crystal structures provides a detailed view of the structural conformation for the hydrophobic cavity and the binding site for quinol. The proposed quinol binding site is lined with a number of highly conserved residues with the residues R96, R118 and T219 thought to be involved in quinol binding[171]. A bottle neck formed by two leucine residues (L122 and L212) within the quinol binding site may help to direct the substrate into the correct position[172]. However, the diversity between amino acid residues within the hydrophobic cavity of AOX species may question the importance of those particular residues. The structural diversity within the hydrophobic cavity may determine differences in both inhibitor sensitivity and enzyme kinetics[171].

The mechanism by which quinol oxidation occurs has been proposed by Young *et al*[173,174], using similarities to that of other diiron proteins RNR and MMO (**Figure 13**). The proposed mechanism proceeds with binding of oxygen to form a superoxo species with the diiron core (Fe-O-O*) following the transfer of one electron from one iron atom to O_2 resulting in a divalent Fe^{2+}/Fe^{3+} system. This superoxo species is then reduced to the hydroperoxo species (FE-O-OH) following hydrogen extraction of an adjacent tyrosine (Y220) to form a tyrosine radical. The iron core then undergoes a rearrangement to form the divalent peroxo species with a loss of water and through to a diamond core which has been predicted in MMO and RNR di-iron proteins. The diamond

core is oxidised with a proton and electron donated from the W247 amino acid which is the final residue in the PCET network. The final step sees the step wise transfer of two electrons from quinol returning the di-iron core to its diferrous state. The remaining electrons and protons from the oxidation of quinol, quench the W247 and Y220 radicals, completing the reaction mechanism with loss of water.

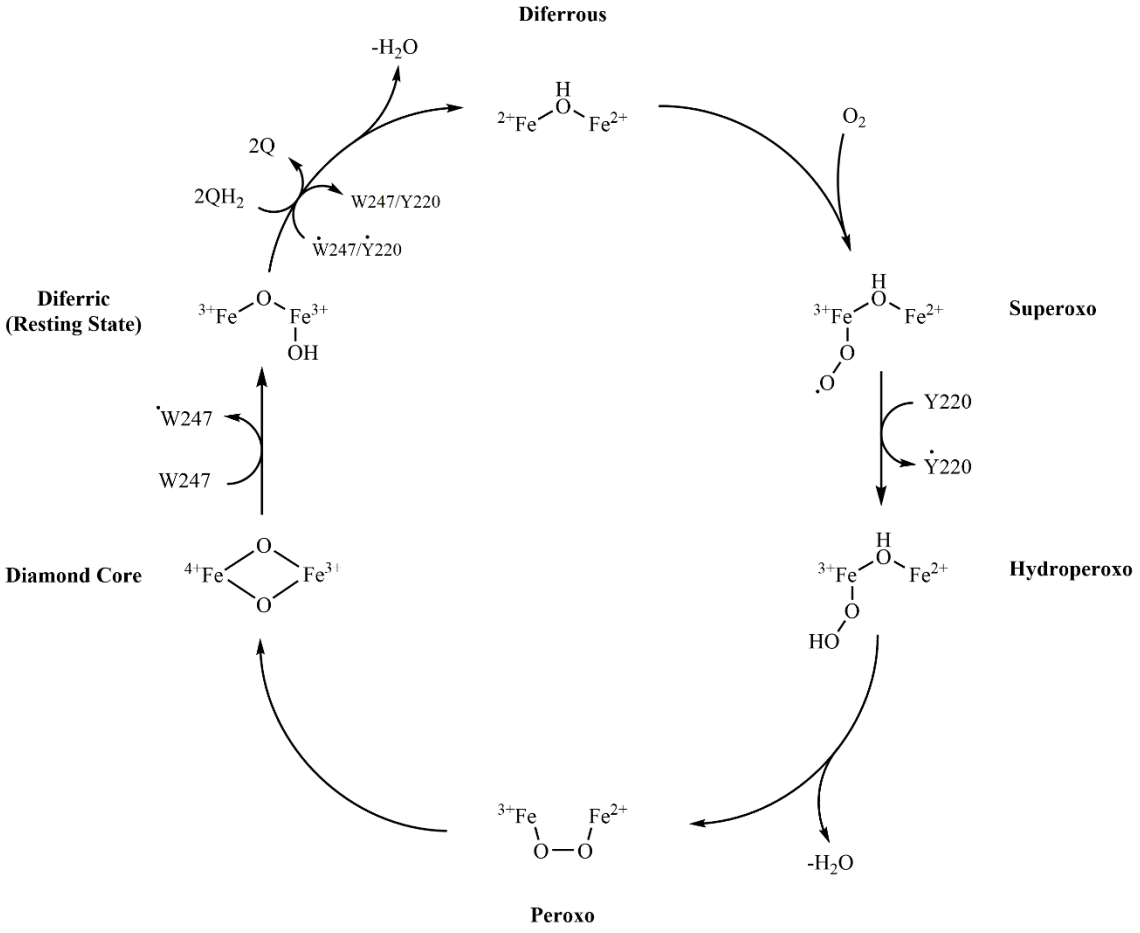

Figure 13 - Catalytic AOX Mechanism proposed by Young et al[172,173]

1.7 Resistance Mechanisms in Fungi and the role of the AOX

There are an increasing amount of highly resistant fungal species affecting our most economically important crops and considerably reducing the efficacy of fungicide classes[175]. Studies[33,176] with a number of common fungicides have implicated a number of mechanisms by which resistance occurs in phytopathogenic fungicides. Understanding the mechanisms by which resistance occurs helps to focus future fungicide design and disease management protocols.

1.7.1 Alterations in the Fungicide Target Site

Mutations in the target site is the primary mechanism which has been implicated in the resistance of fungal species to Q_oIs, SDHIs and azoles. Q_oI fungicides lose sensitivity in particular to mutations within the cytochrome *b* subunit which prevent fungicide binding to their target site. As mentioned previously, the most notable mutations within this category include the G143A, F129L and G137R which are present in a number of fungal strains[38,39,41,86–90,93,177]. The increased usage of the SDHI fungicides has led to the development of mutation within the Q_P site of the SdhB subunit. The major mutation conferring resistance is H227Y which has now been found in a number of field isolates but has yet to be fully established. The triazole family of fungicides confers resistance[33] within the CYP51 enzyme with the greatest number of mutations occurring within *S. tritici* fungal strains[40]. Contrary to resistant strains within other target sites, the CYP51 enzyme has previously selected for double mutant strains, Y137F-S542T, however, new triazole compounds have eliminated its prevalence[40].

1.7.2 Overexpression of Target Protein/Enzyme

The overexpression of the fungicide target site has only been observed within the target for DMI fungicides with documented resistance from this mechanism for *S. tritici*[40], *V. inaequalis*[178] and *Monilinia fructicola*[179] fungal species. Overexpression of the target protein results in a decreased sensitivity of the azole fungicides and therefore a higher threshold for lethal cellular concentrations. Changes in the promoter region of the CYP51 gene through an insertion of tandem repeats or transposable elements, facilitates the overexpression of the target enzyme.

1.7.3 Efflux Transporters

The removal of lethal concentrations of fungicide within plant pathogens through the overexpression of efflux transporters has been reported for both Q_oIs[180,181] and DMIs[182–184]. For both fungicide classes the same family of efflux transporters are responsible for removing inhibitors out of the cell, namely the ABC transporters. In *S. tritici*[181], the AtrB gene encodes for the ATB transporter involved in Q_oI sensitivity. Often resistant fungal strains also contain cytochrome *b* mutations complicating the specific contribution from each mechanism. Deising *et al*[180] confirmed efflux transporters as a resistance mechanism through the combination of efflux inhibitors and Q_oI fungicides, which restored resistant fungal strains sensitivity to fungicides. The

resistance to DMIs was seen in *B. cinerea*[182] with the ABC transporter, encoded by BcatrD, overexpressed in azole insensitive fungal species. Mutations removing the BcatrD gene, showed an increased sensitivity to azole fungicides.

1.7.4 Alternative Respiration via the AOX

Alternative respiration *via* the AOX has been implicated as a possible resistance mechanism with its induction following the use of single site-specific fungicides. The inhibition of the classical cytochrome pathway from Q_oIs results in respiration *via* the AOX albeit with lower energy efficiency[185]. Since mitochondrial DNA mutates at a faster rate than nuclear DNA[186], the opportunity for the selection of mutations within the cytochrome *b* gene is high. Furthermore, the ability for fungal cells to survive with only Complex I and the AOX functioning demonstrates a viable mechanism for resistance[149].

The upregulation of the alternative oxidase following the application of Q_oI fungicides has been most commonly seen within *S. tritici* fungal strains[185,187–189]. Field isolates obtained by Miguez *et al*[185] demonstrated the ability of resistant fungal strains to switch metabolic activity to an AOX pathway following Q_oI treatment. This protection *via* the AOX provides continued growth within the host; and therefore, opportunity for mutation selection. This study is supported by O_2 assays for *S. tritici* mitochondria whereby continued oxygen consumption is apparent following the inhibition of the cytochrome pathway with Antimycin A and Azoxystrobin [187,188].

Further *in vitro* studies on fungal pathogens such as *S. sclerotiorum*, *Magnaporthe grisea*, *Microdochium nivale*, *U. maydis and M. perniciosa* provide further evidence of the role of the AOX following Q_oI treatment. Consistently the use of Azoxystrobin induced AOX gene expression during mycelial growth of the fungus. This latent respiration is inhibited by the AOX specific inhibitor SHAM, confirming the alternative respiratory pathway. AOX gene deletion studies for *Ustilago maydis*[114] showed full inhibition of fungal cells to cytochrome inhibitors for AOX deficient mutants. Whereas continued growth was seen in the presence of these respiratory inhibitors with the AOX gene included. Thomazella *et al*[151] provides further evidence of alternative respiration *via* the AOX as a resistance mechanism. The use of Azoxystrobin prevented the switch from biotrophic to necrotrophic growth but a combination of an AOX specific inhibitor and Azoxystrobin halted growth in all instances and growth phases.

Rebuttals to the influence of AOX in pathogenicity and resistance have highlighted two problems with alternative respiration as mechanism[189,190]. Firstly, the energy efficiency of the AOX respiratory pathway is 40% lower than that of the cytochrome pathway. Fungal pathogens require

large amounts of energy during spore germination and host penetration to successfully establish growth within a plant system. Secondly, the plant's natural antioxidant defence systems (flavones) interfere with the induction of the AOX gene and therefore AOX influence would not be seen *in planta*.

Current research suggests that energy requirements are in fact much lower during latent periods of fungal pathogen growth[114,189]. Furthermore; the influence of the AOX as a rescue mechanism during periods of oxidative stress and fungal survival is a beneficial trade off to lower energy efficiency. Research suggesting that fungal survival *via* AOX respiration is valid has been shown in a number of studies[114,149,185,187–189]. *In planta* studies[111,153,185] as well as a mechanism by which the fungal AOX is activated by purine nucleotides[160,161], disproves the flavone hypothesis. Nevertheless; the establishment of the AOX as a primary resistance mechanism requires further evaluation to confirm previous studies.

1.8 AOX Inhibitors

The first inhibitors of the AOX were discovered by Umbach and Siedow[191] and their use is still seen in research today as they are relatively inexpensive (**Figure 14**). Salicylic hydroxamic acid (SHAM) is still considered a specific inhibitor of AOX within the ETC despite inhibition of cellular tyrosinase, peroxidases[192,193] and urease activity[194]. Historical studies on the inhibitory effect of SHAM on *Arabidopsis thaliana* and *Arum maculatum* suggest a high inhibitory effect with a magnitude of inhibition in the μM range. A more recent study shows the inhibitory effect of SHAM varies depending the species of AOX[171] but still requires a high dose response. The gallates (**Figure 14**) offered improved inhibitory effect over SHAM for the *Trypanosoma brucei brucei* AOX (TAO) with the addition of the hydrophobic tail moiety[195,196].

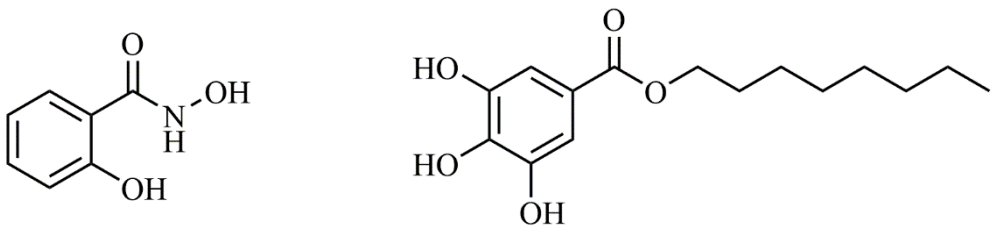

SHAM Octyl Gallate

Figure 14 - Classical AOX Inhibitors

The establishment of TAO as potential therapeutic drug target for the treatment of African trypanosomiasis[146], led to the discovery of number of natural products conferring sensitivity to the AOX. Ascofuranone, a natural metabolite from *Acremonium sclerotigenum*[197], has exhibited a selectivity to the AOX with 0.13 nM IC_{50} values for TAO[198] and a much larger dose required for the cytochrome bc_1 complex at 16 μM[199]. Ascofuranone has shown trypanosidal activity for both *in vitro*[198,200,201] and *in vivo*[202–204] studies offering a suitable candidate for lead modification. The addition of glycerol increased the activity of these compounds by inhibiting the glycerol production pathway. Two structurally similar natural derivatives, colletochlorin B and ascochlorin (**Figure 15**), also exhibit AOX activity but without selectivity to the alternative or cytochrome dependent pathway[199].

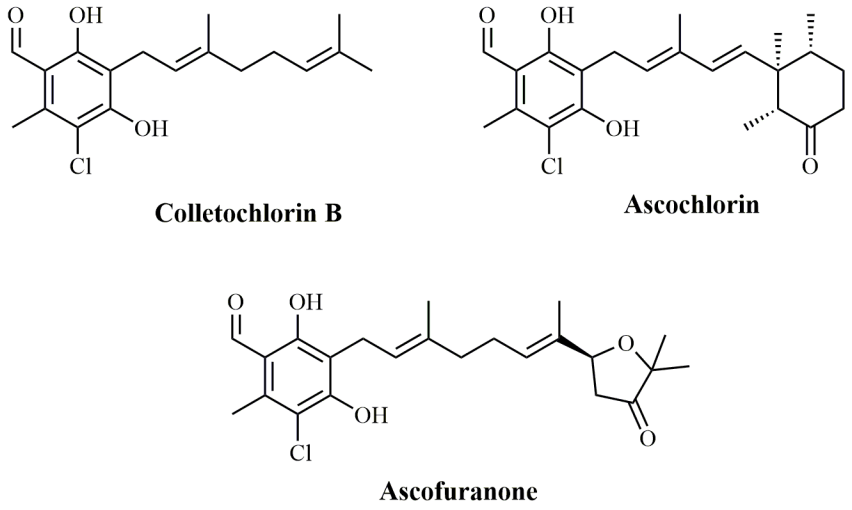

Figure 15 - Natural products exhibiting AOX efficacy extracted from the fungus Acremonium sclerotigenum.

Identification of a pharmacophore for ascofuranone and its inhibition of TAO was carried out by Saimoto *et al*[198]. A series of inhibitors were synthesised demonstrating the importance of functional groups within the head group for potent trypanocidal inhibition. Recent work[200,201] by the Ward group has further expanded on drug design by Shiba *et al*[198] to elucidate more chemical structure requirement for TAO inhibition. The work by both groups contradicts each other with uncertainty surrounding important features of the aromatic head group of ascofuranone like derivatives. Unfortunately, sensitivity to AOX inhibitors is not universal across all species[171] and therefore further work is required to elucidate structural features required for different species of AOX.

1.9 Concluding Remarks

The regulation or banning of multi-target site fungicides, due to their inherent non-target organism toxicity[3,9,16,17], has considerably reduced the number of effective fungicides available to treat phytopathogenic fungi. Typically, the design of new classes of fungicides has focussed on targeting the specific multi-enzyme complexes within the fungal ETC, effectively reducing ATP synthesis and respiration. This selective design has produced some of the most economically important classes of fungicides (Q_oI and SDHIs) whilst offering low non-target toxicity. However, a simple mutation within the fungicide binding site of these respiratory complexes can reduce the sensitivity or render the fungicide completely insensitive; thereby increasing the selection pressure for this mutation[38,39,41,86–90,93,177]. To my knowledge there are no fungicides described in the literature, or in use commercially, that target multiple sites of inhibition within the mitochondrial respiratory chain to reduce the opportunity for development of resistant fungal species. The treatment of fungicide resistant phytopathogenic fungi through the use of multiple target site fungicides has been encouraged by FRAC[205] and provides farmers with an effective treatment for crops with low risk of resistance.

Septoria tritici devastates wheat crops within Europe and the UK[206,207] and leads to the extensive use of fungicide treatments[208] leading to the development of resistant strains to important fungicide classes[183,206,209–211]. Alternative respiration *via* the AOX has been implicated[185,187–189] as a causal mechanism for resistance development for *S. tritici* as highlighted in **Section 1.7.4**. Furthermore; studies have shown that the upregulation of the AOX occurs following the treatment with Q_oI fungicides[185,187–189] with AOX inhibition providing potentiating effects when used in combination with azoxystrobin[151–154].

Strategies and research efforts towards inhibition of the AOX has focussed on the causative agent for African sleeping sickness, *Trypanosoma brucei brucei* (TAO). The design of these inhibitors has been led by the structure of TAO; and therefore, any alterations to improve inhibitory activity may not translate to the fungal AOX. The published literature on fungal AOXs in general is limited and there remains only a few studies[185,187,188] on the AOX found in *Septoria tritici* (StAOX); however there are no published protocols on the isolation, purification and enzyme kinetics of StAOX. The design of inhibitors targeting either the AOX selectively; or targeting both AOX and cytochrome bc_1 complex, has furthermore, yet to be explored. This presents an area for research within the disciplines of both biochemistry and organic chemistry to investigate the StAOX enzyme and novel inhibitors in order to assess the viability of a new class of phytopathogenic fungicides.

1.10 Research Objectives

Overall aims of the project are:

1. To provide a full characterisation of StAOX assessing its viability as a potential resistance mechanism and fungicide target.

2. Full characterisation also offers the opportunity to assess a previously unstudied AOX protein and elucidate any interspecies similarities/differences with respect to its structure, enzymatic activity and regulation.

3. To design and synthesise compounds that demonstrate either: AOX inhibitory activity; cytochrome bc_1 complex inhibition; or a combination of both.

4. The design of chemically and structurally distinct inhibitors as a basis for probing the shape and size of the quinol binding site for the AOX and the two quinol/quinone binding sites in the cytochrome bc_1 complex.

5. To investigate the binding and inhibition profiles of the natural products colletochlorin B, ascochlorin and ascofuranone from *A. sclerotigenum*; to better understand why ascofuranone shows AOX selectivity.

6. To investigate the sensitivity of established and newly synthesised AOX inhibitors on StAOX and the cytochrome bc_1 complex.

7. Establish new assay techniques to differentiate between structurally similar compounds to direct synthetic routes for fungicide discovery.

8. Identify unique amino acid residues or structural features that will guide selectivity between the cytochrome bc_1 complex and StAOX.

Chapter 2: Materials and Methods

2.1 pET Vector System

A number of plasmids were created using Novagen's pET-15b vector system to facilitate transformation and overexpression of alternative oxidases in *E. coli*, as host cells. The pET-15b vector encodes for a Twin-Strep tag, ampicillin resistance and induction by the addition of IPTG. The heme deficient *E. coli* strain FN102 was used as a host cell for transformation.

2.2 *E. coli* Grow-Up

2.2.1 Competency

The *E. coli* (FN102) cells were grown on L-agar plates containing ALA (50 μg/mL) and kanamycin (100 μg/mL). A single colony was selected from this plate and used to inoculate Luria Broth containing ALA (50 μg/mL) and kanamycin (100 μg/mL) and incubated on a benchtop orbital shaker at 37 °C, 180 rpm for 4 hours. Following incubation, the *E. coli* culture was centrifuged at 1000 x *g* at 4 °C for 5 min. The supernatant was discarded and the pelleted cells were resuspended in $CaCl_2$ (5 mL, 0.1M) and left on ice for 20 min. The centrifugation was then repeated with the resulting pellet resuspended to a volume of 500 μl with glycerol (15%) and $CaCl_2$ (0.075M). The competent cells were then aliquoted into 50 μl samples for transformation and stored at -80 °C.

2.2.2 Transformation

Two 50 μl aliquots of competent FN102 cells were placed on ice and 3 μl (100 ng/μl) of the pET vector plasmid was added to one sample and 3 μl of water was added to the other, to act as a control. The samples were placed on ice for 15 min followed by a heat shock at 42 °C for 2 min. The cells were placed on ice for a further two minutes and then made up to 1 mL with luria broth. The cultures were grown for 1 hr on an orbital shaker at 180 rpm and 37 °C. After growing for 1 hr, the cells were concentrated by centrifugation at 5000 x *g* for 1 min and plated onto sterile agar plates incubated with ampicillin (100 $\mu g.mL^{-1}$), kanamycin (100 $\mu g.mL^{-1}$) and ALA (50 $\mu g.mL^{-}$

[1]). The plates were left to grow overnight in a 37 °C incubator and the following day stored at 4 °C.

2.2.3 E. coli Growth

Table 1

K-Broth Composition /L

Substance	**Weight/ g**
Tryptone	10.0
Yeast Extract	5.0
Casamino Acids	5.0
K_2HPO_4	10.4
KH_2PO_4	3.0
Sodium Citrate	0.74
Ammonium Sulfate	2.5

Note. K-broth prepared in advance of experiments with milli-Q water and was sterilised *via* autoclave.

Table 2

1000x Metal Mix Composition / 10 mL

Substance	**Weight/ g**
$MgSO_4.7H_2O$	0.50
$FeSO_4.7H_2O$	0.25
$FeCl_3$	0.25

Note. Metal mix was prepared in milli-Q water and filter sterilised using Cole-Parmer 0.2 μm pore air filters.

From a fresh transformation plate, a single colony was used to inoculate sterile L-broth (10 mL) supplemented with Ampicillin (100 μg.mL^{-1}), Kanamycin (100 μg.mL^{-1}) and ALA (50 μg.mL^{-1}) and left to grow overnight at 180 rpm and 37 °C in an orbital shaker. Following overnight growth, two 1 mL aliquots were taken from the L-broth culture and used to inoculate two starter culture flasks containing K-Broth (**Table 1**, 50 mL) supplemented with Ampicillin (100 μg.mL^{-1}), Kanamycin (100 μg.mL^{-1}), ALA (50 μg.mL^{-1}), Metal Mix (50 μl, **Table 2**) and Glucose (0.2% w/v). The starter cultures were left to grow at 225 rpm and 37 °C until the OD_{600} was approximately 0.6. The cells were then isolated by centrifugation for 10 minutes at 3000 x *g*, after

which the media was exchanged with K-Broth (50 mL) supplemented with Ampicillin (100 μg.mL^{-1}), Kanamycin (100 μg.mL^{-1}), ALA (50 μg.mL^{-1}), Metal Mix (50 μl) and Glucose (0.2% w/v) in order to remove the ALA from the sample. The media exchange was repeated after further centrifugation with a final resuspension of both samples into K-broth (5 mL) yielding a concentrated inoculum. This concentrated inoculum was then used to inoculate four Erlenmeyer flasks containing K-Broth (1L) supplemented with Carbenicilin (100 μg.mL^{-1}), Kanamycin (100 μg.mL^{-1}), Metal Mix (50 μl) and Glucose (0.2% w/v) to 0.01 OD_{600}. The cultures were incubated at 30 °C and 180 rpm until the OD_{600} measured 0.6, at which point induction was carried out with IPTG (25 μM) added to each flask. The cultures were left to incubate overnight and were harvested the following morning.

2.2.4 Harvest

After approximately 13 hours of growth, cells were harvested by centrifugation at 7000 x *g* for 15 minutes and the supernatant was discarded. The pellets were combined (wet weight approx. 20 g) and resuspended in buffer at 4°C (MOPS 65 mM, pH 7.5 at 23 °C, protease inhibitor tablet (Roche) and $MgSO_4$ (1 mM)). The cells were disrupted using a constant system by passing it through two times at 30 kPa and unbroken cells were removed by centrifugation (15 minutes at 7000 x *g*). The supernatant was isolated and ultra-centrifugation (210,000 x *g* for 1 hr) was carried out to collect membrane fragments containing overexpressed alternative oxidase. The membrane pellets were resuspended in buffer (MOPS 65 mM, pH 7.5 at 23°C, 20 mL) and flash frozen in liquid nitrogen to be stored at -80 °C.

2.3 Purification

2.3.1 Solubilisation and Elution

A membrane sample (20 mL) was thawed on ice from a -80 °C stock and solubilised with solubilisation buffer (20 mL, MOPS (32 mM), glycerol (20%), $MgSO_4$ (200 mM), Octyl-glucoside (1.4%), pH 7.5 at 23 °C for 1 hour. The sample was then centrifuged at 210,000 x *g* for 30 minutes to remove all un-solubilised protein. The Streptactin column was equilibrated with Wash Buffer (2x Column volumes) at 2 mL.min^{-1}. The AKTA Prime was prepared by washing lines A and B with water, elution buffer and then washing buffer. The supernatant collected from centrifugation was filtered through a 0.2 μm filter before loading on to a Streptactin column at 2

$mL.min^{-1}$. The column was then transferred to the AKTA prime plus FPLC and washed with Wash buffer at 0.5 $mL.min^{-1}$ until the absorbance at 280 nm reached baseline. The column was then washed with elution buffer at 0.5 $mL.min^{-1}$ and the fractions containing protein were collected and combined. The Streptactin column was regenerated with regeneration buffer (**Table 4**) until the beads turn from colourless to red. The beads were then washed with AP buffer (pH 10.5 at 23 °C) until the colour turned backed to an off white before further washing with AP buffer (pH 7.5 at 23 °C) and stored at 4°C.

Table 3

All Purpose (AP) Buffer Composition

AP Buffer (1 L)	**Weight/ g**
$MgSO_4$ (50 mM)	12.33
NaCl (160 mM)	9.35
MOPS (26 mM)	2.43
Glycerol (20% v/v)	252

Note. Buffer adjusted with using a dilute KOH solution up to pH 7.5 and stored at -4 °C.

Wash Buffer:

AP buffer + 0.042% DDM (Detergent is AOX dependent)

Elution Buffer:

AP Buffer + 0.042% DDM (Detergent is AOX dependent) + Desthiobiotin (2.5 mM)

Table 4

Regeneration Buffer Composition/ 500 mL

Substance	Weight/ g
Tris-HCl (20 mM)	1.21
NaCl (150 mM)	4.68
HABA (1 mM)	0.12

Note. Buffer was prepared with Milli-Q water and filtered using Merck Steritop vacuum filtration units (0.2 μm pore size). The pH of the regeneration buffer was not adjusted.

2.3.2 Protein Precipitation

For purified protein samples that consisted of a low protein concentration, samples required precipitation to achieve the required 15 μg necessary for running an SDS-page analysis. A volume of acetone pertaining to 4 times the volume required to yield 150 μg of purified protein was added to the sample. The sample was then stored at -20 °C for 24 h and then centrifuged for 10 min at 10,000 x *g*. The supernatant was discarded and the purified protein pellet was left at room temperature for 30 min to ensure any remaining acetone had evaporated. Resuspension of the sample was achieved with the addition of 1x loading dye (**Table 5)** to the correct protein concentration (1.5 μg/mL).

2.4 Protein Estimation

An estimation of protein concentration in both membrane and purified AOX samples was analysed using a Bio-Rad Protein Assay kit. As described in the Bio-Rad Protein Assay, a series of BSA concentration standards (2, 4, 6, 8 and 10 $\mu g.mL^{-1}$) were prepared in triplicate, in order to generate a standard curve, by which unknown protein concentration samples could be measured. Unknown protein samples were diluted appropriately (10:1 dilution for *E. coli* membrane and rat liver mitochondria samples and 1:1 dilution for purified protein samples) and additions of 1-4 μl were added in triplicate to 200 μL (96-well plates) or 1 mL (cuvette assay) of dye mix (deionised water 4:1 Dye Reagent Concentrate). The samples were all mixed vigorously and measured at 595 nm by spectrophotometry. The standard curve for the series of BSA standards was plotted and using the cubic function for the curve, the protein estimation for the unknown samples were determined.

2.5 Rat Liver Mitochondria Preparation

Rat liver mitochondria samples were harvested from wistar rats following euthanasia *via* cervical dislocation and CO_2 asphyxiation. The liver was dissected and transferred into buffer (30 mM MOPS, 1 mM EGTA, 250 mM sucrose, 0.1% (w/v) BSA, 3.5 mM *L*-cysteine at pH 7.4). The liver was then homogenised with 10 passes through a large gap homogeniser followed by 10 passes through a small gap homogeniser. The resultant liquid was filtered through muslin cloth and the filtrate was centrifuged at 1000 x *g* for 10 min. The supernatant was isolated and centrifuged again at 10,000 x *g* for 10 minutes, with the resultant pellet resuspended in wash

buffer (30 mM MOPS, 1 mM EGTA, 250 mM sucrose and 0.1% (w/v) BSA at pH 7.4). A final centrifugation was performed at 10,000 x *g* for 10 minutes and the final pellet was resuspended in wash buffer. All mitochondrial rat liver preparations were kindly carried out by Alicia Rosell-Hidalgo.

2.6 Proteoliposome Preparation

Incorporation of the AOX into proteoliposomes was kindly carried out by Dr. Alice Copsey according to the methodology outlined by Jones *et al*[212].

2.7 Gels

Table 5

General Use Reagents for SDS page and Western Blot analysis

Name	Contents
Loading Dye x2	Tris-HCl (0.1 M, pH 6.8) EDTA (10 mM) SDS (2% w/v) Glycerol (5% w/v) Bromophenol-blue (0.05% w/v)
Running Buffer	Tris-HCl (0.25 M pH 8.3) SDS (1% w/v) Glycine (1.9 M)
TBST	NaCl (1.4 M) Tris-HCl (200 mM pH 7.4) Tween 20 (1% w/v)
Transfer Buffer	Glycine (2 M) Tris-HCl (250 mM)
Blot Rinse	Tris-HCl pH 7.2 EDTA (5 mM)
Block	Milk Powder (5%) BSA (3%)

2.7.1 Sample Preparation

To prepare samples for gel electrophoresis, *E. coli* membrane samples were diluted to afford 150 µg in 50 µl of water. Purified AOX samples were diluted in a similar manner but required concentration *via* acetone precipitation. The 50 µl sample solutions were then further diluted up to 100µl with loading dye (**Table 5**) and denatured on a hot block at 90°C for 3 minutes.

2.7.2 Gel Preparation

Gels for electrophoresis were cast using Bio-Rad Mini-PROTEAN® Tetra Handcast systems, providing 10 cm x 8 cm x 1 mm gels. For each gel, one glass spacer plate and one short spacer plate were assembled in the casting frames and attached to the casting stand with wa*tert*ight gaskets. The resolving gel was prepared as outlined in **Table 6** with the addition of TEMED (10 µl) as the final component. To ensure correct filling of the resolving gel, the level at which the bottom of the 10 well or 15 well combs reached was marked. The combs were removed and the resolving gel was filled to the mark, with the remaining volume filled by propanol. The gels were left to set in an incubator at 37 °C for 1hr, after which the propanol was drained and the top of the gel was washed with water. The stacking gel was prepared as outlined in **Table 7**, once again with the final addition of TEMED (10 µl). The stacking gel was layered on top of the resolving gel with the inclusion of the desired 10 well or 15 well combs. The gel was incubated once again at 37 °C and left to set for 1 hour. The gels were kept in running buffer at 4 °C and used when needed.

Table 6

Resolving Gel Composition for the Preparation of Two Gels

Substance	Volume/mL
H_2O	5.94
Resolving Buffer (1.5 M Tris pH 8.8)	3.75
SDS (10%)	0.15
Acrylamide	5.00
APS	0.15
TEMED	0.01

Table 7

Stacking Gel Composition for the Preparation of Two Gels

Substance	Volume/mL
H_2O	2.825
Stacking Buffer	1.250
SDS	0.050
Acrylamide	0.825
APS	0.050
TEMED	0.010

2.7.3 Electrophoresis and Coomassie Gel Preparation

Two gels were attached to the Bio-Rad Electrophoresis Cassette with each lane void filled with running buffer. The prepared gel samples were loaded with 10 µl in each lane representing 15 µg of protein and with one lane containing the Bio-Rad protein standard ladder (3µl). The cassette was submerged in the electrophoresis cell, with the marked volume of running buffer pertaining to the number of gels. The gels were run at 150 V for approximately 45 min or until the dye front reached the bottom of the gel. Both of the gels were then removed from the cell and cassette, with one of these gels placed in a gel staining tray with Gel Code blue staining solution (20 mL). The gel was left to in the stain for 45 min on a rocking table after which the stain was removed and the gel was left in deionised water (20 mL) overnight.

2.7.4 Western Blot Analysis

The other gel removed from the electrophoresis cell was used for Western Blot Analysis. The gel was placed within a semi-dry transfer stack consisting of two pre-soaked 3 mm blotting filter pads and nitrocellulose membrane. The layer was assembled on the anode of the semi-dry transfer equipment with one blotting filter pad, followed by the nitrocellulose, gel and finally another blotting filter pad. The cathode was placed on top of the transfer stack and the transfer was run at 20 V for 20 minutes.

The nitrocellulose was then removed from the transfer stack and placed in a clean staining tray and stained with ponceau solution (10 mL). The ponceau stain was removed and the nitrocellulose

was washed with deionised water to reveal and confirm the presence of transferred protein bands. The nitrocellulose was then de-stained with 1x TBST solution and placed in 20 mL of block solution to be agitated for 1 hr. The block was drained from the nitrocellulose and either submerged in block (25 mL, **Table 5**) with addition of the primary AOA antibody (10 µl); or submerged in the Twin-Strep antibody solution (Twin-Strep antibody 1:1000 dilution in BSA (3%) and milk powder (5%)). The nitrocellulose was left agitating for 1hr for both antibodies and then washed three times for 10 minutes with 1xTBST (10 mL). The Twin-Strep antibody nitrocellulose film could be taken forward; whereas a secondary AOA antibody (10 µl) was added to the other film and left agitating for 1hr, followed by three washes with 1x TBST for 10 minutes. For each antibody used, the final wash with blot rinse (20 mL) was carried out for 15 min.

2.7.5 Detection

Detection was performed using the GE healthcare chemiluminescence kit to prepare the detection mixture consisting of a 1:1 ratio of both kit solutions. The nitrocellulose film was exposed to the detection mixture (2 mL) for 1 minute and then placed within a contained sheet of saran wrap, ensuring a smooth surface on top of the nitrocellulose. The nitrocellulose is fixated to an exposure cassette and transferred to a dark room. With only the safelight for illumination, X-ray film (Fujifilm Super RX Medical) was removed from its packaging with a corner cut to determine correct orientation after processing. The film is placed in the exposure cassette and left for the desired exposure time (30 s - 5 min) to expose the film to the nitrocellulose membrane. The film is removed and developed in a Konika SRX-101A X-ray developer. The film is removed and the lanes and protein standards are marked on the exposed film.

2.8 Analytical Techniques

2.8.1 O_2 Respirometry

All oxygen consumption assays were performed on an Oroboros Oxygraph-2K with the packaged software. The measurement of AOX activity within *E. coli* membranes was performed in MOPS buffer (65 mM, pH 7.5 (unless stated)) at 25 °C and the addition of substrates with Hamilton micro syringes. The Oroboros Oxygraph-2K was calibrated with deionised water (100%) and sodium dithionite (0%).

2.8.2 Spectrophotometric Plate Assay

Plate assays were carried out using a Thermo Fisher Scientific Multiskan FC Microplate Photometer and packaged software using 96-well microplates. The microplate reader was set to: the wavelength corresponding to the substrate measured (**Table 8**); with 1 min shaking before assay readings and 2 secs between readings; and with readings performed every 5 seconds for 10 minutes. The Microplate reader software package performed both blank subtraction and kinetic reduction analysis for unknown samples.

Table 8

Spectrophotometric Parameters for Substrate Analysis

Substrate	Wavelength/ nm	Extinction coefficient
NADH	340	6200
Cytochrome *c*	550	18500
DCPIP	600	19100
Q_2H_2	278	17000

2.8.3 High Resolution Spectrophotometric Assay

High resolution spectrophotometry was performed using a Cary 400 UV spectrophotometer with the associated kinetics package software. Absorbance measurements required the use of a quartz cuvette with a 1 cm path length. The spectrophotometer was set to the correct wavelength for the substrate and blanked against the biological buffer. The auto-oxidation rate was analysed by addition of the substrate before activity analysis. The purified AOX activity was measured by calculating the absorbance change over time.

2.9 ITC Assay

Purified protein samples were dialysed using Thermo Fisher dialysis cassettes (MW cut off = 20 kDa) in elution buffer for a minimum of 4 h at 4 ˚C. Inhibitor stock solutions were made up in DMSO and diluted so that the final concentration of DMSO was equal to 4% and corresponded to the desired compound concentration. At the moment before ITC measurements were carried out, a volume of DMSO equal to 4% was added to purified protein samples, minimising any protein degradation. ITC experiments were conducted in a Malvern MicroCal PEAQ-ITC with packaged software for binding isotherm and thermodynamic quantity generation.

2.10 Molecular Modelling Software and Crystal Structures

A combination of three molecular modelling software packages (PyMol v2.2[213] and Maestro v11.5[214] by Schrödinger and MOE by Chemical Computing Group[215]) were utilised for both protein visualisation and ligand docking. Ligand/inhibitor docking was primarily carried out on Maestro using the GLIDE plugin[216] and scoring function. AOX proteins without a solved crystal structure were modelled using SWISS-MODEL automated homology server[217]. All crystal structures were obtained from the RCSB Protein Data Bank[218] with **Table 9** outlining the PDB structure entry and crystal structure details.

Table 9

Protein database crystal structures utilised for modelling analysis

PDB code	Description
3W54	TAO with colletochlorin B bound (2.3 Å)
3VVA	TAO with ascofuranone derivative bound (2.6 Å)
3VV9	TAO no inhibitor (2.9 Å)
3H1L	Cytochrome bc_1 complex (chicken) with ascochlorin bound (3.2 Å)
3L71	Cytochrome bc_1 complex (chicken) with azoxystrobin bound (2.84 Å)
1PPJ	Cytochrome bc_1 complex (chicken) with stigmatellin and antimycin A bound (2.1 Å)
3L74	Cytochrome bc_1 complex (chicken) with famoxadone bound (2.76 Å)

2.11 Chemical Synthesis

General Technical Procedures:

All chemicals and solvents were obtained from commercial suppliers, Sigma Aldrich or Fischer Scientific. The thin layer chromatography (TLC) analyses were performed using silica gel (Merck-Millipore 20x20 cm aluminium backed, thickness: 0.2 mm) or amine functionalised glass backed plates (Silicycle 250 μm) which were cut to the appropriate size. TLC compound detection was achieved under UV light (253 and 366 nm) or with one of the listed TLC dips outlined in **Table 10**. Column chromatography was carried out with glass columns of various sizes with silica gel (Fischer Scientific, pore size 60 Å) or amine functionalised silica (Sigma Aldrich 40-75 μm particle size). All ^{1}H and ^{13}C NMR were recorded on a Varian NMR 7600-AS spectrometer at 400 MHz and 101 MHz or 600 MHz and 151 MHz, respectively. NMR readings are reported in ppm on the δ scale relative to the internal TMS standard.

Table 10 - TLC Stains

TLC Stain	Composition	Notes/Uses
Potassium Permanganate	Potassium permanganate (1.5 g) Potassium carbonate (10 g) 10% Sodium hydroxide (1.25 mL) Water (200 mL)	General use. Compound spots develop as white or yellow spots.
Iodine	A few iodine crystals in silica gel	Used for the detection of compounds that do not show under UV light.
Ninhydrin	Ninhydrin (1.5 g) Acetic acid (3 mL) *n*-butanol (100 mL)	Amines show up as purple spots.
Ceric Ammonium Molybdate	Ceric ammonium sulfate (4 g) Ammonium molybdate (10 g) Conc. sulfuric acid (40 mL) Water (360 mL)	General use: Useful for alcohols Compounds develop as blue spots after heating.
2,4-DNP	2,4-Dinitrophenylhydrazine (12 g) Conc. sulfuric acid (60 mL) Water (80 mL) 95% Ethanol (200 mL)	Detects the presence of aldehydes

General procedure for alkyl coupling/tail addition for colletochlorin and ascofuranone like derivatives:

To each solution of 3-chloro-4,6-dihydroxy-2-methylbenzaldehyde (1 equiv) in dry methanol (1-5 mL), alkyl bromide (0.8-1.2 equiv) and $CaCl_2.2H_2O$ (0.6-0.8 equiv) were added. The reaction was kept under an inert atmosphere at 0 °C and stirred for 30 min. Potassium hydroxide (1M solution in dry methanol) was added to the reaction vessel and was left to slowly warm to room temperature overnight. The reaction was quenched with a brine solution, concentrated in vacuo and extracted with ethyl acetate (2 x 50 mL). The organic extract was dried with $MgSO_4$, filtered and purified by preparative TLC or column chromatography using solvents Petroleum ether (40-60)/EtOAc (95/5 – 8/2) with TEA as a supplement to the eluent.

General procedure for the allylic oxidation of geranyl, prenyl and neryl protected alcohols:

To a nitrogen flushed round bottomed flask, protected geranyl, prenyl or neryl alcohol (1 equiv) was added to a solution of selenium oxide (0.1 equiv), salicylic acid (0.1 equiv) and *tert*-butyl hydroperoxide (70% solution in water, 10-30 mL). The solution was left to react at room for 24 h at room temperature (alcohol) or 37 °C for 48 h (aldehyde). The resultant reaction mixture was diluted with toluene (100 mL) and reduced to half of its volume under vacuum. The remaining organic layer was washed with a concentrated NaOH solution (2M) to remove selenium by-products and filtered through a celite pad. The final organic filtrate was concentrated under vacuo and purified by column chromatography (Petroleum ether (40-60) 7:3 EtOAc) yielding the alcohol and aldehyde as pale-yellow oils.

General procedure for reductive amination of allylic aldehydes:

To a flame dried round-bottomed flask, an allylic aldehyde (1 equiv) was added along with the functionalised aniline (1.1 equiv) and dichloroethane (20-120 mL). The solution was stirred for 30 min at room temperature after which glacial acetic acid (1.2 equiv) was added to the reaction mixture. The reaction mixture was left to stir for a further 30 min followed by the addition of sodium triacetoxyborohydride (1.4 equiv) and left to stir overnight at 30 °C. The reaction was then quenched with a saturated solution of $NaHCO_3$ (20 mL), extracted with EtOAc (3 x 75 mL) and dried with $MgSO_4$ to yield a crude product. The crude product was then purified by column chromatography ($CHCl_3$ 95:5 MeOH or $CHCl_3$: MeOH: NH_3, 97:2:1) to yield the desired product.

General procedure for acetate deprotection:

To a round bottomed flask, acetate protected functionalised aniline (1 equiv) was dissolved in methanol (5-30 mL). Potassium carbonate (3 Equiv) was dissolved in water (1-5 mL) and slowly added to the reaction flask. The reaction mixture was left to stir overnight, after which the reaction was quenched with water (10-40 mL). The mixture was then concentrated in vacuo, extracted with DCM (3 x 40 mL), washed with brine (100 mL), dried and the solvent removed under reduced pressure. The crude product was purified by column chromatography ($CHCl_3$:MeOH 95:5 or 80:10:1 NH_3) to yield a yellow crystalline solid.

2,4-Dihydroxy-6-methylbenzaldehyde[219] **(1)**

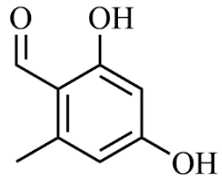

Phosphorus oxychloride (2 mL, 21.4 mmol) was added slowly to DMF (10 mL) in a salt-ice bath (~-2 °C) with rapid stirring over 30 min and left for 1.5 h. 3,5-Dihydroxytoluene (2.063 g, 16.6 mmol) was dissolved in DMF (5 mL) and slowly added to the reaction mixture. The reaction flask was warmed to room temperature and left to stir overnight. The mixture was then cooled under an ice bath (~3 °C), with ice water (25 mL) and NaOH (~25 mL, 20% sol) slowly added until pH 9 was reached. The reaction mixture was heated to 110°C and refluxed for 45 min. Following heating, the flask was allowed to cool to room temperature followed by further cooling in a salt-ice bath (~-2 °C). Acidification was achieved through the slow addition of a 20% solution of HCl (~15 mL) until pH 3 and a white precipitate formed. An off-white powder was isolated following drying and filtration steps (1.605 g, 64%). ^{1}H NMR (400 MHz, Methanol-d_4): δ 9.96 (s, 1H, C*H*O), 6.11 (d, 0.8 Hz, 1H, Ar-*H*), 6.00 (d, *J* = 2.3 Hz, 1H, Ar-*H*), 2.39 (s, 3H, Ar-CH_3); ^{13}C NMR (101 MHz, Methanol-d_4): δ 192.9, 166.1, 165.8, 144.9, 112.6, 110.4, 100.1, 17.0; MS (ESI) *m/z*: 150.850 (M-)

3-Chloro-4,6-dihydroxy-2-methylbenzaldehyde[220] **(2)**

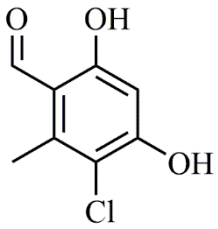

Sulfuryl chloride (0.5 mL, 6.00mmol) was added dropwise into a stirred solution of 2,4–dihydroxy-6-methylbenzaldehyde (0.829 g, 5.45 mmol) dissolved in anhydrous ether (50 mL) within an ice-salt bath (~-2 °C). The reaction was kept at this temperature and left to stir for 3 h or until the starting material was no longer present when assessed by TLC. The reaction mixture was quenched with $NaHCO_3$, washed with brine and then water followed by extraction of the aqueous layer with ethyl acetate (3 x 75 mL). The combined organic extracts were dried with $MgSO_4$ and concentrated in vacuo. Purification of the final product was achieved by column chromatography (Petroleum ether (40-60) 8:2 EtOAc) and yielded a white solid (0.489g, 48%). ^{1}H NMR (400 MHz, Methanol-d_4) δ 10.04 (s, 1H, C*H*O), 6.19 (s, 1H, Ar-*H*), 4.76 (s, 1H, Ar-O*H*) 2.51 (s, 3H, Ar-C*H*$_3$). ^{13}C NMR (101 MHz, Methanol-d_4) δ 193.6, 163.9, 161.0, 141.40, 100.74, 13.34. MS (EI) *m/z*: 184.750 (M-).

(*E*)-3-Chloro-5-(3,7-dimethylocta-2,6-dien-1-yl)-4,6-dihydroxy-2-methylbenzaldehyde (Colletochlorin B)[221] **(3)**

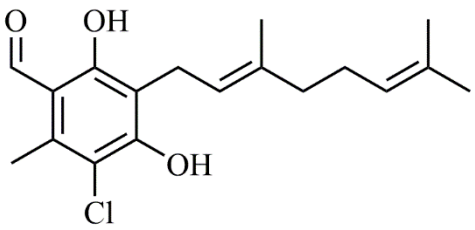

Following the general procedure for alkyl coupling starting from 3-chloro-4,6-dihydroxy-2-methylbenzaldehyde (0.149 g, 0.79 mmol), geranyl bromide (0.13 mL, 0.63 mmol), methanol (0.5 mL) and KOH solution (0.105 g in 2 mL of MeOH). Compound **3** was isolated by column

chromatography (Petroleum ether (40-60) 95:5 EtOAc) as a white solid (0.111 g, 55%). ^{1}H NMR (400 MHz, Chloroform-*d*) δ 12.62 (s, 1H, Ar-O*H*), 10.07 (s, 1H, C*H*O), 6.36 (s, 1H, Ar-O*H*), 5.15 (tq, *J* = 7.1, 1.3 Hz, 1H, C=C*H*), 4.98 (tq, *J* = 8.4, 1.5 Hz, 1H, C=C*H*), 3.36 – 3.30 (m, 2H, C*H*$_2$), 2.53 (s, 3H, Ar-C*H*$_3$), 2.02 – 1.95 (m, 2H, C*H*$_2$), 1.95 – 1.88 (m, 2H, C*H*$_2$), 1.72 (d, *J* = 1.3 Hz, 3H, C*H*$_3$), 1.60 – 1.56 (m, 3H, C*H*$_3$), 1.50 (d, *J* = 1.2 Hz, 3H, C*H*$_3$). ^{13}C NMR (101 MHz, Chloroform-*d*) δ 193.3, 162.2, 156.5, 137.6, 137.0, 131.5, 124.2, 120.7, 114.4, 113.6, 113.3, 39.8, 26.59, 25.66, 22.01, 17.67, 16.18, 14.44. MS (EI) *m/z*: 323.00 (M+)

3-Chloro-4,6-dihydroxy-2-methyl-5-(3-methylbut-2-en-1-yl)benzaldehyde (Colletochlorin D)[221] **(4)**

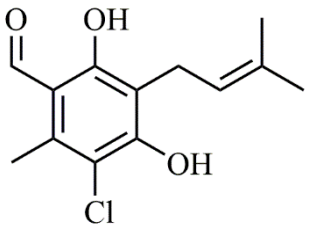

Following the general procedure for alkyl coupling starting from 3-chloro-4,6-dihydroxy-2-methylbenzaldehyde (0.200 g, 1.07 mmol), 3,3 dimethyl allyl bromide (0.15 mL, 0.85 mmol), methanol (3 mL), $CaCl_2.2H_2O$ (0.093 g, 0.64 mmol) and KOH solution (0.111 g, 1.98 mmol). The final compound was isolated by column chromatography (Petroleum ether (40-60) 95:5 EtOAc) as white crystalline solid (26 mg, 12%). ^{1}H NMR (400 MHz, Chloroform-*d*) δ 12.61 (s, 1H, Ar-O*H*), 10.06 (s, 1H, C*H*O), 6.36 (s, 1H, Ar-O*H*), 5.15 (t, *J* = 7.3 Hz, 1H, C=C*H*), 3.31 (d, *J* = 7.2 Hz, 2H, C*H*$_2$), 2.52 (s, 3H, Ar-C*H*$_3$), 1.72 (s, 3H, C*H*$_3$), 1.62 (s, 3H, C*H*$_3$). ^{13}C NMR (101 MHz, Chloroform-*d*) δ 193.3, 162.1, 156.3, 137.6, 133.3, 120.9, 114.4, 113.6, 113.2, 29.7, 25.8, 22.1, 17.8, 14.4. MS (ES) *m/z*: 253.90 (M-)

(±)-1-Bromo-3,7-dimethyloctane (5)

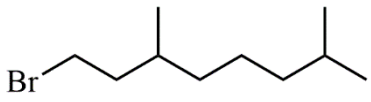

(±)-3,7-Dimethyl octanol (1 mL, 5.23 mmol) and tetrabromomethane (1.959 g, 5.75 mmol) were placed into a 3-necked flask and flushed with nitrogen. Anhydrous dichloromethane (10 mL) was then added to the flask at 0 °C and stirred for 20 min. Triphenylphosphine (1.536 g, 5.75 mmol)

was then dissolved in anhydrous DCM (10 mL) and slowly added to the reaction mixture over the course of 30 min. The reaction was left to stir for 5 h at room temperature. The reaction was stopped and concentrated under reduced pressure. To the concentrated oil, petroleum ether (40-60) was added until a precipitate was seen. The crude product was the take forward without further purification (1.102 g, 95%).

2,2,2-Trifluoro-*N*-(6-hydroxyhexyl)acetamide (6)

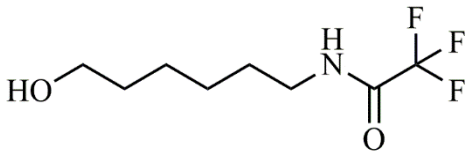

To a solution of 6-aminohexanol (0.760 g, 6.49 mmol) in dichloromethane (10 mL), ethyl trifluoroacetate (0.85 mL, 7.14 mmol) was added slowly. The mixture was left to stir at room temperature overnight and then concentrated in vacuo. The flask was then placed in an ice bath until a crude white crystalline solid formed (1.191 g, 86%), the product was taken forward to the next step without further purification. Crude ^{1}H and ^{13}C NMR with amide peak at ppm 157.5.

***N*-(6-Bromohexyl)-2,2,2-trifluoroacetamide (7)**

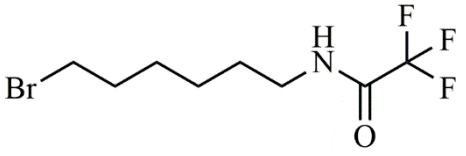

Compound **6** (1.050 g, 4.92 mmol) was placed in an oven dried round bottomed flask. The flask was purged with nitrogen, cooled to 0 °C and compound **6** was dissolved in dry dichloromethane (40 mL). To the flask kept at 0°C, CBr_4 (3.258 g, 9.85 mmol) and triphenylphosphine (2.21 g, 9.64 mmol) were added. The reaction mixture was left to stir at 0 °C for 4 h and quenched with $NaHCO_3$ (30 mL). The organic layer was separated, concentrated in vacuo and washed through a short silica pad. The crude product was used without further purification yielding a brown oil (1.259 g, 93%).

6-((7-Nitrobenzo[*c*][1,2,5]oxadiazol-4-yl)amino)hexan-1-ol[222] (8)

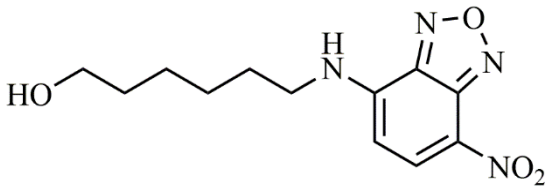

To a solution of 6-aminohexanol (0.287 g, 2.45 mmol) in 0.3M $NaHCO_3$ (aq) (0.302 g, 3.43 mmol), NBD-Cl (0.477 g, 2.45 mmol) was added along with methanol (20 mL). The reaction was then left to stir overnight at room temperature. The solvent was reduced under reduced pressure and purified by column chromatography (Petroleum ether (40-60) 6:4 EtOAc) yielding an orange powder (0.386 g, 56%). ^{1}H NMR (600 MHz, Methanol-d_4) δ 8.50 (d, *J* = 8.8 Hz, 1H, Ar-*H*), 6.32 (d, *J* = 8.9 Hz, 1H, Ar-*H*), 3.55 (t, *J* = 6.5 Hz, 2H, C*H*$_2$), 3.51 (s, 1H, N*H*), 1.78 (m, *J* = 6.9 Hz, 2H,C*H*$_2$), 1.55 (q, *J* = 6.8 Hz, 2H, C*H*$_2$), 1.52 – 1.40 (m, 4H, C*H*$_2$-C*H*$_2$). ^{13}C NMR (151 MHz, Methanol-d_4) δ 137.2, 98.1, 61.4, 43.3, 32.1, 27.8, 26.5, 25.2. MS (EI) *m/z*: 278.950 (M-)

***N*-(6-Bromohexyl)-7-nitrobenzo[*c*][1,2,5]oxadiazol-4-amine (9)**

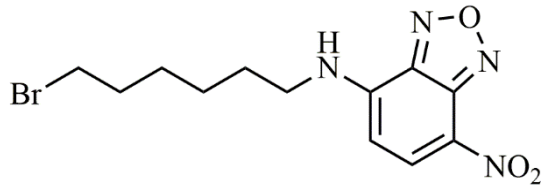

Compound **8** (0.050 g, 0.18 mmol) was placed in an oven dried round bottomed flask and purged with nitrogen. Anhydrous dichloromethane (10 mL) was added to the round bottomed flask to dissolve compound **8** under ice bath cooling (0 °C)**.** To the flask, CBr_4 (0.111 g, 0.36 mmol) and PPh_3 (0.114 g, 0.36 mmol) were added. The reaction mixture was left to stir overnight at room temperature. The reaction mixture was then quenched with $NaHCO_3$ (30 mL) and extracted with EtOAc (2 x 50 mL) and concentrated in vacuo. The resultant oil was dissolved in DCM and filtered through a short silica gel column, yielding a crude yellow oil which was take forward without further purification (0.067 g, 98%).

(2*E*,6*E*)-8-Hydroxy-3,7-dimethylocta-2,6-dien-1-yl acetate[223] (10)

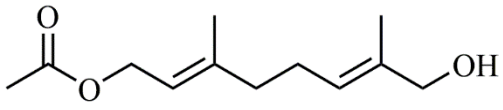

Prepared according to the general procedure for allylic oxidation, starting with geranyl acetate (10 mL, 46.3 mmol), selenium oxide (2.51 g, 23.2 mmol), DCM (150 mL) and *t*-BuOOH (12.5 mL, 92.6 mmol), yielding a pale-yellow oil (4.301 g, 44%). ^{1}H NMR (600 MHz, Chloroform-*d*) δ 5.45 – 5.23 (m, 2H, C=C*H*), 4.57 (d, *J* = 7.1 Hz, 2H, COOC*H*$_2$), 3.98 (d, *J* = 1.4 Hz, 2H, C*H*$_2$OH), 2.21 – 2.12 (m, 2H, C*H*$_2$), 2.12 – 2.05 (m, 2H, C*H*$_2$), 2.04 (s, 3H, C*H*$_3$COO), 1.78 – 1.61 (m, 6H, C*H*$_3$); ^{13}C NMR (151 MHz, Chloroform-*d*) δ 171.2, 141.7, 135.2, 125.2, 118.6, 68.8, 61.4, 39.0, 25.6, 21.0, 16.4, 13.6. MS (ES) *m/z*: 235.00 (M+Na$^+$)

(2*E*,6*E*)-3,7-Dimethyl-8-oxoocta-2,6-dien-1-yl acetate[223] (11)

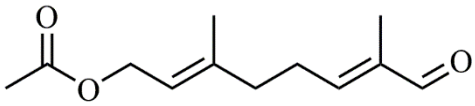

According to the general procedure for allylic oxidation, compound **11** was prepared with geranyl acetate (2.5 mL, 11.6 mmol), selenium oxide (0.131 g, 1.18 mmol), *tert*-butylhydroperoxide (3 mL, 23.2 mmol) and DCM (50 mL), yielding a pale-yellow oil (1.186 g, 49%). ^{1}H NMR (600 MHz, Chloroform-*d*) δ 9.30 (s, 1H, C*H*O), 6.38 (tq, *J* = 7.3, 1.4 Hz, 1H, C*H*=C), 5.30 (tq, *J* = 7.2, 1.4 Hz, 1H, C*H*=C), 4.50 (d, *J* = 7.1 Hz, 2H, COOC*H*$_2$), 2.45 – 2.36 (m, 2H, C*H*$_2$), 2.15 (t, *J* = 7.6 Hz, 2H, C*H*$_2$), 1.96 (s, 3H, C*H*$_3$COO), 1.70-1.61 (m, 6H, C*H*$_3$). ^{13}C NMR (151 MHz, Chloroform-*d*) δ 195.5, 170.9, 153.5, 140.3, 139.5, 119.5, 61.1, 37.6, 26.9, 20.7, 16.3, 9.1. MS (ES) *m/z*: 233.00 (M+Na$^+$)

(2*E*,6*E*)-8-Bromo-3,7-dimethylocta-2,6-dien-1-yl acetate (12)

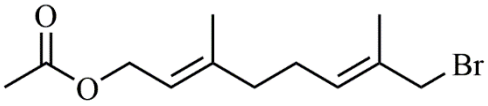

To a solution of compound **11** (1.573 g, 7.41 mmol) in dry diethyl ether (60 mL), phosphorus tribromide (0.7 mL, 9.63 mmol) was added dropwise at 0 °C. The reaction was left to react for 1hr, after which the reaction was quenched with ice cold water (50 mL), diluted with EtOAc (75 mL) and washed with a saturated $NaHCO_3$ solution (50 mL). The organic layer is separated, dried with $MgSO_4$ and then concentrated under reduced pressure. A crude brown oil was isolated without further purification (1.640 g, 80%).

(*E*)-3-Methyl-4-oxobut-2-en-1-yl acetate (13)

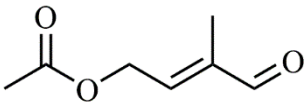

Following the general procedure for allylic oxidation, compound **13** was prepared, starting with 3,3-dimethylallyl acetate (10 mL, 71.4 mmol), selenium dioxide (0.788 g, 7.14 mmol), salicylic acid (1.003 g, 7.14 mmol), *tert*-BuOOH (10 mL) and DCM (150 mL). Compound **13** was isolated as pale-yellow oil (4.237 g, 38%). ^{1}H NMR (600 MHz, Chloroform-*d*) δ 9.35 (s, 1H, C*H*O), 6.42 (t, *J* = 6.0 Hz, 1H, C=C*H*), 4.81 (d, *J* = 6.0 Hz, 2H, COOC*H*$_2$), 2.02 (s, 3H, C*H*$_3$COO), 1.70 (s, 3H, C*H*$_3$); ^{13}C NMR (151 MHz, Chloroform-*d*) δ 194.2, 170.7, 145.9, 140.3, 60.8, 20.6, 9.3. MS (ES) *m/z*: 165.06 (M+)

(2*Z*,6*E*)-8-Hydroxy-3,7-dimethylocta-2,6-dien-1-yl acetate (14)

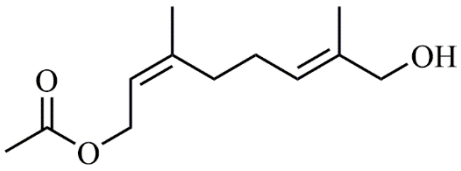

Compound **14** was prepared according to the general procedure for allylic oxidation, starting with neryl acetate (20 mL, 93.2 mmol), selenium dioxide (1.027 g, 9.32 mmol), salicylic acid (1.295 g, 9.32 mmol), *tert*-BuOOH (30 mL) and DCM (80 mL). A colourless oil was isolated (11.234 g, 56%). ^{1}H NMR (600 MHz, Chloroform-*d*) δ 5.34 - 5.30 (m, 1H, C*H*=C), 5.28 (td, *J* = 7.2, 1.6 Hz, 1H, C*H*=C), 4.49 (dd, *J* = 7.2, 1.1 Hz, 2H, COOCH_2), 3.90 (s, 2H, CH_2OH), 2.28 (s, 1H, O*H*), 2.08 (d, *J* = 3.4 Hz, 4H, CH_2), 1.97 (s, 3H, CH_3COO), 1.70 (s, 3H, CH_3), 1.59 (s, 3H, CH_3). ^{13}C NMR (151 MHz, Chloroform-*d*) δ 171.2, 141.9, 135.5, 124.5, 119.4, 68.4, 61.1, 31.7, 25.9, 23.29, 20.9, 13.5. MS (ES) *m/z*: 234.950 ($M+Na^+$)

(2*Z*,6*E*)-8-Bromo-3,7-dimethylocta-2,6-dien-1-yl acetate (15)

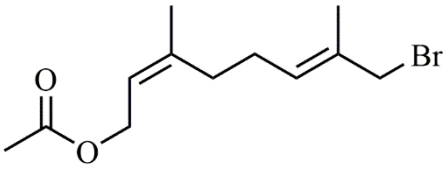

Compound **14** (2.502 g, 11.8 mmol) was placed in a nitrogen purged, flame dried round bottom flask and dissolved in dry diethyl ether (30 mL). The solution was stirred and kept at 0 °C whilst phosphorus tribromide (0.52 mL, 7.07 mmol) was added dropwise to the flask. The reaction was left to stir for 1 hr and was then quenched with cold water (30 mL) followed by $NaHCO_3$ (40 mL). The mixture was diluted with EtOAc (50 mL), separated and dried with $MgSO_4$. The organic solvent was removed under reduced pressure to yield a crude oil which was used without further purification (2.014 g, 62%).

(2*E*,6*E*)-8-(3-Chloro-5-formyl-2,6-dihydroxy-4-methylphenyl)-3,7-dimethylocta-2,6-dien-1-yl acetate (16)

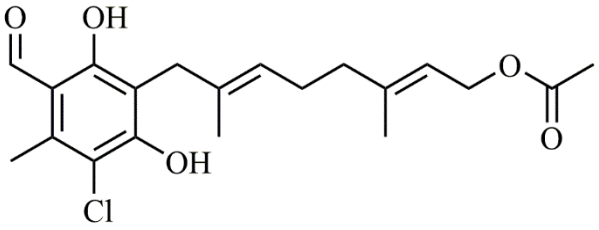

Compound **16** was prepared according to the general procedure for alkyl coupling, using compound **2** (0.306 g, 1.60 mmol), alkyl bromide **12** (0.528 g, 1.92 mmol), methanol (12 mL). $CaCl_2.2H_2O$ (0.140 g, 0.96 mmol) and a KOH solution (0.194 g, 3.2 mmol). The crude product was purified by pTLC (Petroleum ether (40-60):EtOAc:TEA, 79:20:1) yielding a pale-yellow oil (121mg, 20%). ^{1}H NMR (400 MHz, Chloroform-d) δ: 12.50 (s, 1H, Ar-O*H*), 10.07 (s, 1H, C*H*O), 6.27 (s, 1H, Ar-O*H*), 5.49 (tq, *J* = 7.1, 1.3 Hz, 1H, C*H*=C), 5.28 (tq, *J* = 7.1, 1.3 Hz, 1H, C*H*=C), 4.50 (d, *J* = 7.0 Hz, 2H, COOCH_2), 4.42 (s, 2H, CH_2), 2.55 (s, 3H, Ar-CH_3), 2.16 (q, *J* = 7.3 Hz, 2H, CH_2), 2.04 (dd, *J* = 9.0, 6.2 Hz, 2H, CH_2), 1.98 (s, 3H, CH_3COO), 1.66 (d, *J* = 1.4 Hz, 6H, CH_3); ^{13}C NMR (101 MHz, Chloroform-*d*) δ 193.2, 171.1, 164.5, 161.3, 141.4, 140.5, 129.9, 128.9, 118.9, 115.4, 113.4, 99.4, 74.9, 61.3, 38.8, 25.8, 21.1, 16.4, 14.6, 13.7. LC-MS (ESI) *m/z*: 379.00 (M-), 90% purity, retention time 23.0 min.

3-Chloro-4,6-dihydroxy-5-((2*E*,6*E*)-8-hydroxy-2,6-dimethylocta-2,6-dien-1-yl)-2-methylbenzaldehyde (17)

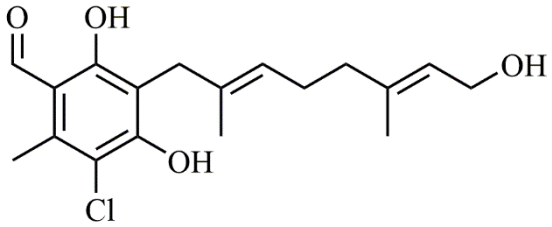

Compound **17** was prepared according to the general procedure for alkyl coupling, using compound **2** (1.003 g, 5.35 mmol), alkyl bromide **12** (1.069 g, 3.88 mmol), methanol (8 mL),

$CaCl_2.2H_2O$ (0.473 g, 3.21 mmol) and a KOH solution (0.539 g, 10.7 mmol). The crude product was purified by pTLC (Petroleum ether (40-60) 6:4 EtOAc) and recrystallised from Hexane/$CHCl_3$ yielding colourless crystals (58 mg, 4%). ^{1}H NMR (400 MHz, Chloroform-d) δ 12.66 (s, 1H, Ar-O*H*), 10.08 (s, 1H, C*H*O), 5.29 (tq, *J* = 6.9, 1.4 Hz, 1H, C*H*=C), 5.09 (tq, *J* = 7.0, 1.4 Hz, 1H, C*H*=C), 4.09 (d, *J* = 6.9 Hz, 2H, CH_2), 3.35 – 3.30 (m, 2H, CH_2), 2.55 (s, 3H, Ar-CH_3), 2.09 (dd, *J* = 9.4, 4.7 Hz, 2H, CH_2), 2.09 (t, *J* = 7.1 Hz, 2H, CH_2), 1.56 (s, 6H, CH_3). ^{13}C NMR (101 MHz, Chloroform-*d*) δ 193.3, 162.3, 157.7, 139.0, 138.4, 133.1, 125.4, 123.9, 113.5, 112.5, 59.5, 39.1, 32.4, 25.7, 16.1, 15.9, 14.5. MS (ESI) *m/z*: 337.00 (M-); 91% purity, retention time 19.4 min.

(2*Z*,6*E*)-8-(3-Chloro-5-formyl-2,6-dihydroxy-4-methylphenyl)-3,7-dimethylocta-2,6-dien-1-yl acetate (18)

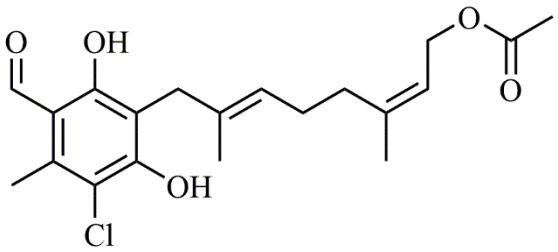

Compound **18** was prepared according to the general procedure for alkyl coupling, starting from compound **2** (0.5032 g, 2.68 mmol), alkyl bromide **15** (0.910 g, 3.22 mmol), $CaCl_2.2H_2O$ (0.275 g, 1.88 mmol), KOH solution (0.300 g, 5.36 mmol) and methanol (8 mL). The final product was purified utilising pTLC (Petroleum ether (40-60) 98:2 EtOAc) yielding a pale-yellow oil (47 mg, 5%). ^{1}H NMR (400 MHz, Chloroform-*d*) δ 12.64 (s, 1H, Ar-O*H*), 10.09 (s, 1H, C*H*O), 6.68 (s, 1H, Ar-O*H*), 5.27 (t, *J* = 7.2 Hz, 1H, C*H*=C), 5.08 – 4.91 (m, 1H, C*H*=C), 4.45 (dd, *J* = 7.2, 1.1 Hz, 2H, COOCH_2), 3.30 (s, 2H, CH_2), 2.56 (s, 3H, Ar-CH_3), 2.03 (d, *J* = 2.5 Hz, 4H, CH_2), 1.99 (s, 3H,CH_3COO), 1.71 – 1.65 (m, 3H, CH_3), 1.58 (d, *J* = 1.6 Hz, 3H,CH_3); ^{13}C NMR (151 MHz, Chloroform-*d*) δ 192.3, 170.4, 161.4, 156.2, 141.1, 137.2, 132.4, 123.0, 118.3, 112.4, 111.6, 60.5, 36.2, 30.3, 25.3, 20.1, 15.3, 13.5, 13.1. MS (ESI) *m/z*: 379.00 (M-); 60% purity, retention time 23.01 min.

3-Chloro-4,6-dihydroxy-5-((2*E*,6*Z*)-8-hydroxy-2,6-dimethylocta-2,6-dien-1-yl)-2-methylbenzaldehyde (19)

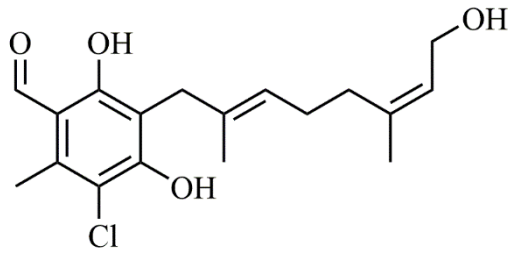

Compound **19** was prepared according to the general scheme for alkyl coupling, with compound **2** (1.083 g, 5.77 mmol), alkyl bromide **15** (1.973 g, 6.93 mmol), $CaCl_2.2H_2O$ (0.696 g, 4.74 mmol), KOH solution (0.643 g, 11.5 mmol) and methanol (10 mL). The final product was isolated *via* pTLC (Petroleum ether (40-60):EtOAc:TEA,79:20:1) yielding a colourless oil (0.148 g, 7%).^{1}H NMR (400 MHz, Chloroform-d) δ 12.64 (s, 1H, Ar-O*H*), 10.08 (s, 1H, C*H*O), 6.70 (s, 1H, Ar-O*H*), 5.27 (td, *J* = 8.6, 1.5 Hz, 1H, C*H*=C), 5.01 (td, *J* = 5.7, 1.6 Hz, 1H, C*H*=C), 4.44 (dd, *J* = 7.2, 1.1 Hz, 2H, COOCH_2), 3.30 (s, 2H, CH_2), 2.55 (s, 3H, Ar-CH_3), 2.17 (d, *J* = 4.3 Hz, 2H, CH_2), 2.09 (t, *J* = 6.8 Hz, 2H, CH_2) 1.67 (q, *J* = 1.1 Hz, 3H, CH_3), 1.57 (d, *J* = 1.4 Hz, 3H, CH_3), 1.19 (d, *J* = 1.9 Hz, 1H, O*H*).^{13}C NMR (101 MHz, Chloroform-*d*) δ 193.3, 162.5, 157.2, 142.2, 138.2, 133.4, 124.0, 119.3, 113.5, 113.3, 112.6, 61.5, 32.16, 32.0, 26.3, 23.5, 21.1, 16.3. MS (ESI) *m/z*: 337.00 (M-) 100% purity, retention time 19.4 min.

(2*E*,6*E*)-8-((2-Chloro-4-cyanophenyl)amino)-3,7-dimethylocta-2,6-dien-1-yl acetate (20)

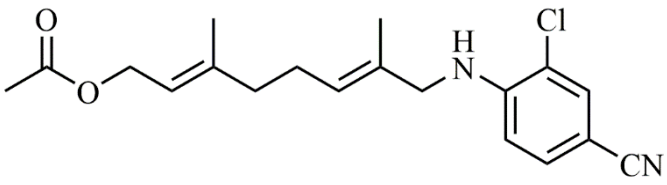

According to the general procedure for reductive amination, compound **20** was prepared starting with allylic aldehyde **11** (0.494 g, 2.35 mmol), 4-amino-3-chlorobenzonitrile (0.435 g, 2.82

mmol), acetic acid (0.16 mL, 2.82 mmol), sodium triacetoxyborohydride (0.692 g, 3.27 mmol) and DCE (25 mL). Purification was carried out by column chromatography ($CHCl_3$:MeOH, 95:5) to yield a brown solid (0.610 g, 75%). ^{1}H NMR (400 MHz, Chloroform-*d*) δ 7.46 (d, *J* = 1.9 Hz, 2H, Ar-*H*), 7.27 (dd, *J* = 8.4, 1.9 Hz, 2H, Ar-*H*), 6.68 (d, *J* = 8.4 Hz, 2H, Ar-*H*), 5.89 (s,1H, N*H*) 5.34 – 5.23 (m, 2H, C*H*=C), 4.52 (d, *J* = 7.0 Hz, 2H, COOCH_2), 3.93 (s, 2H, CH_2NH), 2.15 - 2.10 (m, 2H, CH_2), 2.05 – 2.01 (m, 2H, CH_2), 1.98 (s, 3H, CH_3COO), 1.62 (dd, *J* = 16.6, 1.4 Hz, 6H, CH_3); ^{13}C NMR (151 MHz, Acetone-d_6) δ 170.1, 148.7, 141.1, 132.9, 131.9, 123.3, 119.0, 118.5, 115.1, 99.0, 67.3, 60.6, 39.0, 29.4, 25.6, 19.9, 15.5, 12.8. MS (ES) *m/z*: 348.600 (M+)

3-Chloro-4-(((2*E*,6*E*)-8-hydroxy-2,6-dimethylocta-2,6-dien-1-yl)amino)benzonitrile (21)

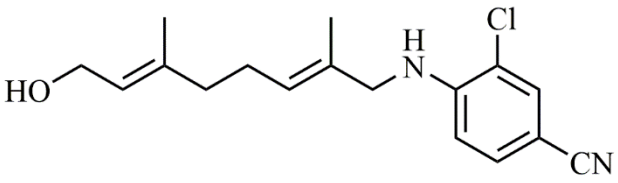

Compound **21** was prepared according to the general scheme for acetate deprotection, starting with compound **20** (0.610 g, 1.76 mmol), potassium carbonate (0.730 g, 5.28 mmol), water (3 mL) and methanol (5 mL). Purification was carried out with column chromatography ($CHCl_3$:MeOH:NH_3(aq), 80:10:1) to yield a crystalline yellow solid (0.377 g, 70%). ^{1}H NMR (600 MHz, Acetone-d_6) δ 7.60 (d, *J* = 1.9 Hz, 2H, Ar-*H*), 7.39 (dd, *J* = 8.5, 1.9 Hz, 2H, Ar-*H*), 6.95 (d, *J* = 8.5 Hz, 2H, Ar-*H*), 5.89 (s, 1H, N*H*), 5.42 – 5.32 (m, 2H, C*H*=C), 4.06 (d, *J* = 6.7 Hz, 2H, CH_2OH), 3.90 (s, 2H, CH_2NH), 2.86 (s, 1H, O*H*), 2.18 – 2.09 (m, 2H, CH_2), 2.02 (dd, *J* = 9.1, 6.3 Hz, 2H, CH_2), 1.68 – 1.54 (m, 6H, CH_3). ^{13}C NMR (151 MHz, Acetone-d_6) δ 170.1, 148.7, 132.9, 131.9, 125.3, 123.7, 118.5, 117.2, 115.1, 112.1, 99.0, 67.5, 58.3, 39.1, 25.8, 15.3, 12.8. MS (ES) *m/z*: 305.00 (M+)

2-(((2*E*,6*E*)-8-Acetoxy-2,6-dimethylocta-2,6-dien-1-yl)amino)-4-chlorobenzoic acid (22)

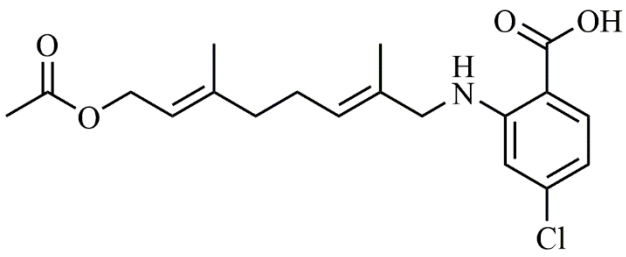

According to the general scheme for reductive amination, compound **22** was prepared starting with allylic aldehyde **11** (2.618 g, 12.5 mmol), 2-amino-4-chlorobenzoic acid (2.160 g, 12.6 mmol), acetic acid (0.9 mL, 15.0 mmol) and sodium triacetoxyborohydride (3.814 g, 17.9 mmol). Purification was carried by column chromatography ($CHCl_3$ 95:5 MeOH) yielding brown semi-solid (1.463 g, 32%). ^{1}H NMR (600 MHz, Acetone-d_6) δ 7.88 (dd, *J* = 8.5, 2.6 Hz, 2H, Ar-*H*), 6.72 (d, *J* = 9.9 Hz, 2H, Ar-*H*), 6.56 (d, *J* = 8.5 Hz, 2H, Ar-*H*), 5.43 (t, *J* = 7.2 Hz, 1H, C*H*=C), 5.31 (t, *J* = 7.0 Hz, 1H, C*H*=C), 4.52 (d, *J* = 7.0 Hz, 2H, CH_2COO), 3.86 – 3.79 (m, 1H, N*H*), 3.25 (q, *J* = 7.2 Hz, 2H, CH_2NH), 2.20 (q, *J* = 7.4 Hz, 2H, CH_2), 2.07 (t, *J* = 7.4 Hz 2H, CH_2), 2.01 – 1.90 (m, 3H, CH_3COO) 1.76 – 1.61 (m, 3H, CH_3), 1.27 (t, *J* = 7.2 Hz, 3H, CH_3); ^{13}C NMR (151 MHz, Acetone-d_6) δ 169.0, 140.9, 140.3, 133.5, 133.4, 125.2, 119.3, 114.3, 114.0, 111.2, 110.4, 60.5, 49.8, 38.9, 37.0, 25.7, 21.1, 19.9, 13.7. MS (ES) *m/z*: 362.750 (M-)

4-Chloro-2-(((2*E*,6*E*)-8-hydroxy-2,6-dimethylocta-2,6-dien-1-yl)amino)benzoic acid (23)

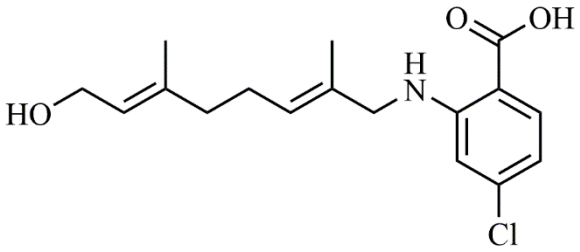

Compound **23** was prepared according to the general scheme for acetate deprotection, using compound **22** (2.061 g, 5.62 mmol), potassium carbonate (3.161 g, 20.5 mmol), methanol (60 mL) and water (20 mL). Following column chromatography ($CHCl_3$ 95:5 MeOH) yielding a off white semi-solid (0.214 g, 12%). ^{1}H NMR (400 MHz, Acetone-d_6) δ 7.77 (dd, *J* = 8.5, 3.4 Hz, 2H, Ar-*H*), 6.52 (d, *J* = 9.9 Hz, 2H, Ar-*H*), 6.37 (d, *J* = 8.1 Hz, 2H, Ar-*H*), 5.39 – 5.17 (m, 2H,

C*H*=C), 4.87 – 4.41 (m, 1H, N*H*), 3.98 – 3.90 (m, 1H, O*H*), 3.77 (d, *J* = 1.3 Hz, 2H, C*H*$_2$OH), 3.08 (q, *J* = 7.1 Hz, 2H, C*H*$_2$NH), 2.11 – 1.95 (m, 2H, C*H*$_2$), 1.91 – 1.85 (m, 2H, C*H*$_2$), 1.55 – 1.44 (m, 3H, C*H*$_3$), 1.36 – 0.83 (m, 3H,C*H*$_3$); ^{13}C NMR (101 MHz, Acetone-d_6) δ 152.0, 139.6, 133.8, 126.2 125.3, 123.8, 113.9 , 110.1, 67.5, 58.3, 39.2, 39.1, 37.0, 25.8, 15.3, 13.7, 12.8. MS (ES) *m/z*: 321.850 (M-).

(*E*)-2-((4-Acetoxy-2-methylbut-2-en-1-yl)amino)-4-chlorobenzoic acid (24)

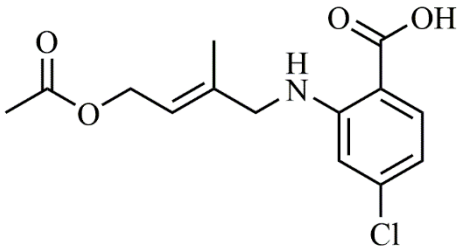

Compound **24** was prepared according to the general scheme for reductive amination, starting with allylic aldehyde **13** (2.469 g, 15.8 mmol), 2-amino-4-chlorobenzoic acid (2.460 g, 14.3 mmol), glacial acetic acid (1.1 mL, 19.0 mmol), sodium triacetoxyborohydride (4.067 g, 22.1 mmol) and DCE (60 mL). Purification was carried out by column chromatography ($CHCl_3$ 95:5 MeOH with AcOH (1%)) yielding a yellow semi-solid (2.030 g, 50%). %). ^{1}H NMR (600 MHz, Acetone-d_6) δ 8.26 (s, 1H, COO*H*), 7.89 (d, *J* = 8.5 Hz, 1H, Ar-*H*), 6.86 (d, *J* = 2.1 Hz, 1H, Ar-*H*), 6.69 (d, *J* = 2.0 Hz, 1H, Ar-*H*), 5.56 (tq, *J* = 5.9, 1.4 Hz, 1H, C*H*=C), 4.61 (dd, *J* = 6.9, 1.2 Hz, 2H, COOC*H*$_2$), 3.90 (d, *J* = 5.1 Hz, 2H, C*H*$_2$NH), 1.95 (s, 3H, C*H*$_3$COO), 1.81 – 1.75 (m, 3H, C*H*$_3$); ^{13}C NMR (151 MHz, Acetone-d_6) δ 170.1, 140.2, 137.4, 133.5, 133.2, 119.4, 115.4, 115.1, 114.6, 111.1, 60.2, 49.1, 19.9, 13.9. MS (ES) *m/z*: 297.950 (M+).

(*E*)-4-((2-Chloro-4-cyanophenyl)amino)-3-methylbut-2-en-1-yl acetate (25)

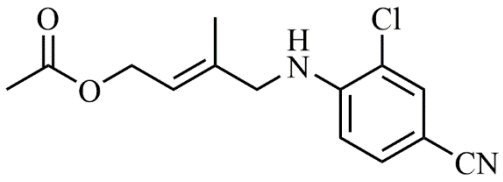

According to the general scheme for reductive amination, compound **25** was synthesised, starting with allylic aldehyde **13** (2.020 g, 12.9 mmol), 4-amino-chlorobenzonitrile (1.943 g, 12.7 mmol), glacial acetic acid (0.9 mL, 15.5 mmol), sodium triacetoxyborohydride (4.470 g, 21.1 mmol) and DCE (60 mL). The crude product was purified by column chromatography ($CHCl_3$ 95:5 MeOH) yielding a yellow crystalline solid (1.202 g, 33%). ^{1}H NMR (600 MHz, Acetone-d_6) δ 7.59 (dd, *J* = 5.4, 1.9 Hz, 2H, Ar-*H*), 7.38 (dd, *J* = 8.5, 1.9 Hz, 2H, Ar-*H*), 6.94 (d, *J* = 8.5 Hz, 2H, Ar-*H*), 5.87 (s, 1H, N*H*), 5.55 (tq, *J* = 5.9, 1.5 Hz, 1H, C*H*=C), 4.12 (d, *J* = 6.4 Hz, 2H, CH_2COO), 3.89 (d, *J* = 6.1 Hz, 2H, CH_2NH), 3.64 (s, 1H), 1.67 – 1.64 (m, 3H, CH_3COO), 1.41 – 1.07 (m, 3H, CH_3); ^{13}C NMR (151 MHz, Acetone-d_6) δ 148.7, 132.9, 132.2, 131.9, 125.9, 118.9, 118.6, 117.3, 115.1, 111.4, 99.0, 58.1, 49.4, 13.6. MS (ES) *m/z*: 277.750 (M-).

(*E*)-3-Chloro-4-((4-hydroxy-2-methylbut-2-en-1-yl)amino)benzonitrile (26)

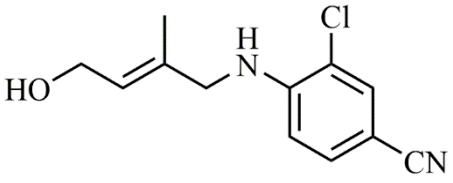

Compound **26** was prepared according to the general procedure for acetate deprotection, starting with compound **25** (0.621 g, 2.23 mmol), potassium carbonate (0.934 g, 6.68 mmol), methanol (20 mL) and water (2 mL). Purification of the crude product was achieved by column chromatography ($CHCl_3$:MeOH:NH_3(aq), 80:10:1) yielding a pale yellow semi-solid (0.121 g, 23%). ^{1}H NMR (600 MHz, Acetone-d_6) δ 7.59 (dd, *J* = 5.4, 1.9 Hz, 2H, Ar-*H*), 7.38 (dd, *J* = 8.5,

1.9 Hz, 2H, Ar-*H*), 6.94 (d, *J* = 8.5 Hz, 2H, Ar-*H*), 5.87 (s, 1H, N*H*), 5.55 (tq, *J* = 5.9, 1.5 Hz, 1H, C*H*=C), 4.12 (d, *J* = 6.4 Hz, 2H, COOCH_2), 3.89 (d, *J* = 6.1 Hz, 2H, CH_2NH), 2.85 (s, 1H, O*H*), 1.67 – 1.64 (m, 3H, CH_3); ^{13}C NMR (151 MHz, Acetone-d_6) δ 149.7, 132.9, 132.2, 131.9, 125.9, 118.6, 115.1, 111.4, 99.0, 58.1, 49.4, 13.6. MS (ES) *m/z*: 236.700 (M+).

Chapter 3: The Characterisation of StAOX

3.1 Introduction

The phytopathogenic fungus *Septoria tritici* is the most prevalent fungal pathogen in the UK and Europe[207], devastating the yield of the second most globally important crop[224], common wheat (*Triticum aestivum*). *S. tritici* is the causal agent of *Septoria tritici* blotch (STB), with documented[206] yield losses of 30-50% to untreated wheat cultivars. Within the UK specifically, typical yield losses for susceptible wheat varieties average to around 20% of a typical harvest, without fungicide treatment or crop management[207,225]. Any reduction in the UK or global crop production efficiency, will hamper the FAO[226] and peer reviewed estimates[227,228] for future food demands, which is stated[227,229] to increase by 60-110% by 2050.

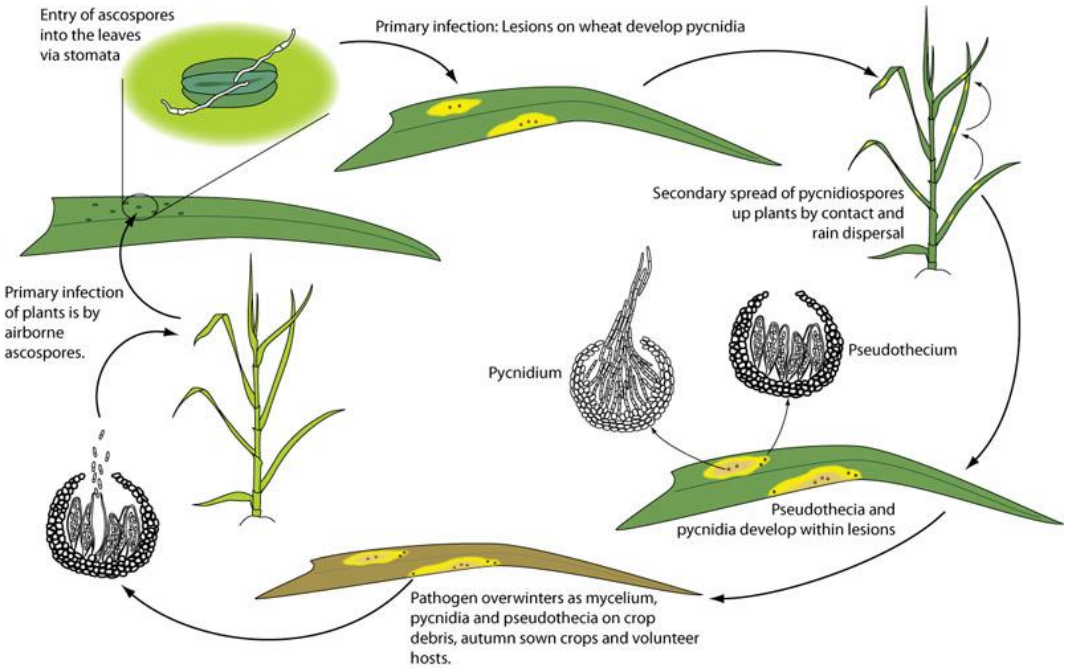

Figure 16 - Septoria tritici Fungal Life Cycle and Pathogenesis of Wheat Plants[241].

The primary infection of wheat by *S. tritici* is initiated through the spread of airborne pycnidiospores[230] or ascospores[231], produced from the pseudothecia or fungal fruiting bodies, contacting the leaf surface. After contact with the leaf surface, the ascospores germinate and switch to hyphal growth, penetrating the wheat host *via* the stomata[232,233]. The nutrient source and growth of the hyphae within the intracellular structure of the plant remains enigmatic[234], with no

generation of fungal feeding structures; metabolic changes of the host; or development of visible symptoms[232–235]. This period of growth is commonly referred to as the latent or biotrophic phase[236]. The symbioses between the fungi and the plant occurs through attenuation of the plants immune system, preventing host recognition or any fungal apoptosis[237,238]. This relationship between the host and fungal pathogen presents a challenging identification and treatment strategy for infected crop fields.

Following the latent period and substantial hyphae growth, the development of pycnidia is initiated[239]: with visible symptoms including lesions and necrotic areas forming on the leaf surface. The development of these symptoms characterises the transition from biotrophic to necrotrophic growth, with the secretion of cell wall degrading enzymes[240]; and thus, the collapse of host cells. The release of nutrients following cell death, provides fuel for the increase in fungal biomass and formation of mature pycnidia[43]. Pycnidiospores develop from mature pycnidia, in order to spread the infection within the plant or to adjacent plant foliage, thereby completing the fungal life cycle (**Figure 16**)[241]. The dissemination of these spores is aided by rainfall[242,243], with optimum conditions[244] for growth between 15-20°C, making the UK an ideal climate for the spread of STB.

The treatment of STB can be achieved through a number of classes of fungicides with varying modes of action. As mentioned in **Chapter 1**, the respiration and oxidative phosphorylation of *S. tritici* is often inhibited with the use of compounds which target the mitochondrial enzymes Complex II (SDHIs)[245,246] or Complex III (Q_oIs)[247–249]. The targeting of fungal respiration is used as a preventative application and provides mostly fungistatic efficacy[80,245], with only a few respiratory inhibitors[250] providing fungicidal and curative properties. Once the appearance of lesions on the leaf are presented, and the necrotic phase precedes, the use of respiratory inhibitors fails to rescue the infected plant[251,252]. The de-methylation inhibitor (DMI) class of fungicides target an enzyme in the biosynthesis of ergosterol, which is essential for fungal cell wall integrity. This group of inhibitors offer curative properties at an early necrotrophic stage[253], due to their effective translocation and xylemic distribution throughout the leaf. The treatment of STB can still be effectively treated with both of these common classes of compounds but their specific single site of action has led to the selection of resistant *S. tritici* strains[40,85,177,208,210,211].

The evolution of resistant strains consistently stems from a target site mutation in response to single site inhibitors[37,39,98,183]. The role of the *S. tritici* alternative oxidase (StAOX) in this process, and pathogenicity, has yet to be fully established. Work by Miguez *et al*[185] provides evidence to suggest that the StAOX reduces the sensitivity of traditional Q_oI fungicides following infection. Alternative respiration[187,188] could facilitate the survival of resistant fungal strains during the

biotrophic or latent stage of growth when ATP demands are considerably reduced. Further evidence to prove these studies *in vitro* or *in planta* have yet to be undertaken for *S. tritici*.

To investigate the function and role of StAOX, a full characterisation of the enzyme and its specific activity is required. Since a protocol specific to fungal AOXs has yet to be determined, a methodology adapted from the well-studied *Trypanosoma brucei brucei* (TAO) provides a useful template. Isolated and membrane bound TAO protein will also be used as a tool for comparison when evaluating StAOX. This chapter outlines: homology modelling and sequence alignments for AOX species; the optimisation for the expression and purification of StAOX within an *E. coli* membrane; the regulation of StAOX *via* allosteric ligands; and a newly designed liposome preparation for the purified fungal AOX.

3.2 Sequence Alignment

The amino acid sequence for StAOX contains 342 residues with Blast analysis showing a sequence similarity of 41% with that of TAO and between 55-70% for the AOXs of over 70 fungal species. The mitochondrial targeting sequence for StAOX was identified using the Mito Prot algorithm[254] and consisted of 61 amino acids at the N-terminus of the protein, representing 18 % of the total number of amino acids for the protein. In comparison, TAO has a targeting sequence of only 24 amino acids (7%), and following application of the algorithm across AOX fungal species a large variation was seen, ranging from 25-64 amino acids. **Figure 17** shows a multiple sequence alignment using Clustal Omega highlighting targeting regions, as well as important structural features between a series of fungal AOXs and TAO.

The multiple sequence alignment in **Figure 17** shows a high conservation between StAOX and other fungal AOXs as well as with TAO. The glutamic acid (TAO numbering: E123, E162, E213 and E266) and histidine residues (TAO numbering: H165 and H269) responsible for ligating to the iron core are highly conserved throughout all AOX species (**Figure 17**). The residues that make up the proposed proton-coupled electron transport (PCET) network (TAO numbering: W65, N161, W247 and D265) and were fully conserved apart from W65 which is found to be a tyrosine residue (StAOX numbering: Y85) in StAOX. The catalytically important tyrosine residue (TAO numbering: Y220) was also found to be conserved across all species.

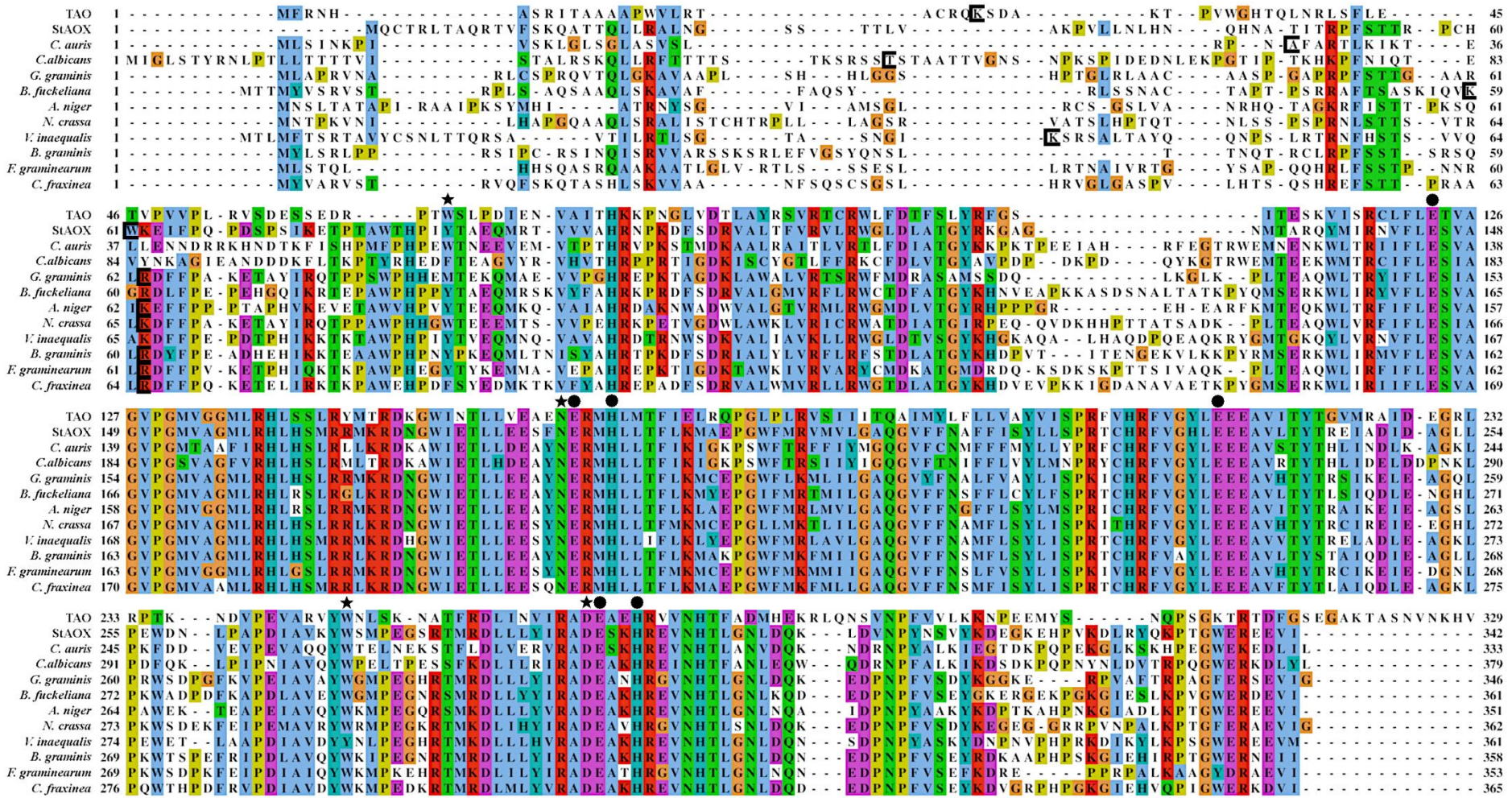

Figure 17 - Multiple Sequence Alignment between fungal AOXs in comparison to TAO. Accession codes as follows: TAO =Q26710; StAOX = F9XCX9; C. auris = A0A0L0NPQ3; C. albicans = O93853; G. graminis = J3P8W0; B. fuckeliana = Q8NJ59; A. niger = O74180; N. crassa =Q01355; V. inaequalis = Q9P429; B. graminis = Q8X1N9; F. graminearum = K3W1T7. Residues responsible for: Iron ligation = ●; PCET = ★. [= start of the N-terminus sequence following leader sequence removal.

3.3 Homology Modelling

The results of the multiple sequence alignment identified that StAOX shared a number of catalytically important residues with full conservation across both TAO and fungal AOX species. However, the blast analysis also identified only 41% conservation between the entire protein sequences of these two AOX species. To understand how these similarities and differences correlate to the overall structure of both the StAOX protein, and its hydrophobic cavity, a detailed assessment *via* molecular modelling was required. The solution of the TAO crystal structure to within a resolution of 2.3 Å with colletochlorin B bound[165], allows for detailed assessment of the enzyme. A crystal structure for StAOX, or for any fungal AOX, remains unsolved; and therefore, required the generation of a homology model *via* SWISS Model software[217] for the analysis of its structure.

Figure 18 presents an overview and side by side comparison of the TAO and StAOX structures. **Figure 18A** and **B** demonstrated that the surface and overall profile of the proteins was largely the same, suggesting that the overall structure of the AOX protein is unaffected by the 59% of non-conserved amino acid residues. **Figure 18C** and **D** provided further analysis of the secondary structure of the protein, and supported the molecular surface results, demonstrating that the position and orientation of the helices (α1-6) that make up the AOX protein are comparable between TAO and StAOX. The four-helix bundle (α2, 3, 5 and 6) that surrounds the diiron core, characteristic of diiron proteins, is also consistent between StAOX and TAO. The final comparisons made between TAO and StAOX (**Figure 18E** and **F)** are ones relating to the PCET network (TAO numbering: W65, N161, W247 and D265; StAOX numbering: Y85, N183, W270, D289), which is critical for catalysis in the O_2 reduction pathway. As stated in the multiple sequence alignment the only point difference between the two proteins is the presence of a tyrosine residue (Y85) in StAOX in place of a tryptophan residue (W65) in TAO.

A more detailed analysis of the active sites of both TAO and StAOX are displayed in **Figure 19**, highlighting the residues in close proximity to the diiron core and at the quinol head group binding site. The residues that make up the primary ligation sphere (TAO numbering: E123, E162, E213, E266, H165 and H269) along with the tyrosine (TAO numbering: Y220) that is involved in the catalytic mechanism are in the same orientation between TAO and StAOX. The residues responsible for binding to the quinol head group (TAO numbering: R93, R118 and T219), and the leucine residues (TAO numbering: L122 and L212) introducing a bottle- neck within the quinol binding site, are orientated in consistent manner across both proteins. This suggests that the 3D dimensional shape of the active site is consistent across both proteins. However, the cysteine residue (C119 in TAO) in close to proximity to the primary ligation sphere (**Figure 19A**) and catalytically important residues are not conserved in StAOX protein (**Figure 19B**) which

contains an aspartic acid residue (D141). How this aspartic acid residue affects the structure of the active site can only be confirmed through determination of the StAOX crystal structure.

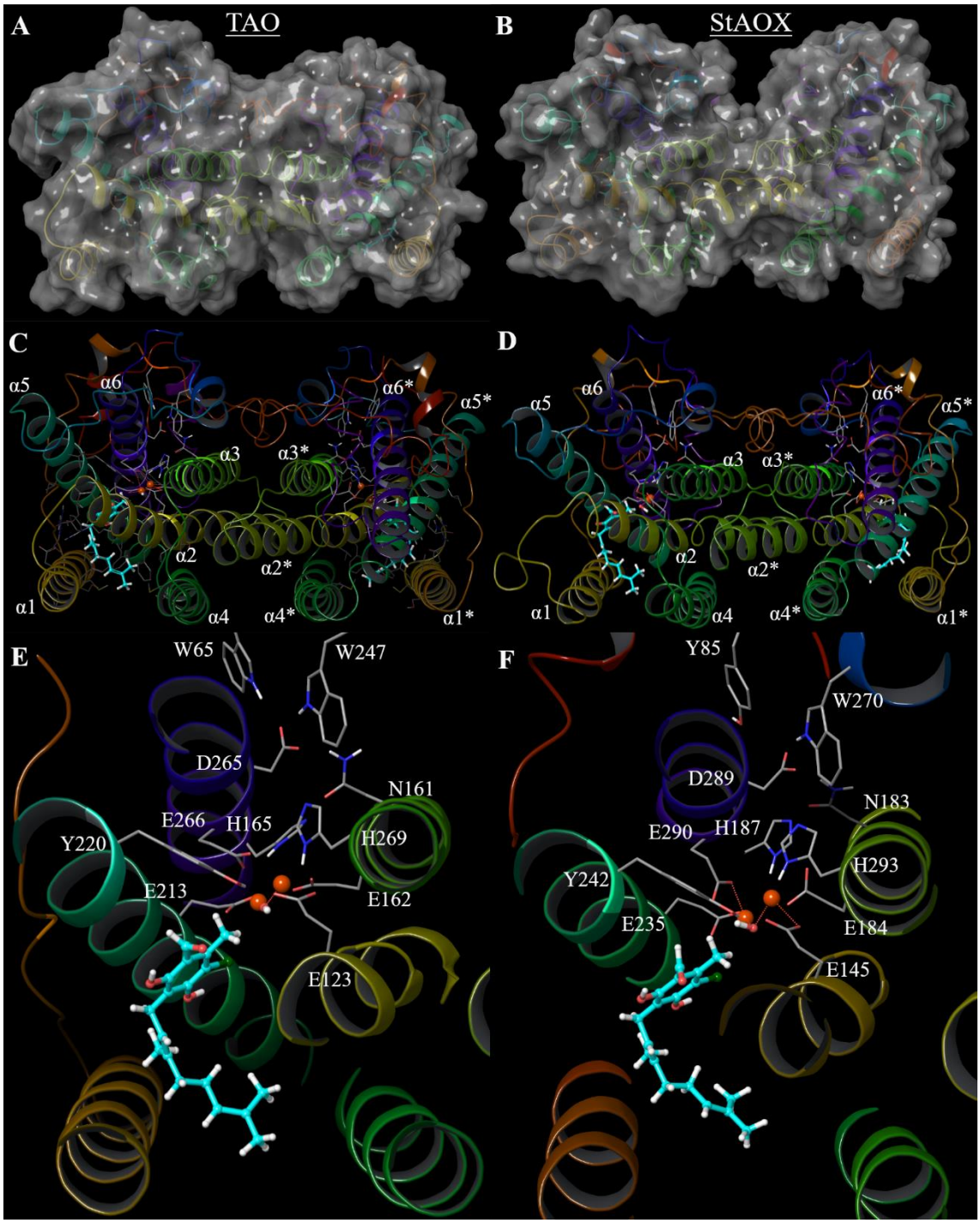

***Figure 18** - Overview of Structural Differences between the TAO crystal structure (PDB code: 3W54) and the StAOX Homology model generated from SWISS model with the AOX inhibitor, colletochlorin B, bound. A = Surface model of TAO; B= Surface model of StAOX; C= Ribbon view of TAO with colletochlorin B bound; D= Ribbon view of TAO with colletochlorin B bound; E= Detailed view of TAO the PCET network and diiron active site; F= Detailed view of StAOX PCET network and diiron active site.*

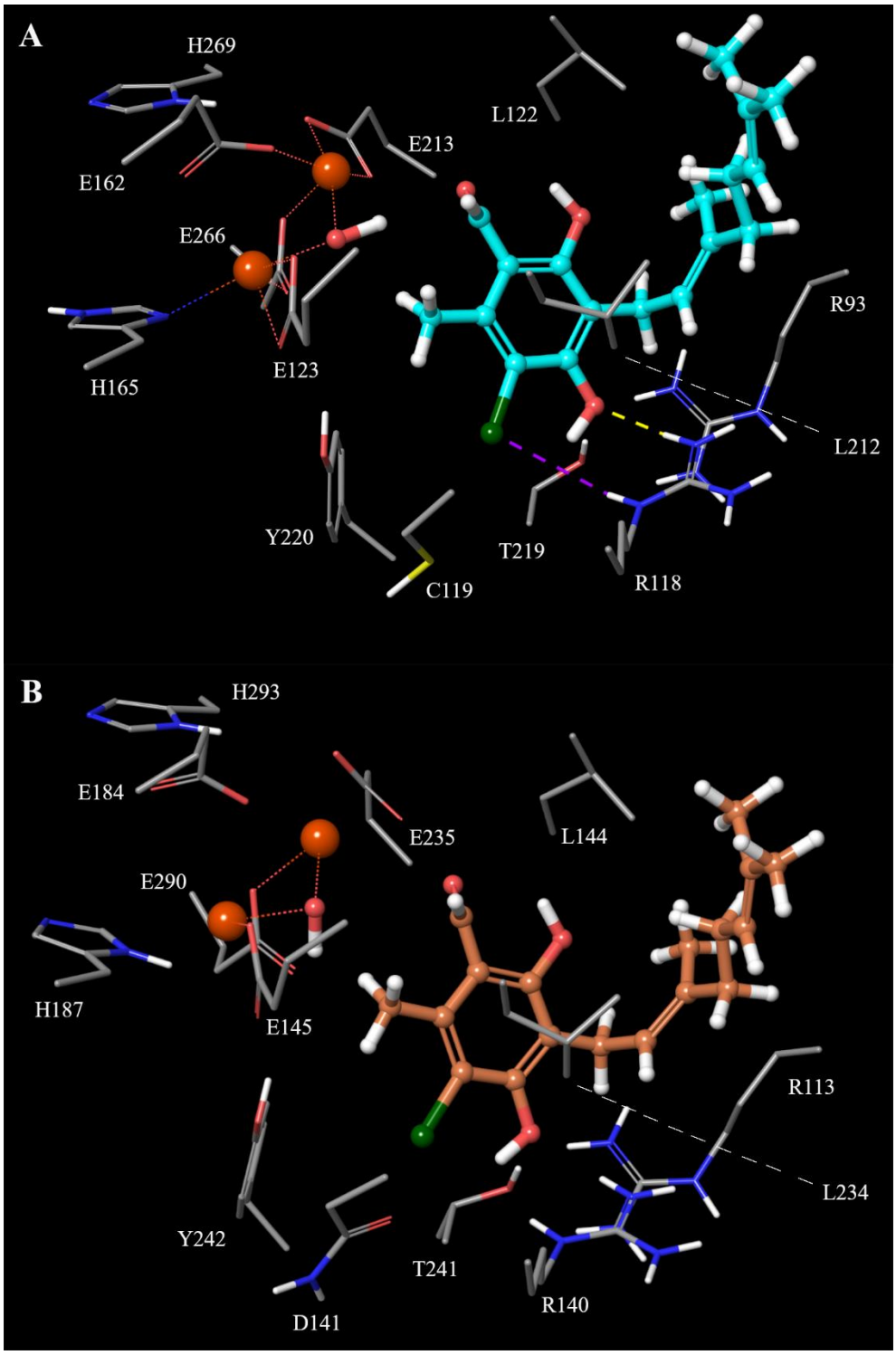

Figure 19 - Active sites of both TAO and StAOX with colletochlorin B bound, highlighting full conservation of important residues within the TAO (A) and StAOX (B) apart from the C119 residue in TAO and D141 residue in StAOX.

3.4 Overexpression and Optimisation of recombinant *S. tritici* and *T. brucei* AOX

The transformation and overexpression of recombinant TAO and StAOX in the FN102 *E. coli* strain was achieved according to the methodology outlined in **Section 2.2**. Initial results indicated a substantial difference in yields between TAO and StAOX *E. coli* membrane cultures, with average wet weights from a 4x 1L growth of 34 g and 22 g respectively. To investigate any significant differences between the size of the protein or level expression, a Coomassie and Western Blot analysis were carried out using the His-Tagged antibody (**Figure 20**). From the Western Gel analysis in **Figure 20A**, a clear difference in intensity can be seen between both bands. Since the same concentration of membrane was loaded from each sample (15 μg), the difference in intensity can be correlated to an increase in AOX expression.

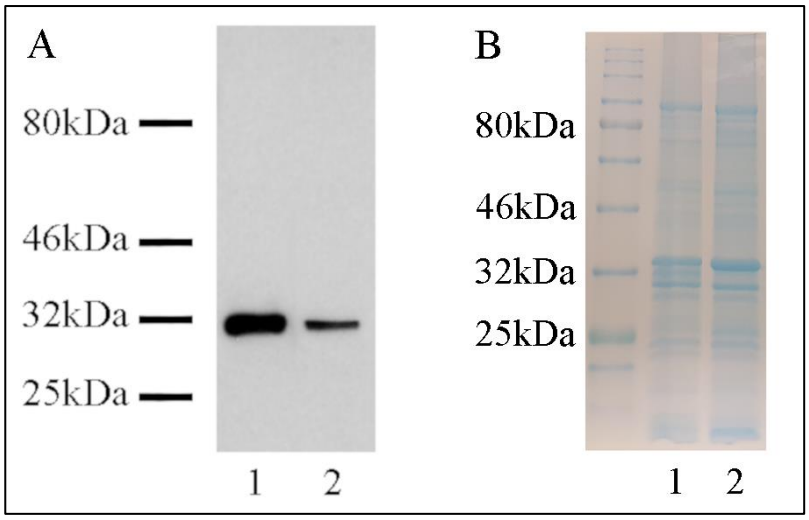

Figure 20 - Western Blot analysis (A) and Coomassie Gel (B) displaying TAO vs StAOX membrane samples. Sample lanes from Left to Right: 1 = TAO, 2 = StAOX each loaded with 15μg. Western Blot detected using His Tagged Antibody.

To determine whether the low expression and yield of StAOX protein was the result of either, the overexpression and *E. coli* growth experimental conditions, or a result of the activity or structure of StAOX, a thorough optimisation process was required. The variables influencing StAOX expression and activity including: structure (His or Twin-Strep Tag with and without leader sequence), biological buffer, inducer concentration (IPTG) and incubation temperature were investigated.

3.4.1 Structural Alterations

It was important to investigate the variables that influence protein folding such as changes to the StAOX amino acid sequence and thus structure. The removal of the mitochondrial targeting sequence has been found[212] to improve the specific activity of TAO and the incorporation of a Twin- Strep tag showed an improvement in purification efficiency. The creation of a new bacterial plasmid incorporating the Twin-Strep tag and without the mitochondrial targeting sequence was used to compare expression and specific activity of StAOX to that of the original His tagged plasmid (**Table 11**).

Table 11

Investigation into Structural Alterations to the StAOX protein

StAOX Purification Tag	Leader Sequence Cleavage Length	Specific Activity/ nmol of O_2 mg^{-1}. min^{-1}
His-Tag	-	15.6 ± 0.6
Twin-Strep Tag	Δ61	23.6 ± 1.2

Note. All assays performed in Tris buffer (pH 7.5, 50mM) with the addition of KCN (1 mM) and NADH (1.25 mM) and with measurements carried out on an Oroboros O2-k Respirometer. Sequence cleavage length determined using the Mito Prot algorithm[254].

3.4.2 Buffer Influence

The buffering capacity, ionic strength and ability to complex with metal ions are important factors to consider when selecting the correct buffer. The first use of a biological buffer occurs during harvest of *E. coli* membranes and resuspension in Tris buffer (pH~ 7.5) and is present during disruption, centrifugation, assay and storage. The use of a Good's buffer[255], MOPS, and its effect on the specific activity of StAOX following a successful harvest was analysed. MOPS buffer was selected due to its effective pH range within typical biological conditions (pH 6.5-7.9) and suitability for redox studies due to its lack of chelation to metal centres[256].

Figure 21 presents the specific activity of StAOX following harvest in MOPS and Tris, with comparable assay conditions in each corresponding buffer. An approximate two-fold increase in specific activity between a MOPS and Tris harvest is determined when assayed in MOPS. The

activity of the Tris harvest can also be enhanced following measurements in MOPS assay, suggesting the dilution of Tris buffer during assay measurements rescues StAOX activity.

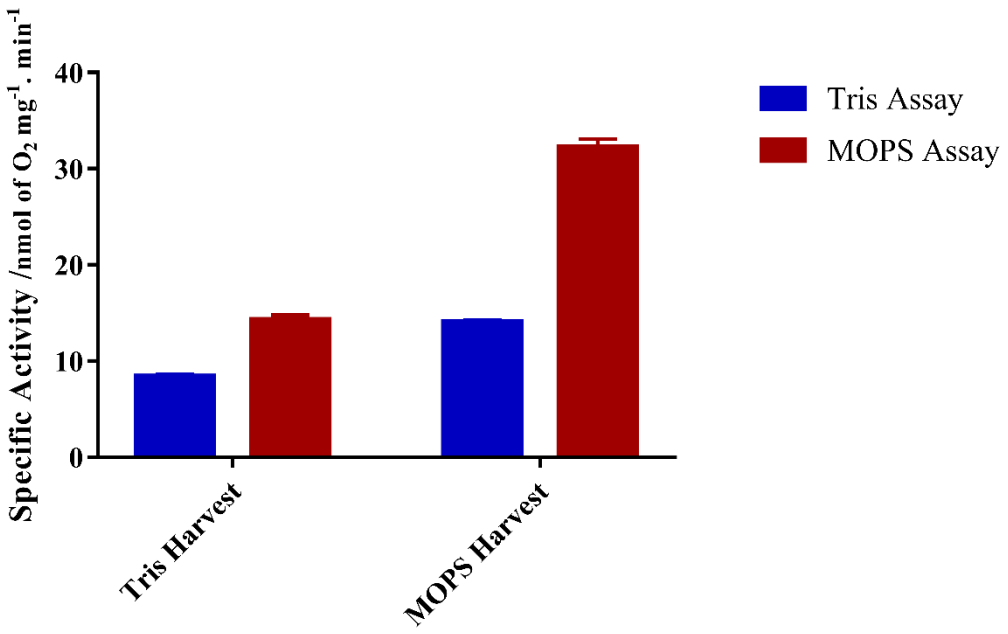

Figure 21 - The influence of Buffer on the Specific Activity of StAOX membrane samples. All assays performed at 25 °C in the appropriate buffer (2 ml) with the addition of KCN (1 mM) and the substrate, NADH (1.25 mM), to initiate AOX turnover.

To investigate the effect of the buffer change on the stability of the StAOX membranes; specific activities were also assessed following incubation of the samples over 24 hours for a series of typical temperatures. **Figure 22** displays the specific activity for StAOX samples following storage at both 4 °C and -20 °C in either MOPS or Tris buffer as well as under both buffer assay conditions. Following storage at 4 °C and 20 °C the MOPS harvest samples consistently retained the most activity when assayed in the same buffer and the overall baseline activity was significantly higher than Tris. In contrast, when measurements were performed in Tris buffer and the *E. coli* membranes were harvested in Tris, the StAOX activity was diminished. Furthermore; assay measurements performed in MOPS buffer rescued the activity lost after a Tris harvest and provided an increase in baseline activity after storage at -20 °C. These results are important to consider when performing inhibition studies, as the measured activity should correlate to a dose response rather than deterioration of the StAOX protein.

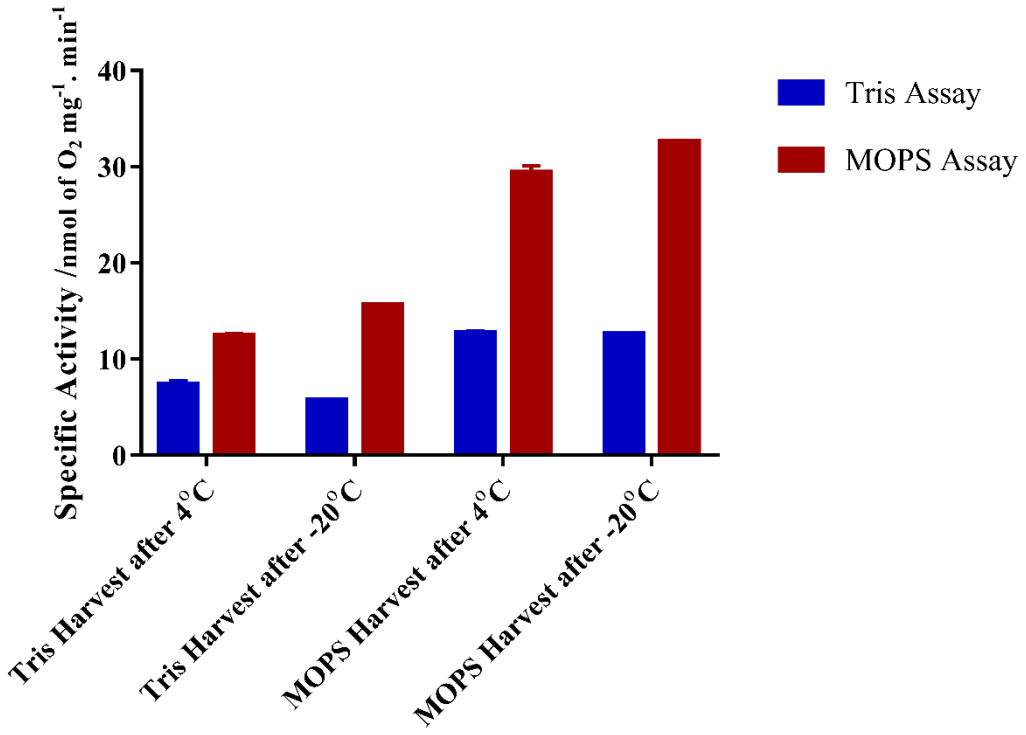

Figure 22 – Stability of enzymatic activity of StAOX E. coli membrane samples following 24 hr storage at 4 °C and -20 °C under both Buffer Harvest and Assay Conditions. All assays performed with the appropriate buffer at pH 7.5 (2 ml), KCN (1 mM) and NADH (1.25 mM). Baseline activities (nmol of O_2 $min^{-1}.mg^{-1}$) prior to storage: Tris Harvest with Tris Assay = 8.38 and MOPS Assay = 14.08; MOPS Harvest with Tris Assay = 14.28 and MOPS Assay = 32.26.

3.4.3 IPTG Concentration

The effect of the concentration of the protein expression inducer, IPTG, was investigated to determine whether the lack expression was a consequence of insufficient sugar concentration to transcribe the *lac operon* operator. The effect of differential concentrations of IPTG was evaluated by wet weight, western blot and enzyme specific activity. **Figure 23** provides an overview for the influence of IPTG concentration on the specific activity and wet weight yield for a given StAOX *E. coli* expression. The wet weight per litre of broth was largely unaffected by the concentration of IPTG but the enzymatic activity was shown to be maximised at 300 μM.

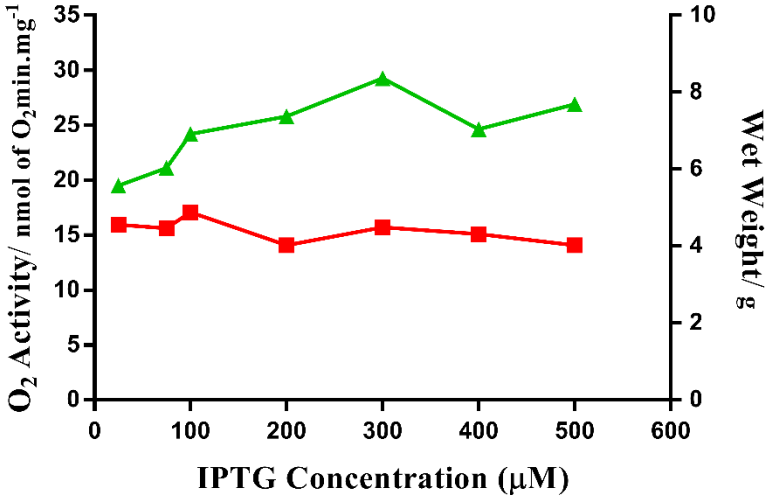

Figure 23 - Effect of IPTG on StAOX Expression. Wet weight of E. coli membrane /L of broth (Red) and Specific O_2 Activity (Green)

The western blot analysis (**Figure 24**) showed a slight increase in expression for the 300 µM band, in accordance with the increase in enzymatic activity, but still remained lower respectively than that of TAO. It was clear that a small advantage may be gained from using an IPTG concentration of 300 µM, but not significant enough to produce comparable expression to that of TAO.

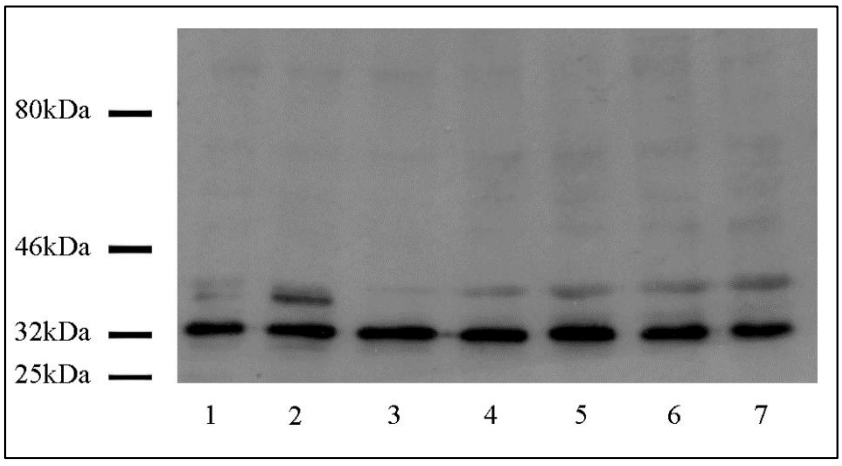

Figure 24 - Western Blot Analysis displaying IPTG Concentration Screen. Sample lanes from Left to Right: 1= 25 µM, 2 = 75 µM; 3 = 100 µM; 4 = 200 µM; 5 = 300 µM; 6= 400 µM; 7 = 500 µM. Loaded with 15 µg of protein and detected using the Twin-Strep antibody.

3.4.4 Incubation Temperature

The incubation temperature for batch *E. coli* membrane preparations has a significant influence on the protein quality and biomass production. An increase in post induction temperature was used to investigate any promotion in *E. coli* cell growth or overall protein expression. As shown in **Table 12**; a post induction temperature rise provided a boost in wet weight combined with an increase in enzymatic activity.

Table 12

Effect of temperature on the specific activity and yield of a typical StAOX overexpression preparation

Temperature	Wet Weight/ g	Specific Activity/ nmol of O_2 min^{-1}. mg^{-1}
30 °C	7.29	25.57 ± 0.52
37 °C	7.63	30.53 ± 1.17

Note. All assays performed in MOPS (65 mM, pH 7.5) with the addition of KCN (1 mM) and NADH (1.25 mM). When carrying out the *E. coli* membrane preparation methodology outlined in **Section 2.2**, incubation temperature was increased following AOX induction with IPTG (300 μM).

3.4.5 Final StAOX Yield and Activity Comparisons

The optimisation of the experimental conditions and structural alterations for the overexpression of the StAOX *E. coli* membrane protocol, demonstrated an improvement in both wet weight yield and specific activity of the protein. The yield of StAOX *E. coli* membrane samples was increased by 45% and the enzymatic activity was effectively doubled as shown in **Table 13**. Comparisons were also made to both protozoan (TAO) and plant (SgAOX) AOX species, highlighting a significant difference in specific activity between the enzymes. StAOX turnover only is only 9.6% of the plant activity and 21% of the protozoan activity. Since the expression protocol was optimised through the alteration of a series of parameters, it could be suggested that the low AOX turnover is characteristic of the protein itself. However, the bacterial *E. coli* membrane system is far removed from the native StAOX membrane found in the mitochondria of fungi. It should therefore be noted that further optimisation of the expression of StAOX may improve this baseline activity further.

Table 13

Measured Specific Activity and Wet Weight Yields for E. coli Membrane preparations

AOX Preparation	Wet Weight/ g	Specific Activity/ nmol of O_2 $min^{-1}.mg^{-1}$
StAOX - Original	22 ± 0.5	15.6 ± 0.6
StAOX - Optimised	32 ± 0.7	32.6 ± 0.1
TAO	34 ± 0.2	685 ± 9.4
SgAOX	N/A	313 ± 18*

Note. *Unpublished data carried out by Fei Xu. All assays performed in MOPS (65 mM, pH 7.5) with the addition of KCN (1 mM) and NADH (1.25 mM) except for the original StAOX preparation which was carried out in Tris buffer (50 mM, pH 7.5). Stated values are the average of 3 isolations ± standard deviation.

3.5 Regulation of StAOX

3.5.1 Screening of Classical Regulators

Since the baseline enzymatic activity could not be improved through optimisation of the overexpression protocol, it could be that the StAOX is activated and regulated through a stress response pathway, to increase its biological activity when required. Our understanding of the plant AOX shows a regulation through the use of the α-keto acid, pyruvate, providing an activation through an allosteric ligand. As mentioned earlier, StAOX does not contain either the QDC/ENV motifs or regulatory cysteines to provide a site for activation through pyruvate; but it is yet to be reported as to whether StAOX responds to allosteric ligands at an alternative binding site. To investigate potential regulation, a series of classical regulators were investigated by measuring the specific activity of StAOX in *E. coli* membrane samples.

Figure 25 shows the response of the specific activity of the StAOX when incubated with a range of purine nucleotides and keto-acids. The lack of regulation from pyruvate was confirmed supporting the hypothesis that both the ENV/QDC motif and the regulatory cysteines are required for activation. Incubation with GMP (1.5mM) and IMP (1.5mM) showed a dramatic increase in specific activity for oxygen, with 4 times the basal rate for both nucleotides. However, the structurally related AMP (1.5mM) showed a similar, yet significantly smaller activation of StAOX (2.5 times fold change), suggesting a structural property or biosynthetic pathway unique to both GMP or IMP is important for activation. These results corroborate with previous work by Siedow *et al*[164] suggesting the fungal AOX is activated by nucleotides, however the activation was found to be smaller in the literature.

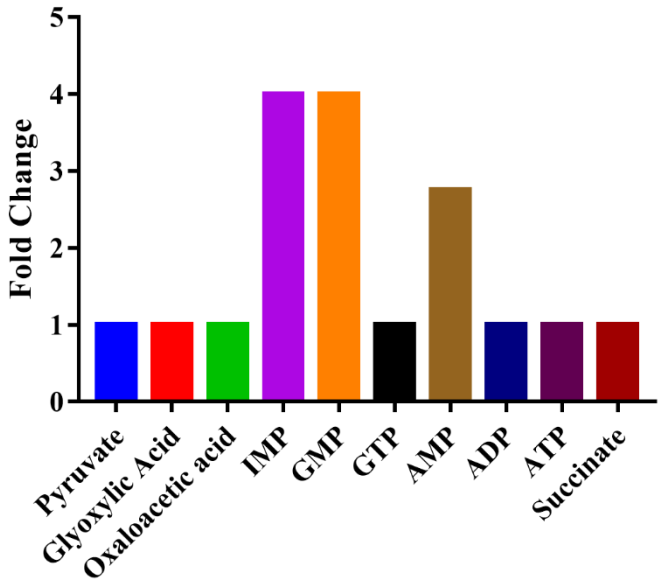

Figure 25 – Influence of Classical Regulators on the Specific Activity of StAOX as measured by fold change. All regulators were used at a concentration of 1.5 mM. Regulators were added after KCN (1mM) and NADH (1.25 mM) additions against StAOX E. coli membrane samples in MOPS buffer (65mM, pH 7.5). Baseline activity for StAOX E. coli membrane samples = 30.21 ± 0.8 nmol of O_2 $mg^{-1}.min^{-1}$.

Further assessment of the GMP activator was also carried out to ascertain the maximal concentration for effective StAOX stimulation. The maximum concentration correlating to a maximum fold change in activity was 7 mM of GMP (**Figure 26**).

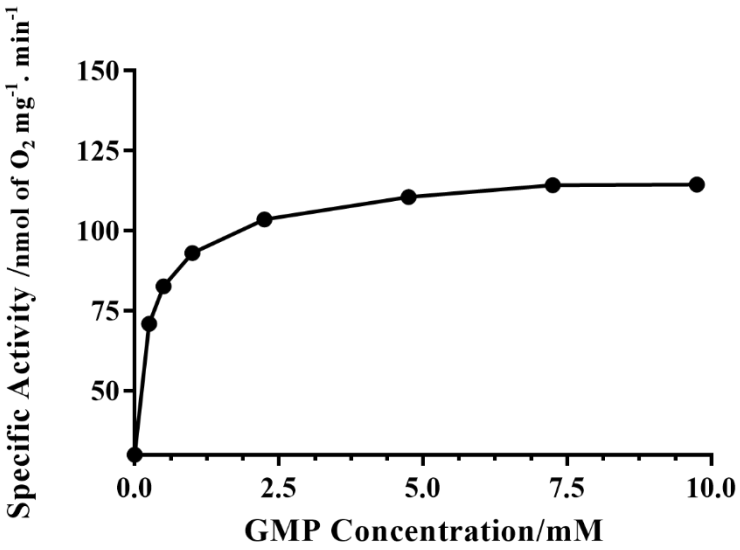

Figure 26 - Titration of GMP on StAOX E. coli membrane samples to determine the maximum concentration for activation. All assays carried out in MOPS buffer (65 mM, pH 7.5), KCN (1 mM) and NADH (1.25 mM). Baseline Activity for StAOX = 32. 08 ± 0.3 nmol of O_2 mg^{-1}.min^{-1}.

3.5.2 In silico evaluation of regulator binding sites

The discovery that StAOX is activated by purine nucleotides allowed for an *in-silico* assessment of potential binding sites for the activation of the enzyme. Using MOE and Maestro molecular modelling software, a suitable site for nucleotide binding was found on the matrix side of the protein surface, as well as at the dimer interface. Docking of the GMP and IMP molecules within the monomer and dimer binding sites generated docking scores that correlate to a requirement for millimolar concentration of the purine nuceltoides (**Table 14**). The nucleotide AMP was also docked in the same monomer site with a lower docking to score to that of GMP and IMP (**Table 14**) which correlated to the activation data shown in **Figure 25**.

Table 14

Purine Nucleotide Docking Scores to the StAOX Homology Model

	Docking Score (S)	
Purine Nucleotide	*Monomer*	*Dimer*
GMP	-7.08	-6.56
IMP	-6.94	-6.21
AMP	-6.71	-5.67

Note. StAOX structure energy minimised according to Maestro and MOE molecular modelling software guidelines.

Using GMP as an example, an overview of the interaction at both monomer and dimer binding sites for purine nucleotides is displayed in **Figure 27**. **Figure 27A** and **B** display the GMP binding position on the matrix side of the StAOX surface model for the monomer and dimer, respectively. Further analysis of the StAOX helices show that the monomer binding site (**Figure 27C**) is created by both α3 and α6 helices whereas the dimer binding position (**Figure 27D**) is created at the dimer interface between α3 and α3*. To provide further context as to the position of the GMP binding sites on the StAOX structure; **Figure 27D** and **E** provides a view of GMP binding in relation to the diiron active site and PCET network for both sites. **Figure 28** highlights the residues potentially responsible for the interactions at these binding sites, with hydrogen bonds at residues P83, E179, T176 and K292 for the monomer binding site and hydrogen bonds with the E179 on α3 helix and the E175 on α3* helix. The interactions with the purine nucleotides are clearly reduced in the dimer position which are highlighted by the lower docking scores in **Table 14**.

It is, however, important to note that the site mapping results obtained from the analysis of the StAOX homology model is preliminary and purely theoretical. Mutagenesis studies of the key residues P83, E179, T176 and K292 at the monomer binding site would be required to confirm the presence of this binding site. Equally the stabilisation of a dimeric conformation of the enzyme, together with a nucleotide binding site between each StAOX monomer, would require investigation through circular dichroism. However, careful analysis of both the TAO (protozoa) and SgAOX (plant) amino acid sequence aligned with the StAOX protein, highlight the absence of the residues implicated in the monomer binding site. For example, the TAO protein does not contain the E179 or K292 residues. Similarly, the SgAOX sequence displays a lack of conservation for residues P83, T176 and K292 within the StAOX monomer nucleotide binding site. Since neither of these enzymes respond to nucleotide activation (unpublished data), this analysis supports the site mapping data and docking results from MOE and Maestro software.

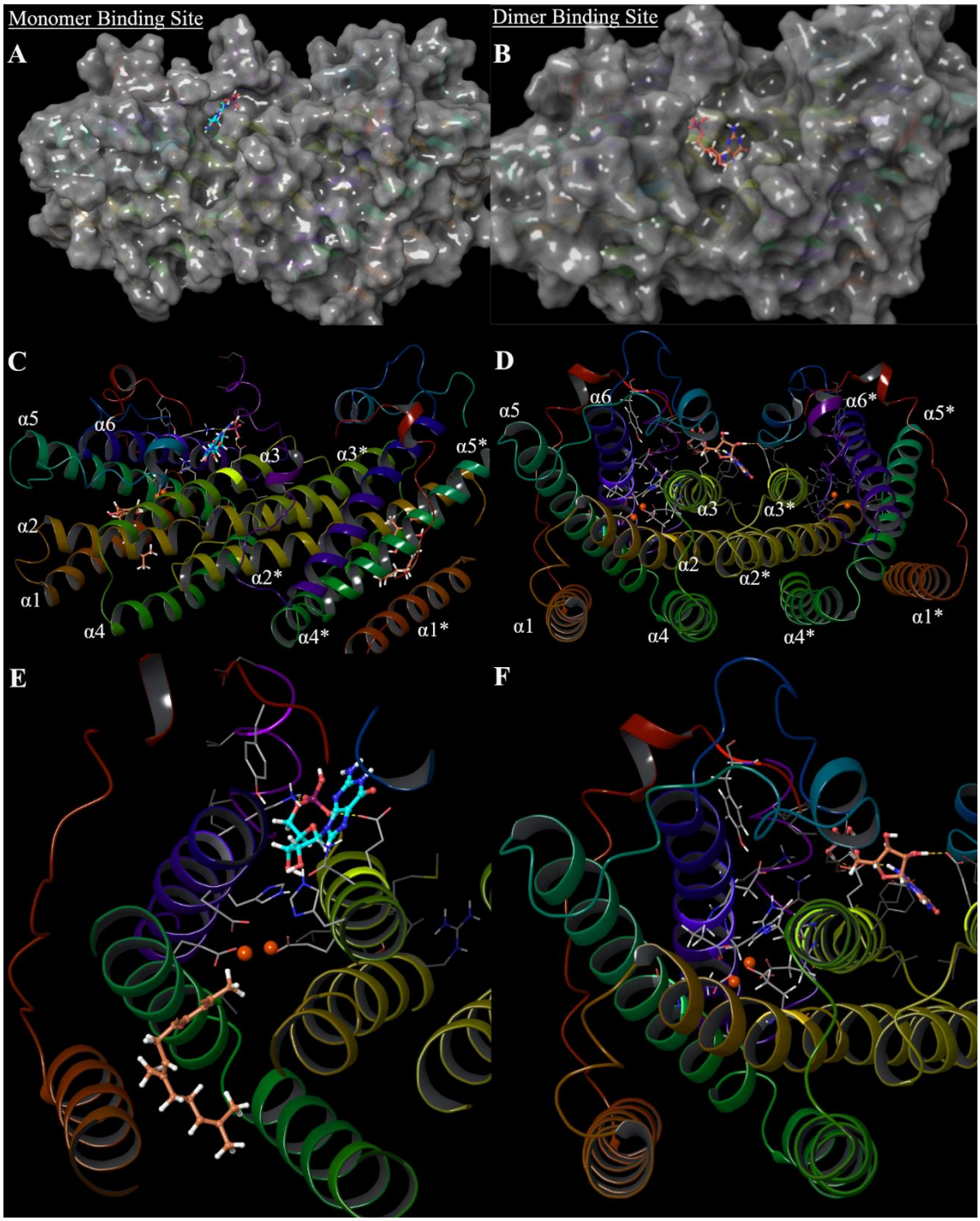

Figure 27 - Docking results on the StAOX homology model for the allosteric ligand, GMP, including colletochlorin B bound, the PCET network and the iron ligation sphere. I. A= Surface model for monomer bound GMP; B= Surface model for Dimer interface binding; C= Ribbon Representation of GMP bound monomer; D= Ribbon representation of GMP bound at Dimer Interface; E= GMP location in regards to the PCET network; F= GMP binding at the dimer interface with the PCET network highlighted.

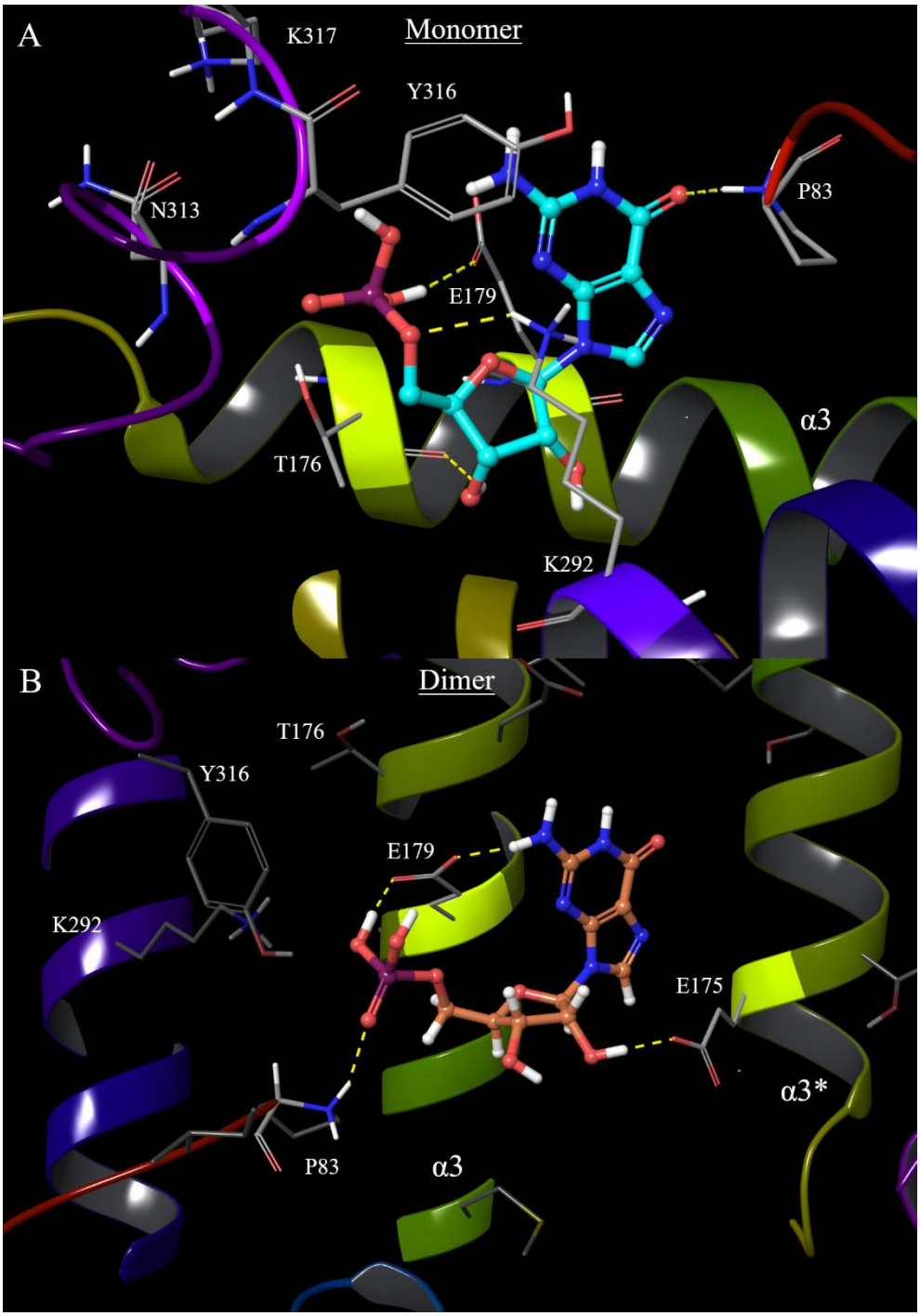

Figure 28 - Binding modes of GMP on the StAOX homology model at both monomer (A) and dimer (B) sites. All H-bond interactions with residues that make up the respective GMP binding sites are represented by the yellow dotted lines.

3.6 Purification of TAO

In order to evaluate an isolated inhibition and binding interaction between the AOX protein and the compounds synthesised in **Chapter 4**, a purified AOX protein sample was required. The only established protocol for purification of the AOX protein is that from TAO; and therefore, it would be beneficial to purify the TAO protein to act as a comparison to that of any purified StAOX samples. Although the results for inhibiting the TAO protein may not correlate directly with StAOX protein it will still help to clarify the binding site differences outlined in Section.

The inclusion of either the His or Twin Strep tag on the N-terminus of the AOX protein provided a means for facile purification for the *T. brucei* species. The purification for TAO was performed according to the published[257–259] methodology outlined in **Section 2.3**: with the use of either TALON® beads for the His-tagged protein; or the high affinity Strep-Tactin® beads for the Strep-tagged proteins. Previous studies for TAO[257,259] found that the optimal conditions required the use of Octyl Gallate (1.4%) for the solubilisation of the protein, and the use of a low concentration of DDM (0.042%) to provide stability for the eluted protein. The purified protein was analysed by measuring its enzymatic activity (**Table 15**), in regards to its substrate quinol, as well as using Western Blot Analysis (**Figure 29**).

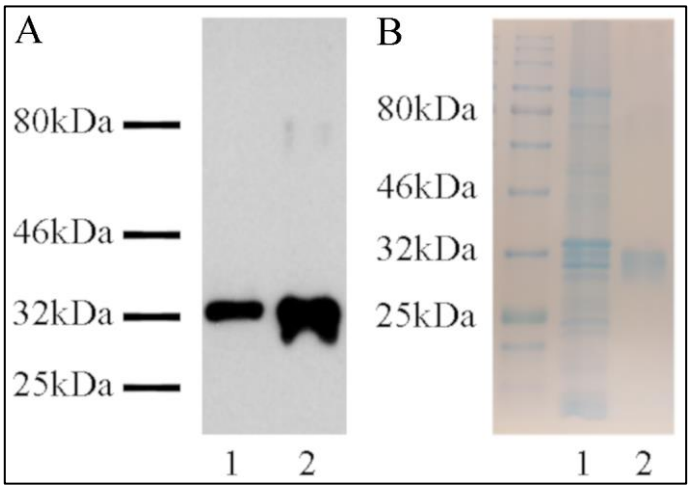

Figure 29 - Western blot analysis (A) and Coomassie gel (B) for TAO membrane and pure protein. Sample lanes: 1= TAO membrane; 2 = TAO pure. Western blot analysis analysed using the AOA1 antibody. Each lane loaded with 15 µg of protein.

Table 15

Purified TAO Specific Activity and the Effect of the Purification Tag

Purified TAO sample	Specific Activity/ μmol of Q_2H_2 mg^{-1}. min^{-1}
TAO- His	17 ± 0.7[†]
TAO- Twin-Strep	79.4 ± 6.3

Note. [†]His-tagged protein contains the full StAOX sequence and the Twin-Strep protein is without the mitochondrial targeting sequence (Δ61). All assays performed spectrophotometrically measuring at 278 nm in MOPS (65 mM, pH 7.5) and with the addition of Q_2H_2 (150 μM).

3.7 Purification of StAOX

Since the isolation and purification of StAOX is yet to be determined in the published literature to date; the established purification protocol for TAO required modification to accommodate the fungal AOX. The net charge on the Δ61 Twin-Strep StAOX protein differs in comparison to that of the Twin-Strep TAO protein, with isoelectric points of 6.67 and 8.42, respectively. It was unclear what role the charge on the protein will have following solubilisation and elution, it wass therefore important to investigate the influence of varying conditions and detergents on both recovery and enzymatic activity. The incorporation of either a His or Twin Strep tag provided a means of separation in a similar manner to that of TAO. The StAOX *E. coli* membrane samples without the leader sequence (Δ61) and the Twin-Strep tag were taken forward through purification optimising steps, in the expectation that a similar improvement in yield and specific activity, could be achieved as reported by Jones *et al*[260].

3.7.1 Solubilisation

The most critical stage for purification of membrane bound proteins occurs upon solubilisation of the target enzyme away from its natural lipid environment. The use of mild detergents ensures sufficient disruption of the lipid membrane to cleave the desired protein and lipids into stabilising micelles. The strength and concentration of the detergent play a significant role in the amount of lipid and protein incorporated into the final detergent micelle, and the subsequent stability of the membrane protein. Therefore, a range of detergents containing both positively and negatively charged moieties were analysed and both protein recovery and enzymatic activity were determined.

Table 16

Solubilisation Buffer Screening for StAOX

Detergent	Protein Recovery/ mg	Specific Activity/ μmol of Q_2H_2 mg^{-1}. min^{-1}
Dodecyl Maltoside (DDM)	1.25	0.002
Octyl glucoside (OG)	0.33	0.0031
FC12	3.32	0.04
UDAO	0.05	-
MEGA-9	0.04	-

Note. All assays performed spectrophotometrically measuring at 278 nm in MOPS (65 mM, pH 7.5) and with the addition of Q_2H_2 (150 μM).

The Western analysis in **Figure 30** shows that the detergents DDM, OG and FC12 provide good solubilisation with only trace quantities present in the unsolubilised fraction. However, from Western blot analysis, a clear distinction between the detergents could not be made, and therefore a focus on the highest protein recovery and enzymatic activity were assessed. It is clear from **Table 16**, that FC-12 provided the best solubilisation, with the highest protein recovery and specific activity for the substrate quinol.

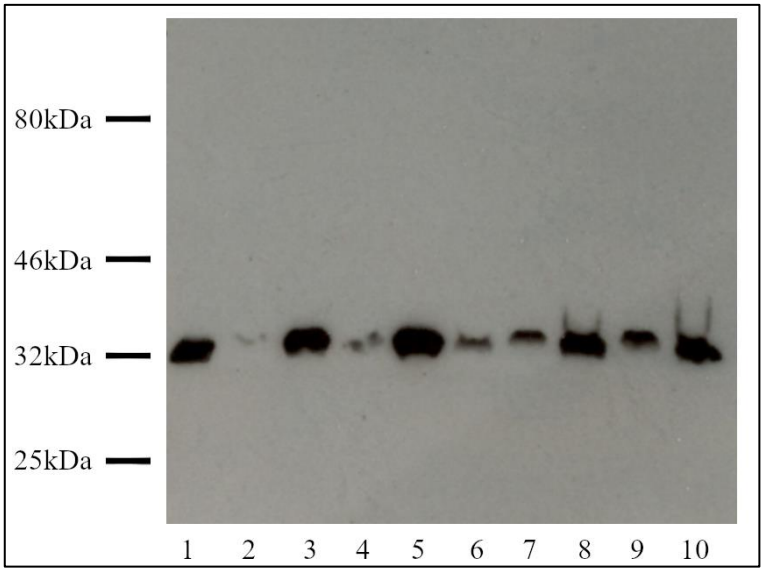

Figure 30 - Western blot analysis investigating the optimal deteregnt for StAOX solubilisation. Sample Lanes: 1 = DDM sol.; 2 = DDM pellet; 3= OG sol.; 4 = OG pellet; 5 = FC-12 sol.; 6 = FC-12 pellet; 7 = UDAO sol.; 8 = UDAO pellet; 9 = MEGA-9 sol.; 10= MEGA-9 pellet. Western blot analysed using a Twin-Strep antibody. All sample lanes loaded with 15 μg of protein.

The salt concentration present in the solubilisation buffer can affect both the solvation sphere surrounding the protein-lipid micelles, as well as stabilising the charge on the protein in solution. The effect of a range of NaCl concentrations were assessed in similar manner as the detergent screen with both enzymatic activity and protein recovery assessed in **Figure 31**. The data presented in **Figure 31** shows that maximal enzymatic activity was achieved at a salt concentration of 200 mM with the second highest protein recovery. Western Blot Analysis (**Figure 33A**) was also carried out to identify the highest specific AOX concentration within the solubilised StAOX sample. A concentration of 500 mM displayed the highest concentration of AOX, however, since this optimisation investigation was concerned with maximising enzymatic activity a salt concentration of 200 mM was taken forward to further optimisation steps.

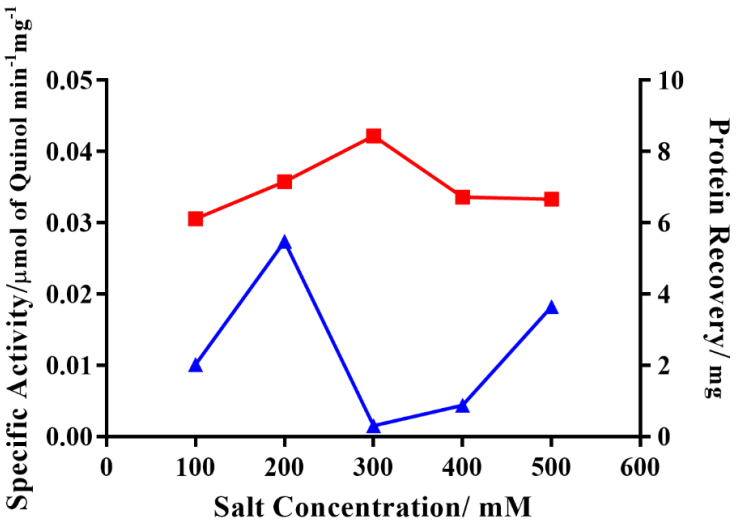

Figure 31 - Effect of Salt concentration on the Specific activity (Blue) and Protein recovery (Red) on solubilised StAOX. Specific activity assays performed spectrophotometrically measuring at 278 nm in MOPS (65 mM, pH 7.5) and with the addition of Q_2H_2 (150 µM).

To understand the effect of pH on the enzymatic activity and effective solubilisation of the StAOX protein, a series of MOPS buffers containing FC-12 (2%) and NaCl (200 mM) were prepared. The specific activity and protein recovery data shown in **Figure 31**, along with the Western Blot Analysis (**Figure 33B**), supported the use of a pH close to biological conditions (pH 7.5).

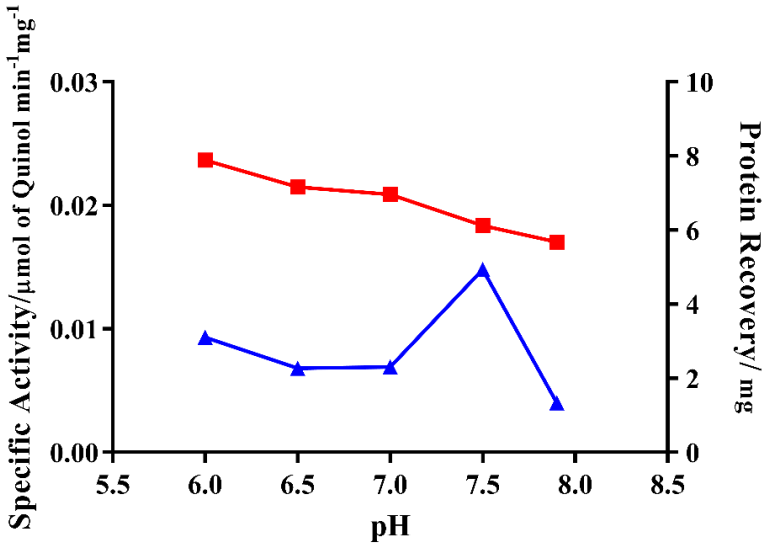

Figure 32 - Effect of pH on the Specific Activity (Blue) and Protein Recovery (Red) on solubilised StAOX. Specific activity assays performed spectrophotometrically measuring at 278 nm in MOPS (65 mM, pH 7.5) and with the addition of Q_2H_2 (150 µM).

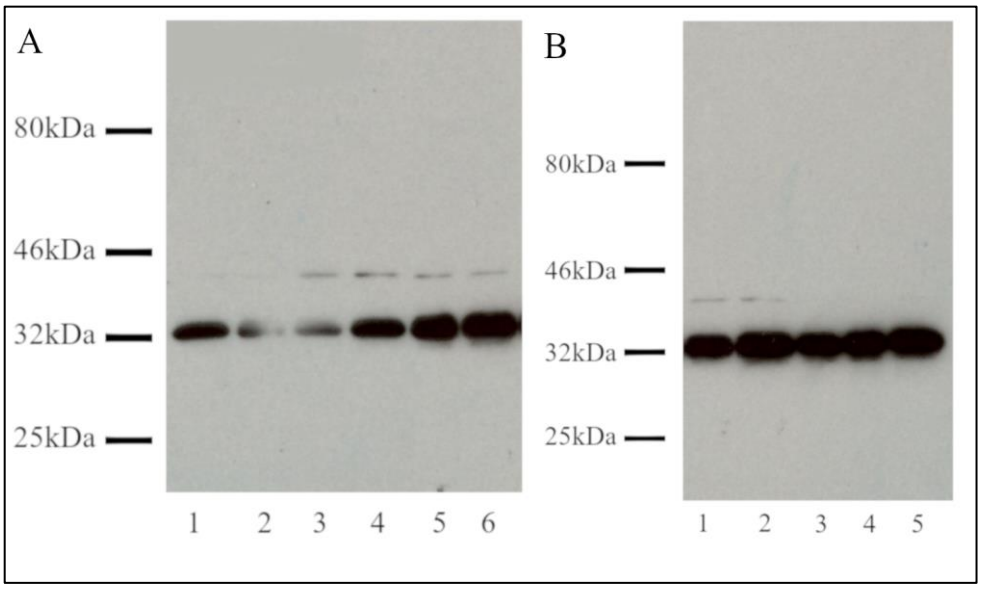

Figure 33 - Western blot analysis investigating the influence of Salt Concentration (A) and pH (B) on solubilised StAOX protein. Samples lanes A: 1 = 200 mM $MgSO_4$; 2 = 100 mM NaCl; 3 = 200 mM NaCl; 4 = 300 mM; NaCl 5 = 400 mM NaCl; 6 = 500 mM NaCl. B: 1 = MES pH 6; 2 = MOPS pH 6.5; 3 = MOPS pH 7; 4 = MOPS pH 7.5; 5 = MOPS pH 7.9. Analysis carried out using the Twin-Strep antibody.

As described earlier, the extent to which the lipid membrane is disrupted and incorporated into a protein-lipid micelle is dependent on the detergent concentration. A series of detergent concentrations were analysed according to both specific enzymatic activity and protein recovery in a similar manner to previous optimisations as shown in **Figure 34.** Western Blot Analysis (**Figure 35**) demonstrated good solubilisation across all detergent concentrations, however the increase in enzymatic activity and protein recovery favoured the use of a 2% FC-12 detergent concentration.

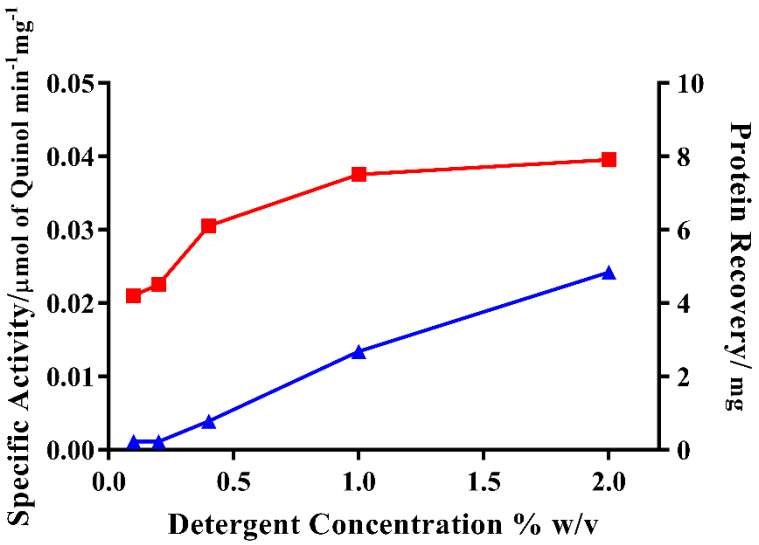

Figure 34 - Effect of detergent concentration on the Specific Activity (Blue) and Protein Recovery (Red) on solubilised StAOX. Specific activity assays performed spectrophotometrically measuring at 278 nm in MOPS (65 mM, pH 7.5) and with the addition of Q_2H_2 (150 µM).

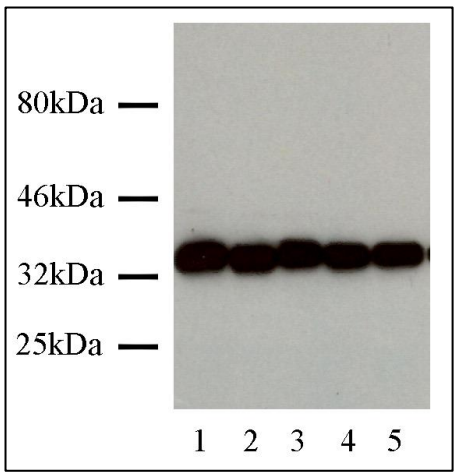

Figure 35 - Western Blot analysis for solubilised StAOX protein and the influence of FC-12 concentration on StAOX recovery. Samples lanes: 1 = 0.1%; 2 = 0.2%; 3 = 0.4%; 4 = 1%; 5 = 2%. Analysis performed using Twin- Strep antibody and with samples lanes loaded with 15 µg.

3.7.2 Elution

The best solubilisation buffer conditions for StAOX were taken forward, and acted as a comparison when establishing the optimal stabilising elution detergent. The concentration of the elution detergent was reduced by ten-fold, as a high concentration was no longer required to disrupt lipid membranes. The stabilising effect of the elution detergent and buffer, ensure the correct folding of membrane proteins within a detergent micelle; and therefore, the elution detergent required screening in the same manner as solubilisation.

Table 17

Specific Activity in Response to Different Elution Buffer Conditions

	Protein Recovery (mg)	
Detergent	*DDM*	*FC12*
DDM	0.04	0.05
OG	0.003	0.012
FC-12	0.33	0.40
UDAO	0.005	-
MEGA -9	0.07	-

Note. Specific activity assays were performed spectrophotometrically measuring at 278 nm in MOPS (65 mM, pH 7.5) and with the addition of Q_2H_2 (150 μM).

Analysis by Western blot (**Figure 36**) showed that following solubilisation and purification, an elution buffer containing either FC12 or DDM provides the highest StAOX concentration. The estimation of the protein recovery listed in **Table 17** supported this analysis.

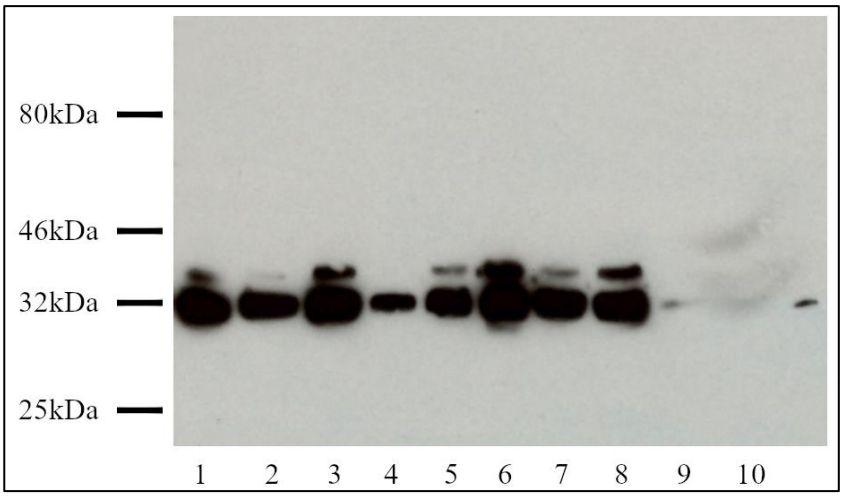

Figure 36 - Western Blot analysis investigating a series of elution detergents under both DDM and FC-12 solubilisation conditions for StAOX. Analysed using the Twin- Strep antibody. Samples loaded with 10 µl of purified StAOX protein sample.

3.7.3 Final Optimised Purified StAOX Conditions

Following extensive optimisation of the conditions for purifying StAOX, it was found that the purified protein still exhibited a low specific activity and recovery weight in comparison to TAO. However, purification of the His-tagged protein demonstrated a considerable increase in specific activity in comparison to the Twin-Strep tag protein (***Table 18***). It could be suggested that either the loss of the leader sequence or difference in purification Tag was responsible for the loss in activity. However, it may also be the case that the StAOX is more reliant on the lipid membrane to exhibit high quinol oxidation.

Table 18

Purified StAOX Specific Activity and the Effect of the Purification Fusion tag.

Purified StAOX Sample	Specific Activity/ µmol of Q_2H_2 mg^{-1}. min^{-1}
StAOX - His	0.450 ± 0.025
StAOX – Twin- Strep (Δ61)	0.0242 ± 0.002

Note. Specific activity assays were performed spectrophotometrically measuring at 278 nm in MOPS (65 mM, pH 7.5) and with the addition of Q_2H_2 (150 µM).

3.8 Proteoliposome Incorporation

The assessment of enzymatic activity of purified StAOX was further evaluated in a self-assembled artificial membrane system, known as a proteoliposome, complete with a quinone reduction cycle. This artificial membrane system mimics the natural lipid environment for membrane bound proteins, as well as facilitating the use of the native substrate for the AOX, Q_{10}, which due its hydrophobicity, prevents its use with purified protein samples. In contrast to the *E. coli* membrane samples, the concentration of the substrate can be determined, allowing for the measurement of precise enzyme kinetics such as K_m and V_{max} constants. The proteoliposomes were prepared according to a modified protocol by Jones *et al*[212], incorporating solubilised Twin-Strep StAOX, an external NADH dehydrogenase (NDI) and the natural isoprenoid substrate quinone (Q_{10}). **Figure 37** provides an overview of the proteoliposome system and quinone reduction cycle.

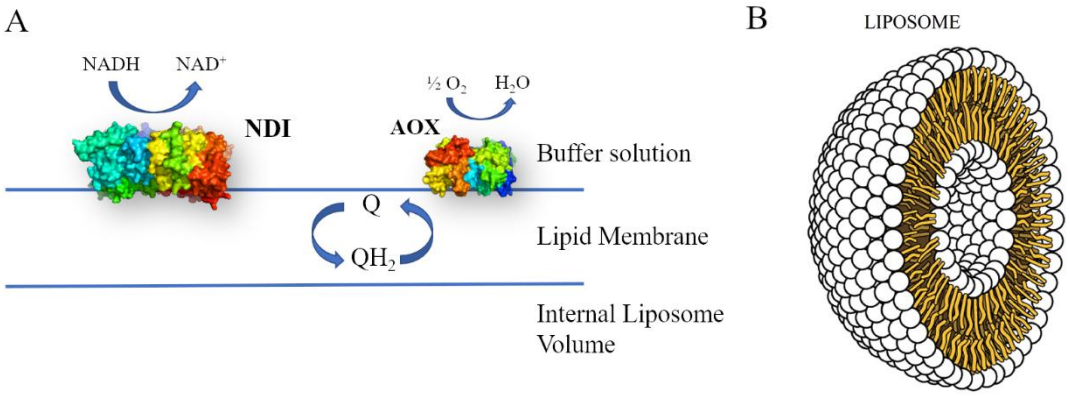

Figure 37 - A = Overview of Quinone reduction cycle in the Proteoliposome system. B = Representation of Proteoliposome Lipid Bilayer (Image from http://lipolife.co.uk).

The reduction cycle was initiated with the addition of NADH (1.25 mM) and StAOX activity was indirectly measured spectrophotometrically by measuring NADH consumption at 340 nm. The inclusion of an excess of NDI within the liposome system, ensured the AOX was rate limiting and that in fact the measured NADH reduction was equal to quinol oxidation through the AOX. The incorporation of the purified StAOX within the proteoliposome system was kindly carried out by Dr. Alice Copsey. **Table 19** outlines the enzymatic activity for the Twin- Strep StAOX protein under both the detergent and lipid environment. A significant increase in enzymatic activity was measured following incorporation of the purified StAOX sample into the proteoliposome with over 3 orders of magnitude increase in activity. The data obtained provides an indication that StAOX is sensitive to either its lipid environment or the substrate that used.

Table 19.

Specific Activity for purified StAOX protein in Different Lipid/Detergent Environments

Detergent/ Lipid Environment for Pure StAOX	Specific Activity (μmol of Quinol mg. min^{-1})
Solubilised (FC-12)	0.0242 ± 0.020
Proteoliposome bound	81.5 ± 2.35

Note. Specific activity assays were performed spectrophotometrically measuring at 278 nm in MOPS (65 mM, pH 7.5) and with the addition of Q_2H_2 (150 μM).

3.9 Conclusions

The literature supporting the role of StAOX in pathogenesis and in the development of resistance fungal strains is limited, but there is however a large number of studies on the fungal AOXs from other species. The intra species Blast analysis was used to corroborate these findings and present a role for similar phytopathogenic fungal AOXs. The Blast analysis of the StAOX amino acid sequence showed an average similarity of around 60% with over 75 fungal species suggesting a similar tertiary structure and phylogenetic relationship. The highly conserved residues necessary to chelate to the iron centre and residues that make up the PCET network are fully conserved, apart from the amino acid residue W65 in TAO and Y85 in StAOX. The influence of this residue on O_2 reduction catalytic mechanism and PCET remains enigmatic, and therefore will require investigation through future mutagenesis studies. However, the difference in specific activity between TAO and StAOX in regards to O_2 consumption suggests it may influence AOX turnover. The residues in close proximity to the diiron active site are also conserved between AOX species except for the C119 in TAO which is replaced by a D141 as shown in **Figure 38A**. In fact, this residue is not conserved between the fungal AOXs or TAO and its effect on the structure or enzymatic activity has yet to be determined.

The sequences for TAO and the fungal AOXs differ at the entrance to the hydrophobic cavity, presenting the opportunity for differential binding poses for the isoprenoid tail of the natural substrate. More specifically, the phenylalanine residue, F212, located in StAOX is highly conserved throughout fungal species but is not present in TAO. The significance of these residues on the overall structure of StAOX and binding of quinol, became clearer following homology modelling and comparisons to that of the crystal structure for TAO (**Figure 38B**).

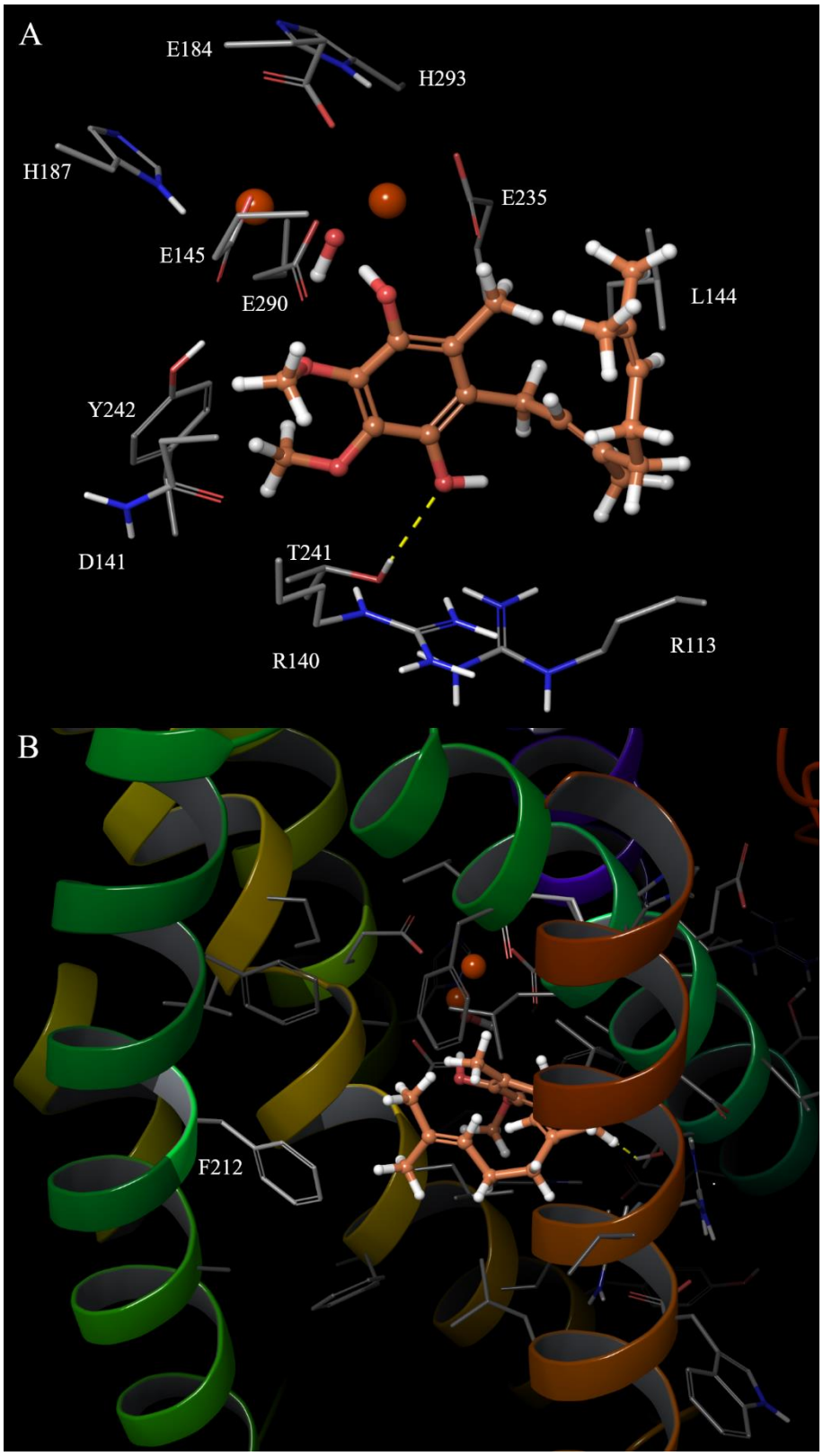

Figure 38 - StAOX binding site with docked quinol substrate (Q_2) displaying differences in the active site with the presence of the D141 residue (A) and the presence of the F212 residue at the opening to the quinol binding site (B).

The homology model and structure of StAOX is predicted from the crystal structure for TAO (PDB code: 3W54) and can therefore only be used as a guide in regards to internal distances and exact residue locations. The high conservation of important residues surrounding the diiron core and hydrophobic cavity residues, however, allows reasonable presumptions to be made. For instance, the F212 residue that is located at the entrance to the hydrophobic cavity clearly reduces the size and entrance for the quinol substrate (**Figure 38B**). Also, the D141 residue is in close proximity to the diiron core to influence the binding and affinity for the quinol substrate (**Figure 38A**). Overall the structure of StAOX is similar to that of TAO with a 4-helix bundle surrounding a diiron core and membrane bound helices adjacent to the entrance to the active site.

Initial attempts for the overexpression of StAOX highlighted a significant reduction in expression and yield in comparison to TAO. Specific activity measurements also revealed an enzymatic activity considerably lower than that of TAO and the plant species, *S. guttatum*. It was therefore important to optimise the protocol for the fungal AOX to boost total yield and expression. An increase in the concentration of the inducing reagent, IPTG, from 25μM to 300μM saw a negligible increase in the expression and total yield, but provided a 50% increase in enzymatic activity. The influence of a higher post induction temperature of 37°C provided an expected increase in total cell yield and expression of StAOX, matching the reported optimal growth conditions of *E. coli*. The removal of the mitochondrial targeting sequence and inclusion of the smaller Twin-Strep tag once again failed to dramatically enhance the specific activity or expression. Since the optimisation failed to increase expression and total wet weight of cells it could be suggested that the protein itself is responsible for the lack of improvement. The haem deficient *E. coli* strain is heavily dependent on the AOX for growth following induction, and since the specific activity of StAOX is low, the opportunity for hindered respiration and cell death is high. The diminishing returns from further optimisation of the expression protocol for StAOX prevented an investigation of additional variables; and therefore, an increase in batch size would suffice and yield the desired increase in total protein.

In contrast to these findings, the introduction of the MOPS buffer provided both an increase in specific activity, and reduction in a loss of activity following sample storage. The improvement of stability and function of StAOX could be attributed to the temperature dependence of Tris and MOPS buffers to pH. The temperature dependence to pH can be represented by the relationship $\Delta pK_a/\Delta T$, the value of which is -0.028 for Tris buffer and 0.015 for MOPS. In practicality, this represents a fluctuation of pH for a Tris buffer from pH = 7.5 at 25 °C to pH = 8.76 at -20 °C, whereas for MOPS buffer the pH at -20 °C is only 6.8, representing only half the change in pH. The results of this buffer change were seen in TAO membrane samples as well, suggesting that the performance of other species of AOX benefit from smaller pH swings.

Following optimisation, the baseline activity of StAOX was still shown to be lower than that of AOXs from other species and still raised questions as to its importance within a bioenergetic system. The regulation of StAOX through the nucleotides GMP, IMP and AMP, suggests there is a mechanism for a biological switch to enhance the normal physiological activity of the enzyme when required. The conditions in which this would occur could be when the use of Q_oI fungicides interrupt the ETC within the mitochondria or following attack from the host plant defence systems occurring during the latent phase of growth. Such a suggestion would make sense from an evolutionary perspective, since an AOX with high baseline activity would negate the function of the cytochrome *bc₁* complex and disrupt proton pumping, and ATP generation, due to an overly oxidised quinone pool. It would also follow an analogous role to that of the AOX in plants, which is highly regulated through the generation of the keto acid, pyruvate.

Using the site mapping algorithm on both Maestro and MOE molecular modelling software, a site for allosteric ligand binding was discovered spanning across both of the monomers and at the dimer interface on the matrix side of the protein. The docking of GMP, IMP and AMP onto the mapping surface identified the monomer and dimer binding sites outlined in **Section 3.5.2** . The proximity of the monomer purine nucleotide binding site to the PCET network suggests it could play a role in aiding the transfer of protons and electrons from molecular O_2 to oxidise quinol. However, this hypothesis is purely theoretical and would require extensive mutagenesis and photochemical studies[170] around the GMP binding site to ensure its validity. In contrast, the suggested purine nucleotide binding site at the dimer interface may offer a conformational alteration of the StAOX enzyme to enhance the enzyme turnover. Once again, further studies using circular dichroism (CD) will be required to support the theory of altered conformation of the protein following purine nucleotide binding.

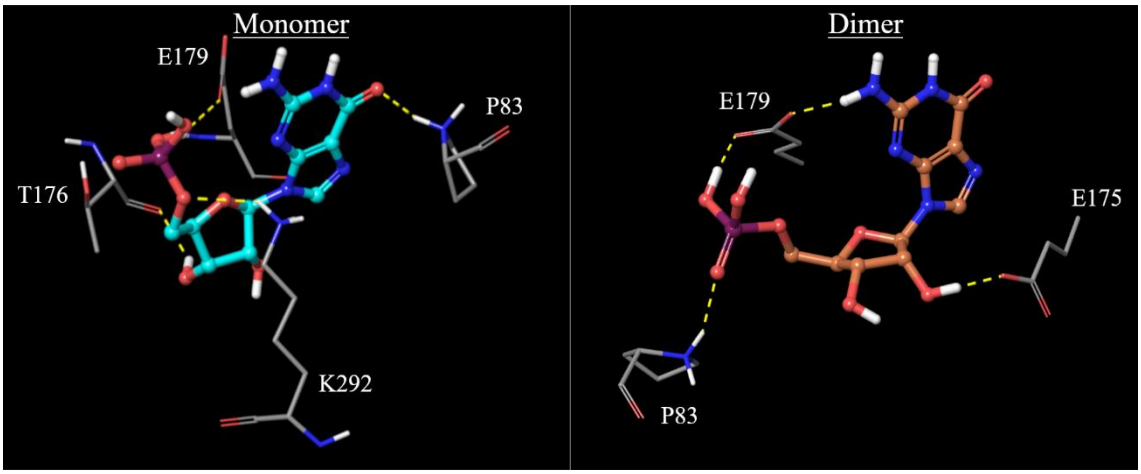

Figure 39 - Residue interactions between GMP and the StAOX homology model at both Monomer and Dimer Binding sites.

A detailed view of the suggested residues responsible for binding to the purine nucleotide molecule, GMP, can be shown in **Figure 39**. At the monomer binding site (**Figure 39A**) the E179, K292 and P83 residues allow for hydrogen bonding to both the guanosine nucleotide and phosphate group of the GMP molecule. A further hydrogen bond interaction can be seen between the hydroxyl group on the pentose sugar ring with the backbone of residue T176. The dimer binding site (**Figure 39B**) displays fewer hydrogen bond interactions but binds to both the E179 and P83 residues found in the monomer binding site. The differences in the number of residues interacting with the purine nucleotide is reflected in the docking scores presented in **Section 3.5.2** Docking of the purine nucleotide, AMP, generated a lower score across both sites in comparison to that of both IMP and GMP, which correlates to the lower activation of StAOX shown in **Figure 25**. However; to fully investigate the interaction between purine nucleotides and StAOX, purified StAOX protein was necessary to clarify whether the activation found in *E. coli* membrane samples was through a direct or indirect mechanism.

An attempt was made to purify the StAOX protein to evaluate its enzyme kinetics, with and without purine nucleotide activation; as well as to assess direct interactions or inhibtion with fungicide candidates synthesised in **Chapter 4**. Purification of StAOX was achieved for both the His and Twin-Strep tagged proteins but highlighted a clear disadvantage following the introduction of the new vector, containing the Δ61- StAOX sequence and Twin-Strep fusion tag. The His-tagged protein exhibited a 20-fold increase in specific activity in comparison to the Twin Strep tagged protein as shown in **Table 20**. The addition of the new Twin-Strep tag was shown in unpublished studies to improve the purification of TAO upon binding to the Strep-tactin® column and subsequent recovery. The addition of this tag as shown in **Table 20** has no negative consequences on the specific activity of TAO and is therefore unlikely to be responsible for the reduction in StAOX activity. The removal of the StAOX mitochondrial targeting sequence represents a loss of 18% from the full-length sequence, reducing the isoelectric point to 6.67. In comparison, the isoelectric point and net charge of the TAO protein is largely unaffected from removal of the targeting sequence representing just 7% of the protein. It is therefore important to note that the restricted length StAOX protein may have an influence on the purified protein activity and its stabilisation within the lipid-detergent micelle.

Table 20

Differences in Specific Activity and pI following AOX Purification

	Specific Activity (μmol of Quinol mg^{-1}. min^{-1})		Isoelectric Point (pI)*	
Enzyme	*His*	*Twin-Strep*	*His*	*Twin-Strep*†
TAO	17.3 ± 0.7	79.4 ± 6.3	8.80	8.42
StAOX	0.450 ± 0.025	0.0242 ± 0.002	8.47	6.67

Note. *Calculated using *Kozlowski, L.P., 2016. IPC–isoelectric point calculator. Biology direct, 11(1), p.55.* http://isoelectric.org/,† Includes the removal of the mitochondrial targeting sequence. Restriction length TAO = Δ24, StAOX = Δ60

Nevertheless; the solubilisation for the Twin-Strep tagged StAOX protein was taken forward and optimised to achieve the highest activity and protein recovery. The zwitterionic detergent, FC-12, provided the best protein recovery and stabilisation following solubilisation. StAOX was also sensitive to the percentage of FC-12 utilised and benefited from the highest concentration of detergent (2% w/v). The salt conditions were altered to affect the solvation sphere surrounding the protein micelle as well as to stabilise charges on the protein. The investigation of the highly kosmotropic salt $MgSO_4$ used for TAO purification was analysed along with a titration of the weakly kosmotropic salt NaCl. The negative charge on the AOX protein showed an improved specific activity following the use of 200 mM NaCl. The pH of the protein was expectedly highest at physiological conditions (pH=7.5) and the effect of altering the charge on the protein at pH 6 did not improve enzymatic activity. The elution buffer was found to stabilise the protein at a 10-fold reduction in comparison to the solubilisation concentration. The optimisation of these conditions failed to improve the StAOX enzymatic activity to any significant degree, suggesting the StAOX is far more sensitive to the stabilising presence of a natural lipid membrane in comparison to TAO and the plant AOX.

The development of a new technique by Jones *et al*[260] provided the opportunity to reconstitute the purified StAOX protein within an artificial membrane known as a proteoliposome. The establishment of an artificial quinone:quinol redox cycle *in vitro* was afforded through the inclusion of the monotopic external dehydrogenase, NDI. The enzymatic activity of StAOX was dramatically increased from 0.024 to 81.5 μmol of Q_2H_2 $min^{-1}.mg^{-1}$, confirming an increased sensitivity to the stabilising effect of a lipid membrane.

The distinct characteristics and differences between AOX species are highlighted in this chapter, especially between the parasite and fungal species. The biological roles of these two proteins are

very different and this reflects on their structure and enzymatic activity. The StAOX is not necessary under normal physiological conditions as has been highlighted by studies on a similar fungal AOX *Ustilago Maydis*[114]. The role of StAOX *in planta* requires considerable investigation, but for the analysis of novel fungicide candidates, *in vitro* testing is sufficient. The corroborating data with similar phytopathogenic fungal AOXs supports StAOX role in pathogenesis and resistance management and presents a novel target for fungicide development.

Chapter 4: Synthesis of Novel AOX and cytochrome *bc₁* complex Inhibitors

4.1 Introduction

The natural products ascochlorin, colletochlorin B and ascofuranone (**Figure 40**), isolated from the fungus *Acremonium sclerotigenum*, offer potential as lead compounds for the inhibition of both the AOX and cytochrome *bc₁* complex. In particular, ascofuranone has been shown[199] to substantially increase the selectivity between these two mitochondrial enzymes. Ascochlorin and Colletochlorin B, on the other hand, have shown[199] little to no selectivity between the AOX and the cytochrome *bc₁* complex. However; selectivity alone between these complexes does not suffice for the identification of a lead fungicide compound. It is therefore important to highlight work carried out by Young *et al*[259] confirming the fungicidal activity of ascochlorin and colletochlorin B against wild-type and Q_oI resistant (G143A) fungal strains. Moreover, the use of an AOX specific inhibitor has been shown to potentiate Q_o inhibitors efficacy *in vitro*[114,151–153] and *in planta*[261]; and therefore, presents a unique mode of action for a class of fungicides. The synthetic route for ascofuranone and ascochlorin, however, is low yielding and requires a number of transformative steps. The necessity to improve on this synthetic route and design a new route for a large library of compounds was apparent.

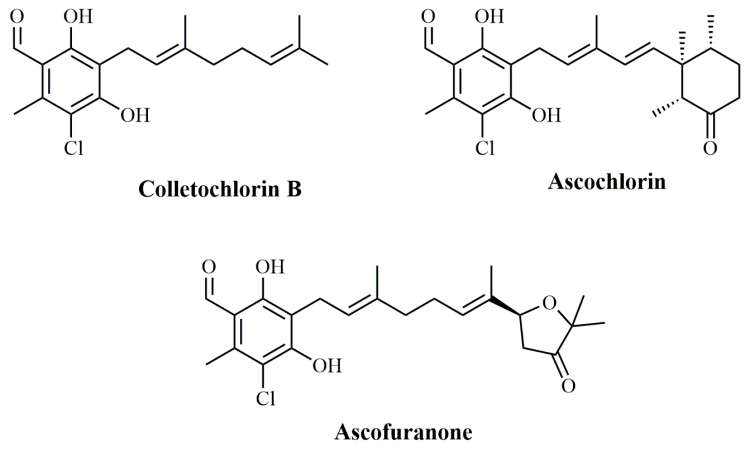

Figure 40 - Natural Products with AOX and Cytochrome bc₁ Complex Efficacy

The methodology for the total synthesis of ascofuranone and colletochlorin derivatives, was described by both Mori *et al*[262–264] and Joullie *et al*[220,265,266] in the mid-80s. The routes taken by both research groups offered significantly different synthetic schemes for ascofuranone, ascochlorin and colletochlorin B derivatives. The principal difference in the Mori synthesis is the alkyl coupling to the cyclohexadiene, followed by the mild oxidation of the head group with *N*-chlorosuccinimide (NCS) and dehydrochlorination with the strong base 1,8-diazabicyclo [5.4.0]undec-7-ene (DBU) (**Figure 41**). The alkyl coupling transformation occurs under harsh conditions of *t*-BuLi as the base with step yield of 67%[264]. This coupling step tolerated alkyl halides such as geranyl bromide, for the synthesis of colletochlorin B, or with the protected ketone furanone alkyl halide, for the synthesis of ascofuranone[263]. Conversely; for unprotected functional groups, the alkyl coupling with *t*-BuLi, demonstrated by Mori *et al*[262–264] would suffer from unwanted side product formation.

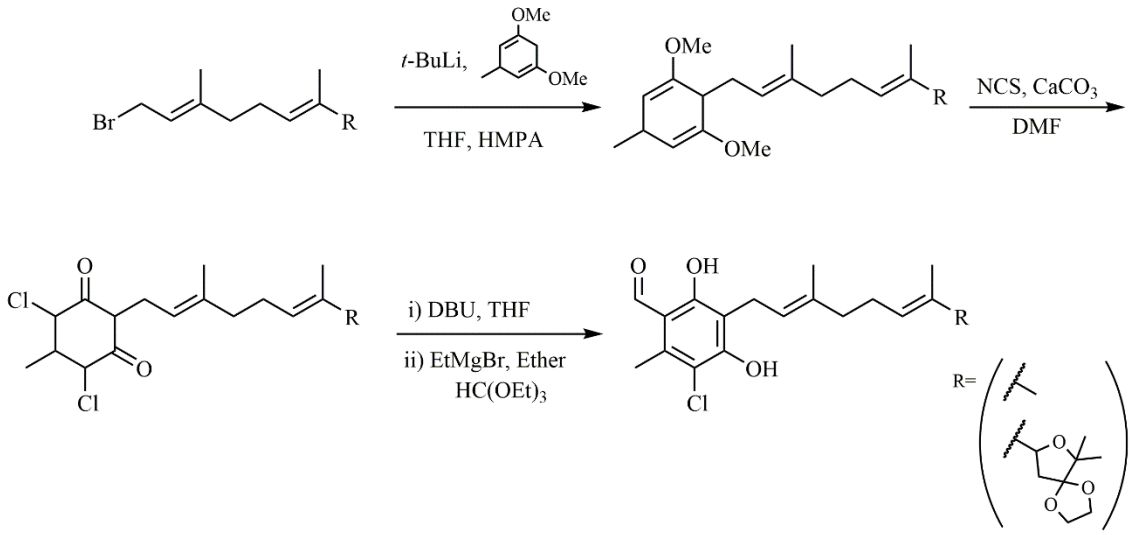

Figure 41 – Abbreviated Synthetic Route for Colletochlorin B and Ascofuranone as developed by Mori et al [257-259].

The synthetic route proposed by Joullie *et al*[220,265,267], affords the natural products of ascochlorin, ascofuranone and colletochlorin B, with the alkyl coupling step performed under milder conditions (**Figure 42**). The appropriate alkyl bromide is coupled to the hexa-substituted benzene ring (head group) directly with a potassium hydroxide solution. The advantage of this second route was the tolerance to a wide range of possible alkyl bromide derivatives without the formation of unwanted side products.

Saimoto *et al*[268] further improved on the synthesis for ascofuranone and colletochlorin derivatives taking features from both synthetic routes (**Figure 43**). The protection of the alcohol and aldehyde functional groups on the head group of ascofuranone allows for the tolerance of the harsh conditions in using *tert*-BuLi alkyl coupling. The alkyl coupling achieved a yield of 62% but the following steps to remove the protecting groups on the final compound, significantly reduced the total yield for the final inhibitor[268]. In order to improve the synthetic efficiency of the reaction, work by the same research group[221] adapted the original coupling step from Joullie *et al*[220,266,267] to improve the overall yield of colletochlorin and ascofuranone derivatives. The addition of $CaCl_2$ along with a potassium hydroxide solution and under a nitrogen atmosphere, improved the yield of the final alkyl coupling to 35% for ascofuranone, reducing ether side product formation and potential alkyl halide elimination. This methodology improved the total yield in comparison to all previous synthetic routes and tolerated most alkyl bromide derivatives. This route has been favoured for the generation a library of inhibitors for TAO, the target for the treatment of African sleeping sickness.

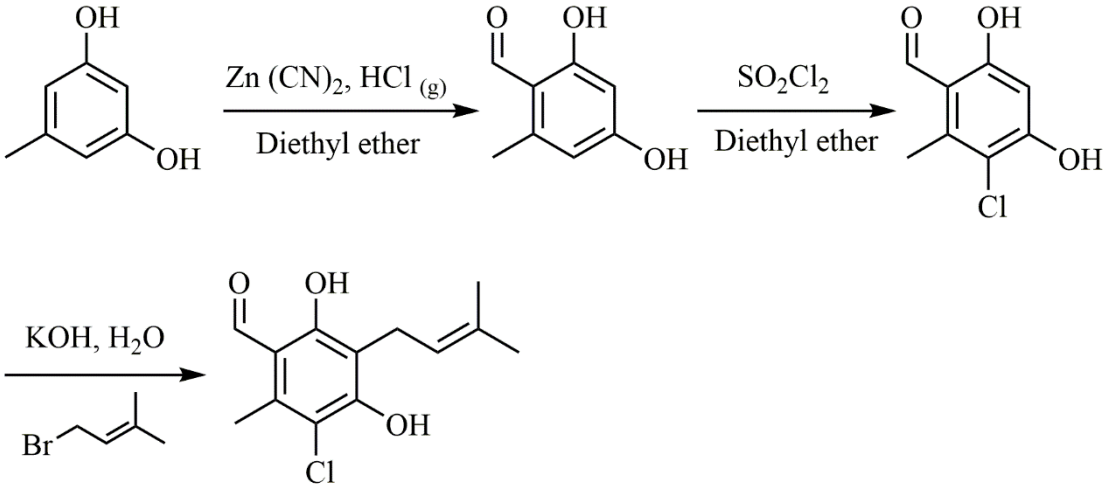

Figure 42 - Abbreviated Synthetic Route for colletochlorin D as developed by Joullie et al[261-263].

Previous work on the design and synthesis of novel AOX inhibitors has focussed on the *Trypanosoma brucei brucei* species[198,200]. Since there are structural differences between StAOX and TAO binding sites, the previous pharmacophore evaluation[198] can only be used as a reference. Synthesising and testing a series of novel compounds may shed light on the differences between the inhibitor binding sites of both the AOX species; and between the AOX and cytochrome bc_1 complex. To improve outcomes for the selection of a possible fungicidal candidate, design features to improve selectivity and binding energy have to be considered. The modelling of the

AOX/cytochrome *bc*$_1$ complex structures, and inhibitor binding sites, would provide an outline for rational inhibitor design. Since the natural product ascofuranone has shown selectivity towards AOX[84], it would be pertinent to understand the discriminating features the inhibitor possesses for one enzyme over the other. Furthermore, a selective inhibitory effect for AOX will improve the outcomes for a future fungicide active ingredient and reduce the chances of cytotoxicity. As mentioned earlier; the natural products ascochlorin and colletochlorin B show[259] efficacy against a resistant strain of *S. tritici in vitro*. The design of inhibitors to match the binding orientations exhibited by these two compounds, would also provide structural features required to navigate common amino acid mutations in resistant fungal species.

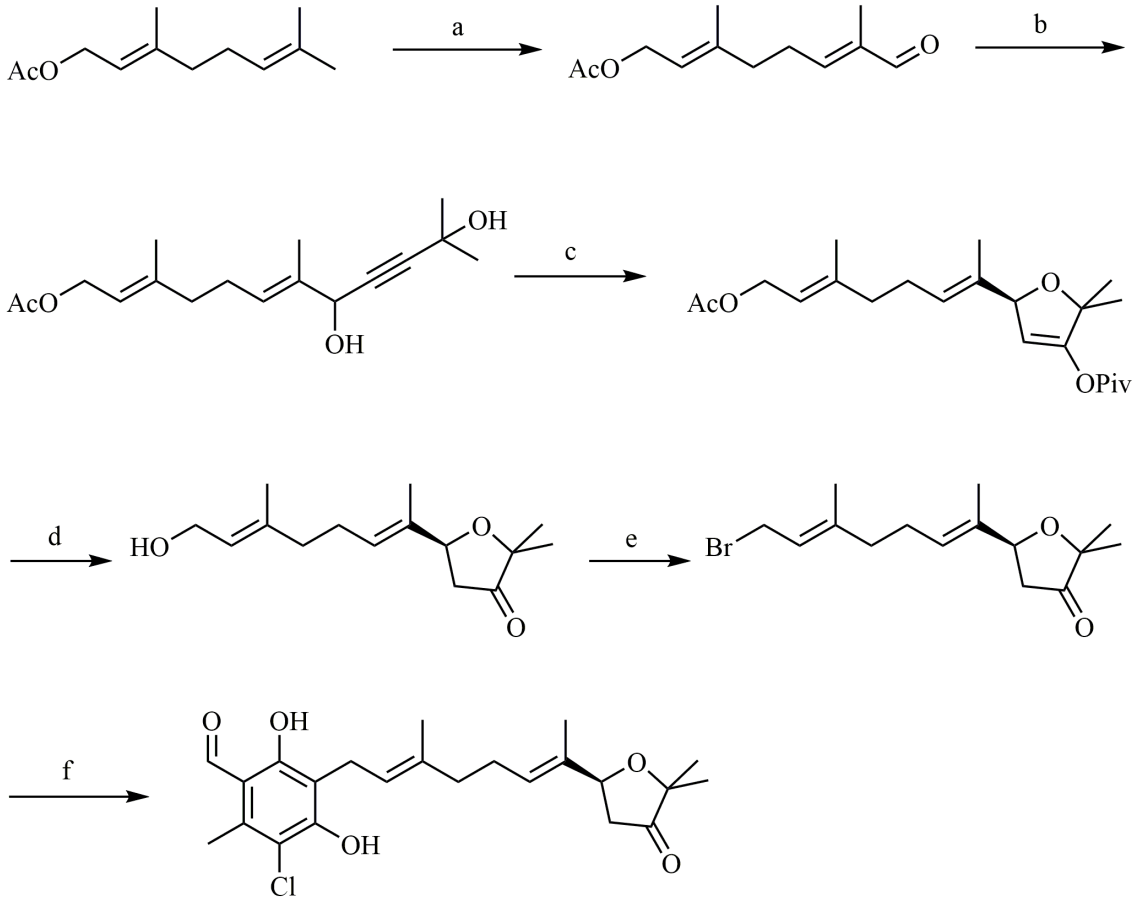

Figure 43 - Synthetic route for Ascofuranone as developed by Saimoto et al[264]. Experimental conditions: a = SeO_2, EtOH, reflux, 54%; b = 2-methyl-3-butyn-2-ol, n-BuLi, THF, -50 °C, 68%; c = i) t-BuCOCl, DMAP, pyridine, $CHCl_3$, 0 °C, 97% ii) $AgBF_4$, toluene, 80 °C, 63%; d = NaOMe, MeOH, 25 °C; e = CBr_4, $(n\text{-}C_8H_{17})_3P$, Et_2O, 0 °C; f = compound 2, $CaCl_2$, KOH, MeOH, 0 °C.

4.2 Designing Novel Inhibitors

A critical evaluation of the binding sites for both the AOX and the cytochrome bc_1 complex, was required to focus the design and synthesis towards novel inhibitors. The differences between AOX species was considered between the most well characterised AOX protein (TAO) and StAOX. For the evaluation of a potential fungicide, a comparison was made between the cytochrome bc_1 complex and StAOX. The crystal structure for TAO (PDB code: 3W54), cytochrome bc_1 complex (PDB code: 3H1L) and the homology model for StAOX, created by SWISS model, facilitated the evaluation of the binding sites of each enzyme. All molecular modelling was carried out using Maestro software package.

4.2.1 Interspecies Differentiation of AOX Inhibitor Binding Sites

A detailed assessment of the binding residues, in close proximity to the tail group, between the StAOX homology model and TAO crystal structure can be shown in **Figure 44.** The entrance to the hydrophobic cavity is significantly different in StAOX in comparison to TAO as can be seen by the surface model presented in **Figure 44A** and **B**. The entrance to the StAOX hydrophobic cavity is dramatically hindered by the presence of the F212 residue which is not conserved in the TAO structure. Although the presence of the F212 residue limits potential fungicide candidates through steric hinderance to within an 8-carbon chain length away from the active site, this residue also provides a unique binding opportunity with either π stacking or cation-π interactions at the terminus of the inhibitor tail.

Below the terminal isoprene on the docked colletochlorin B molecule we can see two hydrophilic residues in the TAO structure (**Figure 44E)**, namely T186 and S182, which provides the opportunity for multiple hydrogen bond interactions. In contrast, the StAOX (Figure 1F) does not contain these residues but contains A208 and M204 which could be an interesting point of contrast when evaluating binding enthalpies. The targeting of these hydrophilic residues present in the TAO structure may provide a point of selectivity and validate the homology model. The A208 residue in StAOX also provides a potential opportunity for selectivity between the AOX species; by simply reducing the space occupied in comparison to the T186 residue in TAO. Above the terminal carbon of colletochlorin B we can only see only a few residue differences between TAO and StAOX. The position of the two phenylalanine residues (F193 and F216) provide an opportunity for selectivity due to differences in their orientation and their potential for inhibitor interactions.

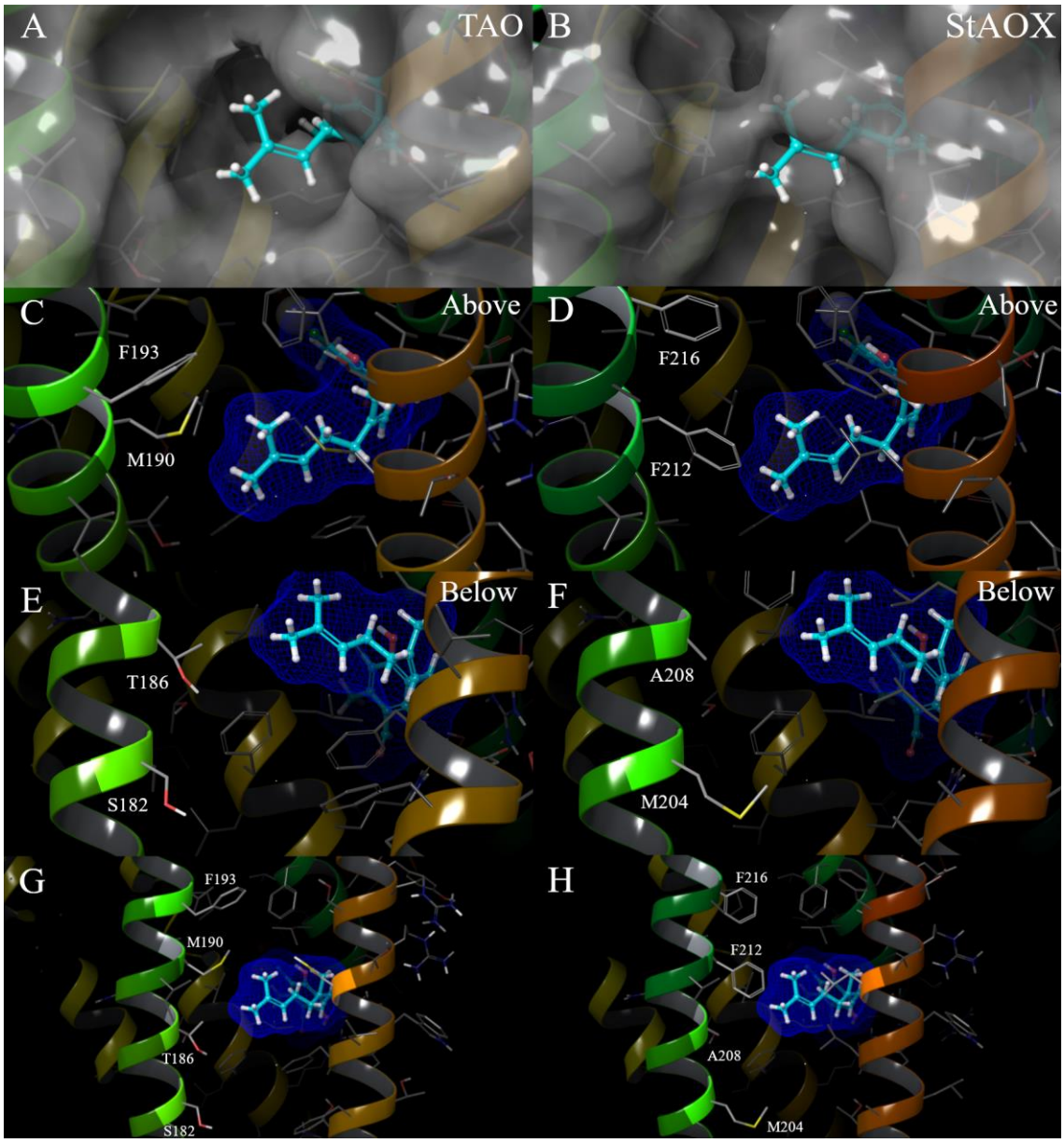

Figure 44 - Inhibitor Binding Site Comparisons between the TAO crystal structure (PDB code: 3W54) and the StAOX homology model. A surface model of the hydrophobic cavity with colletochlorin B bound highlights the restriction of the hydrophobic cavity for StAOX (B) in comparison to that of TAO (A). The differences in residues above the hydrophobic inhibitor binding site are displayed for TAO (C) and StAOX (D), as well as the residues below the inhibitor binding site for TAO (E) and StAOX (F). A final comparison is made between TAO (G) and StAOX (H).

4.2.2 Binding Site Differences between the AOX and Cytochrome bc_1 complex

A detailed assessment of the differential binding residues, between StAOX and the cytochrome *bc_1* complex, was not necessary for rational inhibitor design but **Figure 45** explores the receptor surface differences between the AOX and the cytochrome *bc_1* complex and provides a general overview as to the shape of the binding cavities. **Figure 45** shows the space above and below a typical 8 carbon chain quinol analogue, such as colletochlorin B and ascochlorin, is restricted in the Q_o site in comparison to the StAOX species. This presents an opportunity for selective design for novel AOX inhibitors, due to unfavourable steric effects following an inhibitor/enzyme binding event. The presence of a large functionalised aromatic ring on the terminal end of the colletochlorin B would present both the opportunity for π-stacking interactions within the AOX, as well as, preventing binding to the Q_o site. Equally, a large bulky tail moiety or a cis orientated terminal alkene would sufficiently alter the structure of an inhibitor to prevent binding. From **Figure 45** it is clear the terminal ketone on ascochlorin comes into close contact with **α helix 1** and could potentially hydrogen bond with the peptide chain. The extra carbon length on ascofuranone could prevent binding to the Q_o site by clashing with **α helix 1** and could provide a route to gain selectivity.

The Q_i site cavity of the cytochrome *bc_1* complex is distinctively shorter than both the AOX and Q_o sites; and therefore, opens fully to the lipid environment after an inhibitor chain length of approximately 8 carbon lengths binds. The opening to the Q_i site is much larger than that of the Q_o site and would still be susceptible to inhibition following the introduction of bulky tail moieties, and would therefore, require differentiation through head group manipulation. ascochlorin binds to the Q_i site in a similar fashion to the Q_o site with the terminal ketone in close proximity to alpha helix 2. The proximity of α helix 2 may prevent favourable binding of the longer ascofuranone inhibitor due to steric hinderance; but this requires further investigation. In comparison to the cytochrome *bc_1* complex, StAOX possesses a narrow binding cavity up until the terminal carbon of the bound colletochlorin B (**Figure 45**). The space above and below this terminal carbon is sufficient to allow for the binding of a functionalised colletochlorin B inhibitor. This feature is not consistent with both the Q_o and Q_i binding sites and therefore provides a point of difference for synthesising a selective *bc_1* complex inhibitor.

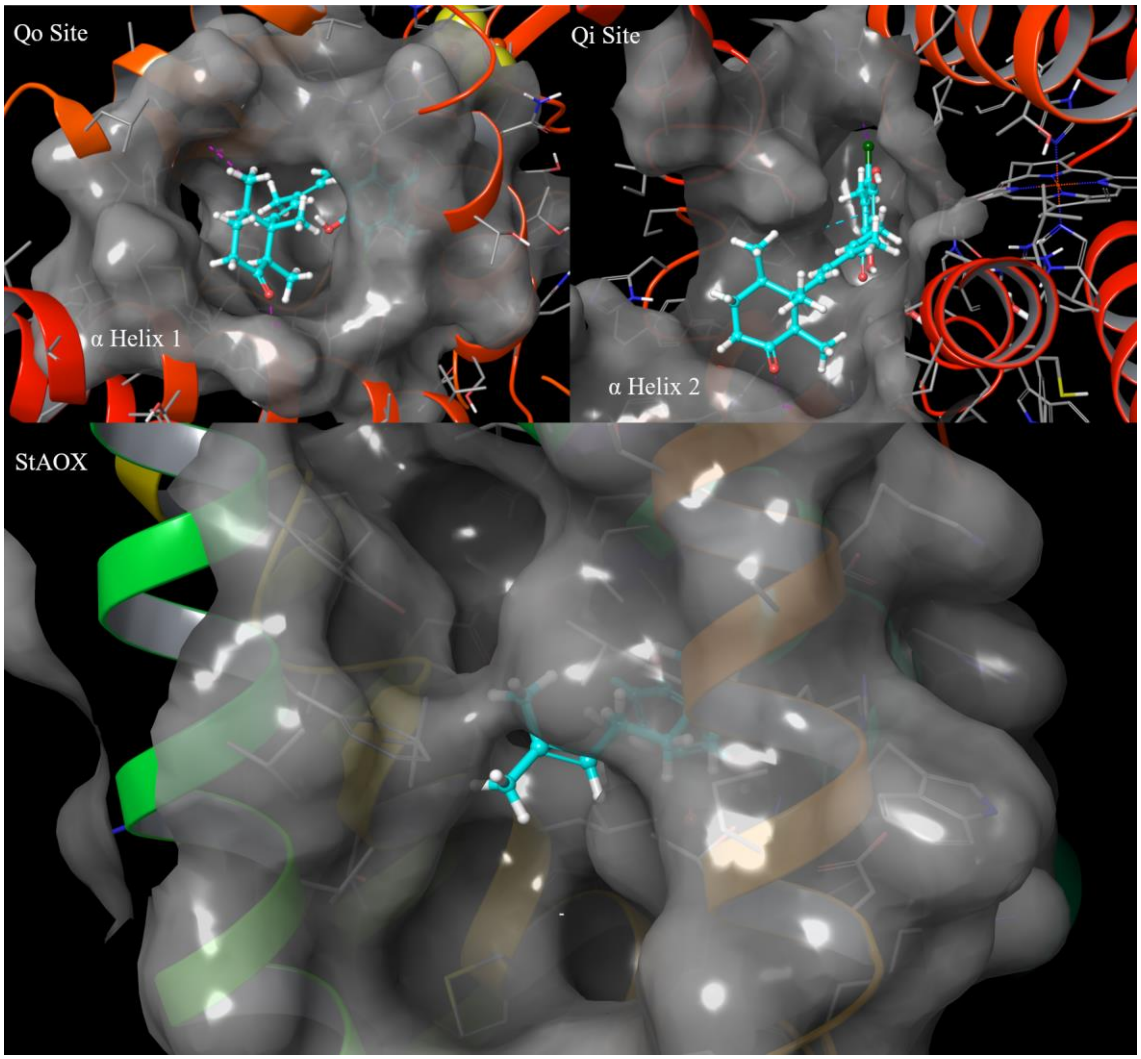

Figure 45 - Binding sites of the cytochrome bc_1 complex with ascochlorin at Q_o and Q_i Binding Sites (PDB Code: 3H1L) and the homology model for StAOX with colletochlorin B bound.

4.2.3 Chemical Structure Templates for Novel Fungicide Candidates

4.2.3.1 Investigating the Size of the Hydrophobic Cavity

To investigate the differences between the size of the opening to the hydrophobic cavity for TAO and StAOX, a freely rotatable tail linker, along with a large or small terminal functional group, would need to be synthesised. The chemical structures shown in **Figure 46**, demonstrate significant differences between their size and electronegativity. The 7-nitrobenz-2-oxa-1,3-diazole (NBD) group offers high electron density as well as considerable size. Through analysis of the crystal structure of TAO in **Section 4.2.1**, it can be expected that the NBD group could be accommodated within the large opening to the inhibitor binding site. In contrast, the StAOX homology model suggested a highly hindered opening to the inhibitor binding site and would therefore fail to accommodate the NBD group. This point of difference should be reflected in each respective inhibitor assay, with a reduced potency expected for the NBD inhibitor (**Figure 46**) against the StAOX protein, due to the proposed steric effects of the F212 residue (**Figure 44**).

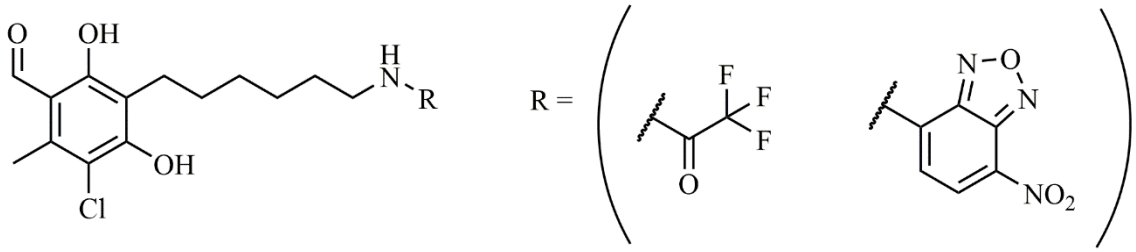

Figure 46 - Chemical Structure Template for investigating the size of the opening to the AOX hydrophobic cavity.

The trifluoroacetamide group shown in **Figure 46** affords a significantly smaller but equally electron dense group to the freely rotatable saturated linker. This compound should bind equally as well to both the TAO and StAOX structures and would therefore act as a comparison to the large NBD compound.

4.2.3.2 Investigating the Space Above and Below the Hydrophobic Cavity Entrance

The two commercially available *E/Z* diastereoisomers, neryl and geranyl acetate, present the opportunity to synthesise the compounds shown in **Figure 47**. The significant deviation in the direction of the terminal acetate or hydroxyl functional group, allows for the assessment of potential hydrogen bonding interactions to residues T186 and S182 within the TAO structure, as highlighted in **Figure 44**. The compounds may also help to confirm the steric influence of the F212 residue within the StAOX structure, with the *Z* - isomer affording the opportunity to avoid this residue and bind in a more favourable conformation.

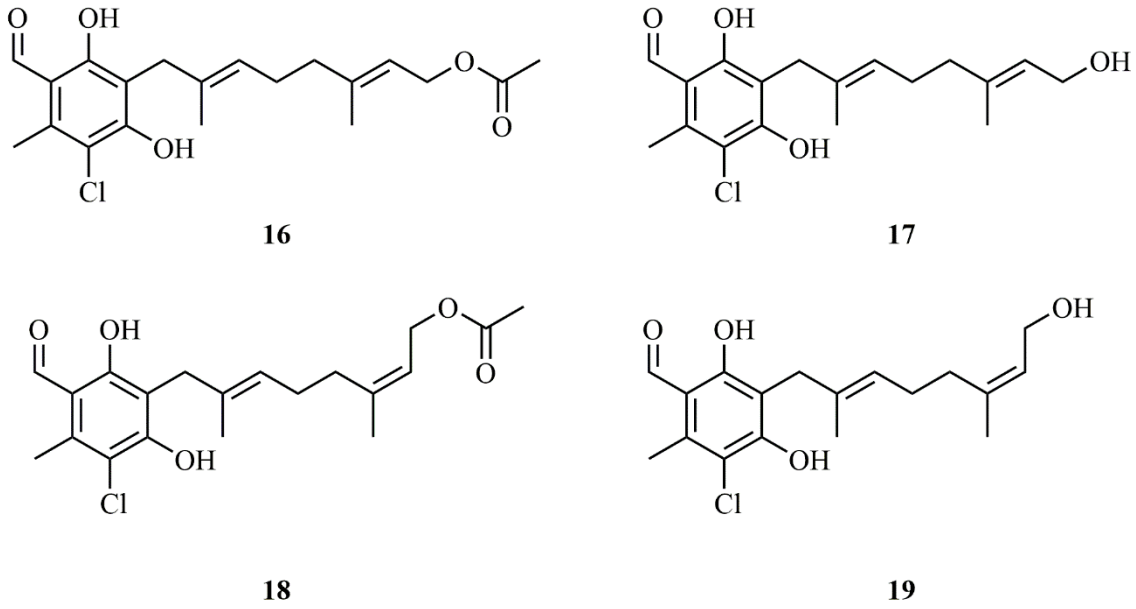

Figure 47 – Acetate protected and deprotected diasteroeisomers in order to investigate the opening to the hydrophobic cavity.

As described in **Section 4.2.2**, the Q_o and Q_i binding sites of the cytochrome bc_1 complex exhibit a narrow binding site for prospective inhibitors within an 8 carbon chain length. The protected and deprotected *Z* isomer shown in **Figure 47** should help to confirm this evaluation through inhibition data, with the straight chain *E* isomers acting as respective comparative compounds. If in fact the *Z* isomer binds favourably to the AOX versus the cytochrome bc_1 complex, then the potential for the generation of future fungicidal compounds exhibiting a specificity to the AOX would follow on from this chemical structure template.

4.2.3.3 Investigating potential Hydrogen Bond Interactions and Length of Binding Sites

To help identify potential hydrogen and halide bond interactions within the cytochrome bc_1 complex, TAO and StAOX, a chemical template allowing for a series of hydrophilic groups was required. As previously discussed, the lead compounds of ascofuranone and ascochlorin demonstrate a differential sensitivity between the AOX and the cytochrome bc_1 complex; and therefore, the chemical template should include features from both of these compounds. The carbon chain length of ascochlorin is noticeably shorter than that of ascofuranone but both share hydrogen bond acceptors at the terminal tail moiety. These features are included in the template show in **Figure 48**, with the inclusion of hydrogen bond acceptors at the terminal moiety and varying carbon chain length, with either the prenyl or geranyl starting materials.

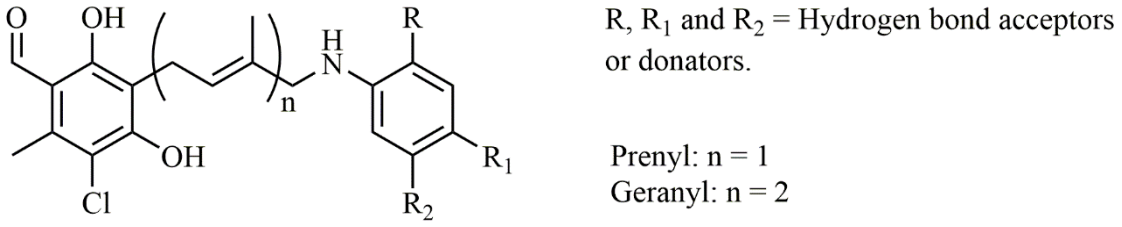

Figure 48 - Chemical template for ascochlorin and ascofuranone like fungicide candidates

From the structure analysis in **Section 4.2.1**, the geranyl length compounds should be accommodated into the TAO inhibitor binding site and potentially interact with T186 and S182 residues. However, due to the presence of the F212 residue within the StAOX homology model blocking the entrance to the binding site, the geranyl length inhibitor may not bind preferentially within the binding site. The shorter length compounds utilising the prenyl starting material should, however, bind within the StAOX hydrophobic cavity, providing more data to confirm validity of the homology model.

The compounds in **Figure 48** may also present an opportunity for selectivity between the cytochrome bc_1 complex and the AOX. It could be suggested that the lower inhibition exhibited by ascofuranone is a product of the carbon chain length of the compound, effectively preventing the favourable binding within either the Q_o or Q_i binding sites of the cytochrome bc_1 complex. It is also apparent that both colletochlorin B and ascochlorin are shorter than ascofuranone but also exhibit potent inhibition of the cytochrome bc_1 complex. The compounds synthesised according to the chemical structure template in **Figure 48** should therefore provide evidence to prove this hypothesis.

4.3 General Reaction Scheme for Natural Products and Analogues

4.3.1 Optimisation and Establishment of a General Reaction Scheme

The first step of the general reaction **Scheme 1** involves the formylation of orcinol *via* the Vilsmeier-Haack reaction. This formylation step was carried out according to the protocol established by Xie *et al*[219]; but required modifications to achieve a suitable yield to carry forward. The original methodology suggested a yield of 93%[219], but after several attempts a maximum yield of 43% was achieved. The critical step in the Vilsmeier-Haack reaction occurs when the iminium salt is formed from the addition of $POCl_3$ to DMF. By increasing the time for this salt to form, and maintaining a slow addition of $POCl_3$, the overall reaction yield was enhanced from 43% to 62%. Furthermore; increasing the equivalents of $POCl_3$ to orcinol from 1.1 to 1.3, improved the final yield by ensuring the iminium salt was in excess. The formylated product (**1**) of this reaction is weakly soluble in DMF and precipitates out upon the acidification process, aided by an excess of water; nevertheless, it was found that a significant yield could be extracted from the remaining filtrate. These modifications provided a new experimental protocol with an improved yield of 64%, which was suitable to be taken forward to the chlorination step; albeit lower than the yield found in the literature.

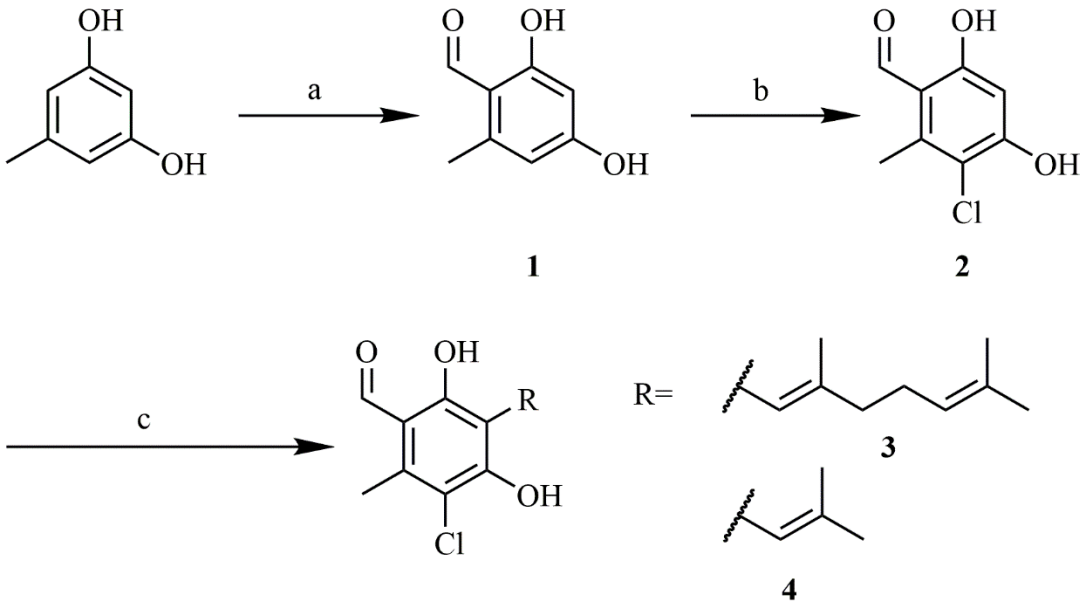

Scheme 1 - General Reaction Scheme for colletochlorin derivatives. Experimental conditions: a = $POCl_3$, DMF, 16 h, -2 – 110 °C, 64%; b = SO_2Cl_2, Diethyl ether, -2 °C, 3 h, 48%; c = Br-R, $CaCl_2.2H_2O$, KOH, MeOH, 0 °C, 14 h, compound 3 = 55% and compound 4 = 12%.

The chlorination step was adapted from syntheses described by Moore *et al*[269] and Safaryn *et al*[220] with a final yield of 48%. The formylated phenol (**1**) is chlorinated by sulfuryl chloride but requires precise addition of the correct stoichiometry in order to reduce unwanted side products. Early attempts with diluted SO_2Cl_2 resulted in an incomplete reaction and a very challenging purification. The starting material and final chlorinated product (**2**) have a very similar R_f value (0.68 and 0.62 in light petroleum 8:2 EtOAc) when assessed by TLC in most solvent conditions. To aid the purification of the crude product, the equivalents of sulfuryl chloride were lowered from 1.3 to 1.1. This ensured that the amount of SO_2Cl_2 was sufficiently high enough to run the reaction to completion, but low enough in order to avoid over chlorination on both aromatic protons. The addition of neat sulfuryl chloride, in a dropwise fashion to a salt bath cooled reaction vessel, reduced the reaction time from 8 hours to as low as 2 hours to yield a mixture of the both the di-chlorinated and mono-chlorinated (**2**) products, which were separated by column chromatography.

The final coupling step between the alkyl chain and the aromatic head group (**2**) required precise optimisation of a number of conditions in order to achieve suitable yields. The proposed mechanism by which compound **2** couples to the alkyl chain, is shown in **Figure 49**. The reaction proceeds with the formation of a potassium salt upon addition of one equivalent of potassium hydroxide dissolved in dry methanol. The potassium salt stabilises the deprotonated aromatic intermediate, leaving a weak nucleophile to attack the brominated alkyl chain. The rate determining step in this mechanism is mediated by the concentration of both the aromatic nucleophile and the alkyl halide with second order kinetics. The major product is this reaction is favourable towards the meta position (in regards to the formyl group) but the two minor side products can be attributed to ether formation, owing to the stability of the aromatic resonance structures.

The first route attempted based on a report from Chiarello *et al*[270] required isolation of the potassium salt of compound **2** to selectively add the isoprenoid chain at the nucleophilic position between the two hydroxyl moieties. The isolation of the aforementioned salt was unsuccessful following several attempts, which can be attributed to a number of factors. One of the factors resulting in the experimental failure, was the difficulty in isolating the aromatic salt from methanol azeotropically. The salt did not precipitate out, and therefore, could not be isolated. This aromatic salt can be formed around the most acidic proton or through one of the hydroxyl moieties but will only form under sufficiently strong alkali conditions. Forming this aromatic salt in situ would alleviate these problems as well as ensuring no water comes into contact with this intermediate. It was therefore concluded that an alternative method would be used to reduce the opportunity of incomplete or unsuccessful reactions.

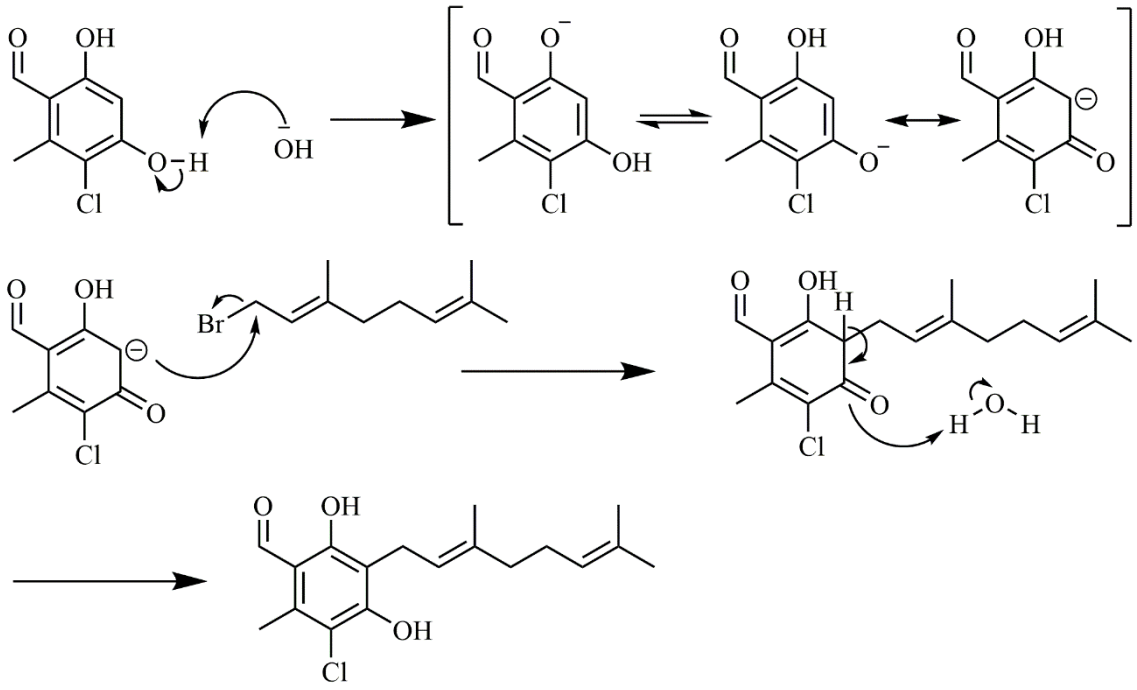

Figure 49 - Tail Addition Mechanism of Colletochlorin B and its Derivatives

The methodology proposed by Haga *et al*[271] for the final coupling step in the synthesis of ascofuranone provided a facile route to alkyl coupling to compound **2**; without the need to isolate the salt intermediate. This method also introduced $CaCl_2$, which may act as desiccant or Lewis acid, to help improve the yield and success of the reaction. Once again, the reaction was found to initially require extremely dry conditions and starting materials to limit the formation of water-halogen complexes which have been shown to disrupt typical S_N2 reactions[272]. Initial experiments successfully isolated the natural product colletochlorin B (**3**) with an overall percentage yield of between 30-40%. The low yield for this final step was attributed to a mixture of two factors: the first was due to unreacted starting material; and the second was due to product loss in the aqueous layer following extraction. To reduce the amount of unreacted starting materials, the effective concentration of potassium hydroxide was increased by increasing the molar equivalents and decreasing the total methanol volume. To improve extraction of the final product from the aqueous layer, the methanol/water layer was concentrated *in vacuo* after quenching the reaction. This step removed the remaining methanol from the reaction; and would therefore, reduce the opportunity for product loss within the aqueous layer. The final coupling step total yield, for colletochlorin B (**3**) and colletochlorin D (**4**), were improved to 55% from 30% and to 45% from 20%, respectively.

4.4 Saturated Tail Synthetic Route

4.4.1 Synthetic route for Functionalised Saturated Inhibitors

It has yet to be reported as to whether the double bonds found in the aforementioned natural products have any significant influence in binding to StAOX; or for that matter, improve selectivity towards any specific enzyme in the respiratory chain. To investigate this inhibitor property a proposed reaction scheme for saturated natural product derivatives was created, which can be shown in **Scheme 2**. This synthetic route benefits from the abundance of a variety of cheap starting materials with different chemical and binding properties. Since the natural product derivatives have a carbon chain length of between 8-10, and pharmacophore profiling by Saimoto *et al*[198] showed an optimal range between 9-10; the shorter 6 carbon chain linker of 6-amino hexanol was selected to allow for further functionalisation to reach the final desired chain length. The strong nucleophilic nature of the terminal amine group of 6-aminohexanol allows for straightforward preparation of secondary amines, when reacted with aryl halides or esters, without the need for hydroxyl protection. The use of a polar protic solvent, such as methanol, will further attenuate the nucleophilicity the hydroxyl group and therefore reduce the possibility of unwanted ether formation. The hydroxyl group can then be brominated *via* the Appel reaction to be taken forward to the final coupling step outlined in **Scheme 1**.

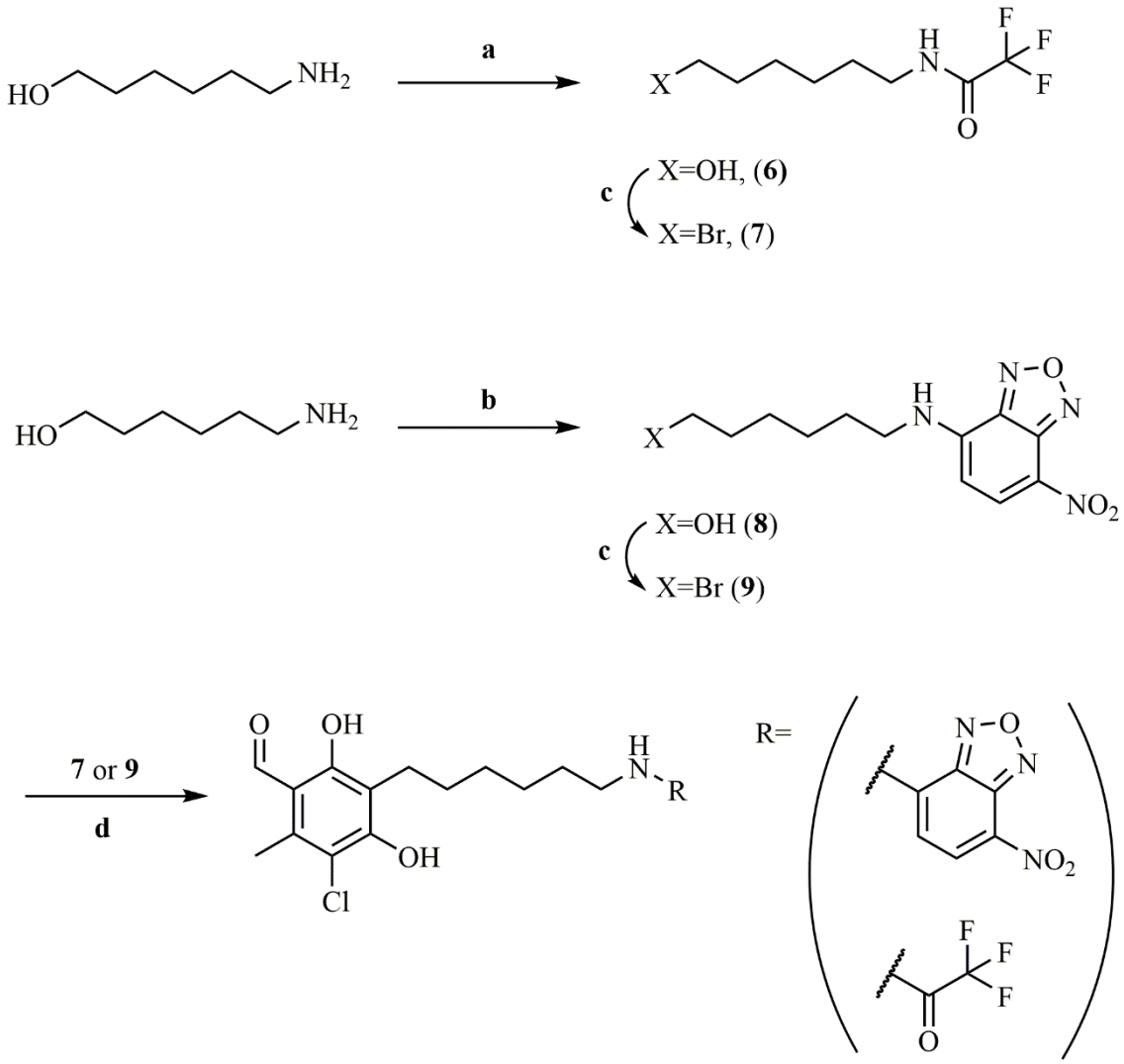

Scheme 2 - Synthetic route for functionalised saturated colletochlorin derivatives. Experimental conditions: a = CF_3CO_2Et, DCM, 25 °C, 12 h, 86%; b = $NaHCO_3$ (0.3M), NBD-Cl, MeOH, 25 °C, 12 h, 56%; c = CBr_4, PPh_3, 0 °C, 4 h, compound 7 = 93% and compound 9 = 98%; d = KOH (aq) (1M), $CaCl_2.2H_2O$, MeOH, compound 2, 0 °C, 12 h.

The bromination reaction of various alcohols was utilized throughout all synthetic routes, often with small amounts of starting material; therefore, it was important to understand the specific reaction mechanisms and troubleshoot the common problems encountered before synthesising new saturated natural products. The saturated analogue for colletochlorin B was attempted several times through the bromination of 3,7-dimethyl-1-octanol followed by the final coupling step outlined in **Scheme 2**. The bromination of 3,7 dimethyl-1-octanol was first attempted using the common brominating reagent phosphorus tribromide (PBr_3) in diethyl ether; but it proved to be largely unsuccessful. The PBr_3 reaction proceeds with the formation of a phosphorus ester followed by an S_N2 substitution around the saturated primary alcohol. The lack of success in this

particular reaction was not immediately attributed to either step of the reaction mechanism outright; therefore, an alternative route for bromination was assessed.

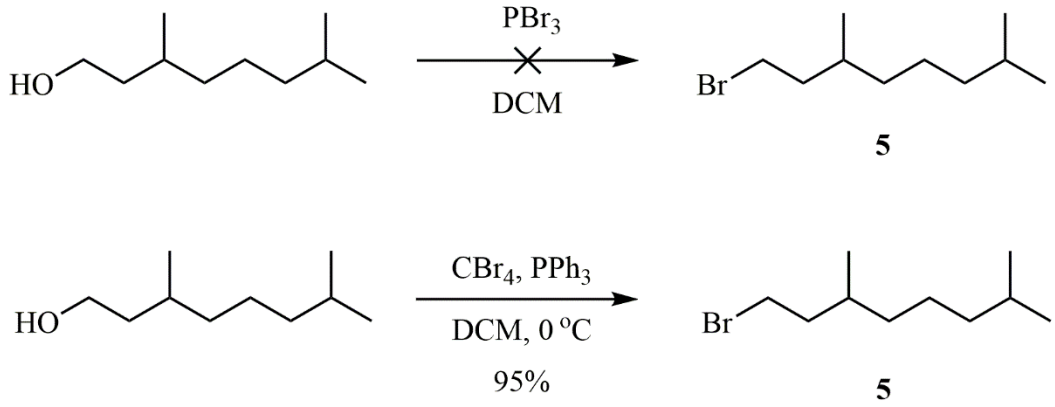

Scheme 3 - Bromination of 3,7-dimethyl-1-octanol with PBr_3 or the Appel reaction.

The Appel reaction, using triphenyl phosphine (PPh_3) and carbon tetrabromide (CBr_4), occurs through a similar reaction mechanism to PBr_3. The major differences between the two reactions include the deprotonation of the alcohol forming an alkoxide, followed by a displacement of the bromide to form a PPh_3 intermediate. A methodology adapted from Asghari *et al*[273] in which two equivalents of CBr_4 and PPh_3 were used for each equivalent of free alcohol proved successful, with a quantitative yield of the alkyl halide. Since the S_N2 substitution mechanism is consistent between both the Appel reaction and the PBr_3 reaction, it could be assumed that the bromination with PBr_3 was failing to activate the saturated alcohol and provide a suitable leaving group. This hypothesis seems unlikely as this primary alcohol is not sterically hindered to any considerable degree. The PBr_3 reaction was repeated with the polar aprotic solvent DMF and the alkyl halide was formed albeit with a lower than quantitative yield. It could be postulated, that the failure to brominate the alkyl halide with PBr_3 was due to the choice of solvent, rather than a mechanistic hinderance of the reagent. Nevertheless; bromination *via* the Appel reaction was favoured over the PBr_3 reaction for all saturated alkyl tail groups, due to its quantitative yield; ease of purification; and tolerance to common solvent systems.

4.4.2 Saturated Alkyl Halides Synthesis and Tail Addition Coupling

As previously described; synthesising an inhibitor that probes the size of the hydrophobic cavity, as well as the possible inhibitor/enzyme interactions, should provide *in vitro* data to support and validate the StAOX and TAO homology models. The fluorescent probe 7-nitrobenz-2-oxa-1,3-diazole (NBD) contains both a large conjugated ring system, providing potential π stacking interactions; and a terminal nitro group with two hydrogen bond acceptors. The NBD moiety has also been utilised extensively in microscopy and spectroscopy,[222,273,274] owing to its fluorescent properties in the visible spectrum.[275,276] Accordingly, efforts were made to incorporate this moiety into our emerging series of inhibitors.

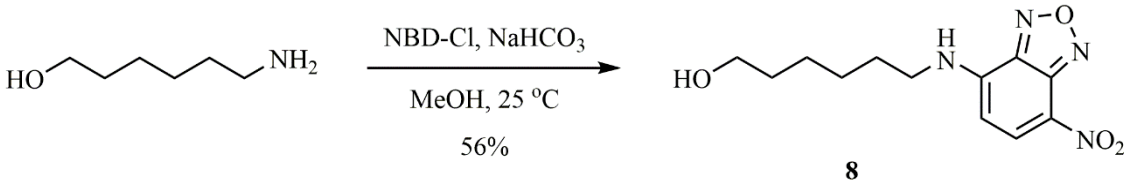

Scheme 4 - The arylation of 6-aminohexanol to yield the NBD-functionalised saturated tail (8)

The arylation of 6-aminohexanol with NBD was carried out with minor modifications according to the procedure by Watanabe[222] with an overall yield of 56% (**Scheme 4**). The yield of this initial arylation step, albeit modest, was considered a success. Fortunately, the NBD moiety contains a strong electron withdrawing group para to the aromatic halogen, which helps to stabilise the charged aromatic intermediate and leads to the loss of the halide group to reintroduce aromaticity. The bromination step of the NBD alcohol was achieved *via* the Appel reaction in DCM with a quantitative yield, which was then taken forward without further purification to the final tail addition step. The final coupling step for the brominated NBD alkyl chain was achieved, following many unsuccessful attempts, but failed to yield a sufficient amount to fully characterise the final compound.

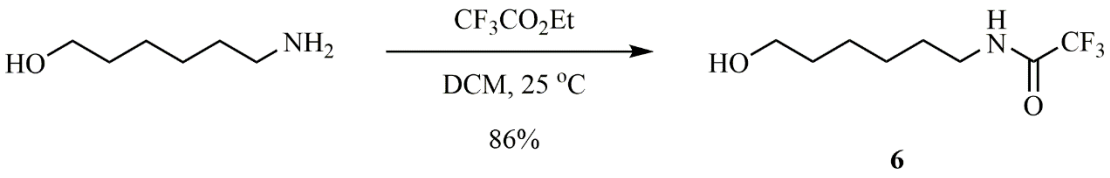

Scheme 5 – Secondary amine preparation of 6-aminohexanol to include the trifluoroamide moiety (6)

The second moiety that was introduced to the saturated tail was the smaller, but highly electronegative, trifluoroacetyl group. The trifluoro group is often included in pharmaceuticals as a classical bioisostere to methyl groups due to its metabolic inertness, high electronegativity and its small size[277,278]. The amine protection was achieved with an 86% yield at room temperature by a straightforward procedure which involved dissolving the 6-aminohexanol in a suitable solvent with a slow addition of ethyl trifluoroacetate (**Scheme 5**). The final product (**5**) was then carried forward without further purification and was brominated *via* the Appel reaction with an overall yield of 93%. The trifluoroacetamide group is susceptible to hydrolysis under relatively mild conditions; and therefore, requires careful coupling under the conditions of the final alkylation step. The trifluoroacetamide group was successfully coupled to the head group but suffered from the same issue as the NBD coupling; namely, a difficult purification. The trifluoro amide group may have been cleaved in this final coupling step due to the high pH (9-10) conditions; but the initial low temperature of the reaction should have prevented the occurrence of this side reaction. The final compound could not be fully characterised or included as part of any inhibitor analysis due to the low final yield and insufficient purity.

The lack of success with the saturated tail synthesis route outlined **Scheme 2** could be solely attributed to the final alkyl coupling step and could not be improved by altering the reaction conditions. It could therefore be assumed that the reason for the failure of the final coupling step was an inherent property of the functionalised saturated alkyl chain, which may favour the elimination of the alkyl halide, or the nucleophilic nature of the new amine group affecting the alkyl coupling mechanism. However, a new synthetic route involving the coupling of an unsaturated tail with a secondary amine would need to be developed to investigate these hypotheses.

4.5 Unsaturated Tail Functionalisation

4.5.1 Synthetic Route for Functionalised Unsaturated Alcohols

The initial studies into the synthesis of novel saturated alkyl inhibitors highlighted some issues with isolation of the final compound. The final coupling could be affected by either the saturated nature of the chain or the terminal amine introduced. It was therefore important to investigate these possible issues, as well as derive a new synthetic route for compounds with greater similarity to the natural products. The synthetic route outlined in **Scheme 6** follows the functionalisation of geranyl acetate *via* an allylic oxidation followed by a reductive amination to yield a functionalised

isoprene. The functionalised isoprene can then be deprotected and brominated to allow for coupling to the head group of colletochlorin B.

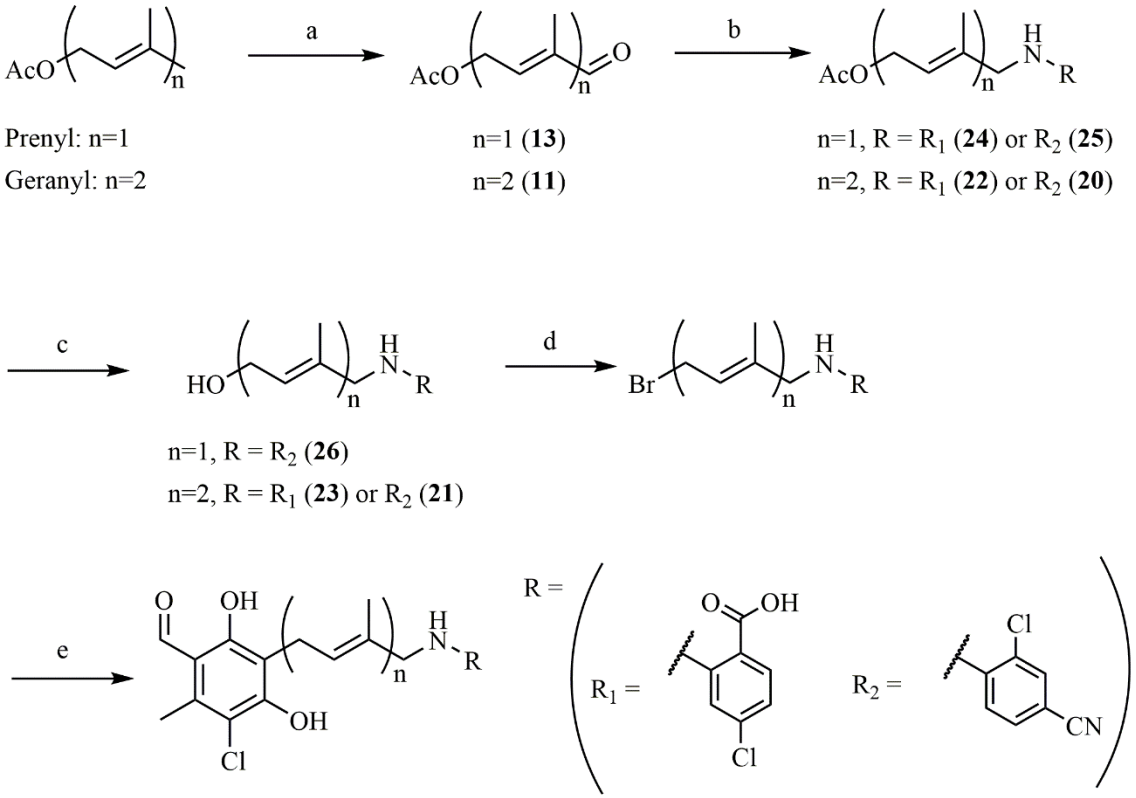

Scheme 6 - Synthetic Route for Functionalised Unsaturated Alcohols. Experimental conditions: a = SeO_2, t-BuOOH, Salicylic acid, 37 °C, 48 h, compound 11 = 49% and compound 13 = 38%; b = $NaBH(OAc)_3$, AcOH, DCE, H_2N-R, 25 °C, 13 h, compound 20 = 75%, compound 22 = 70%, compound 24 = 50% and compound 25 = 33%; c = K_2CO_3, MeOH, 25 °C, 12 h, compound 21 = 70%, compound 23 = 12% and compound 26 = 23%; d = PBr_3, THF, 25 °C, 12 h; e = KOH, MeOH, $CaCl_2.2H_2O$, compound 2.

4.5.2 Allylic Oxidation

The initial step of Scheme 3 involves the functionalisation of geranyl acetate to produce the terminal aldehyde necessary for reductive amination, which was achieved through an allylic oxidation (**Scheme 7**). The allylic oxidation of geranyl acetate with selenium oxide (SeO_2) required careful consideration for most of the reaction parameters; but also, for the removal of the toxic selenium by-products. The allylic alcohol and aldehyde are the two major products formed in this oxidation and the yield for each of these products was improved by altering both the

temperature, and the selenium oxide equivalents. The reaction mechanism for the allylic oxidation of geranyl acetate, proceeds with the ene type reaction of selenium oxide followed by 2,3-sigmatropic rearrangement[279]. The decomposition of the selenium intermediate produces the allylic alcohol and further oxidation will then form an allylic aldehyde.

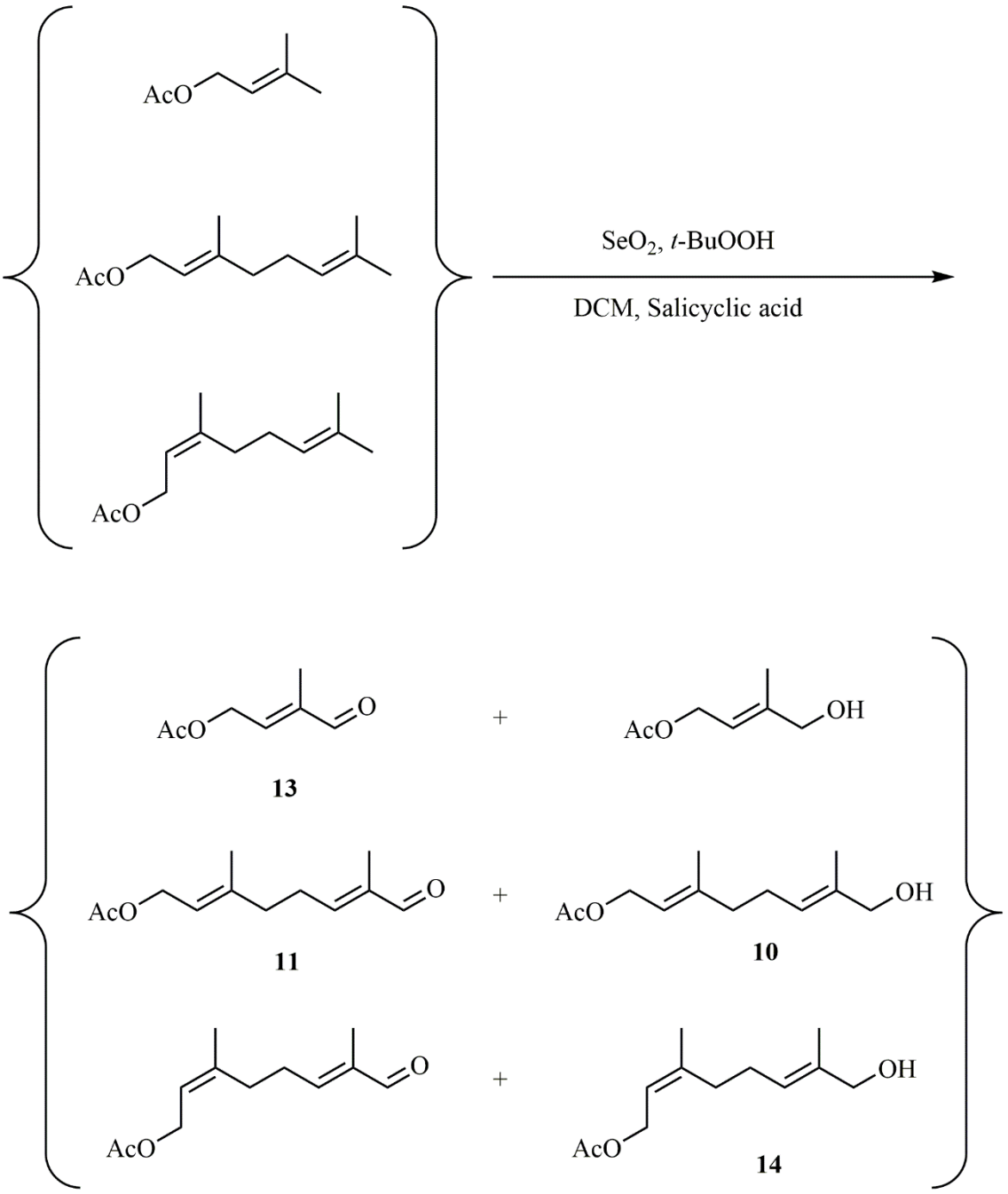

Scheme 7 - Allylic oxidation via the Sharpless Procedure for prenyl, geranyl and neryl acetate. Experimental yields: compound 10 = 44%; compound 11 = 49%; compound 13 = 38%; compound 14 = 56%). Experimental conditions: alcohol 25 °C and 24 h; aldehyde 37 °C and 48 h.

The first oxidation methodology was adapted from Jackson *et al*[280], it involved stoichiometric equivalents of selenium dioxide and was carried out under reflux and dry conditions. The crude product contained a mixture of allylic oxidation products as well as insoluble selenium oxide by products, which were subsequently filtered through a Celite pad. The filtrate containing the mixture of crude products was then purified by column chromatography isolating the aldehyde in 49% yield. The ease of the removal of the toxic selenium by products was facile by this methodology, which eliminated any contamination of the final product. Ultimately, the high temperature conditions and stoichiometric equivalents of SeO_2 led to a number of oxidation products around both of the isoprenes; resulting in a challenging purification. The difficulty in purifying the target compound *via* this method, led to a large variability in final yield and therefore required altering.

It was clear that a reduction in the amount of SeO_2 used would benefit both the purification and reduce the amount unwanted side products formed. The Sharpless procedure[223] uses *tert*-hydroperoxide, in order to re-oxidise the reduced selenium compounds, along with catalytic amounts of SeO_2. The Sharpless procedure tolerated milder conditions and produced cleaner products with reliable yields. Under these milder conditions the dominant product was the allylic alcohol, which was subsequently isolated and utilised for other reactions, or treated with manganese dioxide to form the aldehyde. The new procedure isolated the allylic alcohol with a yield of 55% of which 83% was successfully converted to the aldehyde following treatment with MnO_2. Through further optimisation of this procedure; it was found that the MnO_2 step was unnecessary, and that the ratio of alcohol to aldehyde could be skewed in the desired direction. By increasing the temperature to 37 °C and leaving the reaction to run to completion over 48 h, the aldehyde was the dominant product with a yield of 52%. If the allylic alcohol was desired, then the reaction was kept under the milder Sharpless conditions with a yield of 55%. The purification of the crude product under both of these conditions was straightforward, owing to the milder conditions and reduced SeO_2 equivalents. The removal of the toxic selenium by products through this method was achieved through several washings with a 1M NaOH solution and followed by filtration through a celite pad. The *tert*-butylhydroperoxide was found to be difficult to remove through the method described by Sharpless *et al*[223] but the addition of several washing steps, and the dilution with toluene as a solvent, removed all but trace amounts of the starting material. This allylic oxidation methodology was applied to both neryl and prenyl acetates with similar reaction profiles and yields.

4.5.3 Reductive Amination and Acetate Deprotection

The generation of an aldehyde group on the terminal end of the unsaturated chain, provided the opportunity of carbonyl conversion through to an amine by reductive amination. Interconversion through this method affords a wide range of commercially available amines with varying chemical functionalities. One such group is 2-amino-4-chlorobenzoic acid, which provides an opportunity to investigate potential π stacking, halogen and hydrogen bond interactions around the entrance to the hydrophobic cavity of both TAO and StAOX. To further investigate the effect of chain length on selectivity to potential fungicides, the reductive amination was carried out on both prenyl and geranyl acetate aldehydes (**Scheme 8**).

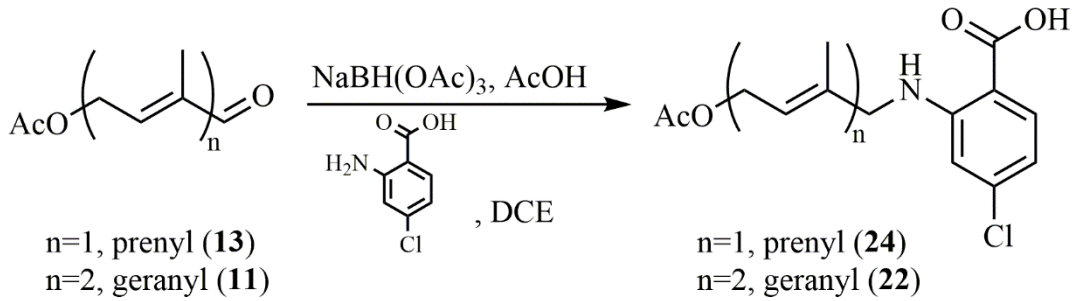

Scheme 8 - Reductive amination of prenyl (13) and geranyl acetate (11) to yield the chlorinated benzoic acid derivatives (24) in 50% and (22) in 70%, respectively.

The method employed was adapted from Gao *et al*[281] using sodium triacetoxyborohydride as the mild and selective reducing agent, with acetic acid as a catalyst. The reaction proceeds with the formation of a hemiacetal which dehydrates to form the imine intermediate. The $NaBH(OAc)_3$ will then selectively reduce the imine to form the alkylated amine. This procedure formed the desired product for both the geranyl (**22**) and prenyl (**24**) alkyl chains but presented a new problem upon purification. The product formed contains both acidic and basic properties as well as a high polarity, which offered a challenging separation under normal phase column chromatography. To improve separation of the starting materials and final products, both silica type and solvent conditions were tested. The use of either TEA or ammonia did not improve separation of the final product nor did the use of the amine functionalised silica, which usually improves the typical purification of amines or highly polar molecules. Nevertheless; the separation of the crude product was best achieved with normal phase silica with a mixture of chloroform and methanol affording both geranyl (**22**) and prenyl (**24**) amines in yields of 34% and 28%, respectively.

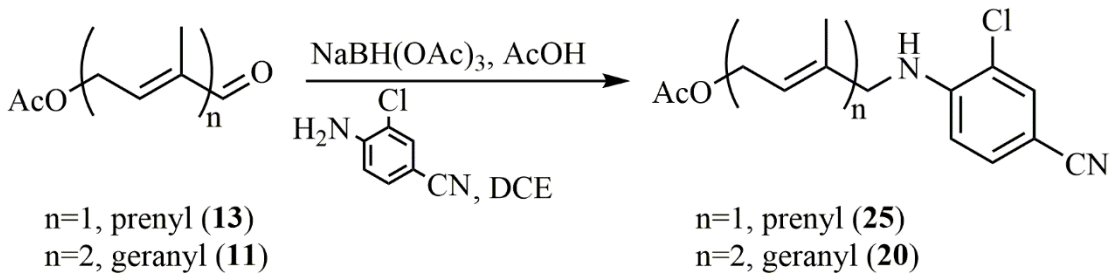

Scheme 9 - Reductive amination of prenyl (13) and geranyl (11) to yield the benzonitrile group derivatives (25) in 33% and (20) in 75%, respectively.

The reductive amination with the 4-amino-3-chloro benzonitrile group introduced a strong hydrogen bond acceptor group to investigate the relevance of the T186 residue for inhibitor binding with TAO (**Scheme 9**). The procedure was carried out in a similar manner set out for the benzoic acid above but encountered similar purifications issues. The use of acetic acid helped to dissolve the compound prior to column chromatography and was incorporated in the eluent system, which alleviated the issues with the compound precipitating in the column. An alternative method for purification was attempted through the slow addition of a copper sulfate solution. The desired product contains a secondary amine which should complex with the copper ions more readily than primary amines. However, this purification attempt failed and the final yield for the prenyl (**25**) and geranyl benzonitrile (**20**) derivatives remained at 33% and 75%, respectively.

Using a concentrated potassium hydroxide solution, acetate deprotection was achieved for compounds **20**, **22**, and **25**. The deprotection for the benzonitrile and benzoic acid derivatives produced the free alcohols in varying yields (12-70%). The benzonitrile derivatives (**21**) suffered from similar issues as with the reductive amination step, with a loss in yield following purification. The eluent system was altered again for column chromatography with the addition of ammonia and a higher ratio of methanol (80:10:1, $CHCl_3$:MeOH:NH_3). The improved eluent system yielded prenyl (**26**) and geranyl (**21**) alcohol benzonitrile derivatives in 23% and 70%, respectively. The addition of ammonia could not be utilised in the eluent system for the purification of the geranyl (**23**) or prenyl benzoic acid derivatives, owing to its acidic nature. The isolation of the geranyl benzoic acid alcohol (**23**) was achieved with only 12% overall yield but the prenyl benzoic acid alcohol could not be isolated owing to the difficult purification.

4.5.4 Unsaturated Alkyl Coupling

The procedure to carry out the tail addition of the unsaturated chains was unmodified and carried out according to the final step in the general reaction **Scheme 1**. The functionalised unsaturated chains provided a useful insight into the differences in the tail addition kinetics between functionalised and non-functionalised and saturated and unsaturated alkyl chains.

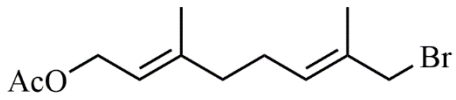

12

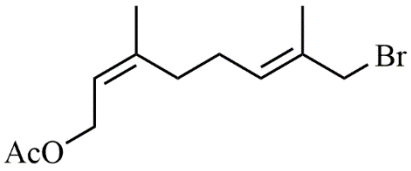

14

Figure 50 - Brominated tails for alkyl coupling. E-isomer (12) and Z (14).

The allylic oxidation of neryl, prenyl and geranyl acetates provided a number of structural analogues; presenting interesting points of comparison to their natural derivatives. **Figure 50** shows the two isomeric equivalents used to probe the AOX and complex III binding cavities. The neryl acetate oxidation presents a terminal *Z*-isomer; effectively directing the acetate group perpendicular to the rest of the chain. This structural property will effectively explore the space above and below the entrance to the hydrophobic cavity. The homology model for StAOX suggests restricted access to the active site in comparison to TAO and therefore the Z isomer should explore the validity of this model. Similarly, the Q_o binding site of the bc_1 complex has a narrow opening to the inhibitor binding site; and therefore, the *Z*-isomer should show some selectivity to the AOX.

The *Z*-isomer inhibitor was prepared according to the final tail addition step outlined in scheme 1 with a yield of 8%. The low initial yield for this step can be attributed to both the synthesis of unwanted side products and difficulties in purification. As previously described, the mechanism of the tail addition leads to the O-alkylation of the aromatic phenol groups. The opportunity for these unwanted side products to form was less apparent with the synthesis of the natural product derivatives and was therefore ignored during the optimisation process. Removal of these side products required altering the purification solvent system to include TEA and required isolation by preparative TLC. The basic conditions of this reaction also led to the formation of the deprotected *Z* -isomer, which was ultimately more attractive, as it could be used in future inhibitor assays as a comparison. The allylic oxidation of geranyl acetate affords the geranyl acetate alcohol, in a similar manner to its stereoisomer, which was subsequently brominated and used for

alkyl coupling step. The synthesis of the *E*-isomer presented the same issues as was seen with the *Z*-isomer but was isolated in much higher yields, with 20% for the final alkyl coupling step. The basic conditions of the reaction also produced the deprotected analogue of the full compound to provide further basis for comparison.

The amine functionalised tails produced in **Scheme 6**, failed to provide sufficient quantities of starting material to attempt an alkyl coupling. The low yields prevented any analysis, and means of comparison, between saturated and unsaturated amine functionalised alkyl coupling. It also prevented further structural insights into the proportionality between: the length of the alkyl chain; and selectivity between respiratory enzymes.

4.6 Conclusions

It was clear that the established routes for the natural compound derivatives required optimisation to achieve suitable yields and to create a platform for novel inhibitor synthesis. The improved yields for the first two steps of **Scheme 1**, affording the common head group, proved to be important since it was often used in high quantities and throughout all novel reaction schemes. The final coupling step was found to be the most problematic due to the synthesis of unwanted side products and the sensitivity to reaction conditions. Nevertheless; improvements were made through the use of $CaCl_2$ as a Lewis acid, effectively activating the alkyl halide and reducing the activation energy of the rate determining step of the reaction. It was also improved through the minor alterations of reactant equivalents; solvent volume; purification techniques; and the reaction temperature. However, the improvements made for the natural products could not be applied and reproduced in the novel synthetic routes.

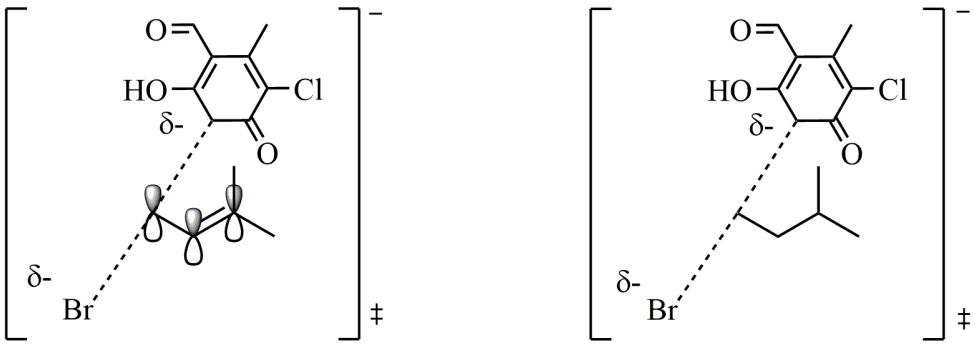

Allylic stabilised transition state Unstabilised transition state

Figure 51 - Allylic stabilisation of the rate determining step of the tail addition mechanism.

It could be hypothesised that the lack of success with the coupling of saturated alkyl chains to the Colletochlorin B head group was mainly due to mechanistic factors. The optimised tail addition step outlined in **Scheme 1** produced yields of up to 55% but the saturated tail addition failed to provide a product yield of over 1%. The key step in the tail addition mechanism involves the attack on the electrophile by the aromatic anion. This attack briefly forms a stable intermediate followed by deprotonation and a restoration of the aromaticity within the benzene ring. The rate determining step within the tail addition mechanism is the attack on the electrophile which briefly forms a transition state between the vacating halogen and incoming nucleophile. As shown in **Figure 51**, the allylic system helps to stabilise this transition state and may offer an explanation as to why the saturated tail synthesis failed to yield suitable quantities of the final compounds according to **Scheme 2**.

The successful synthesis of the unsaturated tail derivatives, shown in **Figure 52**, supports the hypothesis that the ability for the alkyl chains to stabilise the rate determining transition state, lowers the activation energy of the tail addition reaction. Since the activation energy for the rate determining step is lower, the reaction will favour the formation of the desired unsaturated alkyl product. The final tail addition step afforded the compounds shown in **Figure 52** in yields of approximately 30%, a substantial increase from the final tail addition step for functionalised saturated alkyl chains in **Scheme 2**. This data is supported by studies investigating the reactivity of allylic systems and their activation towards S_N2 mechanised reactions[282,283]. The synthesis of these unsaturated inhibitors also provided a useful comparison for the tail addition reaction mechanism, but will also explore the unique binding site characteristics of each enzyme outlined in **Section 4.2**

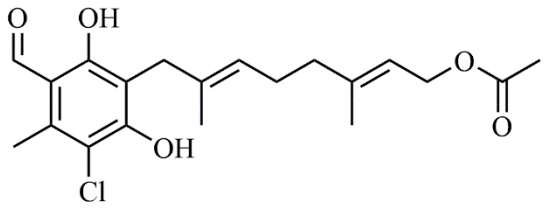

16

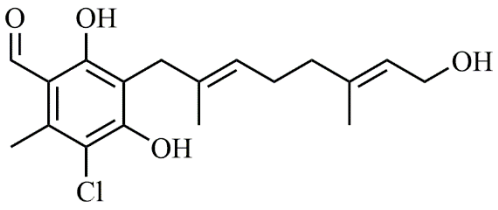

17

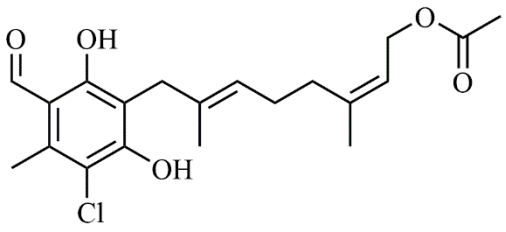

18

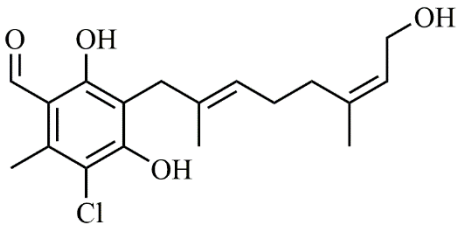

19

Figure 52 - Synthesised Derivatives of Natural Fungicides

The synthetic route for a series of functionalised unsaturated compounds outlined in **Scheme 6** failed to yield sufficient quantities of the alkyl halide starting material. The fundamental reason for the lower yield taken forward on each step in **Scheme 6** was due to the strong binding of both the polar products and starting materials to the silica gel, hampering purification efforts. Efforts to change the solvent system and type of silica gel used did not successfully improve the final yield for any step up to the free alcohol. Since the final alkyl coupling step is also often completed in low yields, a high amount of alkyl halide was required to fully characterise and isolate the final fungicide candidate. Therefore, **Scheme 6** did not yield any potential fungicide candidates to take forward to inhibition studies in **Chapter 5.**

The synthesis of amine functionalised unsaturated alkyl chains would have further supported the theory that the saturated nature of the compounds in **Scheme 2**, inhibited the progress of the tail addition rather than the terminal amine group. Furthermore, the reductive amination step **Scheme 6** would have expanded the possible tail moieties due to the abundance of commercially available starting materials. Nevertheless, progress has been made for future development of colletochlorin B derivatives through established coupling techniques and with the common natural product head group.

Chapter 5: Inhibition of the AOX and cytochrome *bc*$_1$ complex

5.1 Introduction

The discovery and identification of novel phytopathogenic fungicides relies on accurate assaying techniques to effectively discriminate between structurally similar compounds and their inhibition of a target enzyme. Traditionally, the evaluation of fungicides within the agrochemical industry focussed on random screening *via* an *in planta*[284] or *in vitro* assay systems. As described by Clarke/Delaney[285], Tice[286] and others[287–289], chemical properties such as lipophilicity, pK_a, molecular weight and solubility, can influence the efficacy of a fungicide within these systems; and therefore, may not represent an increased binding affinity to the desired target. It is important to consider the efficacy of a fungicide across a broad spectrum of assay techniques; from binding affinity (K_D) for a purified target to a whole system pot trial screen. The use of advanced *in silico* docking and QSARs can support the biological data, effectively reducing the capital and resource costs, along with the number of fungicide candidates required for evaluation.

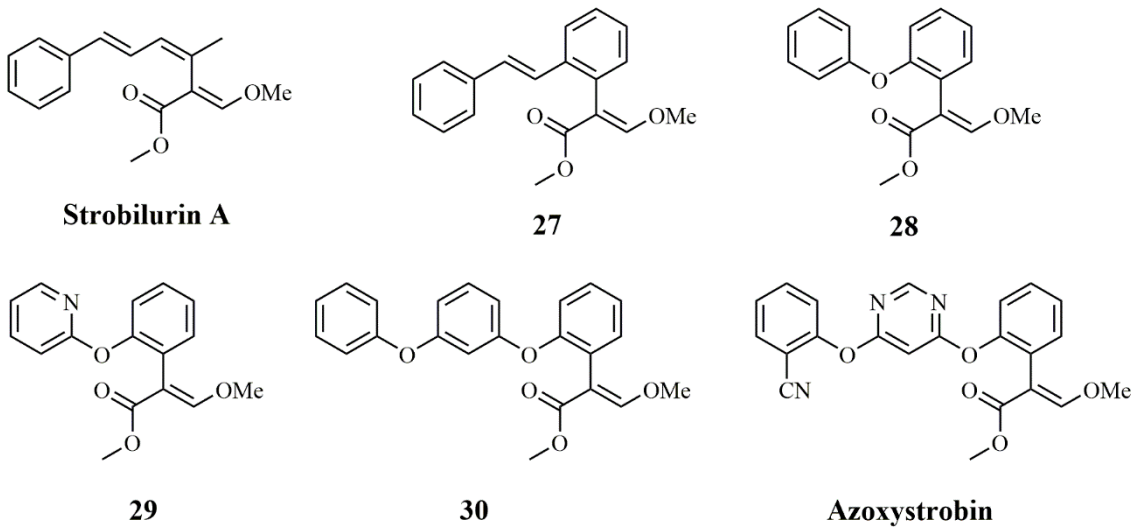

Figure 53 - Notable strobilurin fungicides candidates along with the lead compound strobilurin A and final compound azoxystrobin.

The notable cytochrome *bc1* complex fungicide, Azoxystrobin, required the synthesis of over 1400 compounds[290] prior to selection as a commercial product. Strobilurin A, the lead compound, proved ineffective following screening through *in planta* studies but showed efficacy during fungal plate assays. It was later found[291] that the (Z)-olefinic bond adjacent to the methoxy acrylate group shown in **Figure 53** was subject to photodegradation and volatility, and its replacement with an ortho substituted benzene ring (Compound **27**) reduced this volatility. A further reduction in photolytic degradation of the compound was improved by introducing the diphenyl ether as an alternative to the remaining olefinic bond linking the two benzene rings and enhancing membrane permeability[80,290,291]. Through trial and error, a large number of fungicide candidates (Compounds **27-30** in **Figure 53**) were investigated to improve systemic distribution and mobility within plants, before the final compound, Azoxystrobin, was selected.

For researchers at Syngenta, the crystal structure, modelling software and established protocols for the isolation or purification of the cytochrome bc_1 complex, were not available during the discovery of Azoxystrobin. In fact, a crystal structure of any membrane bound high or low molecular weight proteins had yet to be solved. Fortunately, the crystal structure of the bc_1 complex has now been solved for a number of typical inhibitors and modern fungicides by Berry *et al*[292–294] allowing for a better understanding of the mechanism of fungicide binding. The use of physics-based membrane permeability calculations also highlights any differences in distribution and accumulation globally within the plant or within the fungal substructures. The combination of these analyses along with measurement of the differences in binding affinity (K_D) and IC_{50} would have highlighted the reasons for lower efficacy during the lead modification process of the strobilurins.

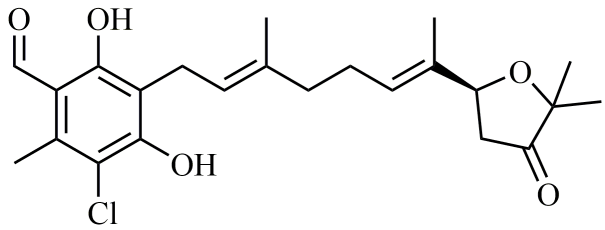

Figure 54 – Chemical structure of ascofuranone

The selection of fungicides targeting the fungal AOX has yet to be established, but research into the development of a therapeutic drug for the treatment of African sleeping sickness, targeting the *Trypanosoma brucei brucei* AOX (TAO), has been investigated. The work by Saimoto *et al*[198] intends to establish a pharmacophore for TAO by screening a number of compounds against

rTAO *E. coli* membranes. The important structural features for a potent TAO inhibitor were hypothesised by obtaining IC_{50} data for a number of ascofuranone derivatives (**Figure 54**). The 1-formyl group, 4 and 6-hydroxyl groups were suggested to interact directly with the enzyme, and the 2-methyl and 3-chloro groups providing conformational stability of the inhibitor (**Figure 55**). The literature also suggests that the furanone ring is not essential for potent inhibition of TAO[198].

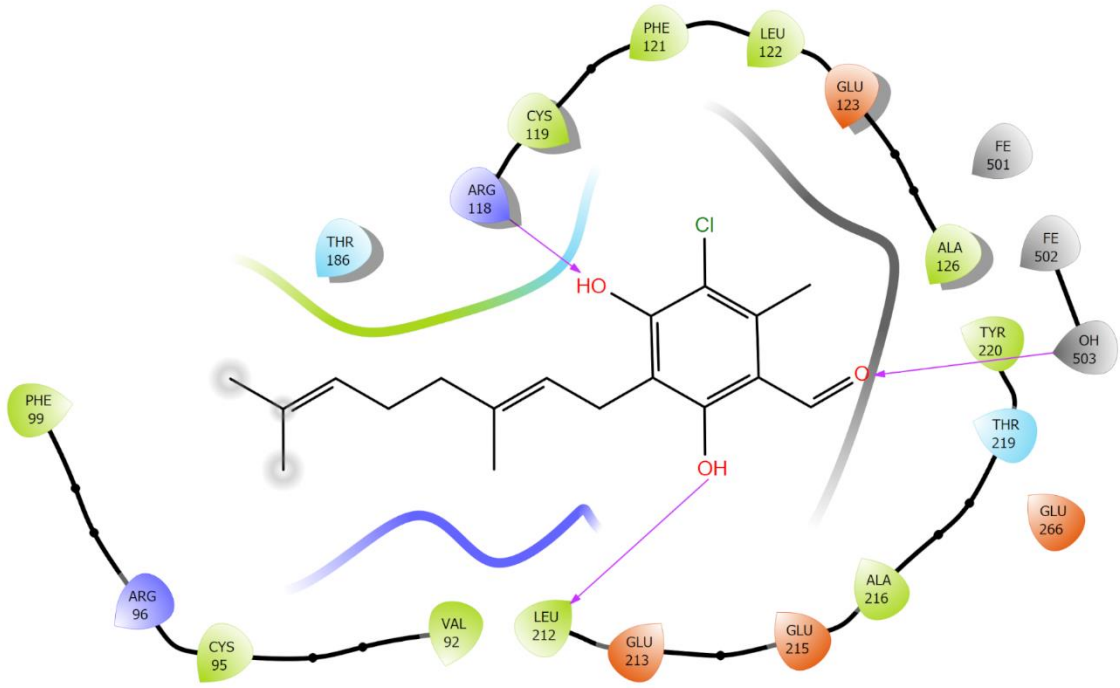

Figure 55 - Molecular interactions of colletochlorin B within the TAO crystal structure (PDB code: 3W54). Hydrogen bond interactions are highlighted by the purple arrows.

More recent studies by West *et al*[200,201] have assayed compounds against purified rTAO, *Trypanosoma brucei brucei* parasites and against human hepatocellular carcinoma cells. The lipophilicity and multiparameter optimisation (MPO) score[295] were also determined within these studies. The MPO score provides a quantitative value for the desirable physicochemical properties of prospective drugs as well as providing a measure of central nervous system enhancing the determination and selection of important inhibitor design features. In contrast to the studies by Saimoto[198], the results obtained by West *et al*[200,201] show that the 4-chloro and 3- methyl groups on ascofuranone confer high potency to rTAO. The removal of the 6-hydroxyl group did not have deleterious effects on potency, nor did substitution of the 1-formyl group with a nitrile group (**Figure 55**). A clear positive correlation between lipophilicity and rTAO inhibition was also seen

in these studies suggesting modifications to the structure of ascofuranone may not relate to improved binding but rather relates to an increased concentration within the rTAO purified lipid environment. Nevertheless, a more complete picture of inhibitor potency can be seen through the inclusion of a greater number of assay methods.

An approach for isolated measurements of inhibitor/enzyme interactions can be achieved through the use of Isothermal Titration Calorimetry (ITC). ITC is often used in the pharmaceutical industry to assess drug/enzyme interactions[296], protein-protein binding[297] and enzyme kinetics[298], providing label free binding affinities (K_D) and full thermodynamic characterisation. The observed enthalpy change (ΔH) for molecular binding event is measured through the titration of a known inhibitor into a purified enzyme solution. The differential power, required to maintain a constant temperature between the sample cell and reference cell is measured. Following saturation of the enzyme binding sites with the known inhibitor, the differential power is equal to zero, allowing for the derivation of the binding enthalpy (ΔH), binding affinity (K_D) and stoichiometry (n). It also allows for the derivation of the apparent thermodynamic constants for the Gibbs Free Energy (ΔG) and change in entropy (ΔS) according to the Gibbs Free Energy Equation (**Equation 1**). For the assessment of novel inhibitors this provides information as to the strength and type of binding to its target. The interactions that predominate the magnitude of the binding enthalpy (ΔH) are hydrogen bonds and electrostatic interactions. The change in entropy (ΔS) for a binding event is often influenced by hydrophobic interactions but can also be affected by a change in conformation of the target enzyme. The utilisation of ITC as a secondary screen for candidate fungicides may provide further details to reduce conflicting information, as highlighted during the screen of anti-parasitic agents targeting TAO.

$$\Delta G = \Delta H - T\Delta S$$

Equation 1. Gibbs Free Energy Equation.

ΔG =Gibbs Free Energy, ΔH = Enthalpy Change of Reaction, T = Temperature and ΔS = Entropy Change of Reaction.

As mentioned earlier, the recent solution of membrane bound crystal structures for mitochondrial respiratory enzyme presents opportunities for new *in silico* drug screening techniques. Homology modelling of enzyme-inhibitor interactions provides another method for quantitative, *in silico* screening for candidate fungicides. Previously, this type of screening would be unavailable for membrane bound proteins due to their notoriously difficult purification and stability in solution when attempting crystallisation. Fortunately, the crystal structure for the cytochrome bc_1 complex

has been solved for a number of species and co-crystallised with a number of established fungicides. The crystal structure for the fungal AOX has yet to be solved, but a homology model derived from TAO provides a good approximation of the binding site structure.

$$\Delta G_{bind} = C_{lipo\text{-}lipo} \sum f(r_{lr}) + C_{hbond\text{-}neut\text{-}neut} \sum g(\Delta r)\ h(\Delta\alpha) + C_{hbond\text{-}neut\text{-}charged} \sum g(\Delta r)\, h(\Delta\alpha) + C_{hbond\text{-}charged\text{-}charged} \sum g(\Delta r)\, h(\Delta\alpha) + C_{max\text{-}metal\text{-}ion} \sum f(r_{lm}) + C_{rotb} H_{rotb} + C_{polar\text{-}phob} V_{polar\text{-}phob} + C_{coul} E_{coul} + C_{vdW} E_{vdW} + \text{solvation terms}$$

Equation 2 - GLIDE Docking Score Derivation

Docking of inhibitors to these structures can be carried out by the GLIDE plugin for Maestro molecular modelling software. The software calculates a score for each docked compound according to an expanded ChemScore function (**Equation 2**). The equation takes into account a number of interactions for the enzyme-ligand complex including: lipophilicity (2^{nd} term); ligand-receptor hydrogen bonding (2^{nd}, 3^{rd} and 4^{th} terms); metal atoms (5^{th} term); rotatable bonds from carbon and hydrogen atoms (6^{th} Term); and biophysical parameters such as coulombic forces and solvation factors. The magnitude of the docking score correlates to an improved binding energy with a visual aid of the possible binding poses of the ligand-enzyme complex. Using docking software may help to eliminate candidate fungicides that show a low docking score, but since the output is theoretical, it should only be used as supporting information rather than primary fungicide selection data.

The combination of the aforementioned techniques has yet to be utilised for the discovery of an AOX targeting fungicide or for the evaluation of existing AOX inhibitors (**Figure 56**). This chapter will investigate the viability of these techniques and use them to screen both existing and newly synthesised (**Figure 57**) fungicide candidates.

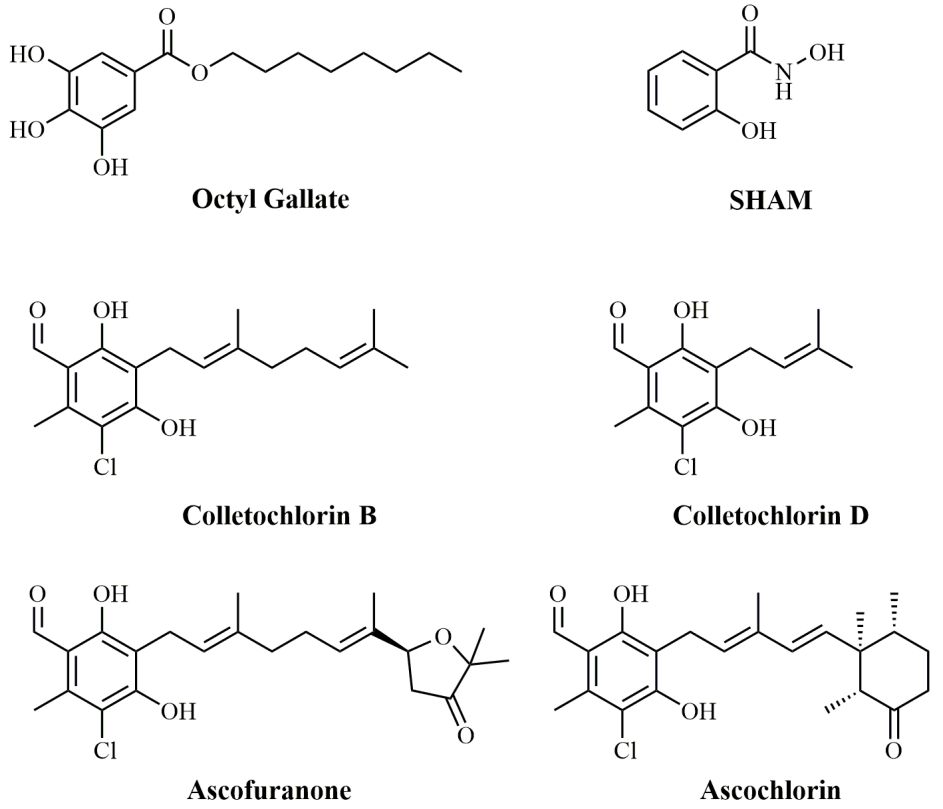

Figure 56 - Established AOX Inhibitors

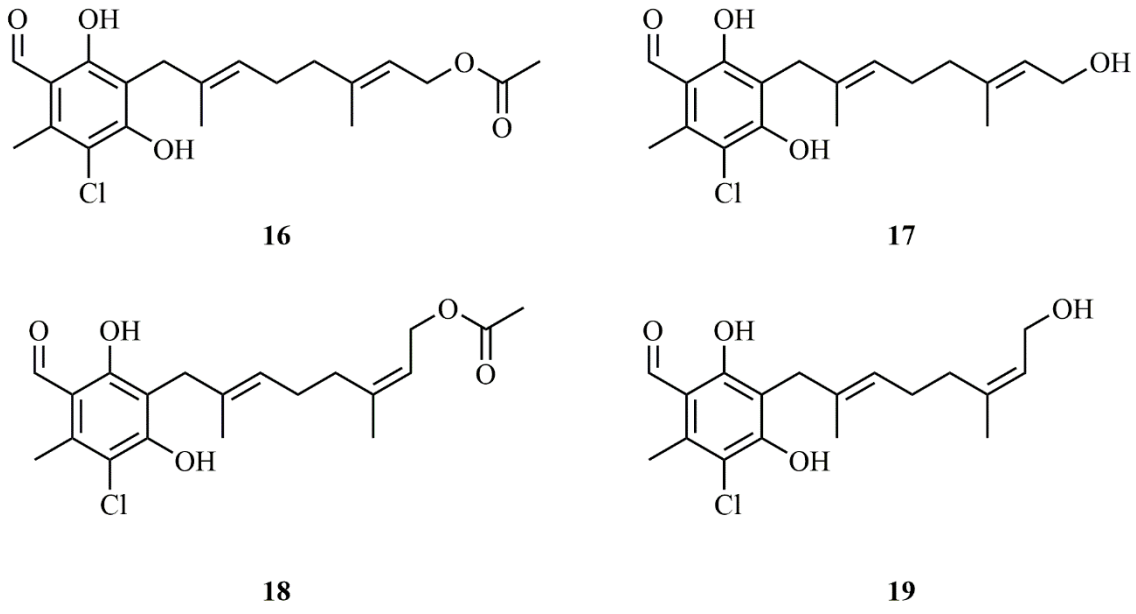

Figure 57 - Newly synthesised fungicide candidates from Chapter 4.

5.2 Chemical properties of Synthesised and Natural Compounds

The chemical properties of each compound (**Table 21**) were assessed in order to assess their viability as fungicide candidates and provide data for fungicide selection criteria. The common properties determined by Clarke/Delaney[285] and Tice[286] for candidate agrochemicals closely follows that of Lipinski's rules[299] and that of the MPO score[295]. The molecular weight (MW), lipophilicity (cLogP), acid dissociation constant (pK_a), hydrogen bond donors (HBD) and total polar surface area (tPSA) were compared to that of well-established fungicide, Azoxystrobin. The limits for each parameter as characterised by Lipinski[286,299] and others[300,301] are: MW < 500 $g.mol^{-1}$; clogP < 6; pKa 4-10; HBD < 5; and tPSA < 140 Å.

Table 21

Physicochemical Properties of Established and Newly Synthesised Candidates Fungicides

Inhibitor	**MW/ $g.mol^{-1}$**	**cLogP**	**pK_a**	**HBD**	**tPSA/ Å**
Azoxystrobin	403.4	3.11	-	0	102.5
SHAM	153.1	0.88	8.36	3	69.6
Octyl Gallate	282.3	4.63	7.73	3	87.0
Colletochlorin D	254.7	4.26	12.07	2	57.5
Colletochlorin B	322.8	6.29	12.06	2	57.5
Ascochlorin	404.9	6.08	12.05	2	74.6
Ascofuranone	420.9	6.02	12.06	2	83.8
Compound **16**	380.9	5.45	12.04	2	83.8
Compound **17**	338.8	4.50	12.04	3	77.8
Compound **18**	380.9	5.45	12.04	2	83.8
Compound **19**	338.8	4.50	12.04	3	77.8

Note. All structure property prediction and calculations were carried out using ChemDraw.

The three most studied natural compounds colletochlorin B, ascochlorin and ascofuranone exhibit poor drug-like properties. In comparison, compounds **16**-**19** synthesised in Chapter 4 fail to meet drug likeness for only one category, acid dissociation constant (pK_a). These compounds also show a reduced lipophilicity in comparison to that of colletochlorin B, ascochlorin and the lead compound ascofuranone. Compounds **16-19** predict physicochemical properties improving on the existing AOX inhibitors and are more closely aligned to that of azoxystrobin.

5.3 *E. coli* Membrane Assays

The *E. coli* membrane samples obtained for the overexpression of AOX species, outlined in Materials and Methods section, provides a system by which AOX activity and inhibition can measured. The reaction pathway is initiated by the addition of an excess of NADH (1.25 mM), reducing quinone to quinol *via* Complex 1, which is then utilised by the AOX to reduce O_2 to H_2O. The quinone reduction cycle shown in **Figure 58** provides a graphical representation of this reaction pathway within the FN102 *E. coli* membrane samples. Since the generation of one mol of quinol is equivalent to 1 mol of NADH consumed, the *E. coli* membrane system allows for the measurement of direct or indirect measurement of AOX activity.

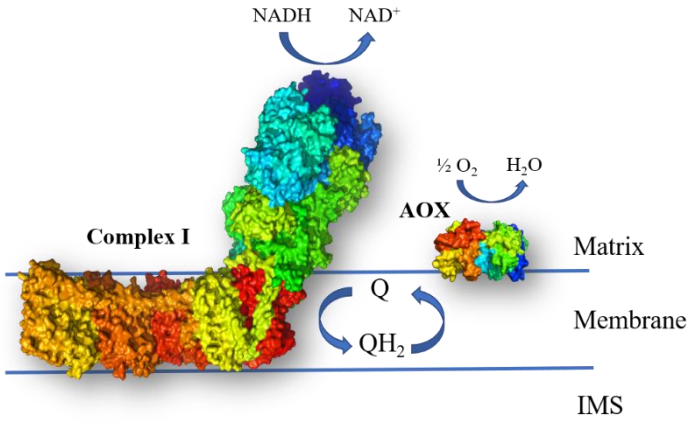

Figure 58 - Quinone Reduction Cycle in FN102* E. coli *membrane system. Complex 1 (PDB code: 6GCS)

5.3.1 O_2 Respirometry Assay

The Oroboros 2K respirometer allows for the direct measurement of AOX activity within the *E. coli* membrane samples, allowing for the generation of dose response curves for each AOX species. The data is analysed by non-linear regression providing an IC_{50} value as described in the Materials and Methods **Section 2.8.1**. **Table 22** summarises the data obtained from the titration of known AOX inhibitors against both TAO and StAOX *E. coli* samples. For ease of comparison the raw IC_{50} data is converted into pIC_{50}, a negative logarithm derivative. The data sets for each inhibitor and for each species are normalised according to the same AOX activity, providing an equal means of comparison. The inclusion of the calculated lipophilicity (cLogP) provides context to the inhibitory effect shown by each inhibitor.

Table 22

Titration of known Inhibitors against TAO and StAOX* E. coli *membrane samples

Inhibitor	cLogP‡	pIC_{50}†	
		TAO*	***StAOX***
SHAM	0.9	5.21 ± 0.19	4.19 ± 0.01
Octyl Gallate	4.6	6.64 ± 0.01	7.07 ± 0.36
Colletochlorin D	4.3	7.48 ± 0.05	7.51 ± 0.18
Colletochlorin B	6.3	8.13 ± 0.05	9.16 ± 0.59
Ascochlorin	6.1	8.16 ± 0.16	6.11 ± 0.21
Ascofuranone	6.0	8.26 ± 0.33	8.86 ± 0.05

Note. † Negative log concentration and standard deviation for 50% inhibition for TAO and StAOX *E. coli* membranes. * Data obtained by Dr. Luke Young[259], ‡cLogP values calculated using ChemDraw software. All assays normalised to the same rate of AOX O_2 reduction and carried out in MOPS (65 mM) with the addition of NADH (1.25 mM) and KCN (1 mM).

The results in **Table 22** demonstrates the range of potencies for the commonly used AOX inhibitors. The inhibition of both TAO and StAOX samples by SHAM is significantly weaker than other inhibitors, which is surprising given its continued use as a specific AOX inhibitor in the literature[114,151–153,261]. The reason for the lack of inhibition is unclear from initial IC_{50} data but the low lipophilicity may account for reduced concentration of inhibitor within the *E. coli* membrane. Octyl gallate shows a significantly improved inhibition in comparison to SHAM for both TAO and StAOX. The increase in inhibitory activity is coupled to an increase in lipophilicity allowing for the accumulation of inhibitor within the membrane. A graphical representation of the dose response curves for each compound is displayed in **Figure 59**.

The natural quinol like derivatives of the colletochlorins, ascofuranone and ascochlorin provide an interesting picture in terms of inhibition. The increase in lipophilicity and carbon chain length from colletochlorin D to colletochlorin B provides an increase in potency by 2 orders of magnitude for TAO and an even greater increase for that of StAOX. The differences in inhibition between the two AOX species with colletochlorin B could not be attributed to differences in cLogP; and therefore, it may be suggested that a preferential binding is responsible. The opposite affect can be seen with the pIC_{50} values for ascochlorin with inhibition 3 orders lower in TAO vs StAOX. The data for ascofuranone suggests a similar binding and inhibition profile which highlights its importance as a universal AOX specific inhibitor and lead compound.

Although IC_{50} measurements for TAO and StAOX using the Oroboros respirometer provides reliable and accurate results, the data acquisition is too time consuming to be employed for

extensive fungicide screening. Nevertheless; it has utility when comparing results to that of existing published inhibition results in the literature.

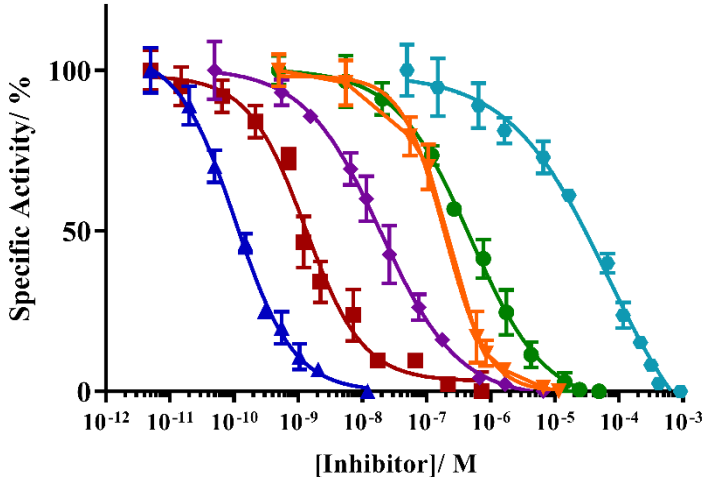

Figure 59 - Normalised Dose Response Curves for Established Inhibitors against StAOX* E. coli *membranes via the O_2 Respirometry Assay. SHAM (Turquoise), Ascochlorin (Green), Octyl Gallate (Orange), Colletochlorin D (Purple), Ascofuranone (Red) and Colletochlorin B (Blue).

5.3.2 Spectrophotometric Plate Assay

The use of a spectrophotometer with 96-well plate scanning capabilities, dramatically reduced the time taken to screen prospective fungicides. The assay technique can be applied to both recombinant *E. coli* membrane and purified AOX samples with the potential for process automation. AOX activity is measured indirectly through the consumption of NADH at 340 nM facilitating the generation of dose response data. StAOX samples required the addition of GMP (1.5 mM) to stimulate enzymatic turnover and generate measurable NADH reduction rates. Although the preparation *E. coli* membrane is carried out in a heme deficient *E. coli* strain, the addition of potassium cyanide ensures AOX activity is measured, by inhibiting any residual bacterial b_d/b_o activity.

To validate this methodology and assess its accuracy in comparison to O_2 assay method, the well-established natural inhibitors were assessed according to pIC_{50}. **Table 23** displays the pIC_{50} results for StAOX *E. coli* membranes when titrated against known AOX inhibitors according to the methodology outlined in Materials Methods **Section 2.8.2**. A graphical representation of the dose response curves for each compound is displayed in **Figure 60**.

Table 23

Dose response and cLogP data for known AOX inhibitors against StAOX* E. coli *membranes.

Inhibitor	cLogP	StAOX pIC_{50}[†]
SHAM	0.9	4.36 ± 0.03
Octyl Gallate	4.6	6.64 ± 0.02
Colletochlorin D	4.3	7.04 ± 0.01
Colletochlorin B	6.3	9.17 ± 0.40
Ascochlorin	6.1	6.17 ± 0.03
Ascofuranone	6.0	8.79 ± 0.15

Note. [†] Negative log concentration and standard deviation for 50% inhibition for StAOX *E. coli* membranes. All assays carried out in MOPS (65 mM) with the addition of NADH (1.25 mM), GMP (1.5 mM) and KCN (1 mM).

The pIC_{50} data obtained from the plate assay screen was shown to produce precise and comparable data to that of the O_2 assay. One notable difference between the O_2 assay and the plate assay, is the reduced standard deviation, and therefore accuracy, of the measurements when performed on the spectrophotometer. The repetition of the assay for known AOX inhibitors also confirms the conclusions made from the O_2 assay. The IC_{50} for colletochlorin B in respect to StAOX is ten times higher than that of TAO. Ascochlorin also exhibits a diminished inhibitory effect in comparison to TAO; both of these results suggest there maybe structural binding site differences.

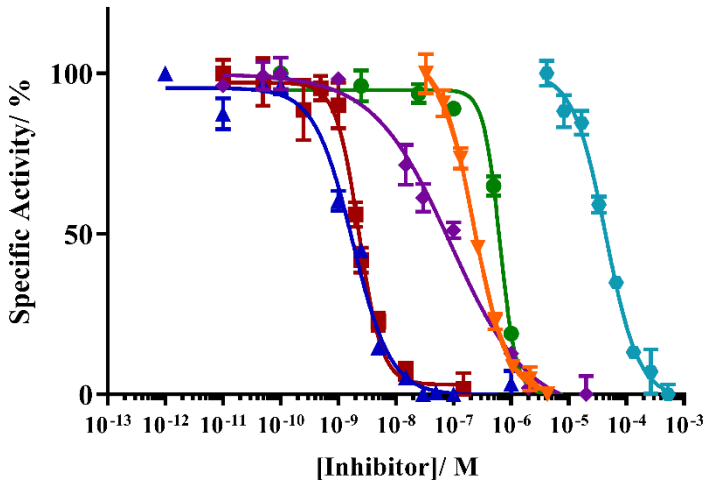

Figure 60 – Normalised Dose Response Curves for Established Inhibitors against StAOX* E. coli *membranes. SHAM (Turquoise), Ascochlorin (Green), Octyl Gallate (Orange), Colletochlorin D (Purple), Ascofuranone (Red) and Colletochlorin B (Blue).

The plate assay protocol provides an efficient and repeatable process for the evaluation of the pIC_{50} for AOX inhibitors. It was therefore taken forward in order to evaluate the compounds designed and synthesised in **Chapter 4** for the inhibition of the fungal AOX and/or cytochrome bc_1 complex (**Figure 61**). **Table 24** presents the data obtained following the evaluation of the aforementioned novel fungicide candidates against StAOX and TAO *E. coli* membranes. The inclusion of the assessment of TAO provides means for comparison between AOX species and between structurally different binding sites.

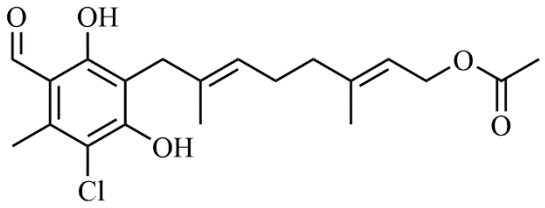

16

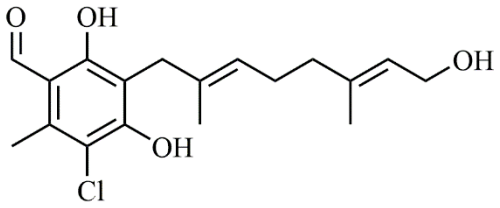

17

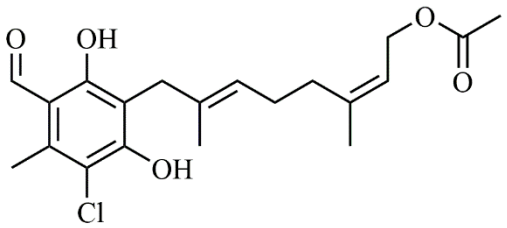

18

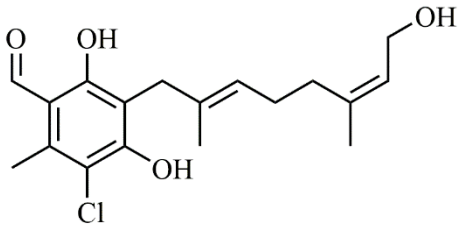

19

Figure 61 - Novel AOX and Cytochrome* bc$_1$ *Complex Candidate Fungicides synthesised in Chapter 4.

The novel fungicide candidates, which have been synthesised and outlined in **Chapter 4**, show a significantly reduced efficacy against StAOX membrane samples in comparison to that of TAO. The absence of any correlation between lipophilicity and pIC_{50} suggests that the inhibition from each of the compounds is influenced by the binding interaction of the inhibitor. The introduction of the (*Z*)-olefinic bond had an improved inhibitory against StAOX effect when compared to both the free alcohols (compounds **17** and **19**) but is removed when comparing the acetate protected compounds **16** and **18**. A correlation between the introduction of the (*Z*)-olefinic bond or acetate protecting group and the inhibition of the StAOX enzyme was not discernible; and therefore, deductions have to be made for each compound individually.

Table 24

Dose Response Data for the Inhibition of TAO and StAOX* E. coli *membranes with Novel Fungicide Candidates

Inhibitor	clogP	pIC_{50}[†]	
		TAO	*StAOX*[*]
Compound **16**	5.4	5.07 ± 0.02	5.71 ± 0.03
Compound **17**	4.4	6.92 ± 0.03	4.95 ± 0.18
Compound **18**	5.4	6.05 ± 0.03	4.23 ± 0.10
Compound **19**	4.4	7.26 ± 0.01	5.40 ± 0.22

Note. [†] Negative log concentration and standard deviation for 50% inhibition of StAOX and TAO E. coli membranes. [*] Inhibition carried out on stimulated specific activity of StAOX with GMP (1.5 mM). All assays performed in MOPS (65 mM) with additions of KCN (1 mM) and NADH (1.25 mM).

The range of pIC_{50} values obtained from the measured inhibition of TAO *E. coli* membranes demonstrates an increased sensitivity to alterations of the length and 3D structure of the novel fungicide candidates. In a similar manner to that of StAOX a correlation between cLogP and pIC_{50} suggest the increased inhibition is not a result of increased membrane concentration but rather a symptom of binding interactions. The addition of the acetate group to both compounds **17** and **19** was deleterious to TAO inhibition. The opposite result was achieved following the introduction of the (*Z*)-olefinic bond in the terminal position of the tail group. The dose response curves to allow for derivation of pIC_{50} values are displayed in **Figure 62** for TAO and **Figure 63** for StAOX.

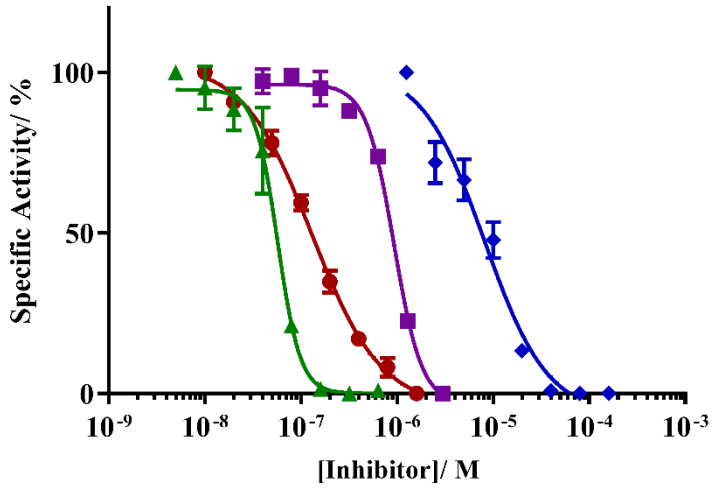

Figure 62 - Dose Response Curves for TAO E. coli membranes. Compound 17 (Red), compound 18 (Purple), compound 19 (Green) and compound 16 (Blue)

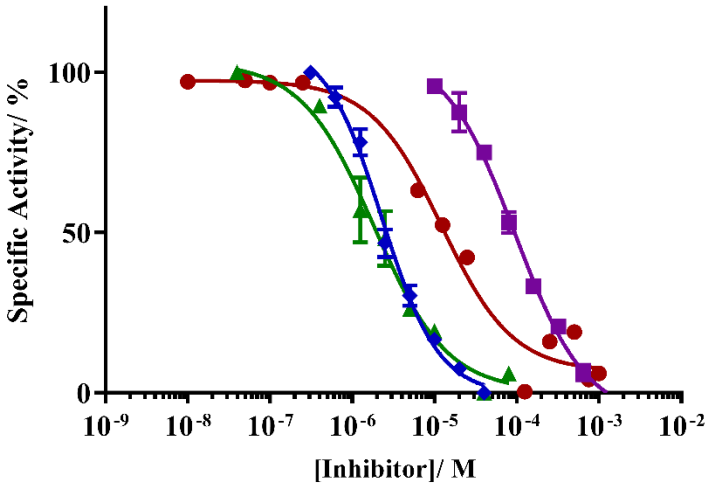

Figure 63 - Dose response curve for StAOX* E. coli *membranes. Compound 17 (Red), compound 18 (Purple), compound 19 (Green) and compound 16 (Blue).

5.4 Mitochondrial Succinate: Cytochrome c Oxidoreductase Assay

The screening of candidate fungicides against whole mitochondria provides an opportunity to assess the inhibitory effect of each compound against both Complex II and Complex III enzymes. The isolation of mitochondria from rat liver, kindly carried out by Alicia Rosell-Hidalgo, also provides information as with respect to whether any non-target or cytotoxic issues occur. All preparations were carried out in accordance to the protocol outlined in Materials and Methods **Section 2.5** and **2.8.2**.

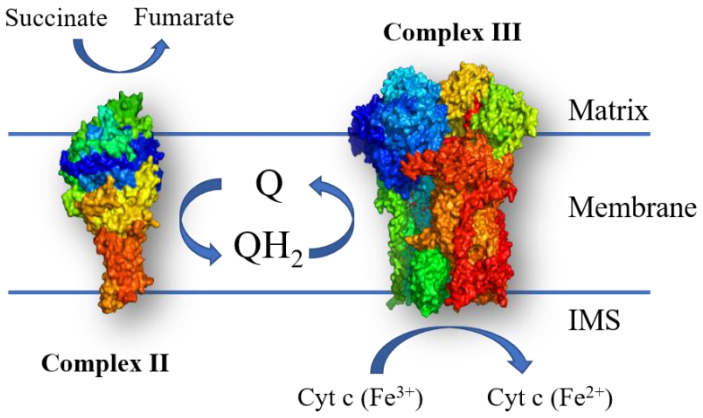

Figure 64 - Mitochondrial pathway for the Measurement of Complex II and III activity in Isolated Mitochondria

The initiation of the reaction pathway is achieved through the addition of succinate to trigger quinone reduction and yield the substrate for cytochrome bc_1 complex, quinol. The reduction of cytochrome c is measured spectrophotometrically providing the enzymatic activity of complex III. An overview of the reaction pathway is summarised in **Figure 64**.

Since the inhibition of Complex II would also see a reduction in the activity of Complex III it was important to perform a further assay to confirm inhibitor binding to complex III. The DCPIP assay allows for the measurement of Complex II activity following the reduction of DCPIP at 600 nM in the presence of antimycin A to inhibit cytochrome bc_1 complex activity. The results of this assay showed no inhibition of Complex II for any of the newly synthesised compounds at double the IC_{50} concentration. These results confirmed that the inhibition of the cytochrome bc_1 complex was due to a direct interaction with the enzyme.

Table 25

Dose Response Data for Candidate Fungicides against Rat Liver Mitochondria

Inhibitor	**cLogP**	**Complex II & III pIC_{50}**
Compound **16**	5.4	N.I.
Compound **17**	4.4	5.27 ± 0.27
Compound **18**	5.4	4.18 ± 0.05
Compound **19**	4.4	5.19 ± 0.01

Note. Negative log concentration and standard deviation for 50% inhibition for cytochrome bc_1 complex activity. All assays carried out in buffer outlined in **Section 2.5** with the addition of cytochrome c (64 μM), ATP (1 mM) succinate (10 mM) and rotenone (1 μM).

The data presented in **Table 25** provides a strong indication that these novel fungicide candidates exhibit weak inhibition of both Complex II or III. The lack of any correlation between cLogP and pIC_{50} supports the suggestion that the inhibition is not wholly influenced by an increased accumulation of inhibitor concentration within the membrane. It can therefore be concluded that the introduction of an acetate protecting group has a deleterious effect on inhibition of both complex II and III mitochondrial enzymes. A 10-fold difference in inhibition can be seen between both compounds **17** and **19** and their acetate protected derivatives. The inclusion of this group increases the carbon chain length of the compound, and thus suggesting a prevention of favourable binding within the size restrictive Q_o binding site in Complex III (highlighted in **Chapter 4**).

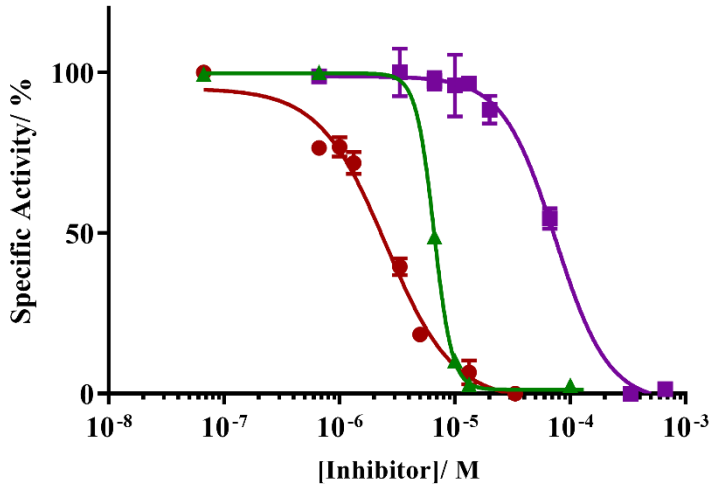

Figure 65 - Dose Response Curves for Novel Fungicide Candidates against Rat Liver Mitochondria.

A graphical representation of the dose response curves for each compound is displayed in **Figure 65**. The difference in inhibition between Compounds **17** and **19** suggests the presence of the (*Z*)-olefinic bond at the terminal end of the inhibitor structure does not severely curtail or enhance inhibition. The increase in inhibitory activity seen for compound **19** when analysing TAO data sets suggests its inclusion could provide a route for selectivity for the AOX. The intolerance for any of the novel fungicide structures suggests that selectivity can be achieved for AOX species.

5.5 Purified Protein Assay (ITC) and Optimisation

The pIC_{50} data obtained from the aforementioned techniques is useful as a primary screen for candidate fungicides but is not sufficiently sensitive for the selection of beneficial chemical properties. For example, the primary screen for rTAO membranes *via* the O_2 assay measures the pIC_{50} for the three structurally dissimilar compounds colletochlorin B, ascochlorin and ascofuranone as 8.13, 8.16 and 8.26, respectively. The marginal differences between the efficacy of these compounds in comparison to a significant change in the chemical structure of the inhibitor tail group, hampers the selection and future design of new inhibitors. It is therefore important to discover the mechanism of inhibition and whether this is due to an increased binding affinity, increased concentration within the membrane or competition with the natural substrate. The use of ITC as secondary screen for candidate fungicides or AOX inhibitors should provide a clearer picture and improve selection outcomes.

Since the extensive optimisation for the purification of StAOX yielded a largely inactive protein, it can be assumed that the binding site lacked structural similarity to its natural form. The analysis of the binding affinity for inhibitors on a misfolded or conformationally altered protein, such as StAOX would not yield accurate or suitable data. The analysis of common inhibitors was therefore considered for rTAO purified protein for which an established and reliable purification protocol was possible. It was hoped that the development of a suitable protocol for rTAO could then be applied to StAOX in the future. However, the existing purification protocol for rTAO required adaptation to be suitable for ITC applications.

5.5.1 Buffer selection

An analysis by ITC involves a precise measurement of the binding enthalpies that occur following a ligand-protein binding event. The sensitivity of this measurement requires precise buffer matching of both ligand and protein solutions. Any heat evolution from the dilution of chemical species not present in one of the solutions will fail to measure an accurate binding event. The use of Tris buffer in the purification of rTAO is unsuitable for ITC measurements since the enthalpy of reaction (ΔH_r) obscures any heat evolved during ligand binding; due to proton cycling between the ligand-enzyme complex and the buffer. The selection of the correct buffer for purified rTAO must also present favourable properties for the correct pH and stabilisation of the protein as well as for ITC analysis.

Table 26

Properties for a Selection of Common Biological Buffers

Buffer	**pK_a**	**pH Range**	**ΔH_r ($kJmol^{-1}$)**	**$d(pK_a)/dT$**
Tris	8.07	7.5-9.0	47.5	-0.028
MOPS	7.18	6.5-7.9	21.1	-0.015
Phosphate	7.19	5.8-8.0	-8, 3.6, 16.0	-0.003
MES	6.27	5.5-6.7	14.8	-0.011
HEPES	7.56	6.8-8.2	20.4	-0.014

Note. All buffer properties described as stated from Ferreira *et al*[256].

The enthalpy released following dilution (ΔH_r) is more than halved by using any of the common buffers outlined in **Table 26**. From the initial selection, MES buffer appears to provide a significant reduction in evolved heat following an inhibitor-enzyme binding event, but was eliminated since the pH range would not be suitable for optimal TAO activity. HEPES buffer would equally suit ITC experiments, but due to its ability to form radical species with H_2O_2 it would not be suitable for redox studies that are often carried out with this protein[302]. Phosphate buffer displays the lowest temperature dependency ($\mathbf{d(pK_a)/dT}$) and enthalpy of dilution (ΔH_r) of all the buffers, but introduces a more complex variable when it comes to controlling ionisation strength. MOPS was therefore examined as an alternative to Tris buffer and assessed to determine the stability of AOX protein within the buffer. The ionisation strength and pH were kept constant to ensure any activity differences were due to the buffer itself.

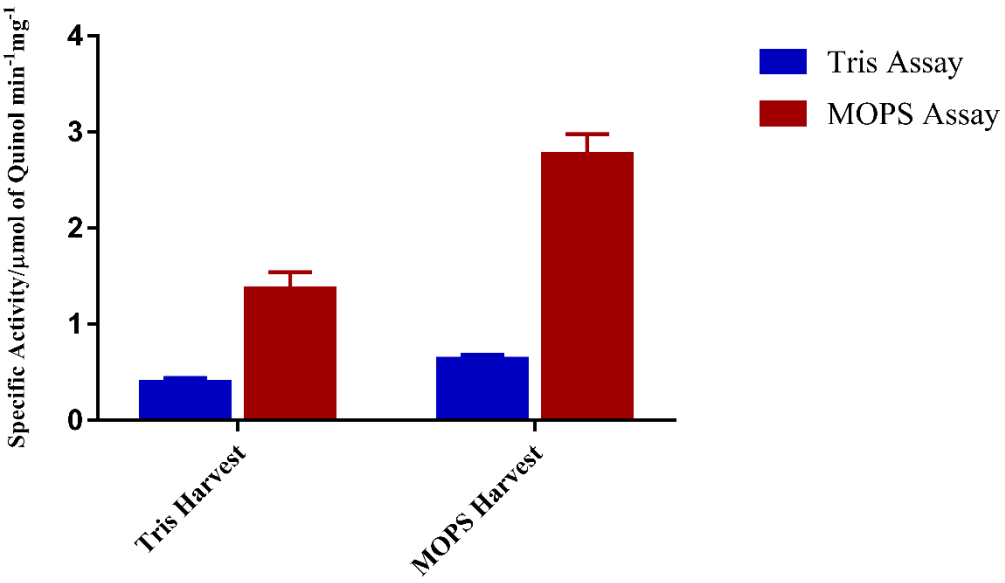

Figure 66 – Specific Activity of purified rTAO in MOPS and Tris buffers.

The change of buffer from MOPS to Tris produced an enhanced activity for purified rTAO samples as shown in **Figure 66**. The reduction in the specific heat of dilution and temperature dependency favours the stability and specific activity of purified TAO with no deleterious effects. It was therefore taken forward as the buffer preference to be used for ITC measurements.

5.5.2 DMSO tolerance

The natural inhibitors to be examined by ITC are not soluble in the water-based MOPS buffer solution and require the addition of DMSO to prevent precipitation. The precise matching of buffers is imperative when carrying out an ITC measurement, therefore the tolerance for the TAO protein to accept the harsh DMSO conditions was examined. The specific activity of rTAO provides a good approximation for the stability and correct conformation of the protein.

As shown in **Figure 67**, a concentration of up to 2% DMSO is tolerated before a substantial loss in activity was observed. At 5% DMSO concentration only 64% of the original activity for rTAO was lost and therefore the balance between AOX stability and inhibitor solubility should be assessed for each compound.

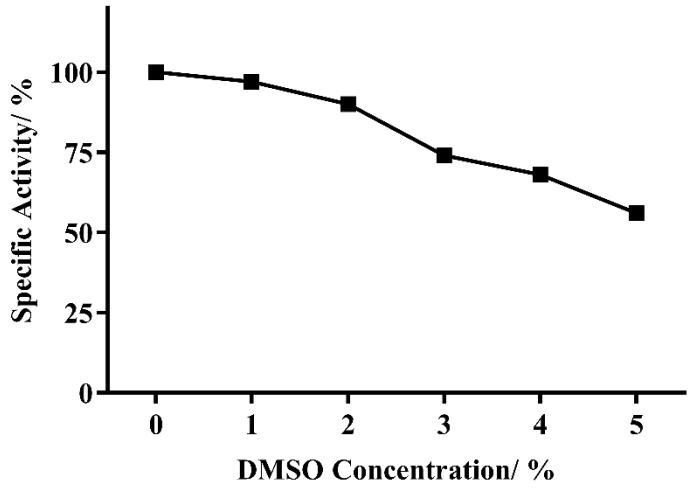

Figure 67 - Effect of DMSO Concentration on the Specific Activity for purified rTAO

5.5.3 ITC results for TAO

The known inhibitors colletochlorin B, ascochlorin and ascofuranone were selected for secondary screening with ITC, due to the close similarity between the compounds O_2 assay pIC_{50} data, which failed to yield discriminatory evidence around the differences in chemical structure. The application of ITC is not suitable as a method of primary screening since the process is time consuming and requires trial and error to optimise the experimental conditions. It was therefore utilised to better understand the binding mechanism of these 3 inhibitors and gain knowledge of the TAO binding site.

The titration was performed by preparing a dialysed rTAO protein solution with a 4% DMSO concentration. A high DMSO concentration was required since the precipitation of ascochlorin and ascofuranone was seen at lower concentrations within the loaded syringe. Inhibitors solutions were prepared from DMSO stock solutions and diluted with the appropriate volume of dialysis buffer, ensuring the concentration of DMSO remained the same in both protein and inhibitor solutions.

The raw isotherm and binding plots for the interactions between rTAO and the known inhibitors are shown in **Figure 68** and **Figure 69**. The stoichiometry (N) for each inhibitor-protein reaction is a third of what is to be expected for an AOX-inhibitor complex. The stoichiometry between an AOX and ligand interaction should be equal to 1 since there is only one binding cavity present for each AOX monomer. The stoichiometry data suggests three structurally similar TAO proteins with differing weights within each purification sample, highlighting an area of improvement for consistent protein purification. The raw data also suggests a unique binding event occurs following a titration of colletochlorin B. The raw isotherm plot in **Figure 68B** displays uneven and jagged spikes when approaching full saturation. This measurement may be due to a change in conformation of the protein or perhaps due to enzymatic conversion of the inhibitor.

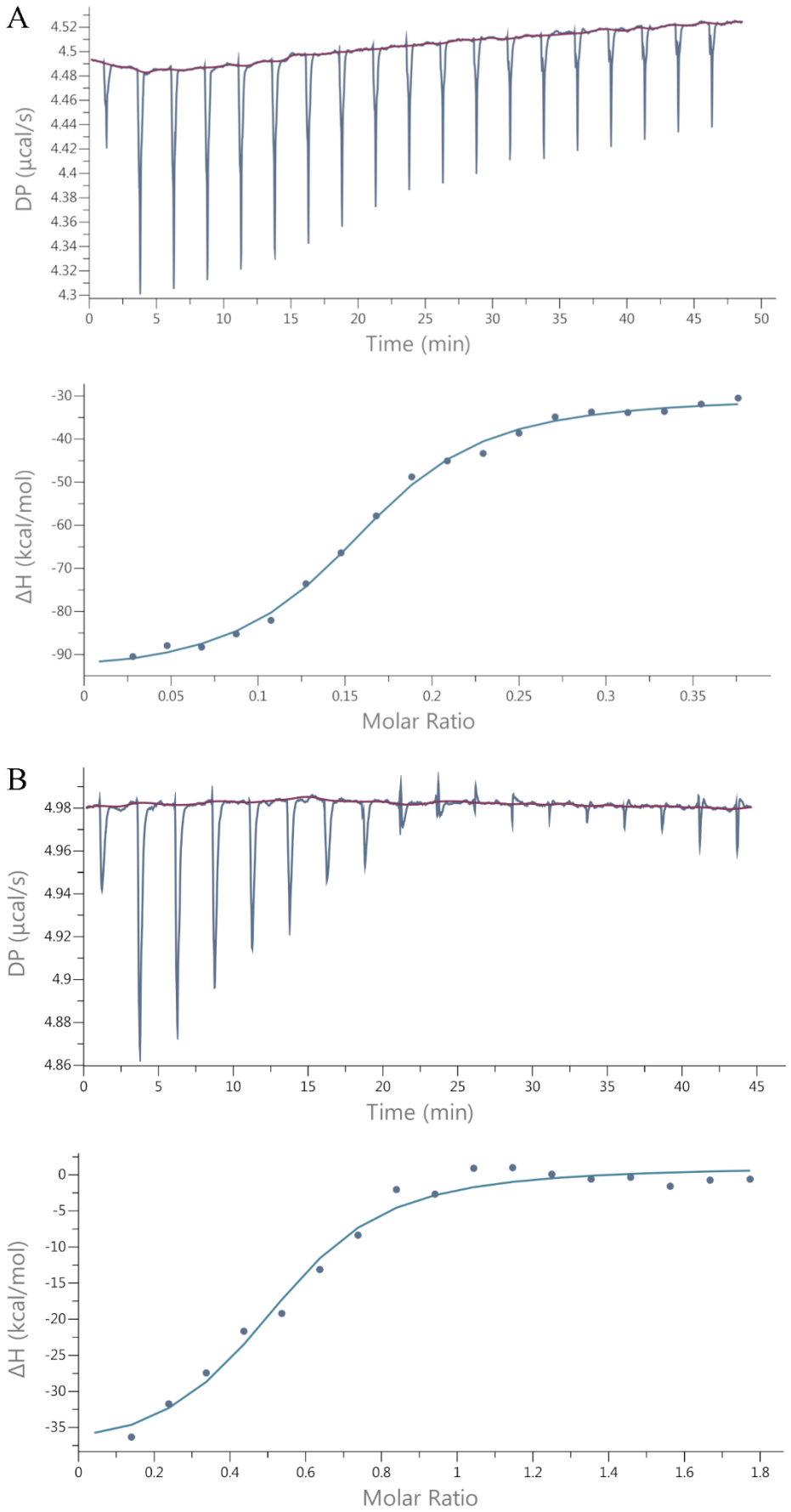

Figure 68 - Raw Isotherm and Binding Plots for TAO against Ascofuranone (A) and Colletochlorin B (B)

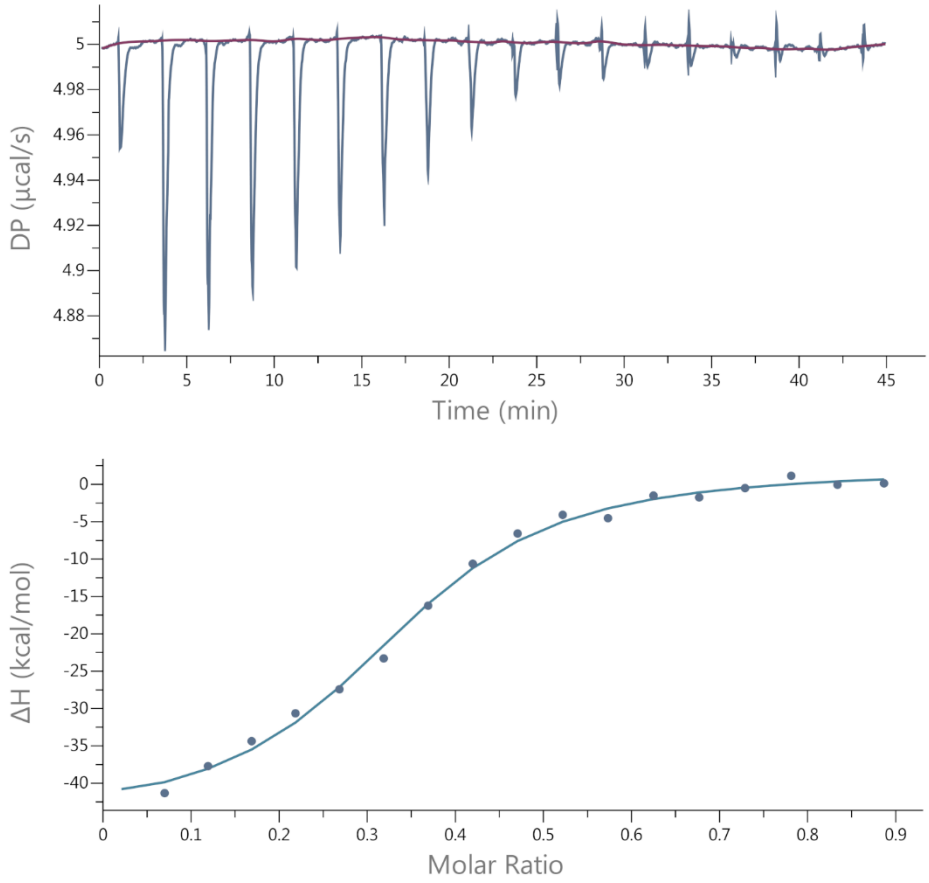

Figure 69 - Raw Isotherm and Binding Plot for TAO against Ascochlorin.

Table 27

Summary of ITC results for known inhibitors of rTAO

			Thermodynamic Parameters		
Inhibitor	***K_d (nM)***	***N***	***ΔH_{obs}***	***ΔG_{obs}***	***$-T\Delta S$***
Ascofuranone	49 ± 2	0.30	-64.4 ± 1.2	- 9.98 ± 0.03	54.4 ± 1.1
Colletochlorin B	165 ± 40	0.32	-36.2 ± 4.7	-9.27 ± 0.2	26.9 ± 4.6
Ascochlorin	132 ± 28	0.34	-41.9 ± 5.5	-8.76 ± 0.5	33.1 ± 5.0

Note. All assays performed in dialysed buffer as described in **Section 2.9.1** with a syringe concentration of 20-50 µM and a purified protein sample in the cell with a concentration of 5 µM. All assays performed at 25 °C with 1 µl injection volume.

The ITC results summarised in **Table 27**, shows the same rank order of inhibition that was seen with the pIC_{50} data from the O_2 assay, with ascofuranone displaying the highest binding affinity ($\mathbf{K_d}$) followed by ascochlorin and colletochlorin B (**Figure 70**). The binding affinity ($\mathbf{K_d}$) supports and reinforces the pIC_{50} data obtained previously but the thermodynamic parameters provide a much clearer picture as to the mode of binding and interactions within the binding site.

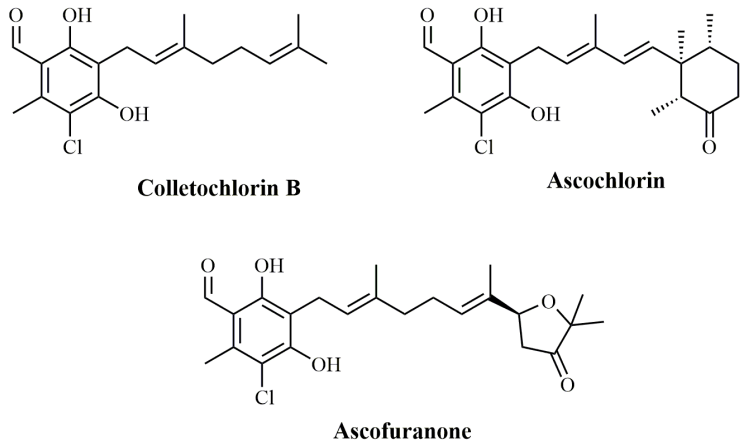

Figure 70 - Known AOX inhibitors evaluated by ITC.

The change in observed enthalpy change ($\mathbf{\Delta H_{obs}}$) represents the summation of H-bonding and electrostatic interactions. The large increase in magnitude of $\mathbf{\Delta H_{obs}}$ for ascofuranone in comparison to colletochlorin B is potentially the result of the inclusion of the furanone ring with both the ether and ketone group involved in binding with the TAO hydrophobic cavity. A similar, but more modest, increase from colletochlorin B to ascochlorin is possibly a result of the hydrogen bonding between the ketone and the TAO structure. The increase in the magnitude of the enthalpic interactions contributes to an increased binding affinity but consequentially increases the entropic term, $\boldsymbol{-T\Delta S}$**.** The entropic term is often lowered by increasing hydrophobic interactions but can be increased by reducing the degrees of freedom for the inhibitor-protein complex. Ascofuranone and ascochlorin exhibit high undesirable entropic terms but due to an increase enthalpic value still result in a favourable Gibbs free energy ($\boldsymbol{\Delta G_{obs}}$) for the molecular interaction. The combined binding curves in **Figure 71** highlights the differences in both: binding enthalpy, represented by the height of the slope, and entropy change, represented by the slope of each curve[303,304].

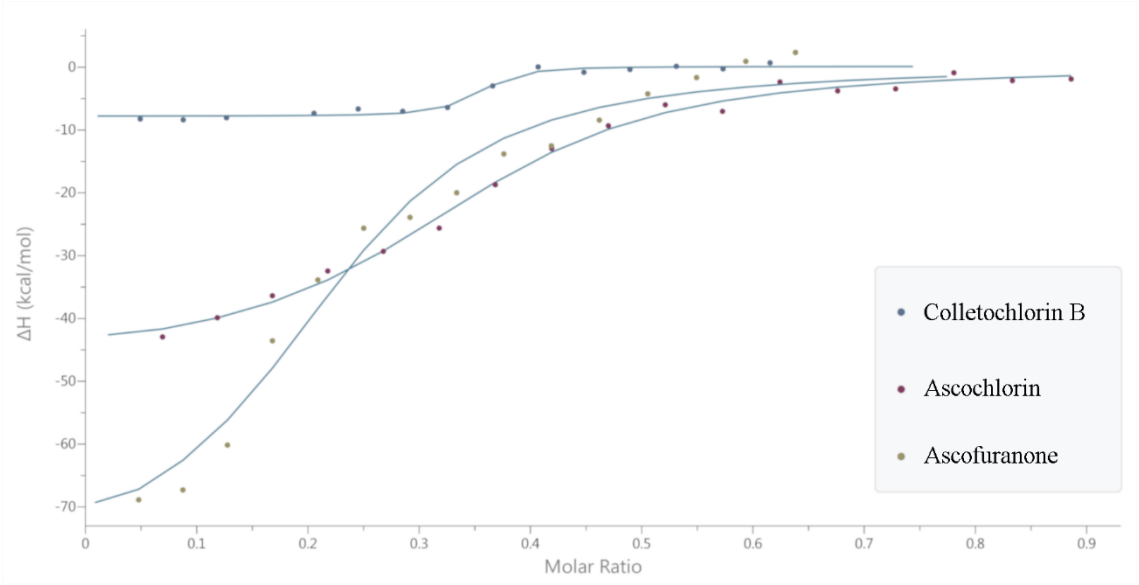

Figure 71 – Normalised and Combined binding curves for Colletochlorin B, Ascochlorin and Ascofuranone.

Initial studies for the titration of ascofuranone against rTAO demonstrated an unwanted endothermic reaction during each injection which may result in inaccurate isotherm curve fitting. This endothermic reaction could be due to a change in conformation of the protein precluding the binding event. An increase in the temperature at which the binding event is measured will decrease the entropic value according to the Gibbs Free Energy equation and increase the enthalpic term. This presented a drastically improved binding isotherm and more accurate curve fitting. **Figure 72** displays the inhibition isotherms obtained when measuring the binding of ascofuranone with a purified rTAO sample at differing temperatures.

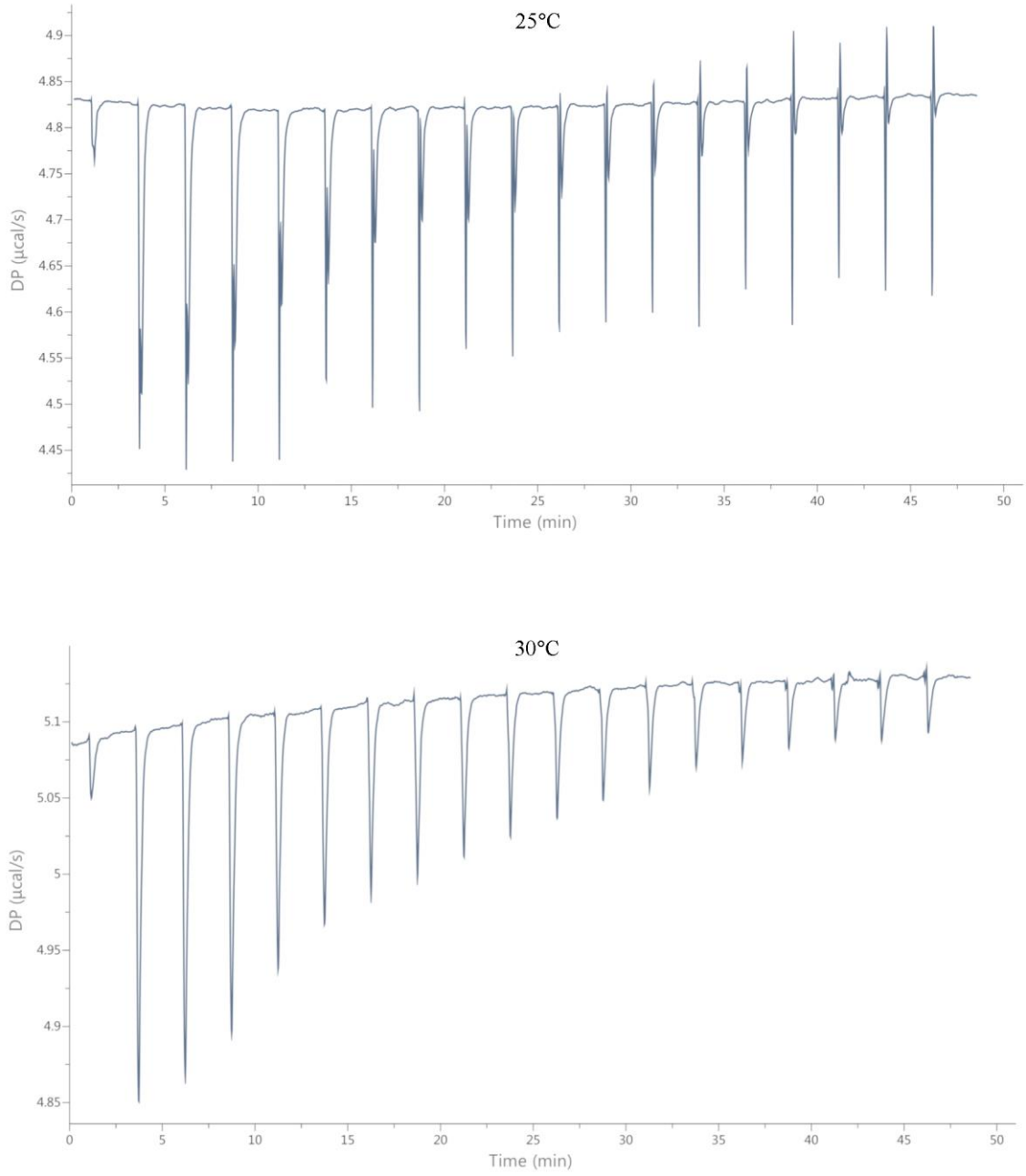

Figure 72 - Raw Binding Isotherms Displaying the Titration of Ascofuranone on purified rTAO protein for both 25 °C and 30 °C.

5.6 *In silico* screening of Novel Fungicides

The use of *in silico* screening can offer further confidence, and data supporting selection criteria, for lead modification and the selection of novel fungicides. This technique provides quantifiable and graphical representation of an inhibitor-enzyme binding event. For the measurement of docking scores, the crystal structures for both cytochrome bc_1 complex and AOX proteins were required. The cytochrome bc_1 complex has been solved with ascochlorin bound[199](PDB code: 3H1L) and was used for the docking of established and new compounds. The crystal structure for StAOX has yet to be solved and therefore a homology model was generated using TAO as a model structure. The docking of compounds was carried out according to Materials and Methods **Section 2.10** using GLIDE plugin for Maestro modelling software[216].

5.6.1 TAO

To provide comparative data and support findings made with previous assay techniques, new and established compounds were docked against the published TAO crystal structure bound with Colletochlorin B (PDB code: 3W54). The results summarised in **Table 28** show that there is a significant increase in docking score for the established inhibitors of ascofuranone and ascochlorin in comparison to the newly synthesised fungicide candidates. The docking pose corresponding to each docking score is displayed in **Figure 73**.

Table 28

Docking scores for Inhibitors against TAO

Inhibitor	GLIDE Docking Score
Colletochlorin B	-8.538
Ascofuranone	-10.187
Ascochlorin	-10.150
Compound **16**	-8.352
Compound **17**	-8.604
Compound **18**	-8.508
Compound **19**	-8.542

Note. All docking studies were carried out using GLIDE plugin for Maestro. The GLIDE scoring function (Equation 2) generates a number corresponding to the strength of binding with more negative value suggesting stronger interaction within the inhibitor binding site.

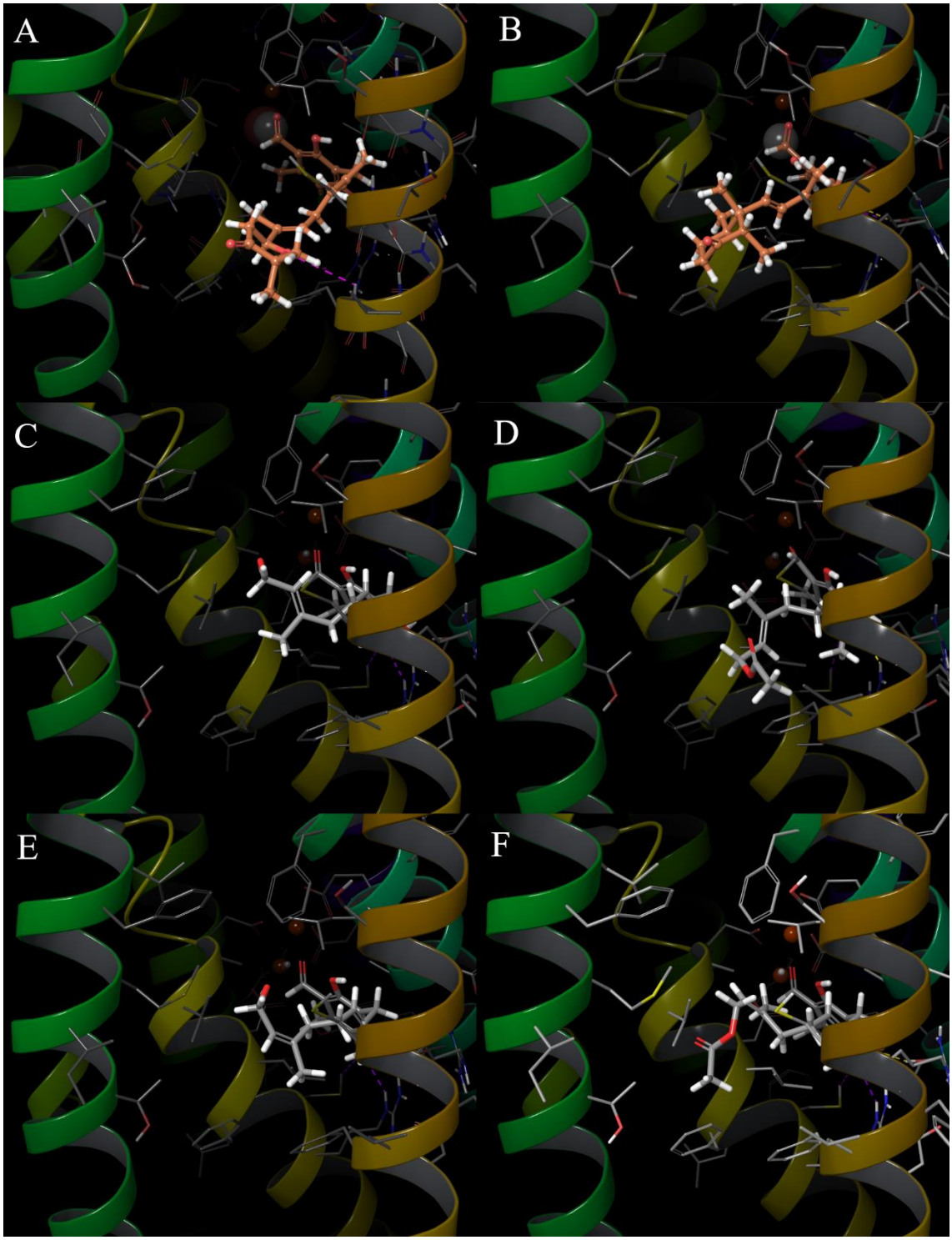

Figure 73 - Docking poses against TAO (PDB code: 3W54) for Established AOX Inhibtors and novel fungicide candidates synthesised in Chapter 4. A = Ascofuranone, B= Ascochlorin, C= Compound 16, D= Compound 17, E= Compound 18, F= Compound 19.

5.6.2 StAOX

The docking of existing inhibitors and new fungicide candidates was carried out against a homology model generated by SWISS model software[305]. The model makes a prediction of the StAOX structure from both the StAOX amino acid sequence and the TAO crystal structure. It is therefore important to consider the results of the docking of new inhibitors will have reduced accuracy in comparison to results from a solved crystal structure.

Table 29

Established and New fungicide Candidates docked against the StAOX Homology Model.

Inhibitor	GLIDE Docking Score
Colletochlorin B	-8.717
Ascochlorin	N/A[†]
Ascofuranone	-6.370
Compound **16**	-6.897
Compound **17**	-5.580
Compound **18**	-5.563
Compound **19**	-5.738

Note. All docking studies were carried out using GLIDE plugin for Maestro. The GLIDE scoring function (Equation 2) generates a number corresponding to the strength of binding with more negative value suggesting stronger interaction within the inhibitor binding site. [†]Ascochlorin failed to bind within the StAOX inhibitor binding site.

The results in **Table 29** provide a clear indication that the docking scores for all inhibitors are considerably reduced in comparison to the scores obtained from the TAO crystal structure. The lack of a high-resolution crystal structure and the use of a homology model for StAOX may hinder the software's ability to correctly process docking scores. Nevertheless, a clear pattern can be seen between the compounds allowing for the analysis of the correlation between experimental pIC_{50} data and docking score. The docking score for ascochlorin could not be obtained and the program failed to dock the compound within the StAOX binding site. **Figure 74** shows the most favourable docking poses for each inhibitor.

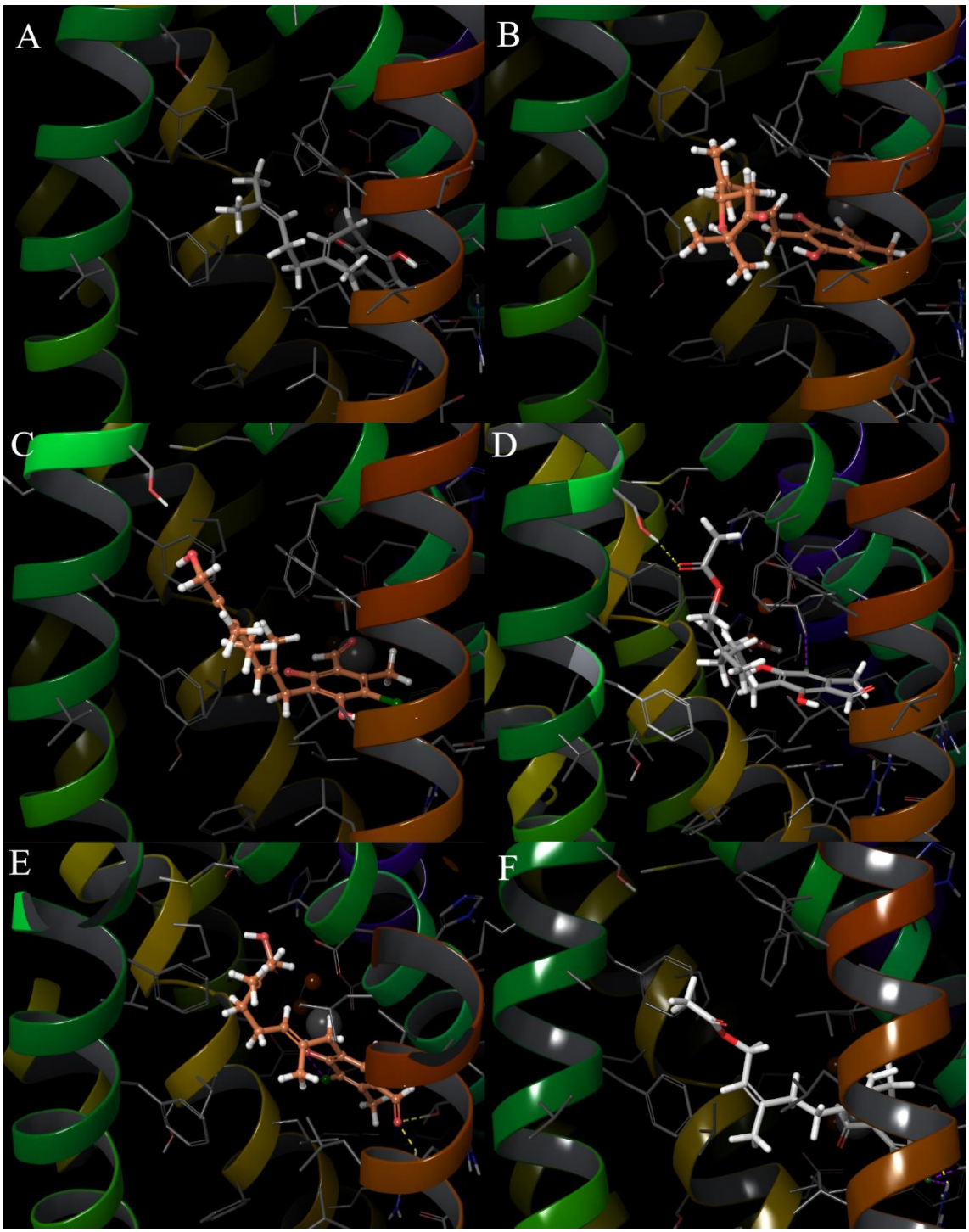

Figure 74 - Docking poses against the StAOX homology model for Established AOX Inhibtors and novel fungicide candidates synthesised in Chapter 4. A = Ascofuranone, B= Ascochlorin, C= Compound 16, D= Compound 17, E= Compound 18, F= Compound 19.

A clear binding pattern can be seen when comparing both TAO and StAOX structures with all compounds overlaid in a single model (**Figure 75**). As previously stated in both **Chapter 3** and **Chapter 4**, the F212 residue considerably reduces the size of the entrance to the hydrophobic cavity for StAOX. In **Figure 75** it is apparent that the F212 residue significantly alters the binding position of the tail which corresponds to a lower docking score for each compound against StAOX in comparison to TAO.

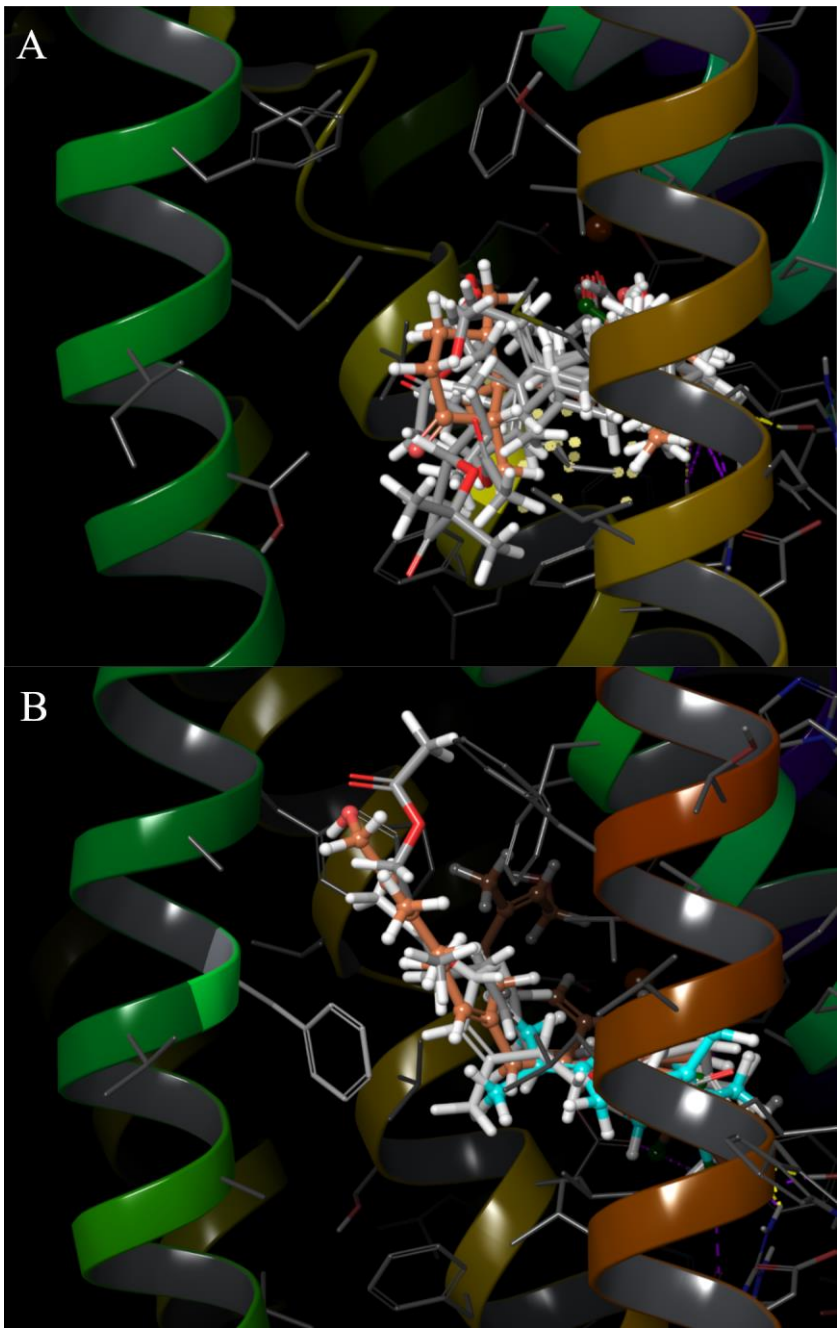

Figure 75 - Combined docking poses for established and novel fungicide candidates synthesised in Chapter 4. A = Combined docking poses against the TAO crystal structure (PDB code: 3W54). B= Combined docking poses against the StAOX homology model.

5.6.3 Cytochrome bc_1 complex

The analysis of the cytochrome *bc_1* complex was carried out utilising the crystal structure from chicken bound with ascochlorin[95]. Performing the docking analysis with the structure from chicken allows for direct comparison from the pIC_{50} results from the rat liver since the Complex III structures are highly conserved among animal orthologues. The docking analysis was carried out on the Q_o site and Q_i site with established and newly synthesised fungicide candidates.

Table 30

The Docking Scores for Established Inhibitors and New Fungicide Candidates

	GLIDE Docking Score	
Inhibitor	***Q_o***	***Q_i***
Ascochlorin	-10.560	-8.634
Colletochlorin B	-9.217	-7.573
Ascofuranone	N/A	N/A
Compound **16**	-9.495	-7.749
Compound **17**	-8.670	-8.560
Compound **18**	-9.108	-7.296
Compound **19**	-9.236	-8.564

Note. All docking studies were carried out using GLIDE plugin for Maestro. The GLIDE scoring function (**Equation 2**) generates a number corresponding to the strength of binding with more negative value suggesting stronger interaction within the inhibitor binding site.

The docking scores for ascofuranone could not be obtained as shown in **Table 30**, which is in accordance its poor inhibition of the cytochrome *bc_1* complex. The newly synthesised compounds show a higher docking score than that of TAO suggesting a higher affinity for the enzyme. **Figure 76** shows the possible docking poses for established and newly synthesised inhibitors for the Q_o site of the cytochrome *bc_1* complex. The docking poses for the Q_i site were not analysed since the

higher docking score values for the Q_o site in general suggest a strong preference for binding over the Q_i site.

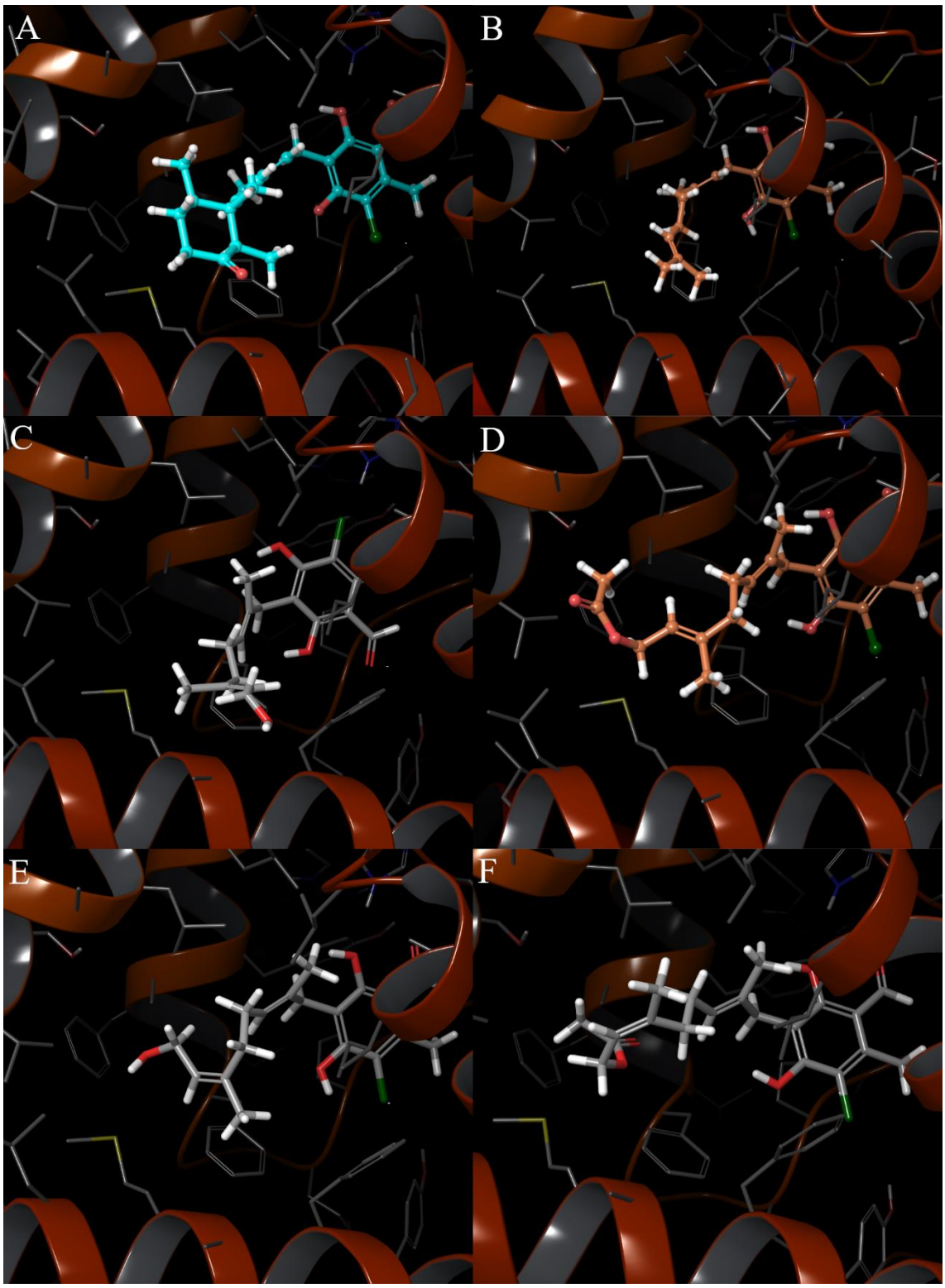

Figure 76 - Docking poses against the Q_o site of the cytochrome bc_1 complex (PDB code: 3H1L) for the Established AOX Inhibitors and newly synthesised fungicide candidates in Chapter 4. A = Ascofuranone, B= Ascochlorin, C= Compound 16, D= Compound 17, E= Compound 18, F= Compound 19.

5.7 Correlation between *in silico* and Experimental Data (QSAR Analysis)

5.7.1 TAO

To determine whether the docking scores generated for each compound provide useful data for the efficacy of novel fungicides, a simple correlation was assessed between docking score and pIC_{50}. The relationship between experimental pIC_{50} and calculated docking score shows a positive correlation with a P value of <0.04 and R^2 value of 0.703. The results are significant and demonstrate the docking scores have value but do not precisely determine the efficacy of a novel fungicide. **Figure 77** displays the relationship between the pIC_{50} data and GLIDE docking scores for TAO.

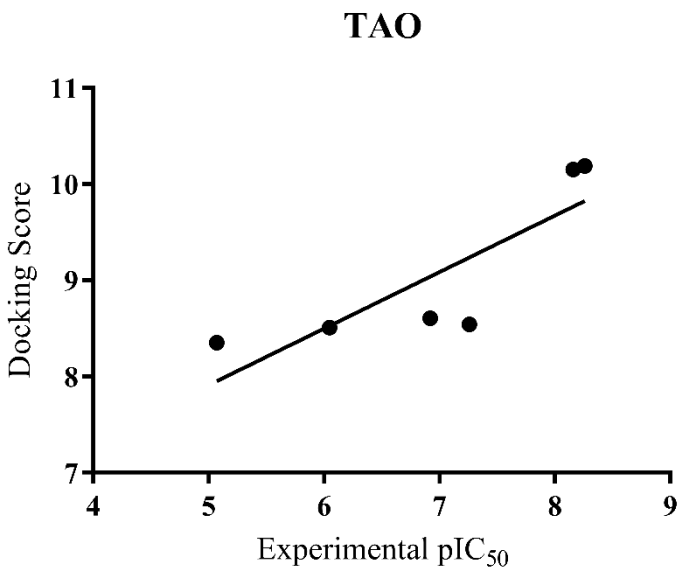

Figure 77 - Relationship between experimental pIC_{50} data and* in silico *GLIDE docking score

5.7.2 StAOX

The same relationship was applied to the results obtained from docking of inhibitors against the homology model for StAOX. Once again, a positive correlation was seen but the high P value ($P > 0.05$) and lower R^2 value (0.643) demonstrate the results do not hold significance. The application of docking to a homology model rather than a solved crystal structure may prevent the docking software from predicting the correct inhibitor binding pose. Nevertheless; the graphical representation of the docked inhibitors demonstrates a significant resemblance to the docked inhibitors within the TAO crystal structure. **Figure 78** displays the relationship between StAOX pIC_{50} and GLIDE docking score.

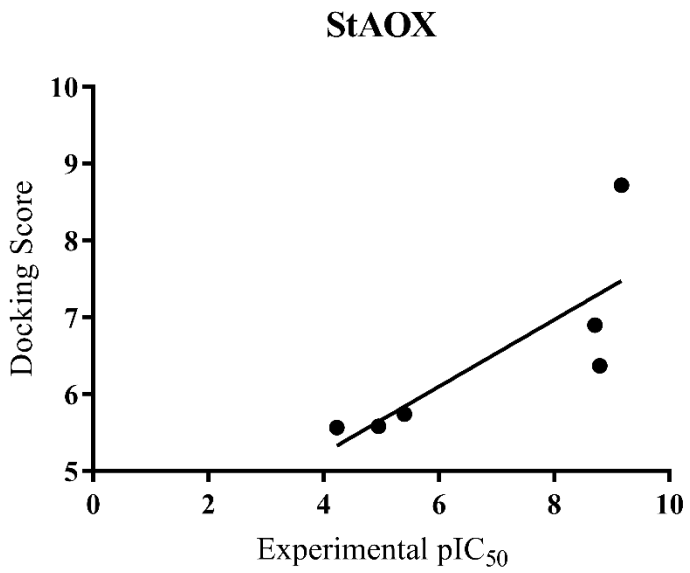

Figure 78 - Relationship between experimental pIC_{50} data and in silico GLIDE docking score

5.7.3 Cytochrome bc_1 Complex

The relationship between pIC_{50} and Glide docking score was again investigated for the cytochrome *bc_1* complex. The highest docking score between both the quinol/ quinone binding sites of the cytochrome *bc_1* complex (Q_O and Q_i) was used since the preference to either docking score should correlate to a stronger binding affinity. The results are displayed in **Figure 79**, with a distinct lack of correlation displayed. The P value for the relationship was greater than 0.5 and an R^2 value of 0.07. It is clear the experimental data significantly differs from the docking score suggesting a more complex interaction when a titration is performed within whole mitochondria.

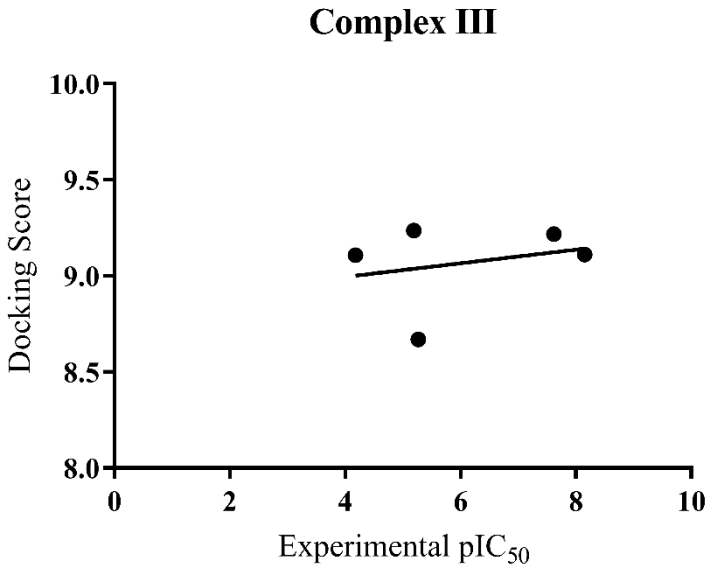

Figure 79 - Relationship between experimental pIC_{50} data and in silico GLIDE docking score

5.8 Conclusions

The development and improvement of assay techniques was necessary to improve efforts to identify the key inhibitor structural features required for AOX or cytochrome bc_1 complex selectivity. Important residues and structural features for each enzyme can then be inferred from these techniques. The newly synthesised fungicides, outlined in **Chapter 4**, display a close structural similarity and therefore require closer scrutiny to determine beneficial chemical features. The use of multiple screening methods, for the newly synthesised and established compounds, has shown utility for fungicide selection.

The results from the O_2 assay suggest that selectivity between AOX species can be achieved, with ascochlorin showing 100 times more efficacy for TAO in comparison to StAOX. In contrast colletochlorin B, ascofuranone and octyl gallate show an increased sensitivity towards StAOX. The inclusion of the lipophilicity data calculated from ChemDraw provided some clarity as to whether an increased concentration within the bacterial membrane was responsible for an increase in pIC_{50}. The data for colletochlorin B and D, highlights the importance for including this chemical property when evaluating enzyme/drug targets within a biological membrane. Colletochlorin B possesses an extra hydrophobic isoprene which contributes very little towards the binding affinity for an enzyme. It could therefore be concluded that the increase potency exhibited by colletochlorin B is due to this increase in cLogP; however, further structural analogues would be required to confirm this.

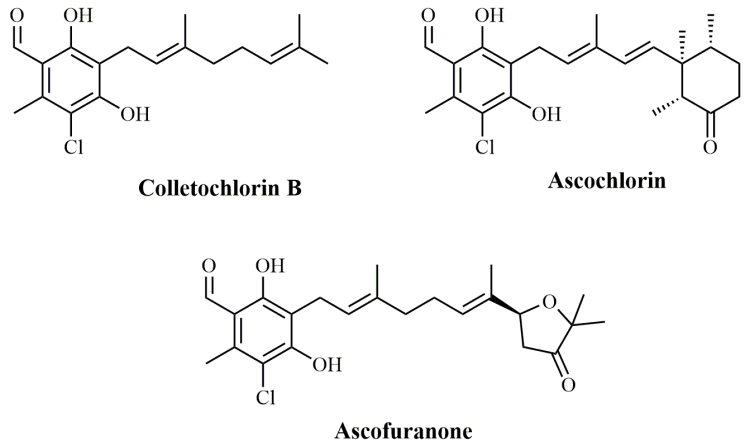

Figure 80 - Established Inhibitors of The AOX and cytochrome bc_1 complex

The use of the O_2 assay for the assessment of AOX inhibitors provides an accurate method for the analysis of potential inhibitors by monitoring substrate specific activity. However, for the screening of larger libraries of compounds, requiring biological and technical replicates, the O_2 assay is too time consuming. The magnitude of the standard deviation (SD) for each compound may present an issue when two structurally similar compounds are investigated. The SD for colletochlorin B against StAOX does not represent sufficient confidence to suggest it is much better than ascofuranone. As a primary screen the O_2 assay may not provide the reliability and efficiency in comparison to the plate assay.

The plate assay results corroborate with the data obtained from the O_2 assay but with much lower SD, shorter processing time and opportunity for full automation. The combined accuracy and precision of this technique meant it was selected for the use against the structurally similar synthesised candidate fungicides. The plate assay results supported those from the O_2 assay for the established inhibitors, confirming its use as a valid screening technique. The lower SD provides more confidence in results obtained; and therefore, suggestions can be made for the possible reasons for the difference in inhibitory activity, between compounds and AOX species.

Ascochlorin displays a significant selectivity between StAOX and TAO presenting the opportunity to highlight the differences in amino acid residues at the entrance to the hydrophobic cavity. The *in-silico* docking for ascochlorin with TAO shows the potential hydrogen bonding interaction between the terminal ketone group and the backbone for the C-95 residue in TAO, highlighted in **Figure 81**. The StAOX amino acid sequence does not contain the C-95 residue but instead contains L-115. This leucine residue introduces a steric hinderance for the cyclohexanone ring of ascochlorin which may prevent binding in StAOX. A similarly located leucine (L-119) residue below L-115 may also introduce some steric hinderance to the cyclohexanone ring of ascochlorin. The use of ITC for StAOX and ascochlroin may have highlighted the drop in $\mathbf{\Delta H_{obs}}$ possibly following a loss in H-bonding interaction, but unfortunately the purified StAOX protein could not be isolated with good structural integrity.

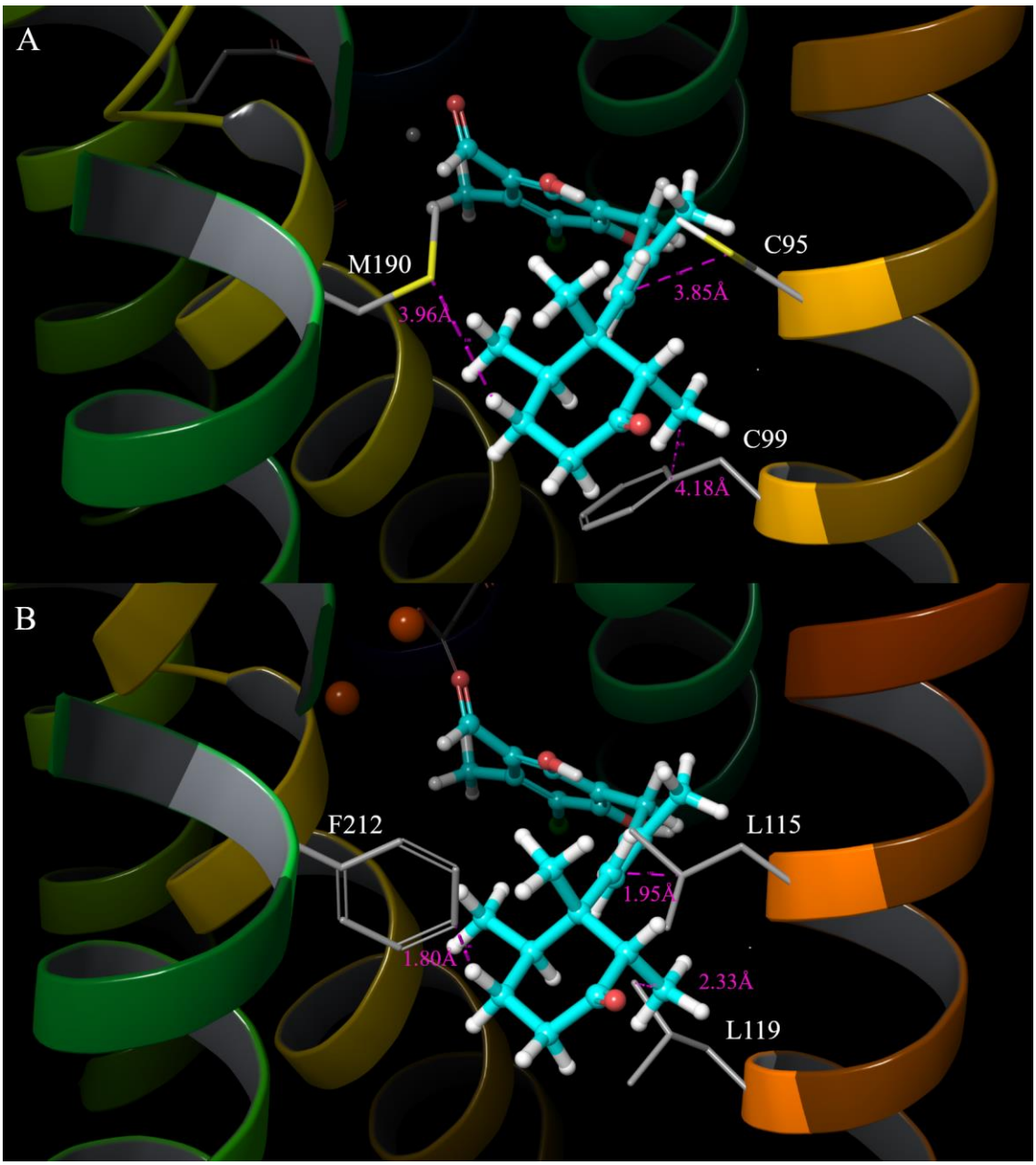

Figure 81 – Docking results displaying the generated pose for Ascochlorin within the binding site of TAO (A) and the overlaid StAOX structure without TAO (B). The difference in distance away from the cyclohexanone ring of ascochlorin is displayed with a clear opportunity for steric hinderance within the StAOX model.

Another interesting result determined from the plate assay screen, showed a 10-fold increase in potency for colletochlorin B against StAOX in comparison to TAO. The F212 residue highlighted in **Figure 81** may allow for beneficial hydrophobic interactions between itself and the terminal methyl groups on colletochlorin B. This would increase favourable entropy of the -TΔS term, within the Gibbs Free Energy equation relating to the ligand-enzyme binding event, and increase the binding affinity, K_D. As mentioned previously, the theories relating to increased binding affinity requires the evidence from a number of assay techniques to confirm their validity.

The evaluation of the newly synthesised fungicide candidates *via* the plate assay system, demonstrated an increased affinity for the TAO protein vs StAOX for all of the compounds. The variance was significantly reduced within the StAOX structure, suggesting the entrance to the hydrophobic cavity is restricted to either an increase in chain length or a drastic change in tail direction. The design of these newly synthesised inhibitors was intended to focus on investigating the space above and below the entrance to the hydrophobic cavity for StAOX. It is clear from these initial results that the hydrophobic binding site is in fact restricted, limiting the candidates for a selective StAOX inhibitor. It may also be the case that the newly synthesised inhibitors are binding in a different pose to that of colletochlorin B. Unfortunately, the lower sensitivity and limited differences in pIC_{50} for each new compound highlighted in **Table 31**, prevents further conclusions.

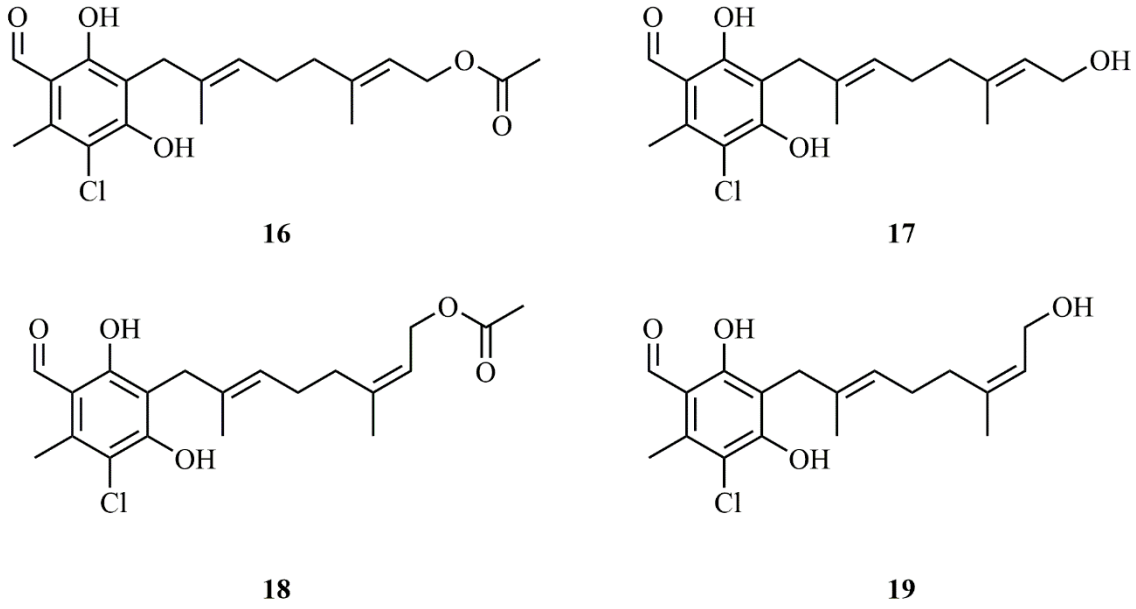

Figure 82 - Fungicide candidates synthesised in Chapter 4.

The range of pIC_{50} data, obtained in the plate assay for the new compounds, displays an almost 10-fold difference in inhibitory activity between each of the compounds displayed in **Figure 82**. The inclusion of the acetate protecting group significantly diminishes activity and therefore suggests a potential clash with an amino acid residue or with the secondary protein structure. The free hydroxyl groups on both compounds **17** and **19** demonstrate a significant improvement in inhibitory activity in comparisons to the acetate protected derivatives. This data suggests an increased binding affinity, which may be due to increased hydrogen bonding to the protein structure. However, *in-silico* modelling of the new synthesised compounds demonstrated very few differences in the orientation of these compounds within the TAO binding site.

Table 31

TAO Inhibition for Novel Fungicide Candidates and their Selectivity in comparison to Complex III.

	TAO Inhibition*	
Inhibitor	***pIC50***	***Selectivity Factor***
Ascofuranone	8.26 ± 0.33†	224
Compound **16**	5.07 ± 0.02	>1000
Compound **17**	6.92 ± 0.03	24
Compound **18**	6.05 ± 0.03	85
Compound **19**	7.26 ± 0.01	114

Note. † Data obtained by Dr. Luke Young[259]. * Negative log concentration and standard deviation for 50% inhibition of TAO *E. coli* membranes. TAO assays performed in MOPS (65 mM) with additions of KCN (1 mM) and NADH (1.25 mM). Selectivity factor determined by dividing IC_{50} results for the rat liver mitochondria assay by the *E. coli* membrane results for TAO measured in **Section 5.3.2** .

The assessment of the novel compounds on rat liver mitochondria allowed an opportunity to evaluate the newly synthesised compounds against the cytochrome bc_1 complex, Complex II and to assess the selectivity between the mitochondrial complexes and TAO. **Table 31** introduces the selectivity factor, which is calculated by dividing the pIC_{50} obtained from inhibition of Complex III by the pIC_{50} data obtained for TAO *E. coli* membrane samples. Compound **19** demonstrates a clear selectivity to TAO suggesting that the Q_o and Q_i binding sites of Complex III have a lower tolerance and space requirements for the (*Z*)-isoprene on compound **19**. However, the data in **Table 31** indicates that ascofuranone still provides the highest selectivity for a TAO inhibitor in comparison to the newly synthesised compounds. The *in-silico* modelling for the cytochrome bc_1 complex suggests a much higher inhibition for the fungicide candidates. This suggests there are some discrepancies with either the experimental data or docking score generation.

The use of ITC provided further clarification on the interactions required for the binding of compounds within the AOX hydrophobic cavity. ITC requires purified protein samples with structural integrity and homogeneity, and therefore, its application using StAOX could not be achieved even following numerous optimisations in solubilisation as highlighted in **Chapter 3**. However; the opportunity to apply a TAO purification protocol in the future to StAOX, presents a useful tool for assessing structurally similar inhibitors. The independence of binding affinity to lipophilicity in an ITC measurement focusses the data to a binding event which emphasises the differences between colletochlorin B, ascochlorin and ascofuranone. Ascofuranone has greater affinity to TAO than the other inhibitors but this leads to a reduction in the degrees of freedom of the protein structure limiting its potential for a low binding affinity. In contrast colletochlorin B has a more entropically favourable interaction with low -TΔS value, but does not bind as strong within the hydrophobic cavity due to the lack hydrogen bonding atoms at the terminus of the tail. Ascochlroin lies in between these two extremes since only possesses one hydrogen bond acceptor within its tail structure. **Figure 83** provides an overview of these thermodynamic parameters measured by ITC.

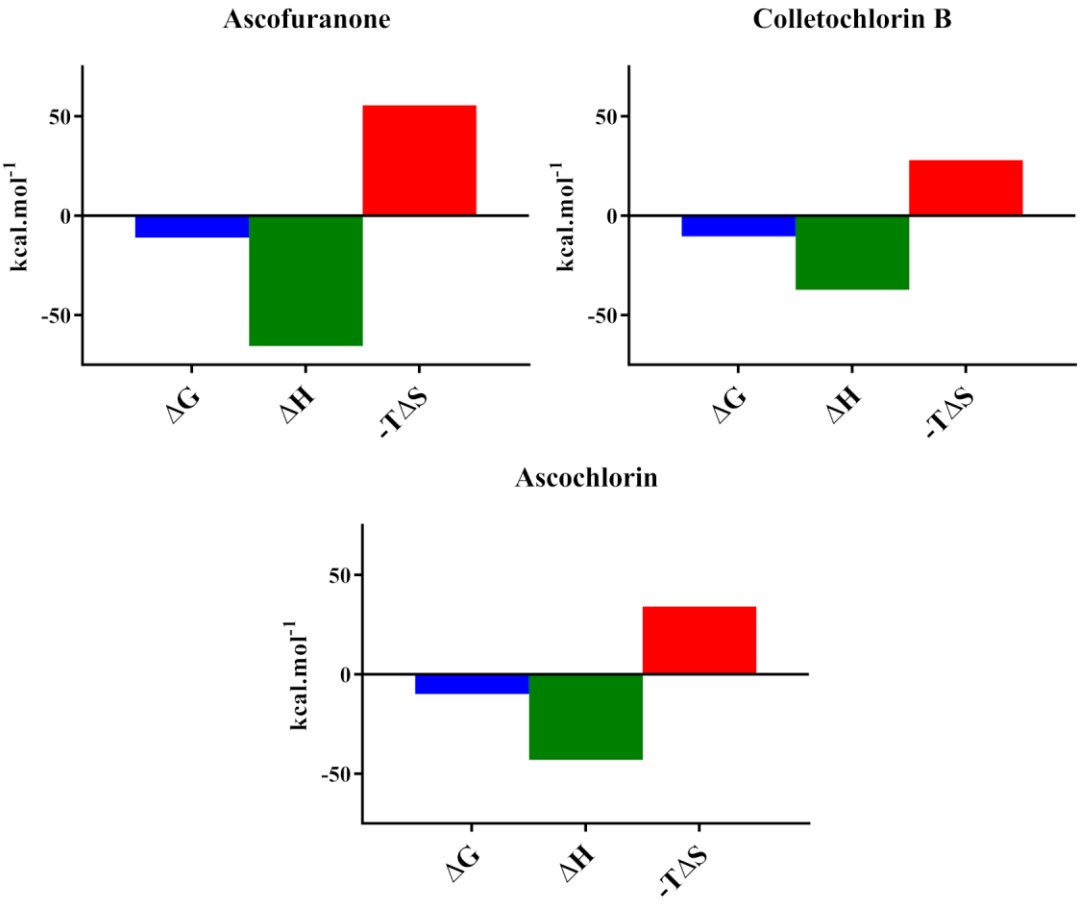

Figure 83 - Thermodynamic Parameters for the Established Inhibitors against purified rTAO generated form the ITC measurements in Section 5.5.3.

The use of *in-silico* docking to support the experimental data provides a useful graphical representation of the binding event and can also offer design features for future fungicide candidates. The docking software positioned the head group of each inhibitor in the correct orientation for all of the enzyme models, which was confirmed when compared to the TAO crystal structure. As mentioned previously, the results are theoretical and therefore may be used a guide for synthesis rather than a determining factor. Whilst this screening technique demonstrated a positive correlation between pIC_{50} and docking score for both TAO and StAOX, the results for Complex III demonstrated that no such correlation existed for the cytochrome bc_1 complex at all. Unfortunately, the data set for TAO was the only relationship which held significance, raising the question as to the validity of docking scores as a useful technique for screening purposes.

It is however important to note that the docking of inhibitors against the target enzyme with molecular modelling software represents an isolated binding interaction. Whereas both the *E. coli* membrane samples and whole mitochondria comprise of a number of multi-enzymes complexes, molecular transporters and lipid membranes which may reduce or increase the efficacy of a particular inhibitor. The ITC assay provides a system with measurements as close to an isolated system as possible and the K_d values obtained for colletochlorin B, ascochlorin and ascofuranone do correlate to the docking scores obtained for TAO. However, a correlation with a sample of size of more than ten would provide a more conclusive assessment of the utility of these dosking score measurements. Aside from the docking score, the poses for each inhibitor demonstrated a similarity to that observed in the TAO crystal structure, with the head group overlaying exactly with that of the crystallised colletochlorin B molecule.

Chapter 6: Final Discussion and Concluding Remarks

The key objectives set out in Section 1.10 were all investigated with varying degrees of success. The characterisation of StAOX demonstrated lower expression and specific activity in comparison to plant (SgAOX) and protozoan (TAO) AOX species. However, the stimulation of the StAOX with purine nucleotides provided a 4-fold increase in the baseline specific activity for the enzyme. The predicted structure of the StAOX was elucidated with major differences at the opening to the hydrophobic cavity which offered the potential for the design of species selective AOX inhibitors.

A number of compounds were synthesised with design features based upon the StAOX homology model and through evaluation of the cytochrome bc_1 complex binding sites (Q_o and Q_i). The binding profiles of the three well established AOX and cytochrome bc_1 complex inhibitors, colleotchlorin B, ascofuranone and ascochlorin, was evaluated through a combination of molecular modelling and experimental data. These results highlighted the differences in inhibitor binding sites between the respiratory complexes which determines the selectivity for ascofuranone towards the AOX.

The sensitivity of the well-established AOX inhibitors and newly synthesised compounds in **Chapter 4** were assessed on TAO, StAOX and the cytochrome bc_1 complex. The compounds demonstrated differing sensitivities to each respiratory complex, providing further data to lead future fungicide design. A number of new assay techniques were developed for the screening of novel fungicide candidates with the most promising results obtained from ITC. The identification of key amino acid residues and unique structural elements to each inhibitor binding site, was elucidated from the inhibitory studies. Once again, this provides data to help lead future fungicide design of both the StAOX and cytochrome bc_1 complex enzymes.

Overall, the aims set out at the start of the research project were achieved, however both a larger library of fungicide candidates, and an active purified StAOX protein, would have generated more data for the continued research into the synthesis of novel AOX and cytochrome bc_1 complex fungicides. On reflection, the research project was an ambitious one, with research spread across both biochemistry and organic chemistry disciplines.

6.1 Enzyme Kinetics, Regulation and Potential Role of StAOX as a Fungicide Target

To date only a few fungal AOXs have been studied to determine the similarities between AOX species; with regards to both amino acid conservation and regulation. However, there remains no published research on the full characterisation of StAOX, or its potential as a fungicide target to both: potentiate existing fungicide treatments[151–154]; and to reduce the selection opportunity for future resistance fungal strains[41]. **Chapter 3** of this thesis presented the optimisation and evaluation of overexpression, purification, enzymatic activity, regulation and structure of StAOX.

Initial overexpression experiments revealed a significant difference in both overexpression and enzymatic activity of the StAOX, in comparison to both plant and protozoan AOX species (**Section 3.4**). Through the optimisation of multiple conditions and parameters, the enzymatic activity was effectively doubled, but still demonstrated only 5% of TAO activity and 10% of plant AOX activity with respect to O_2 consumption rates. In contrast to these results, multiple sequence alignment analysis indicated that the primary ligation sphere and PCET network, which are vital for enzyme catalysis, were fully conserved between all AOXs. However, the terminal residue of the PCET network (W65 in TAO and Y85 in StAOX) was not conserved between TAO and StAOX, however its effect on the O_2 catalytic proton-electron transfer remains enigmatic. Further structural analysis of StAOX, through homology modelling, revealed differences to a number of residues at the entrance to the hydrophobic cavity. These residues contribute to the reduction in enzymatic activity between StAOX and other AOX species. However, further mutagenesis studies would be required to confirm this. The final enzymatic activity for StAOX suggested a modest role for the enzyme in energy metabolism, whilst under normal physiological conditions, with a specific activity of 32.6 nmol of O_2 $mg^{-1}.min^{-1}$, representing 5% and 10% of specific activity rates of protozoan and plants species, respectively.

Previous findings[162,306] of nucleotide regulation for fungal AOXs was confirmed through analysis of the StAOX activity. In particular the addition of the purine nucleotide, GMP, displayed an increase in enzymatic activity of 4 times the un-activated StAOX turnover. As mentioned previously in **Section 3.9**, the build-up of nucleotides such as GMP, AMP and IMP could act as allosteric ligands to upregulate AOX activity following periods of biotic stress[162] or potentially from the use of fungicides that target the ETC. This hypothesis can be taken further when fully analysing the metabolic pathways to the synthesis and degradation of purine nucleotides. As shown in **Figure 84**, the enzymes responsible for a number of transformation steps between IMP, GMP and AMP are ATP dependent. A serious deficiency in ATP production or high concentration

of ADP, would suggest a poorly functioning ETC, since the majority of ATP for the cell is generated from this pathway. The build-up of purine nucleotides would then activate the fungal AOX to alleviate an over reduced quinol pool, reduce ROS and allow for continued ATP production through Complex I and the TCA cycle.

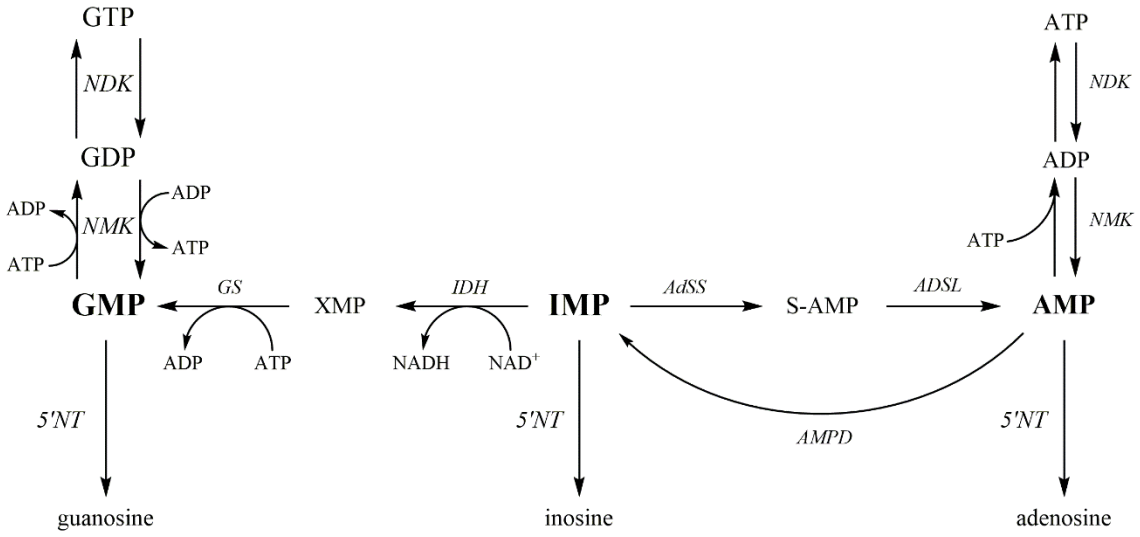

Figure 84 - Purine Nucleotide Metabolism with regulators of the AOX in bold. Abbreviations: AdSS, adenylosuccinate synthetase; ADSL, adenylosuccinate lyase; AMPD, adenylate deaminase; GS, GMP-synthase; IDH, IMP-dehydrogenase; NDK, nucleoside diphosphate kinase; NMK, nucleoside mono-phosphate kinase; 5'NT, 5'-nucleotidase.

Previous studies[307,308], have also shown that the AOX gene is upregulated by the production of ROS, which increases following the inhibition of cytochrome dependent pathway. The activation of the AOX coupled with the upregulation of the AOX gene would offer a powerful response to inhibition of the ETC. The respiration of the fungal cell during these periods may be enhanced[114,151–153,261] allowing for the selection of mutant respiratory complexes through the survival of fungal cells during when affected by fungicides that target the ETC. The AOX should therefore not be disregarded as a potential resistance mechanism or metabolic pathway for reducing fungicide sensitivity.

The regulation by GMP and other purine nucleotides could not be confirmed by way of the purified StAOX, as the absorption wavelength for both the nucleotide and quinol/quinone clash (278 nm). It can therefore not be conclusively determined whether nucleotide activation occurs through a binding interaction with the protein itself or through another mechanism within the *E. coli* membrane. Although the binding sites outlined in **Section 3.5.2** offer a possibility for interaction through dimer formation, conformational change and improvement of the PCET

mechanism after binding to the matrix side of the protein. The purified StAOX protein also did not respond to the same optimisation process as the membrane bound AOX protein. The enzymatic activity of the Δ61 Twin-Strep StAOX was dramatically reduced following removal the biological membrane which was ultimately rescued when reincorporated into the proteoliposome system. The His-tagged protein which contained the mature sequence did not exhibit the same reduction in enzymatic activity following solubilisation. As stated in **Section 3.9**, the N-terminal region of the protein may be the necessary for correct protein conformation or may be involved in dimer formation as stated by Siedow *et al*[306].

6.2 Designing and Synthesising Fungicides for the AOX and Cytochrome *bc₁* complex

The design of selective inhibitors for the StAOX and/or the cytochrome *bc₁* complex required the analysis of three sperate quinol binding sites, one for the AOX and two for the cytochomre *bc₁* complex (Q_o and Q_i). Homology and crystal structure modelling assessed these sites, presenting opportunities for selectivity between AOX species and between AOX and the cytochrome *bc₁* complex. The phenylalanine residue (F212) hindering the entrance to the hydrophobic cavity prevented the synthesis of long carbon chain inhibitors but two hydrophilic residues (S182 and T186) present in TAO provided an opportunity to explore AOX species selectivity. The binding sites of the cytochrome *bc₁* complex differed drastically but both retained narrow cavities within an 8-carbon chain length. The analysis of these binding sites, along with reported data for the selectivity of ascofuranone but not for ascochlorin, highlighted the importance of the tail moiety. The design of fungicides for both respiratory complexes therefore focussed on the tail moiety, with no alterations to the head group.

The natural products and lead compounds, ascochlorin, colletochlorin B and ascofuranone, possess a number of undesirable properties (clogP > 5.6 and pKa >10) for both agrochemical and drug design, according to Lipinski's rules[286,287,299]. The lipophilicity of the compounds is an important chemical property to be altered if future efforts towards an effective fungicide were to be made. The functionalisation of the lipophilic tail allows a more desirable lipophilicity and selectivity between the respiratory complexes. Therefore, a modified synthetic route for the synthesis of colletochlorin B compounds was devised.

The synthetic route to the natural compound colletochlorin B required a large amount of optimisation to improve the overall yield. Although the alkyl coupling was improved for colletochlorin B from 11% to 55%, the results did not translate to that of functionalised tails. In

fact, the final novel compounds **15** and **17** only managed to achieve yields of 20% and 5%, respectively. Furthermore; the coupling of both the saturated and unsaturated functionalised alkyl chains failed to couple at all. The challenging synthetic route prevented the synthesis of many of the intended fungicide candidates and therefore prevented clear structure elucidation in **Chapter 5**. Nevertheless; the synthesis of four structurally related compounds (**15-18**) with similar hydrogen bond acceptors to that of ascofuranone, allowed for evaluation *via* various assay techniques.

The potential to synthesise further compounds from the devised reaction Schemes outlined in **Chapter 4**, for both saturated and unsaturated tails, failed to yield a final compound. The synthesis of allylic functionalised aniline derivatives offered a facile route in theory to a library of compounds, due to the abundance of commercially available amines. Unfortunately, purification of the final compounds significantly reduced the final yields of each step leading up to the final alkyl coupling. The small quantities taken through to the alkyl step failed to couple to head group but the reasons for the failure remain unknown. Both the secondary amine functional group and the already low yielding alkyl coupling step may be responsible.

6.3 Inhibition of the AOX and cytochrome bc_1 complex

The evaluation of the established AOX inhibitors against StAOX revealed a clear difference in sensitivity between the three most potent inhibitors (colletochlorin B, ascochlorin and ascofuranone). These results also emphasised the difference in inhibition between TAO and StAOX, presenting an opportunity for designing species selective inhibitors. The conclusions made in **Chapters 3** and **4** from analysis of the StAOX and TAO structures through molecular modelling software, also supported by this data. Unfortunately, newly synthesised fungicide candidates (compounds **16**-**19**) showed poor inhibition against StAOX. Evaluation of compounds **16**-**19** against the cytochrome bc_1 complex also demonstrated poor inhibition for all of these fungicide candidates. In contrast, compounds **19** and **17** demonstrated an increase sensitivity to TAO with compounds **16** and **19** offering selectivity factors of 1000 and 114, respectively. Although the design of these compounds was intended to offer new fungicide candidates, it follows that the newly synthesised compounds may offer more potential as drugs for the treatment of African sleeping sickness.

The use of a secondary screen, through ITC, provided a novel methodology for assessing AOX inhibitors. This methodology was applied to TAO due to the stability and conformational integrity of the purified protein. However, screening fungicide candidates using ITC analysis could not be achieved for StAOX, due to low protein recovery and specific enzymatic activity. Efforts were

made to improve specific enzymatic activity and protein recovery through a number of optimisations steps in **Chapter 3** but no significant improvement was seen. The thermodynamic quantities obtained from the ITC studies for TAO, however, identified ascofuranone as the strongest binder, with an increased number of H-bond interactions reflected in the increased enthalpic contribution to its overall infinity. Such results are important for leading future inhibitor design but its application to StAOX will require further optimisation of purification protocols.

The use of *in silico* docking, for the evaluation of potential drug candidates, has been successful in supporting QSAR data for over 50 FDA approved pharmaceuticals[309] and is growing as a drug screening technique[310–312]. However, its application towards the synthesis and design of novel agrochemicals has yet to be adopted. Its application for the assessment novel fungicide candidates was explored for TAO, StAOX and the cytochrome bc_1 complex. The docking of compounds within the crystal structure provided a useful visual tool to understand binding interactions and focus future fungicide design. However; the correlation between pIC_{50} and docking scores did not show any statistical significance. It could be suggested that since the evaluation through *in silico* docking calculates an inhibitor/enzyme interaction directly, the relevance of pIC_{50} data, which is influenced by a number of external parameters, does not perfectly correlate. The ITC assay carried out on purified TAO samples provided an isolated system by which to assess enzyme/inhibitor interactions. The correlation between docking scores and K_d data was shown to be positive, however the sample of size of only 3 inhibitor/enzyme interactions precludes any conclusive validity to the *in silico* docking studies. Furthermore, the substantial research efforts described in the literature[309–312] suggest that in silico docking does hold validity under the correct experimental conditions.

6.4 Future Work

The scope for future work extends across both biochemical and organic synthetic aspects of this research topic. The first area of research should be to investigate the influence of the location of purification tag on the StAOX protein and its effects on expression and purified enzymatic activity. The loss of the leader sequence and introduction of the Twin-Strep tag significantly improved the specific activity of the *E. coli* membrane samples, however the purified Twin-Strep tagged StAOX protein showed a 20 times lower specific activity in comparison to the His-tagged purified protein. The loss the leader sequence represented a significant change to the N-terminus for the StAOX protein and therefore it seems to be important for the conformation and activity of the solubilised protein. Including the leader sequence and the effect of moving the purification tag to the C-terminus should be analysed in order to improve the activity of the StAOX purified

protein. A stable and active purified protein may facilitate the use of StAOX in ITC measurements for both inhibitor studies and for the confirmation of GMP as an allosteric regulator. The measurement of the stoichiometry (n) would help to support the hypothesis of 3 binding sites per StAOX dimer molecule as suggested in **Chapter 3**. Measuring the K_D, however, could offer utility through mutagenesis of the residues implicated in the GMP binding site which would see an increase or decrease in GMP binding affinity.

The mixed results from the organic synthesis of candidate fungicides provides a large opportunity for work on new synthetic routes for ascofuranone or colletochlorin B derivatives. The alkyl coupling route did not allow for suitable yields following the transfer from the optimised colletochlorin B synthesis to the new functionalised tail derivatives. **Scheme 10** offers an alternative route for the synthesis of a library of fungicides, which should improve the total yield of the final inhibitor compounds. Important differences in this synthetic route is omission of both the alcohol in the meta position to the formyl group and the formyl group itself. From docking studies in Chapter **5** and published drug design for TAO from West *et al*[200,201] these groups have shown that the alcohol does not contribute to the efficacy and the formyl group can be replaced by other hydrogen bond acceptors. The first step of the proposed scheme involves the protection of the alcohol which can be achieved through the use of TBDMS-Cl in DCM. The generation of the nitrile group could be achieved by generating the Vilsmeier-Haack intermediate through $POCl_3$ and DMF, followed by the addition of an ammonia solution and iodine to form the nitrile. Chlorinating the aromatic ring would be less problematic than the one afforded in Chapter **4**, since di-substituted halogens can be formed at high equivalents of SO_2Cl_2 and high yields. An added benefit would be the possibility of utilising already synthesised isoprenoid alcohols and utilising palladium catalysts, outlined by Beller[313] and Buchwald[314,315], to afford an ether coupling to the

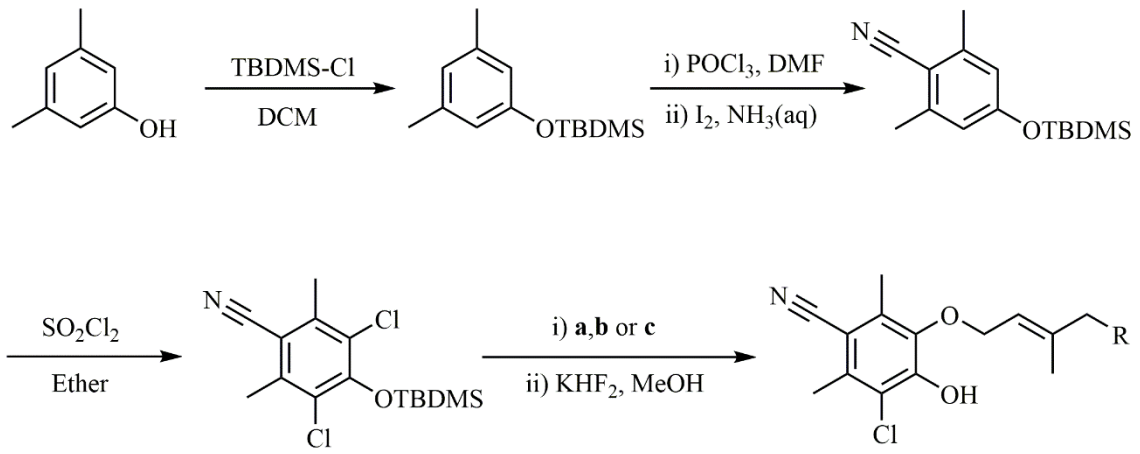

Scheme 10 - Proposed scheme for the generation of candidate fungicides for the AOX or cytochrome bc_1 complex. a = Pd $(OAc)_2$, Cs_2CO_3, toluene, b or c = Buchwald[4,5]

head group in high yields. The introduction of an ether would also reduce lipophilicity and introduce a point of metabolism to ensure rapid degradation within non-target organisms.

The evaluation of prospective fungicides was only evaluated on isolated enzymes and simple metabolic systems. It would therefore be pertinent to screen fungicides on both a whole cell fungal plate assay, with quantification of the effectiveness with of kill-zone measurements, and through *in planta* studies, with visual STB symptoms analysed. With both of these systems Q_oI, SDHI and DMI resistant fungal strains may be used to assess new fungicides sensitivity to these fungi. Ultimately, evaluating AOX inhibitors along with other traditional respiratory fungicide classes (Q_oI and SDHI) may elucidate the potentiating contribution when inhibiting the alternative pathway. Furthermore; it will allow for the understanding of how well these potential fungicides will travel within the plant. The use of phosphor image analysis, coupled with quantitative analysis of a radiolabelled inhibitor, allows for a comprehensive understanding of distribution of a fungicide within its target system[284,316].

It is also important to note both validation of the AOX as a resistance mechanism and role in potentiating existing fungicide formulations has not been confirmed, however, there remains large amounts of studies[33,111,114,149,151–154,176,185,187–189,205] implicating its involvement. The generation of AOX knockout mutants and the effect on the growth, and its ability to adapt to fungicide stress, for *S. tritici*, would further confirm the role the enzyme plays in resistance and pathogenesis. Furthermore, the synthesis of a specfic StAOX inhibitor, and the evaluation of its efficacy combined with a commercial respiratory targeted fungicide, such as Azoxystrobin, may confirm support these suggested roles. It also creates a platform for a novel phytopathogenic fungicide class with lower risk of resistance and high efficacy, whilst delivering low non-target toxicity.

Bibliography

1. Millardet, P. M. A. *The Discovery of Bordeaux Mixture*. (The American Phytopathological Society, 1933). doi:10.1094/9780890545188

2. Li, X., Dong, S. & Su, X. Copper and other heavy metals in grapes: a pilot study tracing influential factors and evaluating potential risks in China. *Sci. Rep.* **8,** 17407 (2018).

3. Merrington, G., Rogers, S. L. & Zwieten, L. Van. The potential impact of long-term copper fungicide usage on soil microbial biomass and microbial activity in an avocado orchard. *Soil Res.* **40,** 749 (2002).

4. Peña, N., Antón, A., Kamilaris, A. & Fantke, P. Modeling ecotoxicity impacts in vineyard production: Addressing spatial differentiation for copper fungicides. *Sci. Total Environ.* **616–617,** 796–804 (2018).

5. de Oliveira-Filho, E. C., Lopes, R. M. & Paumgartten, F. J. R. Comparative study on the susceptibility of freshwater species to copper-based pesticides. *Chemosphere* **56,** 369–374 (2004).

6. Kumar Sharma, Y., Environ Biol, J., Singh, D. & Nath, K. Response of Wheat Seed Germination and Seedling Growth under Copper Stress Article. *J. Environ. Biol.* 409–414 (2007).

7. Ópezalonso, M. L. *et al.* The Effect of Pig Farming on Copper and Zinc Accumulation in Cattle in Galicia (North-Western Spain). *Vet. J.* **160,** 259–266 (2000).

8. Bayram, S., Genc, A., Buyukleyla, M. & Rencuzogullari, E. Genotoxicity and cytotoxicity of copper oxychloride in cultured human lymphocytes using cytogenetic and molecular tests. *Cytotechnology* **68,** 2027–2036 (2016).

9. Wightwick, A., Walters, R., Allinson, G., Fungicides, S. R.- & 2010, undefined. Environmental risks of fungicides used in horticultural production systems. *intechopen.com*

10. EFSA. Review of the existing maximum residue levels for copper compounds according to Article 12 of Regulation (EC) No 396/2005. *EFSA J.* **16,** (2018).

11. Long, J. W. & Siegel, M. R. Mechanism of action and fate of the fungicide chlorothalonil (2,4,5,6-tetrachloroisophthalonitrile) in biological systems: 2. In vitro reactions. *Chem. Biol. Interact.* **10,** 383–394 (1975).

12. Arvanites, A. C. & Boerth, D. W. Modeling of the mechanism of nucleophilic aromatic substitution of fungicide chlorothalonil by glutathione. *J. Mol. Model.* **7,** 245–256 (2001).

13. DeLorenzo, M. E., Wallace, S. C., Danese, L. E. & Baird, T. D. Temperature and salinity effects on the toxicity of common pesticides to the grass shrimp, *Palaemonetes pugio*. *J. Environ. Sci. Heal. Part B* **44,** 455–460 (2009).

14. DeLorenzo, M. E. & Serrano, L. Individual and Mixture Toxicity of Three Pesticides; Atrazine, Chlorpyrifos, and Chlorothalonil to the Marine Phytoplankton Species *Dunaliella tertiolecta*. *J. Environ. Sci. Heal. Part B* **38,** 529–538 (2003).

15. Bringolf, R. B. *et al.* Acute and chronic toxicity of technical-grade pesticides to glochidia and juveniles of freshwater mussels (Unionidae). *Environ. Toxicol. Chem.* **26,** 2086 (2007).

16. Teng, Y. *et al.* Successive chlorothalonil applications inhibit soil nitrification and discrepantly affect abundances of functional genes in soil nitrogen cycling. *Environ. Sci. Pollut. Res.* **24,** 3562–3571 (2017).

17. Zhang, M. *et al.* Cumulative effects of repeated chlorothalonil application on soil microbial activity and community in contrasting soils. *J. Soils Sediments* **16,** 1754–1763 (2016).

18. Tomlin, C. & British Crop Protection Council. *The pesticide manual : a world compendium.* (British Crop Protection Council, 2000).

19. Armbrust, K. L. Chlorothalonil and chlorpyrifos degradation products in golf course leachate. *Pest Manag. Sci.* **57,** 797–802 (2001).

20. Wang, G.-L. *et al.* Lysobacter ruishenii sp. nov., a chlorothalonil-degrading bacterium isolated from a long-term chlorothalonil-contaminated soil. *Int. J. Syst. Evol. Microbiol.* **61,** 674–679 (2011).

21. Mori, T., Fujie, K. & Katayama, A. Bacterial and fungal contributions to chlorothalonil degradation in soil. *Soil Sci. Plant Nutr.* **44,** 297–304 (1998).

22. Tang, L. *et al.* Biodegradation of chlorothalonil by Enterobacter cloacae TUAH-1. *Int. Biodeterior. Biodegradation* **121,** 122–130 (2017).

23. Liang, B. *et al.* Hydrolytic Dechlorination of Chlorothalonil by Ochrobactrum sp. CTN-11 Isolated from a Chlorothalonil-Contaminated Soil. *Curr. Microbiol.* **61,** 226–233 (2010).

24. Wang, H., Xu, S., Hu, J. & Wang, X. Effect of Potassium Dihydrogen Phosphate and

Bovine Manure Compost on the Degradation of Chlorothalonil in Soil. *Soil Sediment Contam. An Int. J.* **18,** 195–204 (2009).

25. Santovito, A. *et al.* Genomic damage induced by the widely used fungicide chlorothalonil in peripheral human lymphocytes. *Ecotoxicol. Environ. Saf.* **161,** 578–583 (2018).

26. Mozzachio, A. M. *et al.* Chlorothalonil exposure and cancer incidence among pesticide applicator participants in the agricultural health study. *Environ. Res.* **108,** 400–403 (2008).

27. Arena, M. *et al.* Peer review of the pesticide risk assessment of the active substance chlorothalonil. *EFSA J.* **16,** (2018).

28. Hou, F., Zhao, L. & Liu, F. Determination of Chlorothalonil Residue in Cabbage by a Modified QuEChERS-Based Extraction and Gas Chromatography–Mass Spectrometry. *Food Anal. Methods* **9,** 656–663 (2016).

29. McDougall, P. *Agriservice report*. (2006).

30. Poole, N. F. & Arnaudin, M. E. The role of fungicides for effective disease management in cereal crops. *Can. J. Plant Pathol.* **36,** 1–11 (2014).

31. Mares, D. *et al.* Emerging antifungal azoles and effects on Magnaporthe grisea. *Mycol. Res.* **110,** 686–696 (2006).

32. Roberts, T. Hutson, D. H. *Metabolic Pathways of Agrochemicals*. (Royal Society of Chemistry, 2007).

33. Price, C. L., Parker, J. E., Warrilow, A. G., Kelly, D. E. & Kelly, S. L. Azole fungicides - understanding resistance mechanisms in agricultural fungal pathogens. *Pest Manag. Sci.* **71,** 1054–1058 (2015).

34. Hou, Y.-P., Chen, Y.-L., Qu, X.-P., Wang, J.-X. & Zhou, M.-G. Effects of a novel SDHI fungicide pyraziflumid on the biology of the plant pathogenic fungi Bipolaris maydis. *Pestic. Biochem. Physiol.* **149,** 20–25 (2018).

35. Young, D. H., Wang, N. X., Meyer, S. T. & Avila-Adame, C. Characterization of the mechanism of action of the fungicide fenpicoxamid and its metabolite UK-2A. *Pest Manag. Sci.* **74,** 489–498 (2018).

36. Butkutė, B., Mankevičienė, A. & Gaurilčikienė, I. A comparative study of strobilurin and triazole treatments in relation to the incidence of Fusarium head blight in winter wheat, grain quality and safety. *Cereal Res. Commun.* **36,** 671–675 (2008).

37. Mounkoro, P. *et al.* Mitochondrial complex III Q i -site inhibitor resistance mutations

found in laboratory selected mutants and field isolates. *Pest Manag. Sci.* (2018).

38. Siah, A., Deweer, C., Morand, E., Reignault, P. & Halama, P. Azoxystrobin resistance of French Mycosphaerella graminicola strains assessed by four in vitro bioassays and by screening of G143A substitution. *Crop Prot.* **29,** 737–743 (2010).

39. Samuel, S. *et al.* Evaluation of the incidence of the G143A mutation and cytb intron presence in the cytochrome bc-1 gene conferring QoI resistance in Botrytis cinerea populations from several hosts. *Pest Manag. Sci.* **67,** 1029–1036 (2011).

40. Cools, H. J. & Fraaije, B. A. Update on mechanisms of azole resistance in *Mycosphaerella graminicola* and implications for future control. *Pest Manag. Sci.* **69,** 150–155 (2013).

41. Brent, K.J., Hollomon, D. W. *Fungicide Resistance: The Assessment of Risk*. *Fractional Global Crop Protection Federation* **2,** (1998).

42. Solomon, P. S., Tan, K.-C. & Oliver, R. P. The nutrient supply of pathogenic fungi; a fertile field for study. *Mol. Plant Pathol.* **4,** 203–210 (2003).

43. Divon, H. H. & Fluhr, R. Nutrition acquisition strategies during fungal infection of plants. *FEMS Microbiol. Lett.* **266,** 65–74 (2007).

44. Papagianni, M., Mattey, M. & Kristiansen, B. The influence of glucose concentration on citric acid production and morphology of Aspergillus niger in batch and culture. *Enzyme Microb. Technol.* **25,** 710–717 (1999).

45. Zickermann, V. *et al.* Structural biology. Mechanistic insight from the crystal structure of mitochondrial complex I. *Science* **347,** 44–9 (2015).

46. Wikström, M. Two protons are pumped from the mitochondrial matrix per electron transferred between NADH and ubiquinone. *FEBS Lett.* **169,** 300–4 (1984).

47. Galkin, A., Dröse, S. & Brandt, U. The proton pumping stoichiometry of purified mitochondrial complex I reconstituted into proteoliposomes. *Biochim. Biophys. Acta - Bioenerg.* **1757,** 1575–1581 (2006).

48. Guénebaut, V., Vincentelli, R., Mills, D., Weiss, H. & Leonard, K. R. Three-dimensional structure of NADH-dehydrogenase from Neurospora crassa by electron microscopy and conical tilt reconstruction. *J. Mol. Biol.* **265,** 409–418 (1997).

49. Hofhaus, G., Weiss, H. & Leonard, K. Electron microscopic analysis of the peripheral and membrane parts of mitochondrial NADH dehydrogenase (Complex I). *J. Mol. Biol.* **221,** 1027–1043 (1991).

50. Abdrakhmanova, A. *et al.* Subunit composition of mitochondrial complex I from the yeast Yarrowia lipolytica. *Biochim. Biophys. Acta - Bioenerg.* **1658,** 148–156 (2004).

51. Baradaran, R., Berrisford, J. M., Minhas, G. S. & Sazanov, L. A. Crystal structure of the entire respiratory complex I. *Nature* **494,** 443–448 (2013).

52. Sazanov, L. A. & Hinchliffe, P. Structure of the hydrophilic domain of respiratory complex I from Thermus thermophilus. *Science* **311,** 1430–6 (2006).

53. *FRAC Code List FRAC Code List ©* 2018: Fungicides sorted by mode of action (including FRAC Code numbering)*. (2018).

54. Kramer, W., Schirmer, U., Jeschke, P. & Witschel, M. *Modern Crop Protection Compounds: Second Edition*. *Modern Crop Protection Compounds: Second Edition* **1–3,** (Wiley-VCH Verlag GmbH & Co. KGaA, 2012).

55. Guan, A. *et al.* Design, synthesis and antifungal activity of new substituted difluoromethylpyrimidinamine derivatives. *J. Fluor. Chem.* **201,** 49–54 (2017).

56. Liu, C. *et al.* Synthesis, Fungicidal Activity and Mode of Action of 4-Phenyl-6-trifluoromethyl-2-aminopyrimidines against Botrytis cinerea. *Molecules* **21,** 828 (2016).

57. Guan, A. *et al.* Discovery of a New Fungicide Candidate through Lead Optimization of Pyrimidinamine Derivatives and Its Activity against Cucumber Downy Mildew. *J. Agric. Food Chem.* **65,** 10829–10835 (2017).

58. Iverson, T. M., Luna-Chavez, C., Croal, L. R., Cecchini, G. & Rees, D. C. Crystallographic Studies of the *Escherichia coli* Quinol-Fumarate Reductase with Inhibitors Bound to the Quinol-binding Site. *J. Biol. Chem.* **277,** 16124–16130 (2002).

59. Iverson, T. M., Luna-Chavez, C., Cecchini, G. & Rees, D. C. Structure of the Escherichia coli fumarate reductase respiratory complex. *Science* **284,** 1961–6 (1999).

60. Maklashina, E. *et al.* Differences in Protonation of Ubiquinone and Menaquinone in Fumarate Reductase from *Escherichia coli*. *J. Biol. Chem.* **281,** 26655–26664 (2006).

61. Tran, Q. M., Rothery, R. A., Maklashina, E., Cecchini, G. & Weiner, J. H. The Quinone Binding Site in *Escherichia coli* Succinate Dehydrogenase Is Required for Electron Transfer to the Heme *b*. *J. Biol. Chem.* **281,** 32310–32317 (2006).

62. Iverson, T. M. Catalytic mechanisms of complex II enzymes: A structural perspective. *Biochim. Biophys. Acta - Bioenerg.* **1827,** 648–657 (2013).

63. Saliola, M., Bartoccioni, P. C., De Maria, I., Lodi, T. & Falcone, C. The Deletion of the

Succinate Dehydrogenase Gene *KlSDH1* in *Kluyveromyces lactis* Does Not Lead to Respiratory Deficiency. *Eukaryot. Cell* **3,** 589–597 (2004).

64. Rutter, J., Winge, D. R. & Schiffman, J. D. Succinate dehydrogenase – Assembly, regulation and role in human disease. *Mitochondrion* **10,** 393–401 (2010).

65. Huang, L. *et al.* 3-nitropropionic acid is a suicide inhibitor of mitochondrial respiration that, upon oxidation by complex II, forms a covalent adduct with a catalytic base arginine in the active site of the enzyme. *J. Biol. Chem.* **281,** 5965–72 (2006).

66. Horsefield, R. *et al.* Structural and computational analysis of the quinone-binding site of complex II (succinate-ubiquinone oxidoreductase): a mechanism of electron transfer and proton conduction during ubiquinone reduction. *J. Biol. Chem.* **281,** 7309–16 (2006).

67. Wang, H. *et al.* Novel trifluoromethylpyrazole acyl urea derivatives: Synthesis, crystal structure, fungicidal activity and docking study. *J. Mol. Struct.* **1171,** 631–638 (2018).

68. Silkin, Y., Oyedotun, K. S. & Lemire, B. D. The role of Sdh4p Tyr-89 in ubiquinone reduction by the Saccharomyces cerevisiae succinate dehydrogenase. *Biochim. Biophys. Acta - Bioenerg.* **1767,** 143–150 (2007).

69. Zhou, Q. *et al.* Thiabendazole inhibits ubiquinone reduction activity of mitochondrial respiratory complex II via a water molecule mediated binding feature. *Protein Cell* **2,** 531–542 (2011).

70. Mitchell, P. The protonmotive Q cycle: a general formulation. *FEBS Lett.* **59,** 137–9 (1975).

71. Mitchell, P. Possible molecular mechanisms of the protonmotive function of cytochrome systems. *J. Theor. Biol.* **62,** 327–67 (1976).

72. Mulkidjanian, A. Y. Proton translocation by the cytochrome bc1 complexes of phototrophic bacteria: introducing the activated Q-cycle. *Photochem. Photobiol. Sci.* **6,** 19–34 (2007).

73. Hunte, C., Solmaz, S., Palsdóttir, H. & Wenz, T. A Structural Perspective on Mechanism and Function of the Cytochrome bc 1 Complex. in *Bioenergetics* 253–278 (Springer Berlin Heidelberg, 2007). doi:10.1007/400_2007_042

74. Zhang, H. *et al.* Quinone and non-quinone redox couples in Complex III. *J. Bioenerg. Biomembr.* **40,** 493–499 (2008).

75. Robertson, D. E. *et al.* Hydroubiquinone-cytochrome c2 oxidoreductase from Rhodobacter capsulatus: definition of a minimal, functional isolated preparation.

Biochemistry **32,** 1310–7 (1993).

76. Lancaster, C. R., Hunte, C., Kelley, J., Trumpower, B. L. & Ditchfield, R. A Comparison of Stigmatellin Conformations, Free and Bound to the Photosynthetic Reaction Center and the Cytochrome bc(1) Complex. *J.Mol.Biol.* **368,** 197–208 (2007).

77. Cooley, J. W., Ohnishi, T. & Daldal, F. Binding Dynamics at the Quinone Reduction (Q i) Site Influence the Equilibrium Interactions of the Iron Sulfur Protein and Hydroquinone Oxidation (Q o) Site of the cytochrome bc1 complex. 10520–10532 (2005).

78. Cape, J. L., Bowman, M. K. & Kramer, D. M. A semiquinone intermediate generated at the Qo site of the cytochrome bc1 complex: importance for the Q-cycle and superoxide production. *Proc. Natl. Acad. Sci. U. S. A.* **104,** 7887–92 (2007).

79. Wikström, M. K. F. & Berden, J. A. Oxidoreduction of cytochrome b in the presence of antimycin. *Biochim. Biophys. Acta - Bioenerg.* **283,** 403–420 (1972).

80. Bartlett, D. W. *et al.* The strobilurin fungicides. *Pest Manag. Sci.* **58,** 649–662 (2002).

81. Balba, H. Review of strobilurin fungicide chemicals. *J. Environ. Sci. Heal. - Part B Pestic. Food Contam. Agric. Wastes* **42,** 441–451 (2007).

82. Fehr, M., Wolf, A. & Stammler, G. Binding of the respiratory chain inhibitor ametoctradin to the mitochondrial bc1complex. *Pest Manag. Sci.* **72,** 591–602 (2016).

83. Berry, E. A., De Bari, H. & Huang, L. S. Unanswered questions about the structure of cytochrome bc1 complexes. *Biochim. Biophys. Acta - Bioenerg.* **1827,** 1258–1277 (2013).

84. Berry, E. A. *et al.* Ascochlorin is a novel, specific inhibitor of the mitochondrial cytochrome bc1complex. *Biochim. Biophys. Acta - Bioenerg.* **1797,** 360–370 (2010).

85. Siah, A., Deweer, C., Morand, E., Reignault, P. & Halama, P. Azoxystrobin resistance of French Mycosphaerella graminicola strains assessed by four in vitro bioassays and by screening of G143A substitution. *Crop Prot.* **29,** 737–743 (2010).

86. Lesniak, K. E., Proffer, T. J., Beckerman, J. L. & Sundin, G. W. Occurrence of QoI Resistance and Detection of the G143A Mutation in Michigan Populations of *Venturia inaequalis*. *Plant Dis.* **95,** 927–934 (2011).

87. Semar, M., Strobel, D., Koch, A., Klappach, K. & Stammler, G. Field efficacy of pyraclostrobin against populations of Pyrenophora teres containing the F129L mutation in the cytochrome b gene. *J. Plant Dis. Prot.* **114,** 117–119 (2007).

88. Leiminger, J. H., Adolf, B. & Hausladen, H. Occurrence of the F129L mutation in

Alternaria solani populations in Germany in response to QoI application, and its effect on sensitivity. *Plant Pathol.* **63,** 640–650 (2014).

89. Sierotzki, H. *et al.* Cytochromeb gene sequence and structure ofPyrenophora teres andP. tritici-repentis and implications for QoI resistance. *Pest Manag. Sci.* **63,** 225–233 (2007).

90. Miessner, S. & Stammler, G. Monilinia laxa, M. fructigena and M. fructicola: Risk estimation of resistance to QoI fungicides and identification of species with cytochrome b gene sequences. *J. Plant Dis. Prot.* **117,** 162–167 (2010).

91. Rodrigues, E. T., Lopes, I. & Pardal, M. Â. Occurrence, fate and effects of azoxystrobin in aquatic ecosystems: A review. *Environ. Int.* **53,** 18–28 (2013).

92. Charvolin, D., Picard, M., Huang, L. S., Berry, E. A. & Popot, J. L. Solution Behavior and Crystallization of Cytochrome bc1in the Presence of Amphipols. *J. Membr. Biol.* **247,** 981–996 (2014).

93. Avila-Adame, C. & Köller, W. Characterization of spontaneous mutants of Magnaporthe grisea expressing stable resistance to the Qo-inhibiting fungicide azoxystrobin. *Curr. Genet.* **42,** 332–338 (2003).

94. FRAC. List of Plant Pathogenic Organisms Resistant To Disease Control Agents. *FRAC - Fungic. Resist. Action Comm.* (2017). doi:10.1016/j.cbpc.2008.01.005

95. Berry, E. A. *et al.* Ascochlorin is a novel, specific inhibitor of the mitochondrial cytochrome bc1 complex. *Biochim. Biophys. Acta - Bioenerg.* **1797,** 360–370 (2010).

96. Sierotzki, H. Respiration Inhibitors: Complex III. in *Fungicide Resistance in Plant Pathogens* 119–143 (Springer Japan, 2015). doi:10.1007/978-4-431-55642-8_9

97. Yang, W. C., Li, H., Wang, F., Zhu, X. L. & Yang, G. F. Rieske Iron-Sulfur Protein of the Cytochrome bc1 Complex: A Potential Target for Fungicide Discovery. *ChemBioChem* **13,** 1542–1551 (2012).

98. Gisi, U., Sierotzki, H., Cook, A. & McCaffery, A. Mechanisms influencing the evolution of resistance to Qo inhibitor fungicides. *Pest Manag. Sci.* **58,** 859–867 (2002).

99. Li, H., Zhu, X. L., Yang, W. C. & Yang, G. F. Comparative kinetics of Qisite inhibitors of cytochrome bc1complex: Picomolar antimycin and micromolar cyazofamid. *Chem. Biol. Drug Des.* **83,** 71–80 (2014).

100. di Rago, J. P. & Colson, A. M. Molecular basis for resistance to antimycin and diuron, Q-cycle inhibitors acting at the Qi site in the mitochondrial ubiquinol-cytochrome c reductase in Saccharomyces cerevisiae. *J. Biol. Chem.* **263,** 12564–70 (1988).

101. Schnaufer, A., Sbicego, S. & Blum, B. Antimycin A resistance in a mutant Leishmania tarentolae strain is correlated to a point mutation in the mitochondrial apocytochrome b gene. *Curr. Genet.* **37,** 234–241 (2000).

102. Geier, B. M. *et al.* Kinetic Properties and Ligand Binding of the Eleven-subunit Cytochrome-c Oxidase from Saccharomyces cerevisiae Isolated with a Novel Large-Scale Purification Method. *Eur. J. Biochem.* **227,** 296–302 (1995).

103. Yoshikawa, S., Muramoto, K. & Shinzawa-Itoh, K. Proton-Pumping Mechanism of Cytochrome *c* Oxidase. *Annu. Rev. Biophys.* **40,** 205–223 (2011).

104. Yoshida, M., Muneyuki, E. & Hisabori, T. ATP synthase - A marvellous rotary engine of the cell. *Nat. Rev. Mol. Cell Biol.* **2,** 669–677 (2001).

105. Walker, J. E. The ATP synthase: the understood, the uncertain and the unknown. *Biochem. Soc. Trans.* **41,** 1–16 (2013).

106. Junge, W. & Nelson, N. ATP Synthase. *Annu. Rev. Biochem.* **84,** 631–657 (2015).

107. Hobler, C. *et al.* Sex-dependent aromatase activity in rat offspring after pre- and postnatal exposure to triphenyltin chloride. *Toxicology* **276,** 198–205 (2010).

108. Moore, A. L. & Siedow, J. N. The regulation and nature of the cyanide-resistant alternative oxidase of plant mitochondria. *Biochim. Biophys. Acta* **1059,** 121–40 (1991).

109. Moore, A. L. *et al.* Unraveling the Heater: New Insights into the Structure of the Alternative Oxidase. *Annu. Rev. Plant Biol.* **64,** 637–663 (2013).

110. McDonald, A. E. & Vanlerberghe, G. C. Origins, evolutionary history, and taxonomic distribution of alternative oxidase and plastoquinol terminal oxidase. *Comp. Biochem. Physiol. Part D Genomics Proteomics* **1,** 357–364 (2006).

111. Avila-Adame, C. & Köller, W. Disruption of the alternative oxidase gene in Magnaporthe grisea and its impact on host infection. *Mol. Plant. Microbe. Interact.* **15,** 493–500 (2002).

112. Miguez, M., Reeve, C., Wood, P. M. & Hollomon, D. W. Alternative oxidase reduces the sensitivity ofMycosphaerella graminicola to QOI fungicides. *Pest Manag. Sci.* **60,** 3–7 (2004).

113. Huh, W. K. & Kang, S. O. Characterization of the gene family encoding alternative oxidase from Candida albicans. *Biochem. J.* **356,** 595–604 (2001).

114. Cárdenas-Monroy, C. A. *et al.* The mitochondrial alternative oxidase Aox1 is needed to cope with respiratory stress but dispensable for pathogenic development in Ustilago

maydis. *PLoS One* **12,** 4–9 (2017).

115. Helfert, S., Estévez, A. M., Bakker, B., Michels, P. & Clayton, C. Roles of triosephosphate isomerase and aerobic metabolism in Trypanosoma brucei. *Biochem. J.* **357,** 117–25 (2001).

116. Jarmuszkiewicz, W., Wagner, A. M., Wagner, M. J. & Hryniewiecka, L. Immunological identification of the alternative oxidase of *Acanthamoeba castellanii* mitochondria. *FEBS Lett.* **411,** 110–114 (1997).

117. Clarkson, A. B., Bienen, E. J., Pollakis, G. & Grady, R. W. Respiration of bloodstream forms of the parasite Trypanosoma brucei brucei is dependent on a plant-like alternative oxidase. *J. Biol. Chem.* **264,** 17770–17776 (1989).

118. McDonald, A. E., Vanlerberghe, G. C. & Staples, J. F. Alternative oxidase in animals: unique characteristics and taxonomic distribution. *J. Exp. Biol.* **212,** 2627–2634 (2009).

119. Rhoads, D. M. & McIntosh, L. Isolation and characterization of a cDNA clone encoding an alternative oxidase protein of Sauromatum guttatum (Schott). *Proc. Natl. Acad. Sci. U. S. A.* **88,** 2122–6 (1991).

120. Ito, K. *et al.* Identification of a gene for pyruvate-insensitive mitochondrial alternative oxidase expressed in the thermogenic appendices in Arum maculatum. *Plant Physiol.* **157,** 1721–32 (2011).

121. Zhu, Y. *et al.* Regulation of Thermogenesis in Plants: The Interaction of Alternative Oxidase and Plant Uncoupling Mitochondrial Protein. *J. Integr. Plant Biol.* **53,** 7–13 (2011).

122. Searle, S. Y. *et al.* Leaf respiration and alternative oxidase in field-grown alpine grasses respond to natural changes in temperature and light. *New Phytol.* **189,** 1027–1039 (2011).

123. Xu, F., Yuan, S. & Lin, H.-H. Response of mitochondrial alternative oxidase (AOX) to light signals. *Plant Signal. Behav.* **6,** 55–8 (2011).

124. Zhang, D. W. *et al.* Effects of light on cyanide-resistant respiration and alternative oxidase function in Arabidopsis seedlings. *Plant, Cell Environ.* **33,** 2121–2131 (2010).

125. Dahal, K. & Vanlerberghe, G. C. Alternative oxidase respiration maintains both mitochondrial and chloroplast function during drought. *New Phytol.* **213,** 560–571 (2017).

126. Vanlerberghe, G. C., Martyn, G. D. & Dahal, K. Alternative oxidase: a respiratory electron transport chain pathway essential for maintaining photosynthetic performance during drought stress. *Physiol. Plant.* **157,** 322–337 (2016).

127. Dahal, K., Wang, J., Martyn, G. D., Rahimy, F. & Vanlerberghe, G. C. Mitochondrial Alternative Oxidase Maintains Respiration and Preserves Photosynthetic Capacity during Moderate Drought in Nicotiana tabacum. *Plant Physiol.* **166,** 1560–1574 (2014).

128. Moore, A. L., Albury, M. S., Crichton, P. G. & Affourtit, C. Function of the alternative oxidase: is it still a scavenger? *Trends Plant Sci.* **7,** 478–481 (2002).

129. Vishwakarma, A., Tetali, S. D., Selinski, J., Scheibe, R. & Padmasree, K. Importance of the alternative oxidase (AOX) pathway in regulating cellular redox and ROS homeostasis to optimize photosynthesis during restriction of the cytochrome oxidase pathway in *Arabidopsis thaliana*. *Ann. Bot.* **116,** 555–569 (2015).

130. Berthold, D. A., Andersson, M. E. & Nordlund, P. New insight into the structure and function of the alternative oxidase. *Biochim. Biophys. Acta - Bioenerg.* **1460,** 241–254 (2000).

131. Costa, J. H. *et al.* Stress-induced co-expression of two alternative oxidase (VuAox1 and 2b) genes in Vigna unguiculata. *J. Plant Physiol.* **167,** 561–570 (2010).

132. Wei, L.-J. *et al.* Ethylene is Involved in Brassinosteroids Induced Alternative Respiratory Pathway in Cucumber (Cucumis sativus L.) Seedlings Response to Abiotic Stress. *Front. Plant Sci.* **6,** 982 (2015).

133. Xu, F., Yuan, S., Zhang, D.-W., Lv, X. & Lin, H.-H. The role of alternative oxidase in tomato fruit ripening and its regulatory interaction with ethylene. *J. Exp. Bot.* **63,** 5705–5716 (2012).

134. Matos, A. R., Mendes, A. T., Scotti-Campos, P. & Arrabaça, J. D. Study of the effects of salicylic acid on soybean mitochondrial lipids and respiratory properties using the alternative oxidase as a stress-reporter protein. *Physiol. Plant.* **137,** 485–497 (2009).

135. Crichton, P. G., Albury, M. S., Affourtit, C. & Moore, A. L. Mutagenesis of the Sauromatum guttatum alternative oxidase reveals features important for oxygen binding and catalysis. *Biochim. Biophys. Acta - Bioenerg.* **1797,** 732–737 (2010).

136. Vishwakarma, A., Bashyam, L., Senthilkumaran, B., Scheibe, R. & Padmasree, K. Physiological role of AOX1a in photosynthesis and maintenance of cellular redox homeostasis under high light in Arabidopsis thaliana. *Plant Physiol. Biochem.* **81,** 44–53 (2014).

137. Yoshida, K., Watanabe, C. K., Terashima, I. & Noguchi, K. Physiological impact of mitochondrial alternative oxidase on photosynthesis and growth in Arabidopsis thaliana. *Plant, Cell Environ.* **34,** 1890–1899 (2011).

138. Hildebrandt, T. M., Grieshaber, M. K., Clauss & Grieshaber. Redox regulation of mitochondrial sulfide oxidation in the lugworm, Arenicola marina. *J. Exp. Biol.* **211,** 2617–23 (2008).

139. Tschischka, K., Abele, D. & Pörtner, H. O. Mitochondrial oxyconformity and cold adaptation in the polychaete Nereis pelagica and the bivalve Arctica islandica from the Baltic and White Seas. *J. Exp. Biol.* **203,** 3355–68 (2000).

140. Gospodaryov, D. V. *et al.* Ciona intestinalis NADH dehydrogenase NDX confers stress-resistance and extended lifespan on Drosophila. *Biochim. Biophys. Acta - Bioenerg.* **1837,** 1861–1869 (2014).

141. McDonald, A. & Vanlerberghe, G. Branched Mitochondrial Electron Transport in the Animalia: Presence of Alternative Oxidase in Several Animal Phyla. *IUBMB Life (International Union Biochem. Mol. Biol. Life)* **56,** 333–341 (2004).

142. Grieshaber, M. K. & Völkel, S. Animal adaptations for tolerance and exploitation of poisonous sulfide. *Annu. Rev. Physiol.* **60,** 33–53 (1998).

143. Suzuki, T. *et al.* Direct evidence for cyanide-insensitive quinol oxidase (alternative oxidase) in apicomplexan parasite Cryptosporidium parvum: phylogenetic and therapeutic implications. *Biochem. Biophys. Res. Commun.* **313,** 1044–52 (2004).

144. Czarna, M. & Jarmuszkiewicz, W. Activation of alternative oxidase and uncoupling protein lowers hydrogen peroxide formation in amoeba *Acanthamoeba castellanii* mitochondria. *FEBS Lett.* **579,** 3136–3140 (2005).

145. Chaudhuri, M., Ott, R. D. & Hill, G. C. Trypanosome alternative oxidase: from molecule to function. *Trends Parasitol.* **22,** 484–491 (2006).

146. Menzies, S. K., Tulloch, L. B., Florence, G. J. & Smith, T. K. The trypanosome alternative oxidase: A potential drug target? *Parasitology* **145,** 175–183 (2018).

147. Johnson, C. H., Prigge, J. T., Warren, A. D. & McEwen, J. E. Characterization of an alternative oxidase activity of Histoplasma capsulatum. *Yeast* **20,** 381–388 (2003).

148. Tudella, V. G., Curti, C., Soriani, F. M., Santos, A. C. & Uyemura, S. A. In situ evidence of an alternative oxidase and an uncoupling protein in the respiratory chain of Aspergillus fumigatus. *Int. J. Biochem. Cell Biol.* **36,** 162–172 (2004).

149. Maas, M. F. P. M., Krause, F., Dencher, N. A. & Sainsard-Chanet, A. Respiratory Complexes III and IV Are Not Essential for the Assembly/Stability of Complex I in Fungi. *J. Mol. Biol.* **387,** 259–269 (2009).

150. Inoue, K., Tsurumi, T., Ishii, H., Park, P. & Ikeda, K. Cytological evaluation of the effect of azoxystrobin and alternative oxidase inhibitors in Botrytis cinerea. *FEMS Microbiol. Lett.* **326,** 83–90 (2012).

151. Thomazella, D. P. T. *et al.* The hemibiotrophic cacao pathogen Moniliophthora perniciosa depends on a mitochondrial alternative oxidase for biotrophic development. *New Phytol.* **194,** 1025–1034 (2012).

152. Kaneko, I. & Ishii, H. Effect of azoxystrobin on activities of antioxidant enzymes and alternative oxidase in wheat head blight pathogens Fusarium graminearum and Microdochium nivale. *J. Gen. Plant Pathol.* **75,** 388–398 (2009).

153. Xu, T. *et al.* Involvement of alternative oxidase in the regulation of sensitivity of Sclerotinia sclerotiorum to the fungicides azoxystrobin and procymidone. *J. Microbiol.* **51,** 352–358 (2013).

154. Steinfeld, U., Sierotzki, H., Parisi, S., Poirey, S. & Gisi, U. Sensitivity of mitochondrial respiration to different inhibitors in Venturia inaequalis. *Pest Manag. Sci.* **57,** 787–796 (2001).

155. Millar, A. H., Wiskich, J. T., Whelan, J. & Day, D. A. Organic acid activation of the alternative oxidase of plant mitochondria. *FEBS Lett.* **329,** 259–62 (1993).

156. Woyda-Ploszczyca, A. M., Sluse, F. E. & Jarmuszkiewicz, W. Regulation of Acanthamoeba castellanii alternative oxidase activity by mutual exclusion of purine nucleotides; ATP's inhibitory effect. *Biochim. Biophys. Acta - Bioenerg.* **1787,** 264–271 (2009).

157. Czarna, M. & Jarmuszkiewicz, W. Activation of alternative oxidase and uncoupling protein lowers hydrogen peroxide formation in amoeba Acanthamoeba castellanii mitochondria. *FEBS Lett.* **579,** 3136–3140 (2005).

158. Grant, N. *et al.* Two Cys or Not Two Cys? That Is the Question; Alternative Oxidase in the Thermogenic Plant Sacred Lotus. *Plant Physiol.* **150,** 987–995 (2009).

159. Kakizaki, Y. & Ito, K. Engineering plant alternative oxidase function in mammalian cells: Substitution of the motif-like sequence ENV for QDT diminishes catalytic activity of Arum concinnatum AOX1a expressed in HeLa cells. *Appl. Biochem. Biotechnol.* **170,** 1229–1240 (2013).

160. Vanderleyden, J., Peeters, C., Verachtert, H. & Bertrand, H. Stimulation of the alternative oxidase of Neurospora crassa by Nucleoside phosphates. *Biochem. J.* **188,** 141–4 (1980).

161. Umbach, A. L. & Siedow, J. N. The cyanide-resistant alternative oxidases from the fungi Pichia stipitis and Neurospora crassa are monomeric and lack regulatory features of the plant enzyme. *Arch. Biochem. Biophys.* **378,** 234–245 (2000).

162. Woyda-Ploszczyca, A. M., Sluse, F. E. & Jarmuszkiewicz, W. Regulation of Acanthamoeba castellanii alternative oxidase activity by mutual exclusion of purine nucleotides; ATP's inhibitory effect. *Biochim. Biophys. Acta - Bioenerg.* **1787,** 264–271 (2009).

163. Joseph-Horne, T., Babij, J., Wood, P. M., Hollomon, D. & Sessions, R. B. New sequence data enable modelling of the fungal alternative oxidase and explain an absence of regulation by pyruvate. *FEBS Lett.* **481,** 141–146 (2000).

164. Umbach, A. L. & Siedow, J. N. The Cyanide-Resistant Alternative Oxidases from the Fungi Pichia stipitis and Neurospora crassa Are Monomeric and Lack Regulatory Features of the Plant Enzyme. *Arch. Biochem. Biophys.* **378,** 234–245 (2000).

165. Shiba, T. *et al.* Structure of the trypanosome cyanide-insensitive alternative oxidase. *Proc. Natl. Acad. Sci. U. S. A.* **110,** 4580–5 (2013).

166. Moore, A. L. *et al.* Compelling EPR evidence that the alternative oxidase is a diiron carboxylate protein. *Biochim. Biophys. Acta* **1777,** 327–30 (2008).

167. Rosenzweig, A. C., Frederick, C. A., Lippard, S. J. & Nordlund, P. Crystal structure of a bacterial non-haem iron hydroxylase that catalyses the biological oxidation of methane. *Nature* **366,** 537–543 (1993).

168. Nordlund, P. & Eklund, H. Structure and Function of the Escherichia coli Ribonucleotide Reductase Protein R2. *J. Mol. Biol.* **232,** 123–164 (1993).

169. Jin, S., Kurtz, D. M., Liu, Z.-J., Rose, J. & Wang, B.-C. X-ray crystal structures of reduced rubrerythrin and its azide adduct: a structure-based mechanism for a non-heme diiron peroxidase. *J. Am. Chem. Soc.* **124,** 9845–55 (2002).

170. Reece, S. Y. & Seyedsayamdost, M. R. Long-range proton-coupled electron transfer in the *Escherichia coli* class Ia ribonucleotide reductase. *Essays Biochem.* **61,** 281–292 (2017).

171. May, B., Young, L. & Moore, A. L. Structural insights into the alternative oxidases: are all oxidases made equal? *Biochem. Soc. Trans.* **45,** 731–740 (2017).

172. Young, L. *et al.* Probing the ubiquinol-binding site of recombinant Sauromatum guttatum alternative oxidase expressed in E. coli membranes through site-directed mutagenesis.

Biochim. Biophys. Acta - Bioenerg. **1837,** 1219–1225 (2014).

173. Young, L. *et al.* The alternative oxidases: simple oxidoreductase proteins with complex functions. *Biochem. Soc. Trans.* **41,** 1305–1311 (2013).

174. Young, L. *et al.* Structure and Mechanism of Action of the Alternative Quinol Oxidases. in 375–394 (Springer, Dordrecht, 2016). doi:10.1007/978-94-017-7481-9_19

175. Hahn, M. The rising threat of fungicide resistance in plant pathogenic fungi: Botrytis as a case study. *J. Chem. Biol.* **7,** 133–41 (2014).

176. Lucas, J. A., Hawkins, N. J. & Fraaije, B. A. *The Evolution of Fungicide Resistance*. *Advances in Applied Microbiology* **90,** (Elsevier, 2015).

177. Estep, L. K. *et al.* Emergence and early evolution of fungicide resistance in North American populations of *Zymoseptoria tritici*. *Plant Pathol.* **64,** 961–971 (2015).

178. Schnabel, G. & Jones, A. L. The 14α-Demethylasse(*CYP51A1*) Gene is Overexpressed in *Venturia inaequalis* Strains Resistant to Myclobutanil. *Phytopathology* **91,** 102–110 (2001).

179. Luo, C.-X. & Schnabel, G. The Cytochrome P450 Lanosterol 14 -Demethylase Gene Is a Demethylation Inhibitor Fungicide Resistance Determinant in Monilinia fructicola Field Isolates from Georgia. *Appl. Environ. Microbiol.* **74,** 359–366 (2008).

180. Reimann, S. & Deising, H. B. Inhibition of efflux transporter-mediated fungicide resistance in Pyrenophora tritici-repentis by a derivative of 4’-hydroxyflavone and enhancement of fungicide activity. *Appl. Environ. Microbiol.* **71,** 3269–75 (2005).

181. Roohparvar, R., De Waard, M. A., Kema, G. H. J. & Zwiers, L.-H. MgMfs1, a major facilitator superfamily transporter from the fungal wheat pathogen Mycosphaerella graminicola, is a strong protectant against natural toxic compounds and fungicides. *Fungal Genet. Biol.* **44,** 378–388 (2007).

182. Hayashi, K., Schoonbeek, H.-J. & De Waard, M. A. Bcmfs1, a novel major facilitator superfamily transporter from Botrytis cinerea, provides tolerance towards the natural toxic compounds camptothecin and cercosporin and towards fungicides. *Appl. Environ. Microbiol.* **68,** 4996–5004 (2002).

183. Leroux, P. & Walker, A.-S. Multiple mechanisms account for resistance to sterol 14α-demethylation inhibitors in field isolates of Mycosphaerella graminicola. *Pest Manag. Sci.* **67,** 44–59 (2011).

184. Nakaune, R., Hamamoto, H., Imada, J., Akutsu, K. & Hibi, T. A novel ABC transporter

gene, PMR5 , is involved in multidrug resistance in the phytopathogenic fungus Penicillium digitatum. *Mol. Genet. Genomics* **267,** 179–185 (2003).

185. Miguez, M., Reeve, C., Wood, P. M. & Hollomon, D. W. Alternative oxidase reduces the sensitivity of Mycosphaerella graminicola to QOI fungicides. *Pest Manag. Sci.* **60,** 3–7 (2004).

186. Bohr, V. A. & Anson, R. M. Mitochondrial DNA Repair Pathways. *J. Bioenerg. Biomembr.* **31,** 391–398 (1999).

187. Ziogas, B. N., Baldwin, C. & Young, J. E. Alternative Respiration : a Biochemical Mechanism of Resistance to Azoxystrobin (ICIA 5504) in Septoria tritici. **50,** 28–34 (1997).

188. Affourtit, C., Heaney, S. P. & Moore, A. L. Mitochondrial electron transfer in the wheat pathogenic fungus Septoria tritici: On the role of alternative respiratory enzymes in fungicide resistance. *Biochim. Biophys. Acta - Bioenerg.* **1459,** 291–298 (2000).

189. Wood, P. M. & Hollomon, D. W. A critical evaluation of the role of alternative oxidase in the performance of strobilurin and related fungicides acting at the Qo site of complex III. *Pest Manag. Sci.* **59,** 499–511 (2003).

190. Fernández-Ortuño, D., Torés, J. A., De Vicente, A. & Pérez-García, A. Mechanisms of resistance to QoI fungicides in phytopathogenic fungi. *Int. Microbiol.* **11,** 1–9 (2008).

191. Siedow, J. N. & Umbach, A. L. Plant Mitochondrial Electron Transfer and Molecular Biology. *Plant Cell* **7,** 821–831 (1995).

192. Rich, P. R., Wiegand, N. K., Blum, H., Moore, A. L. & Bonner, W. D. Studies on the mechanism of inhibition of redox enzymes by substituted hydroxamic acids. *Biochim. Biophys. Acta - Enzymol.* **525,** 325–337 (1978).

193. Singh, A. K. *et al.* Binding modes of aromatic ligands to mammalian heme peroxidases with associated functional implications: crystal structures of lactoperoxidase complexes with acetylsalicylic acid, salicylhydroxamic acid, and benzylhydroxamic acid. *J. Biol. Chem.* **284,** 20311–8 (2009).

194. Hassan, S. S. M., El-Bahnasawy, R. M. & Rizk, N. M. Potentiometric determination of salicylhydroxamic acid (urinary struvite stone inhibitor) based on the inhibition of urease activity. *Anal. Chim. Acta* **351,** 91–96 (1997).

195. Siedow, J. N. & Bickett, D. M. Structural features required for inhibition of cyanide-insensitive electron transfer by propyl gallate. *Arch. Biochem. Biophys.* **207,** 32–39 (1981).

196. Grady, R. W., Bienen, E. J. & Clarkson, A. B. Esters of 3,4-dihydroxybenzoic acid, highly effective inhibitors of the sn-glycerol-3-phosphate oxidase of Trypanosoma brucei brucei. *Mol. Biochem. Parasitol.* **21,** 55–63 (1986).

197. Hijikawa, Y. *et al.* Re-identification of the ascofuranone-producing fungus Ascochyta viciae as Acremonium sclerotigenum. *J. Antibiot. (Tokyo).* **70,** 304–307 (2017).

198. Saimoto, H., Kido, Y., Haga, Y., Sakamoto, K. & Kita, K. Pharmacophore identification of ascofuranone, potent inhibitor of cyanide-insensitive alternative oxidase of Trypanosoma brucei. *J. Biochem.* **153,** 267–273 (2013).

199. Berry, E. A. *et al.* Ascochlorin is a novel, specific inhibitor of the mitochondrial cytochrome bc1 complex. *Biochim. Biophys. Acta - Bioenerg.* **1797,** 360–370 (2010).

200. West, R. A. *et al.* African trypanosomiasis: Synthesis & SAR enabling novel drug discovery of ubiquinol mimics for trypanosome alternative oxidase. *Eur. J. Med. Chem.* **141,** 676–689 (2017).

201. West, R. A., Cunningham, T., Pennicott, L. E., Rao, S. P. S. & Ward, S. E. Toward More Drug Like Inhibitors of Trypanosome Alternative Oxidase. *ACS Infect. Dis.* **4,** 592–604 (2018).

202. Yabu, Y. *et al.* Oral and intraperitoneal treatment of Trypanosoma brucei brucei with a combination of ascofuranone and glycerol in mice. *Parasitol. Int.* **47,** 131–137 (1998).

203. Yabu, Y. *et al.* The efficacy of ascofuranone in a consecutive treatment on Trypanosoma brucei brucei in mice. *Parasitol. Int.* **52,** 155–164 (2003).

204. Yabu, Y. *et al.* Chemotherapeutic efficacy of ascofuranone in Trypanosoma vivax-infected mice without glycerol. *Parasitol. Int.* **55,** 39–43 (2006).

205. FRAC Commitee. Importance of multisite fungicides in managing pathogen resistance. (2018). doi:10.1007/978-4-431-55642-8_4

206. Eyal, Z. & International Maize and Wheat Improvement Center. *The Septoria diseases of wheat : concepts and methods of disease management*. (CIMMYT, 1987).

207. Fones, H. & Gurr, S. The impact of Septoria tritici Blotch disease on wheat: An EU perspective. *Fungal Genet. Biol.* **79,** 3–7 (2015).

208. Torriani, S. F., Brunner, P. C., McDonald, B. A. & Sierotzki, H. QoI resistance emerged independently at least 4 times in European populations of *Mycosphaerella graminicola*. *Pest Manag. Sci.* **65,** 155–162 (2009).

209. McCartney, C., Mercer, P. C., Cooke, L. R. & Fraaije, B. A. Effects of a strobilurin-based spray programme on disease control, green leaf area, yield and development of fungicide-resistance in Mycosphaerella graminicola in Northern Ireland. *Crop Prot.* **26,** 1272–1280 (2007).

210. Amand, O. *et al.* First detection of resistance to QoI fungicides in Mycosphaerella graminicola on winter wheat in Belgium. *Commun. Agric. Appl. Biol. Sci.* **68,** 519–31 (2003).

211. Cools, H. J. & Fraaije, B. A. Are azole fungicides losing ground against Septoria wheat disease? Resistance mechanisms inMycosphaerella graminicola. *Pest Manag. Sci.* **64,** 681–684 (2008).

212. Jones, A. J. Y. *et al.* A Self-Assembled Respiratory Chain that Catalyzes NADH Oxidation by Ubiquinone-10 Cycling between Complex I and the Alternative Oxidase. *Angew. Chemie Int. Ed.* **55,** 728–731 (2016).

213. Schrödinger. The PyMOL Molecular Graphics System, Version 2.0 Schrödinger. (2019).

214. Schrödinger. Release 2019-1: Maestro. (2019).

215. Inc., C. C. G. MOE (The Molecular Operating Environment) Version 2018. 001. (2018).

216. Richard A. Friesner, * *et al.* Extra Precision Glide: Docking and Scoring Incorporating a Model of Hydrophobic Enclosure for Protein−Ligand Complexes. (2006). doi:10.1021/JM051256O

217. Waterhouse, A. *et al.* SWISS-MODEL: homology modelling of protein structures and complexes. *Nucleic Acids Res.* **46,** W296–W303 (2018).

218. Berman, H. M. *et al.* The Protein Data Bank. *Nucleic Acids Res.* **28,** 235–242 (2000).

219. Xie, L., Takeuchi, Y., Cosentino, L. M., McPhail, A. T. & Lee, K. H. Anti-AIDS agents. 42. Synthesis and anti-HIV activity of disubstituted (3′R,4′R)-3′,4′-di-O-(S)-camphanoyl-(+)-cis- khellactone analogues. *J. Med. Chem.* **44,** 664–671 (2001).

220. Safaryn, J. E., Chiarello, J., Chen, K.-M. & Joullie, M. M. A convenient synthesis of (±) ascochlorin. *Tetrahedron* **42,** 2635–2642 (1986).

221. Haga, Y. *et al.* A Short and Efficient Total Synthesis of (±)-Ascofuranone. *Chem. Lett.* **39,** 622–623 (2010).

222. Watanabe, S. Synthesis of fluorescent alkyl lactoside derivatives. *Carbohydr. Res.* **343,** 2325–2328 (2008).

223. Umbreit, M. A. & Sharpless, K. B. Allylic Oxidation of Olefins by Catalytic and Stoichiometric Selenium Dioxide with tert-Butyl Hydroperoxide. *J. Am. Chem. Soc.* **99,** 5526–5528 (1977).

224. Food and Agriculture Organization of the United Nations. *Food and Agriculture Organization of the United Nations: World Food Situation*. (2015).

225. Thomas, M. R., Cook, R. J. & King, J. E. Factors affecting development of Septoria tritici in winter wheat and its effect on yield. *Plant Pathol.* **38,** 246–257 (1989).

226. FAO. *OECD-FAO Agricultural Outlook 2012*. (OECD Publishing, 2012). doi:10.1787/agr_outlook-2012-en

227. Tilman, D., Balzer, C., Hill, J. & Befort, B. L. Global food demand and the sustainable intensification of agriculture. *Proc. Natl. Acad. Sci. U. S. A.* **108,** 20260–4 (2011).

228. Bebber, D. P. & Gurr, S. J. Crop-destroying fungal and oomycete pathogens challenge food security. *Fungal Genet. Biol.* **74,** 62–64 (2015).

229. FAO. *How to Feed the World in 2050*. *The High-Level Expert Forum on How to Feed the World in 2050* (2009). doi:http://www.fao.org/wsfs/forum2050/wsfs-forum/en/

230. Eyal, Z., International Maize and Wheat Improvement Center., A. L., Prescott, J. M. & Ginkel, M. Van. *The Septoria diseases of wheat : concepts and methods of disease management*. (CIMMYT, 1987).

231. Scott, P. R., Sanderson, F. R. & Benedikz, P. W. Occurrence of Mycosphaerella graminicola, teleomorph of Septoria tritici, on wheat debris in the UK. *Plant Pathol.* **37,** 285–290 (1988).

232. Kema, G. Histology of the Pathogenesis of *Mycosphaerella graminicola* in Wheat. *Phytopathology* **86,** 777 (1996).

233. Duncan, K. E. & Howard, R. J. Cytological analysis of wheat infection by the leaf blotch pathogen Mycosphaerella graminicola. *Mycol. Res.* **104,** 1074–1082 (2000).

234. Sánchez-Vallet, A., McDonald, M. C., Solomon, P. S. & McDonald, B. A. Is Zymoseptoria tritici a hemibiotroph? *Fungal Genet. Biol.* **79,** 29–32 (2015).

235. Keon, J. *et al.* Transcriptional Adaptation of *Mycosphaerella graminicola* to Programmed Cell Death (PCD) of Its Susceptible Wheat Host. *Mol. Plant-Microbe Interact.* **20,** 178–193 (2007).

236. Yang, F., Li, W. & Jørgensen, H. J. L. Transcriptional Reprogramming of Wheat and the

Hemibiotrophic Pathogen Septoria tritici during Two Phases of the Compatible Interaction. *PLoS One* **8,** e81606 (2013).

237. Marshall, R. *et al.* Analysis of Two in Planta Expressed LysM Effector Homologs from the Fungus Mycosphaerella graminicola Reveals Novel Functional Properties and Varying Contributions to Virulence on Wheat. *Plant Physiol.* **156,** 756 LP-769 (2011).

238. Ferreira, R. B. *et al.* The role of plant defence proteins in fungal pathogenesis. *Mol. Plant Pathol.* **8,** 677–700 (2007).

239. Eyal, Z. The kinetics of pycnospore liberation in *Septoria tritici*. *Can. J. Bot.* **49,** 1095–1099 (1971).

240. Rudd, J. J. *et al.* Transcriptome and metabolite profiling of the infection cycle of Zymoseptoria tritici on wheat reveals a biphasic interaction with plant immunity involving differential pathogen chromosomal contributions and a variation on the hemibiotrophic lifestyle definition. *Plant Physiol.* **167,** 1158–85 (2015).

241. Ponomarenko A., S.B. Goodwin, and G. H. J. K. Septoria tritici blotch (STB) of wheat. *Plant Heal. Instr.* (2011).

242. Van Ginkel, M., McNab, A., Krupinsky, J. & International Maize and Wheat Improvement Center. *Septoria and Stagonospora diseases of cereals : a compilation of global research : proceedings of the fifth International Septoria Workshop, September 20-24, 1999, CIMMYT, Mexico*. (CIMMYT, 1999).

243. Shaw, M. W. Assessment of upward movement of rain splash using a fluorescent tracer method and its application to the epidemiology of cereal pathogens. *Plant Pathol.* **36,** 201–213 (1987).

244. Chungu, C., Gilbert, J. & Townley-Smith, F. Septoria tritici Blotch Development as Affected by Temperature, Duration of Leaf Wetness, Inoculum Concentration, and Host. *Plant Dis.* **85,** 430–435 (2001).

245. Wieczorek, T. M. *et al.* Impact of DMI and SDHI fungicides on disease control and CYP51 mutations in populations of Zymoseptoria tritici from Northern Europe. *Eur. J. Plant Pathol.* **143,** 861–871 (2015).

246. Fraaije, B. A. *et al.* Risk assessment studies on succinate dehydrogenase inhibitors, the new weapons in the battle to control Septoria leaf blotch in wheat. *Mol. Plant Pathol.* **13,** 263–275 (2012).

247. Ohkawa, H., Miyagawa, H. & Lee, P. W. *Pesticide Chemistry: Crop Protection, Public*

Health, Environmental Safety. *Pesticide Chemistry: Crop Protection, Public Health, Environmental Safety* (Wiley-VCH Verlag GmbH & Co. KGaA, 2007).

248. Marroni, M. V, Viljanen-Rollinson, S. L. H., Butler, R. C. & Deng, Y. *Plant Pathogens Fungicide Timing for the control of Septoria Tritici Blotch of Wheat*. *New Zealand Plant Protection* **59,** (2006).

249. Kildea, S. *et al.* Pyraclostrobin reduces germ tube growth of QoI-resistant Mycosphaerella graminicola pycnidiospores and the severity of septoria tritici blotch on winter wheat. *Plant Pathol.* **59,** 1091–1098 (2010).

250. Schöfl, U. A. & Zinkernagel, V. A test method based on microscopic assessments to determine curative and protectant fungicide properties against Septoria tritici. *Plant Pathol.* **46,** 545–556 (1997).

251. Marroni, M. V, Viljanen-Rollinson, S. L. H., Butler, R. C. & Deng, Y. *Fungicide timing for the control of Septoria tritici blotch of wheat*. *New Zealand Plant Protection* **59,** (2006).

252. Cook, R. J., Hims, M. J. & Vaughan, T. B. Effects of fungicide spray timing on winter wheat disease control. *Plant Pathol.* **48,** 33–50 (1999).

253. Sanssené, J. *et al.* Protective and curative efficacy of prothioconazole against isolates of Mycosphaerella graminicola differing in their in vitro sensitivity to DMI fungicides. *Pest Manag. Sci.* **67,** 1134–1140 (2011).

254. Claros, M. G. & Vincens, P. Computational method to predict mitochondrially imported proteins and their targeting sequences. *Eur. J. Biochem.* **241,** 779–86 (1996).

255. Good, N. E. *et al.* Hydrogen Ion Buffers for Biological Research *. *Biochemistry* **5,** 467–477 (1966).

256. Ferreira, C. M. H., Pinto, I. S. S., Soares, E. V. & Soares, H. M. V. M. (Un)suitability of the use of pH buffers in biological, biochemical and environmental studies and their interaction with metal ions-a review. *RSC Adv.* **5,** 30989–31003 (2015).

257. Kido, Y. *et al.* Purification and kinetic characterization of recombinant alternative oxidase from Trypanosoma brucei brucei. *Biochim. Biophys. Acta - Bioenerg.* **1797,** 443–450 (2010).

258. Elliott, C. *et al.* Purification and characterisation of recombinant DNA encoding the alternative oxidase from Sauromatum guttatum. *Mitochondrion* **19,** 261–268 (2014).

259. Young, L. Structure, function and mechanism of the alternative oxidases. (University of

Sussex, 2014).

260. Jones, A. J. Y. *et al.* A Self-Assembled Respiratory Chain that Catalyzes NADH Oxidation by Ubiquinone-10 Cycling between ComplexI and the Alternative Oxidase. *Angew. Chemie - Int. Ed.* **55,** 728–731 (2016).

261. Avila-Adame, C. & Köller, W. Characterization of spontaneous mutants of Magnaporthe grisea expressing stable resistance to the Qo-inhibiting fungicide azoxystrobin. *Curr. Genet.* **42,** 332–338 (2003).

262. Mori, K. & Fujioka, T. Synthesis of (±)-ascofuranone, in antibiotic with hypolipidemic and antitumor protective properties. *Tetrahedron Lett.* **24,** 1547–1548 (1983).

263. Mori, K. & Takechi, S. Synthesis of the natural enantiomers of ascochlorin, ascofuranone and ascofuranol. *Tetrahedron* **41,** 3049–3062 (1985).

264. Mori, K. & Fujioka, T. Synthesis of (±)-ascochlorin, (±)-ascofuranone and LL-Z1272. *Tetrahedron* **40,** 2711–2720 (1984).

265. Kau-Ming, C. & Joullié, M. M. A simple total synthesis of (±)-ascofuranone. *Tetrahedron Lett.* **25,** 3795–3796 (1984).

266. Guthrie, A. A., Semple, J. E. & Joullie, M. M. Synthetic studies of fungal metabolites: ascofuranone and colletochlorin D. *J. Org. Chem.* **47,** 2369–2376 (1982).

267. Chen, K.-M. & Joullié, M. M. Synthesis of colletochlorin D. *Tetrahedron Lett.* **23,** 4567–4568 (1982).

268. Saimoto, H., Ohrai, S., Sashiwa, H., Shigemasa, Y. & Hiyama, T. Total Synthesis of *dl* -Ascofuranone and Related Compounds. *Bull. Chem. Soc. Jpn.* **68,** 2727–2734 (1995).

269. Anthony, L. M., Albury, M. S., Young, L. E. & Catherine Elliott, B. Compounds for use as inhibitors of alternative oxidase or cytochrome bc1 complex. (2013).

270. Chiarello, J. & Joullié, M. M. Synthetic routes to cristatic acid and derivatives. *Tetrahedron* **44,** 41–48 (1988).

271. Haga, Y., Tonoi, T., Anbiru, Y., Takahashi, Y. & Tamura, S. Supporting Information A Short and Efficient Total Synthesis of (±) -Ascofuranone. *Bioscience* **0052,** 3–7 (2010).

272. Doi, K. *et al.* Microhydration Effects on the Intermediates of the S_N2 Reaction of Iodide Anion with Methyl Iodide. *Angew. Chemie Int. Ed.* **52,** 4380–4383 (2013).

273. Asghari, T. *et al.* Synthesis and Evaluation of a New Series of 3,5-bis((5-bromo-6-methyl-2-t-aminopyrimidin-4-yl)thio)-4H-1,2,4-triazol-4-amines and their Cyclized Products

‘Pyrimidinylthio Pyrimidotriazolothiadiazines’ as 15- Lipo-Oxygenase Inhibitors. *Chem. Biol. Drug Des.* **85,** 216–224

274. Concilio, S. *et al.* A novel fluorescent solvatochromic probe for lipid bilayers. *Supramol. Chem.* **29,** 887–895 (2017).

275. Concilio, S., Bugatti, V., Iannelli, P. & Piotto, S. P. Synthesis and characterization of new photoluminescent oxadiazole/ carbazole-containing polymers. *Int. J. Polym. Sci.* **2010,** 1–7 (2010).

276. Amaro, M., Filipe, H. A. L., Prates Ramalho, J. P., Hof, M. & Loura, L. M. S. Fluorescence of nitrobenzoxadiazole (NBD)-labeled lipids in model membranes is connected not to lipid mobility but to probe location. *Phys. Chem. Chem. Phys.* **18,** 7042–7054 (2016).

277. Hathwar, V. R., Chopra, D., Panini, P. & Guru Row, T. N. Revealing the Polarizability of Organic Fluorine in the Trifluoromethyl Group: Implications in Supramolecular Chemistry. *Cryst. Growth Des.* **14,** 5366–5369 (2014).

278. Yale, H. L. The Trifluoromethyl Group in Medical Chemistry. *J. Med. Pharm. Chem.* **1,** 121–133 (1959).

279. Nakamura, A. & Nakada, M. Allylic Oxidations in Natural Product Synthesis. *Synthesis (Stuttg).* **45,** 1421–1451 (2013).

280. Jackson, H. L., Nadolski, G. T., Braun, C. & Lockwood, S. F. Efficient total synthesis of lycophyll (ψ,ψ-carotene-16,16′- diol). *Org. Process Res. Dev.* **9,** 830–836 (2005).

281. Gao, J. *et al.* Multi-target-directed design, syntheses, and characterization of fluorescent bisphosphonate derivatives as multifunctional enzyme inhibitors in mevalonate pathway. *Biochim. Biophys. Acta - Gen. Subj.* **1830,** 3635–3642 (2013).

282. Erden, I. *et al.* Effect of Allylic Groups on S N 2 Reactivity Scheme 1. Competitive Additions of Nucleophiles onto 1. *J. Org. Chem* **79,** (2014).

283. Robiette, R., Trieu-Van, T., Aggarwal, V. K. & Harvey, J. N. Activation of the SN2 Reaction by Adjacent π Systems: The Critical Role of Electrostatic Interactions and of Dissociative Character. *J. Am. Chem. Soc.* **138,** 734–737 (2016).

284. Humphreys, S. P., Oates, K., Ayres, P. G., Shephard, M. C. & Baldwin, B. C. Distribution of a fungicide at the host-pathogen interface studied by X-ray microanalysis. *Mycol. Res.* **95,** 239–242 (1991).

285. Delaney, J., Clarke, E., Hughes, D. & Rice, M. Modern agrochemical research: a missed opportunity for drug discovery? *Drug Discov. Today* **11,** 839–845 (2006).

286. Tice, C. M. Selecting the right compounds for screening: does Lipinski's Rule of 5 for pharmaceuticals apply to agrochemicals? *Pest Manag. Sci.* **57,** 3–16 (2001).

287. Lipinski, C. A., Lombardo, F., Dominy, B. W. & Feeney, P. J. Experimental and computational approaches to estimate solubility and permeability in drug discovery and development settings. *Adv. Drug Deliv. Rev.* **46,** 3–26 (2001).

288. Manallack, D. T. The acid/base profile of agrochemicals. *SAR QSAR Environ. Res.* **28,** 621–628 (2017).

289. Avram, S. *et al.* Quantitative estimation of pesticide-likeness for agrochemical discovery. *J. Cheminform.* **6,** 42 (2014).

290. Hutson, D. H. (David H. & Miyamoto, J. (Junshi). *Fungicidal activity : chemical and biological approaches to plant protection*. (Wiley, 1998).

291. Godwin, J., Anthony, V., Clough, J. & Godfrey, C. ICIA5504: a novel, broad spectrum, systemic b-methoxyacry- late fungicide. in *Proc Brighton Crop Protect Conf. Pests and Diseases* 435–442 (1992).

292. Gao, X. *et al.* The crystal structure of mitochondrial cytochrome bc1 in complex with famoxadone: The role of aromatic-aromatic interaction in inhibition. *Biochemistry* **41,** 11692–11702 (2002).

293. Berry, E. A. & Huang, L.-S. Conformationally linked interaction in the cytochrome bc1 complex between inhibitors of the Qo site and the Rieske iron–sulfur protein. *Biochim. Biophys. Acta - Bioenerg.* **1807,** 1349–1363 (2011).

294. Esser, L. *et al.* Crystallographic Studies of Quinol Oxidation Site Inhibitors: A Modified Classification of Inhibitors for the Cytochrome bc1 Complex. *J. Mol. Biol.* **341,** 281–302 (2004).

295. Wager, T. T., Hou, X., Verhoest, P. R. & Villalobos, A. Moving beyond Rules: The Development of a Central Nervous System Multiparameter Optimization (CNS MPO) Approach To Enable Alignment of Druglike Properties. *ACS Chem. Neurosci.* **1,** 435–449 (2010).

296. Weber, P. C. & Salemme, F. R. Applications of calorimetric methods to drug discovery and the study of protein interactions. *Curr. Opin. Struct. Biol.* **13,** 115–121 (2003).

297. Leavitt, S. & Freire, E. Direct measurement of protein binding energetics by isothermal titration calorimetry. *Curr. Opin. Struct. Biol.* **11,** 560–566 (2001).

298. Olsen, S. N. Applications of isothermal titration calorimetry to measure enzyme kinetics

and activity in complex solutions. *Thermochim. Acta* **448,** 12–18 (2006).

299. Lipinski, C. A., Lombardo, F., Dominy, B. W. & Feeney, P. J. Experimental and computational approaches to estimate solubility and permeability in drug discovery and development settings. *Adv. Drug Deliv. Rev.* **23,** 3–25 (1997).

300. Fischer, H., Gottschlich, R. & Seelig, A. Blood-brain barrier permeation: molecular parameters governing passive diffusion. *J. Membr. Biol.* **165,** 201–11 (1998).

301. Palm, K., Luthman, K., Ros, J., Grasjo, J. & Artursson, P. Effect of molecular charge on intestinal epithelial drug transport: pH-dependent transport of cationic drugs. *J. Pharmacol. Exp. Ther.* **291,** 435–43 (1999).

302. Zhao, G. & Chasteen, N. D. Oxidation of Good's buffers by hydrogen peroxide. *Anal. Biochem.* **349,** 262–267 (2006).

303. Ladbury, J. E. & Chowdhry, B. Z. Sensing the heat: the application of isothermal titration calorimetry to thermodynamic studies of biomolecular interactions. *Chem. Biol.* **3,** 791–801 (1996).

304. Ladbury, J. E. & Williams, M. A. The extended interface: measuring non-local effects in biomolecular interactions. *Curr. Opin. Struct. Biol.* **14,** 562–569 (2004).

305. Waterhouse, A. *et al.* SWISS-MODEL: homology modelling of protein structures and complexes. *Nucleic Acids Res.* **46,** W296–W303 (2018).

306. Siedow, J. N. & Umbach, A. L. The mitochondrial cyanide-resistant oxidase: Structural conservation amid regulatory diversity. *Biochim. Biophys. Acta - Bioenerg.* **1459,** 432–439 (2000).

307. Vishwakarma, A., Tetali, S. D., Selinski, J., Scheibe, R. & Padmasree, K. Importance of the alternative oxidase (AOX) pathway in regulating cellular redox and ROS homeostasis to optimize photosynthesis during restriction of the cytochrome oxidase pathway in *Arabidopsis thaliana*. *Ann. Bot.* **116,** 555–569 (2015).

308. Polidoros, A. N., Mylona, P. V. & Arnholdt-Schmitt, B. *Aox* gene structure, transcript variation and expression in plants. *Physiol. Plant.* **137,** 342–353 (2009).

309. Jorgensen, W. L. The many roles of computation in drug discovery. *Science* **303,** 1813–8 (2004).

310. Kitchen, D. B., Decornez, H., Furr, J. R. & Bajorath, J. Docking and scoring in virtual screening for drug discovery: methods and applications. *Nat. Rev. Drug Discov.* **3,** 935–949 (2004).

311. Ekins, S., Mestres, J. & Testa, B. *In silico* pharmacology for drug discovery: methods for virtual ligand screening and profiling. *Br. J. Pharmacol.* **152,** 9–20 (2007).

312. Zoete, V., Grosdidier, A. & Michielin, O. Docking, virtual high throughput screening and in silico fragment-based drug design. *J. Cell. Mol. Med.* **13,** 238–248 (2009).

313. Gowrisankar, S. *et al.* A General and Efficient Catalyst for Palladium-Catalyzed C−O Coupling Reactions of Aryl Halides with Primary Alcohols. *J. Am. Chem. Soc.* **132,** 11592–11598 (2010).

314. Cheung, C. W. & Buchwald, S. L. Mild and General Palladium-Catalyzed Synthesis of Methyl Aryl Ethers Enabled by the Use of a Palladacycle Precatalyst. *Org. Lett.* **15,** 3998–4001 (2013).

315. Anderson, K. W., Ikawa, T., Tundel, R. E. & Buchwald, S. L. The Selective Reaction of Aryl Halides with KOH: Synthesis of Phenols, Aromatic Ethers, and Benzofurans. *J. Am. Chem. Soc.* **128,** 10694–10695 (2006).

316. deBoer, G. J., Nott, P. & Kemmitt, G. M. Use of Uptake Spraying Oil to Improve Fungicidal Activity of the Triazole Fungicide Fenbuconazole on *Puccinia triticina* and *Puccinia striiformis* Rusts of Wheat. *Plant Heal. Prog.* **14,** 19 (2013).

Appendix

The following pages provide the raw LC-MS spectra for Compounds **16-19**.

All other ^{1}H, ^{13}C and LC-MS spectra are available on request as part of a supplementary data file.

Compound 16

Shimadzu Open Solution

Project:	Direct Access
Experiment:	am2089_20181005_01
Experiment Description:	
Sample:	JM8
Sample Description:	
Data File Name:	C:\LabSolutions\Data\Project1\am2089_20181005_01\JM8.lcd
Sample Location:	Plate Number: 1 - Position: 76
Run By:	am2089
Run Started:	06 October 2018 03:24:37
Run Finished:	06 October 2018 08:35:58
Method:	Ana 30-95 in 20min

LC Chromatogram

LC#1 : Detector A Channel 1

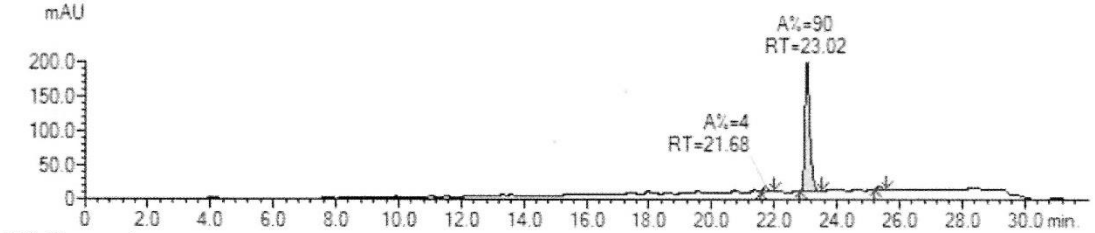

MS Chromatogram

Group#2 Scan(-) EI : TIC

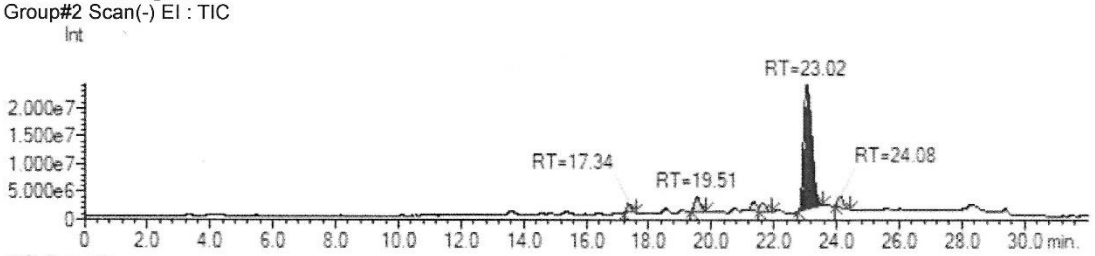

MS Spectrum

Group#2 - MS Peak: 13, RT: 22.74 to 23.54 min

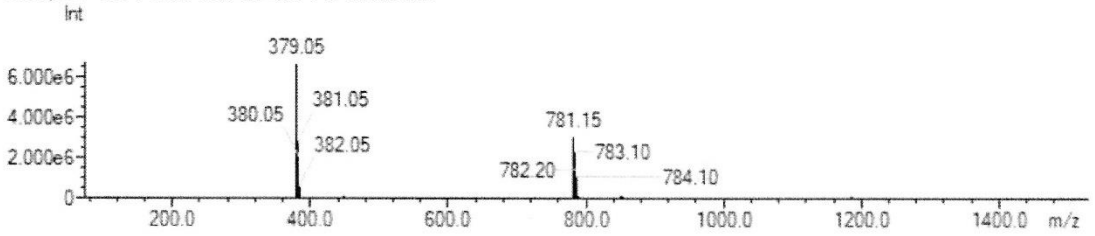

Sample: JM8 **Run By:** am2089 **Run Finished:** 06 October 2018 08:35:58

LC Peak Table

ID	RT	LC Channel	Area %
1	21.68	Detector A Channel 1	3.6
2	23.02	Detector A Channel 1	89.7
3	25.32	Detector A Channel 1	2.1

MS Peak Table

ID	RT	Scan Group	Purity	Purity Source	Area %
4	3.98	1: TIC	0.0		48.9
5	17.34	1: TIC	0.0		2.8
6	19.52	1: TIC	0.0		2.8
7	23.02	1: TIC	89.7	LC#1 : Detector A Channel 1 23.02 min	26.3
8	29.38	1: TIC	0.0		15.0
9	17.34	2: TIC	0.0		3.0
10	19.51	2: TIC	0.0		6.3
11	21.32	2: TIC	0.0		3.6
12	21.60	2: TIC	3.6	LC#1 : Detector A Channel 1 21.68 min	3.8
13	23.02	2: TIC	89.7	LC#1 : Detector A Channel 1 23.02 min	76.4
14	24.08	2: TIC	0.0		4.7

Compound 17

Shimadzu Open Solution

Project:	Direct Access
Experiment:	am2089_20181005_01
Experiment Description:	
Sample:	JM3
Sample Description:	
Data File Name:	C:\LabSolutions\Data\Project1\am2089_20181005_01\JM3.lcd
Sample Location:	Plate Number: 1 - Position: 26
Run By:	am2089
Run Started:	06 October 2018 03:24:37
Run Finished:	06 October 2018 08:35:58
Method:	Ana 30-95 in 20min

LC Chromatogram

LC#1 : Detector A Channel 1

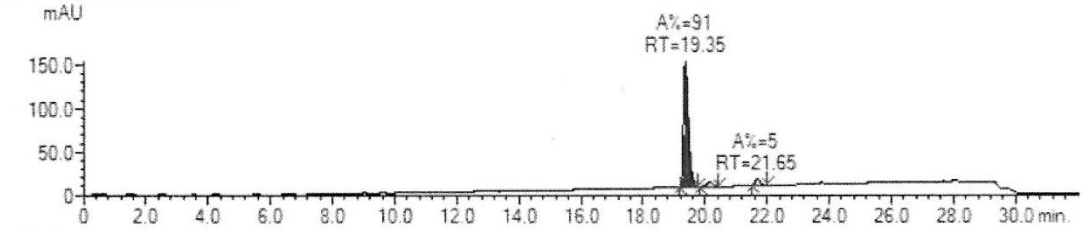

MS Chromatogram

Group#2 Scan(-) EI : TIC

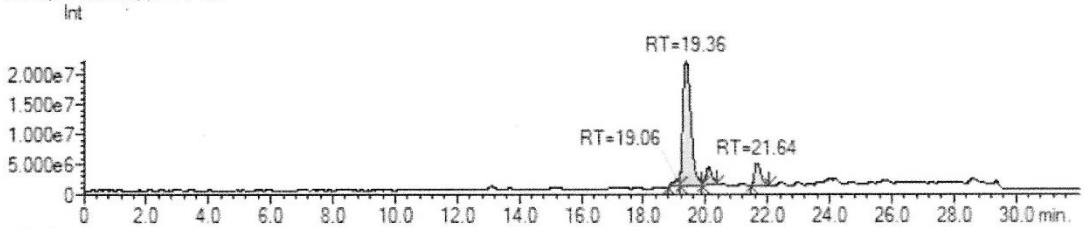

MS Spectrum

Group#2 - LC Peak: 1, RT: 19.15 to 19.77 min

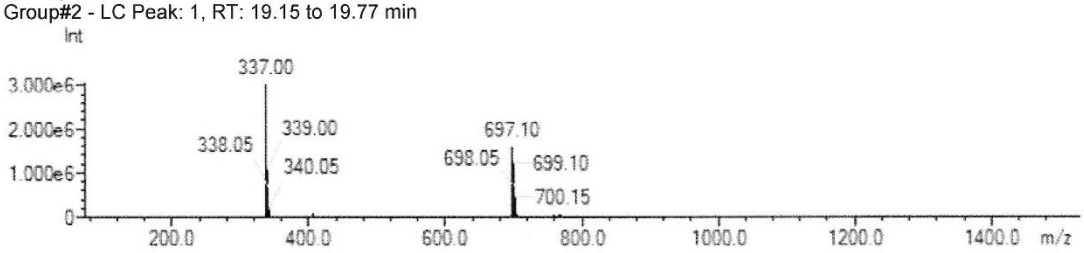

Sample: JM3 **Run By:** am2089 **Run Finished:** 06 October 2018 08:35:58

LC Peak Table

ID	RT	LC Channel	Area %
1	19.35	Detector A Channel 1	90.9
2	20.10	Detector A Channel 1	4.0
3	21.65	Detector A Channel 1	5.1

MS Peak Table

ID	RT	Scan Group	Purity	Purity Source	Area %
4	14.09	1: TIC	0.0		2.6
5	19.36	1: TIC	90.9	LC#1 : Detector A Channel 1 19.35 min	40.8
6	21.64	1: TIC	5.1	LC#1 : Detector A Channel 1 21.65 min	8.1
7	23.85	1: TIC	0.0		3.7
8	24.14	1: TIC	0.0		9.5
9	29.36	1: TIC	0.0		35.2
10	19.06	2: TIC	0.0		3.4
11	19.36	2: TIC	90.9	LC#1 : Detector A Channel 1 19.35 min	76.9
12	20.08	2: TIC	4.0	LC#1 : Detector A Channel 1 20.10 min	8.3
13	21.64	2: TIC	5.1	LC#1 : Detector A Channel 1 21.65 min	10.6

Compound 18

Shimadzu Open Solution

Project:	Direct Access
Experiment:	am2089_20181005_01
Experiment Description:	
Sample:	JM9
Sample Description:	
Data File Name:	C:\LabSolutions\Data\Project1\am2089_20181005_01\JM9.lcd
Sample Location:	Plate Number: 1 - Position: 86
Run By:	am2089
Run Started:	06 October 2018 03:24:37
Run Finished:	06 October 2018 08:35:58
Method:	Ana 30-95 in 20min

LC Chromatogram

LC#1 : Detector A Channel 1

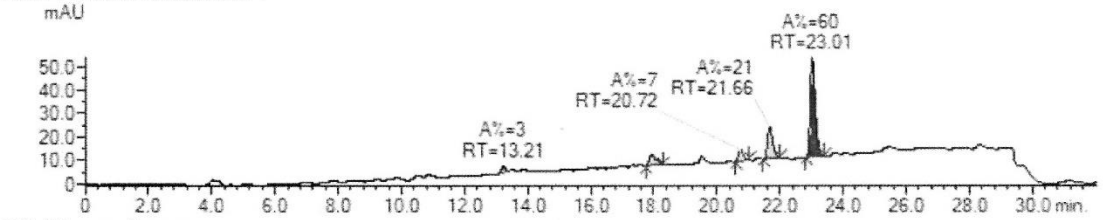

MS Chromatogram

Group#2 Scan(-) EI : TIC

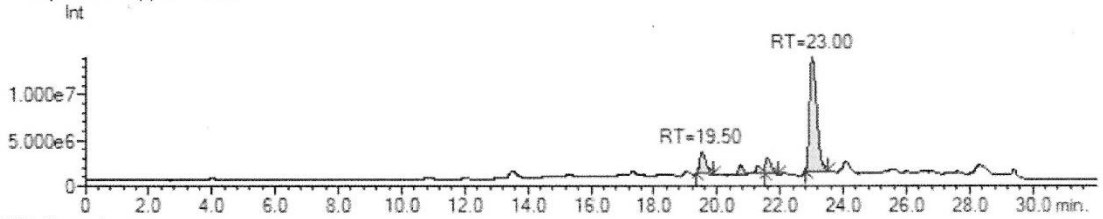

MS Spectrum

Group#2 - LC Peak: 5, RT: 22.80 to 23.37 min

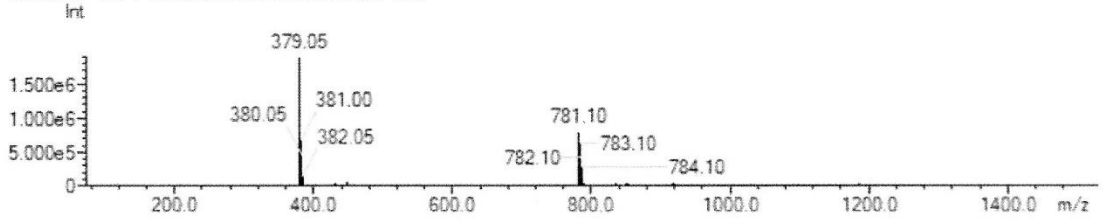

LC Peak Table

ID	RT	LC Channel	Area %
1	13.21	Detector A Channel 1	3.4
2	17.91	Detector A Channel 1	9.2
3	20.72	Detector A Channel 1	6.7
4	21.66	Detector A Channel 1	20.6
5	23.01	Detector A Channel 1	60.1

Sample: JM9 **Run By:** am2089 **Run Finished:** 06 October 2018 08:35:58

MS Peak Table

ID	RT	Scan Group	Purity	Purity Source	Area %
6	3.99	1: TIC	0.0		47.5
7	4.54	1: TIC	0.0		5.2
8	4.67	1: TIC	0.0		5.0
9	4.94	1: TIC	0.0		2.3
10	19.52	1: TIC	0.0		2.8
11	22.99	1: TIC	60.1	LC#1 : Detector A Channel 1 23.01 min	9.1
12	25.47	1: TIC	0.0		5.7
13	29.40	1: TIC	0.0		13.9
14	19.50	2: TIC	0.0		11.6
15	20.72	2: TIC	6.7	LC#1 : Detector A Channel 1 20.72 min	3.7
16	21.25	2: TIC	20.6	LC#1 : Detector A Channel 1 21.66 min	3.2
17	21.58	2: TIC	20.6	LC#1 : Detector A Channel 1 21.66 min	8.1
18	23.00	2: TIC	60.1	LC#1 : Detector A Channel 1 23.01 min	71.8

Compound 19

Shimadzu Open Solution

Project:	Direct Access
Experiment:	am2089_20181005_01
Experiment Description:	
Sample:	JM1
Sample Description:	
Data File Name:	C:\LabSolutions\Data\Project1\am2089_20181005_01\JM1.lcd
Sample Location:	Plate Number: 1 - Position: 6
Run By:	am2089
Run Started:	06 October 2018 03:24:37
Run Finished:	06 October 2018 08:35:58
Method:	Ana 30-95 in 20min

LC Chromatogram

LC#1 : Detector A Channel 1

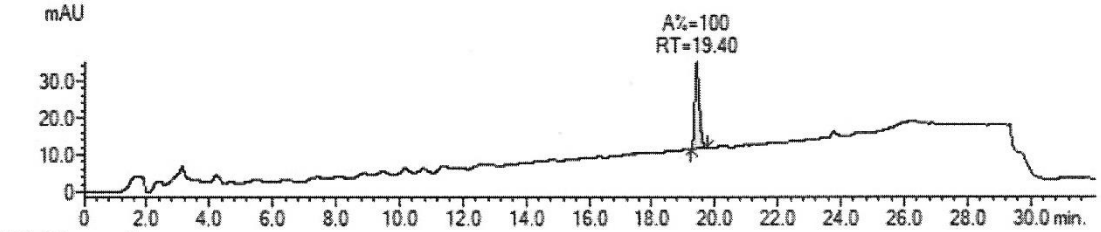

MS Chromatogram

Group#2 Scan(-) EI : TIC

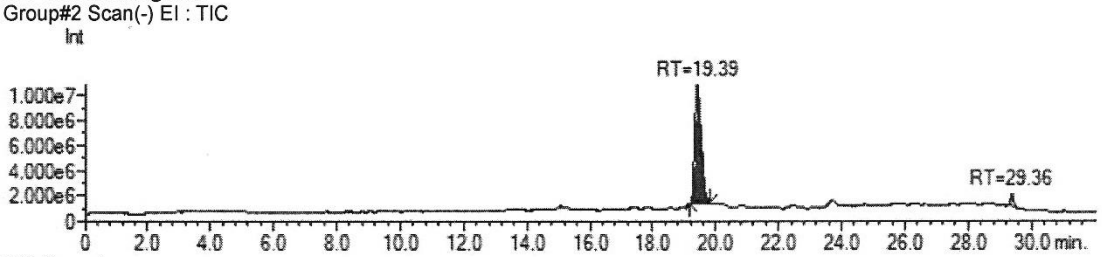

MS Spectrum

Group#2 - MS Peak: 4, RT: 19.17 to 19.79 min

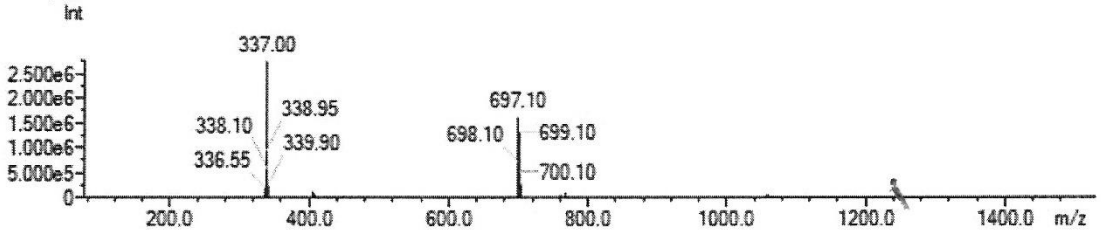

Sample: JM1 **Run By:** am2089 **Run Finished:** 06 October 2018 08:35:58

LC Peak Table

ID	RT	LC Channel	Area %
1	19.40	Detector A Channel 1	100.0

MS Peak Table

ID	RT	Scan Group	Purity	Purity Source	Area %
2	19.40	1: TIC	100.0	LC#1 : Detector A Channel 1 19.40 min	26.1
3	29.37	1: TIC	0.0		73.9
4	19.39	2: TIC	100.0	LC#1 : Detector A Channel 1 19.40 min	96.1
5	29.36	2: TIC	0.0		3.9